# *Giardia duodenalis* – epithelial interaction and barrier function

D I S S E R T A T I O N

zur Erlangung des akademischen Grades

d o c t o r  r e r u m  n a t u r a l i u m

(Dr. rer. nat.)

im Fach Biologie

eingereicht an der

Lebenswissenschaftlichen Fakultät der Humboldt-Universität zu Berlin

von M.Sc. Martin Rolf Kraft

Präsidentin

der Humboldt-Universität zu Berlin

Prof. Dr.-Ing. habil. Dr. phil. Sabine Kunst

Dekan der Lebenswissenschaftlichen Fakultät

der Humboldt-Universität zu Berlin

Prof. Dr. rer. nat. Bernhard Grimm

Gutachter/innen

PD Dr. rer. nat. Anton Aebischer

Prof. Dr. rer. nat. Kai Matuschewski

Prof. Dr. med. Jörg-Dieter Schulzke

Tag der Disputation: 17. Dezember 2019

https://doi.org/10.18452/21045

*Ich will Ihnen das Geheimnis verraten, das mich zum Ziel geführt hat:*
*Meine Stärke liegt einzig und allein in meiner Hartnäckigkeit.*

Louis Pasteur

# Danksagung

An erster Stelle bedanke ich mich herzlichst bei Dr. Toni Aebischer für die Möglichkeit in seiner Fachgruppe am Robert Koch-Institut dieses Promotionsprojekt durchzuführen, der umfassenden Betreuung sowie seiner zahlreichen Anregungen und Ideen.
Ebenfalls bedanke ich mich herzlichst bei Prof. Dr. Jörg-Dieter Schulzke für die Unterstützung, die vielen Ratschläge und die Bereitstellung der humanen Dünndarmbiopsien, dessen Spendern ich gleichfalls danke.

Großer Dank gilt auch Dr. Christian Klotz, der mir stets mit Rat und Tat zur Seite stand und dessen praktische Erfahrung äußerst hilfreich war.
Ebenso Dr. Roland Bücker, der mich den Umgang mit dem Transwell-Kultivierungssystem sowie den elektrischen Widerstandsmessungen lehrte und mir viele Tipps gab.

Ich bedanke mich auch bei Prof. Dr. Ralf Ignatius, der als Mitglied meines *Thesis Advisory Committee* mir ebenfalls mit hilfreichem Feedback zur Seite stand.

Ferner möchte ich mich bei Prof. Dr. Frank Seeber und Dr. Geo Semini sowie meinen stets hilfreichen Kollegen Francesca Torelli, Totta Ehret, Benedikt Fabian, Estefanía Delgado-Betancourt und Stephanie Henkel für die zahlreichen Diskussionen und das freundliche Arbeitsumfeld bedanken.

Mein Dank gilt auch den übrigen Mitarbeitern von FG16, insbesondere den zuvorkommenden TAs, wie Jasmin Gerkrath, Petra Gosten-Heinrich, Gudrun Kliem und Ulrike Laube.

Des Weiteren möchte ich den Studenten, studentischen Hilfskräften und Azubis, wie Wibke Krüger, Julia Plinke und Maximilian Preuß für ihre Unterstützung danken. Insbesondere auch David Holthaus, der eine große Hilfe im Laboralltag war und dem ich als mein Nachfolger, aufbauend auf diesem Projekt, viel Erfolg und gutes Gelingen wünsche.

Ich bedanke mich ebenfalls bei Dr. Susanne Krug und In-Fah Lee von der Charité für die Unterstützung bei der Isolierung von Krypten aus den Biopsien sowie den Ussing-Kammer-Experimenten. Ich danke auch Dr. Michael Laue und Gudrun Holland aus ZBS4 für die elektronenmikroskopischen Aufnahmen.

Zuletzt bedanke ich mich bei Prof. Dr. Susanne Hartmann dafür, dass ich Stipendiat des GRK 2046 sein durfte sowie den damit verbundenen Privilegien und der Finanzierung. Ebenfalls danke ich der Sonnenfeld-Stiftung für das Antje-Bürgel-Stipendium, um diese Arbeit abzuschließen.

# Zusammenfassung

Die Durchfallerkrankung Giardiasis wird durch den einzelligen Parasiten *Giardia duodenalis* ausgelöst. Die Infektion erfolgt durch die Aufnahme von Zysten über fäkal-oralem Weg, meist über kontaminiertes Trinkwasser. Im Magen des Wirts transformieren sich die aufgenommenen Zysten zu Trophozoiten, welche das vegetative und bewegliche Lebensstadium des Parasiten darstellen. Die Trophozoiten kolonisieren das Duodenum und den oberen Teil des Jejunums und heften sich an das Dünndarmepithel, wodurch sie die Krankheitsbeschwerden auslösen. Allerdings sind Details über die Mechanismen der Pathogenese unbekannt. Dazu kommt, dass der Ausgang einer Infektion fallspezifisch starken Schwankungen unterworfen ist, von selbst-limitierend bis chronisch und asymptomatischer Kolonisierung bis hin zur schweren Enteritis. Ein möglicher Pathomechanismus ist der Wegfall der Barrierefunktion des Dünndarmepithels, z.B. durch Beeinträchtigung von *tight junctions* oder Zelltod.

In dieser Arbeit wurden Effekte von *G. duodenalis* auf *in vitro* Modellsysteme des humanen Dünndarmepithels untersucht. Dazu wurden hauptsächlich Daten über die Barrierefunktion sowohl von der weit verbreiteten Caco-2 Zelllinie, als auch über ein neu etabliertes humanes Dünndarmorganoidsystem, erhoben.

Es konnte gezeigt werden, dass mehrere - mitunter in der Literatur als hochvirulent beschriebene - *G. duodenalis* Isolate zu keinerlei Beeinträchtigung der Barrierefunktion oder irgendeiner anderen untersuchten potenziellen Schädigung an zwei unterschiedlichen Caco-2 Zelllinien unter diversen Infektions- und Kulturbedingungen führte. Jedoch andererseits das neu entwickelte Dünndarmorganoidsystem mit pseudo-luminalem Medium TYI-S-33 reproduzierbar die Zerstörung des Epithelmodells mit Zellverlust, Zelltod (apoptotisch und nicht-apoptotisch), Störung der *tight junctions* (Abbau und Dislokation von Claudinen und ZO-1) und den Verlust von Mikrovilli innerhalb ein bis zwei Tage nach Parasiteninfektion zeigen konnte. Zudem wurde das Auftauchen von ClCa-1-Signalen unter andauerndem Infektionsstress beobachtet, was die Differenzierung bzw. Metaplasie zu Becherzellen nahelegt, jedoch keine Wirtsreaktion auf die Gewebszerstörung zu sein scheint.

Solche Funde, die nicht mit dem gängigem Caco-2 Ansatz erzielt werden konnten oder gar mit diesem System unmöglich zu beobachten sind, zeigen klar den Vorteil von organoidbasierten Modellen gegenüber traditionellen Karzinom-abgeleiteten Zellsystemen. Damit wird deutlich, dass diese fortschrittlicheren Alternativen benötigt werden um verlässliche Erkenntnisse von komplexen und schwer fassbaren Erkrankungen, wie Giardiasis, zu bekommen und zukünftige Forschungsarbeiten können sowohl auf den Erkenntnissen, als auch auf dem entwickelten Dünndarmorganoidsystem dieser Arbeit aufbauen.

# Abstract

The protozoan parasite *Giardia duodenalis* is the etiological agent for the intestinal diarrheal disease giardiasis. Infections are acquired via the fecal-oral route, mostly via uptake of cysts from contaminated drinking water. Taken up cysts transform into the trophozoite stage, which is the parasite's motile and vegetative life stage. The colonization of the hosts' duodenum and upper jejunum and the attachment of *Giardia* trophozoites onto the epithelium is the cause of a variety of gastrointestinal complaints but the exact pathomechanisms are unknown. Furthermore, the outcome of *Giardia* infections varies greatly between individuals, ranging from self-limiting to chronic, and asymptomatic to severe enteritis. One proposed mechanism for the pathogenesis is the breakdown of intestinal barrier function, e.g. by tight junction impairment or induction of cell death.

In this work, effects of *G. duodenalis* on *in vitro* models of the human small intestinal epithelium were investigated by studying mainly barrier-related properties and changes of widely used Caco-2 cells as well as newly established human small intestinal organoid-derived monolayers (ODMs).

It could be shown that several isolates of *G. duodenalis*, some described as highly virulent, fail to induce barrier dysfunction or any other investigated pathological effect on two Caco-2 cell lines under various infection and culturing conditions. On the other side, by developing a new organoid-based model system and the use of luminal mock medium TYI-S-33, considerable epithelial disruption (including loss of cells), cell death (apoptosis and non-apoptotic), tight junction impairment (degradation and dislocation of claudins and ZO-1), and microvilli depletion reproducibly induced by *G. duodenalis* trophozoites between one and two days after infection could be observed. Moreover, emergence of ClCa-1 positive cells with ongoing parasite infections suggest epithelial differentiation or metaplasia towards goblet cells, which is furthermore not associated to tissue damage.

Those findings, which were not achieved or even impossible to detect by the popular Caco-2 approach, indicate the advantage of organoid-based models over such traditional carcinoma-derived cell systems. It becomes clear that those advanced *in vitro* models are required to gain robust data from complex and elusive diseases like giardiasis and future research may build upon findings and the developed ODM system of this work.

# Table of Content

# List of Figures

# List of Tables

# List of Abbreviations

| | |
|---|---|
| (ds)RNA | (double stranded) ribonucleic acid |
| 2D | 2 dimensional (flat) |
| 3D | 3 dimensional |
| 3Rs | replacement, reduction, refinement (lab animal guideline) |
| A83-01 | a TGFβ-inhibitor |
| AC | alternating current |
| AJ | adherens junction |
| Akt | protein kinase B |
| ALK [number] | activin receptor-like kinase [number] |
| ALPi | alkaline phosphatase, intestinal |
| ANOVA | Analysis of Variance |
| ATP | adenosine triphosphate |
| BCA | bicinchoninic acid assay |
| BF | bright field |
| BSA | bovine serum albumin |
| CaCC | calcium-dependent chloride channel |
| Casp3 | caspase 3 |
| CBC | crypt base columnar [cells], synonym for ISC |
| CBF | (Charité) Campus Benjamin Franklin; also as designation for isolates |
| CCD | charge-coupled-device |
| CCL[2/20] | chemokine (C-C motif) ligand [2/20] |
| CD4 | cluster of differentiation 4, marker for T helper cells and more |
| CFTR | cystic fibrosis transmembrane conductance regulator |
| ChrA | chromogranin A |
| ClCa-1 | chloride channel accessory 1 |
| cldn-[number] | claudin [number] |
| cLSM | confocal laser-scanning microscopy |
| CTRL+/- | positive/negative control condition |
| CXCL[1/2] | chemokine (C-X-C motif) ligand [1/2] |
| DAPI | 4′,6-diamidino-2-phenylindole |
| DC | direct current |
| DCLK-1 | doublecortin-like kinase 1 |
| DF | dark field |
| DIC | differential interference contrast |
| DM-[1/2] | differentiation medium mix [1/2] |
| DMEM | Dulbecco's modified Eagle's medium |
| DNA | deoxyribonucleic acid |
| dUTP | deoxyuridine triphosphate |
| e.g. | exempli gratia (for example) |
| EC | enterocyte |
| E-cadherin | epithelial cadherin |
| ECM | extracellular matrix |
| EDTA | ethylenediaminetetraacetic acid |
| EEC | enteroendocrine cell |
| EGF | epidermal growth factor |
| EHT | electron high tension |
| ELISA | enzyme-linked immunosorbent assay |
| EM | electron microscopy |
| EtOH | ethanol |
| FA | focal adhesions |
| F-actin | filamentous actin, polymers consisting of G-actin (globular) |
| FBS | fetal bovine serum |
| FGF-2 | fibroblast growth factor 2 |
| FITC | fluorescein isothiocyanate |
| GALT | gut-associated lymphoid tissue |
| GAP | goblet cell associated antigen passage |
| GAPDH | glyceraldehyde 3-phosphate dehydrogenase |

| | |
|---|---|
| GC | goblet cell |
| GJ | gap junction |
| GLUT2 | glucose transporter 2 |
| GLV | Giardia lamblia virus |
| GM-CSF | granulocyte-macrophage colony-stimulating factor |
| GSH/GSSG | glutathione (mono-/dimeric) |
| GSK3 | glycogen synthase kinase 3 |
| HDAC | histone deacetylase |
| IBD | irritable bowel disease |
| IF[A] | immunofluorescence [assay] |
| IFNγ | interferon gamma |
| Ig[A/G] | immunoglobulin type [A/G] (antibodies) |
| IGF-1 | insulin-like growth factor 1 |
| Il-[number] | interleukin [number] |
| ILC2 | innate lymphoid cells group 2 |
| ISC | intestinal stem cell |
| ISC | short-circuit current (charge flow per time when short-circuited) |
| JAM | junctional adhesion molecule |
| LARPII | luciferase assay reagent II |
| Lgr5 | leucine-rich repeat-containing G-protein coupled receptor 5 |
| LN | liquid nitrogen |
| LRC | label-retaining cells, putative quiescent stem cells |
| LRV1 | Leishmania RNA virus-1 |
| M cell | microfold cell |
| mag. | magnified (microscopically) |
| MAPK | mitogen-activated protein kinase |
| MeOH | methanol |
| MOI | multiplicity of infection (here ratio of trophozoites to host cells) |
| Muc2 | mucin 2 |
| MVID | microvilli inclusion disease |
| MW | molecular weight |
| NEAA | non-essential amino acids |
| NFκB | nuclear factor kappa-light-chain-enhancer of activated B cells |
| NKCC | Na+-K+-Cl- co-transporter |
| O/N | over night |
| ODM | organoid-derived monolayer |
| p.i. | *post infectionem* (post infection) |
| P/S | penicillin/streptomycin |
| PAS | periodic acid-Schiff |
| PBS | phosphate-buffered saline |
| PC | Paneth cell |
| PC-transwell-filter | (also PCF) polycarbonate transwell-filter (opaque) |
| PET-transwell-filter | polyethylene terephthalate transwell-filter (translucent properties) |
| PFA | paraformaldehyde, but basically formaldehyde in solution |
| PGC | pepsinogen C |
| PGE2 | prostaglandin $E_2$ |
| pH | negative base 10 logarithm of the molar $H^+$ concentration in solution |
| PI | propidium iodide |
| PI3K | phosphoinositide 3-kinase |
| PLA2 | phospholipase A2 |
| PLB | passive lysis buffer |
| pNP | para-nitrophenyl |
| pNPP | para-nitrophenylphosphate |
| qRT-PCR | quantitative reverse transcriptase polymerase chain reaction |
| Reg3-[β/γ] | regenerating islet-derived protein 3 [beta/gamma] |
| RELMβ | resistin-like molecule beta |
| RI | ROCK-inhibitor |
| RKI | Robert Koch-Institute |
| ROCK | rho-associated protein kinase |
| ROS | reactive oxygen species |

| | |
|---|---|
| RT | room temperature (20-22°C) |
| SB202190 | a p38 MAPK-inhibitor |
| SD | standard deviation |
| SEM | scanning electron microscopy |
| SGLT-1 | sodium-dependent glucose cotransporter 1 |
| SI | sucrase-isomaltase |
| SM | spheroid medium mix (favors stem cell growth) |
| SOX9 | SRY-box 9 |
| sp. | species (unspecified) |
| spp. | species pluralis (multiple unspecified species) |
| SST | somatostatin |
| STAT3 | signal transducer and activator of transcription 3 |
| STEM | scanning transmission electron microscopy |
| TA | transient amplifying [zone/cells] |
| TC | tuft cell, also known as brush cell |
| TdT | terminal deoxynucleotide transferase |
| TEER | trans-epithelial electric resistance |
| TEM | transmission electron microscopy |
| TF | transcription factor |
| Tff3 | trefoil factor 3 |
| TGF-β | transforming growth factor beta |
| TJ[C/P] | tight junction [complex/protein] |
| TLR | toll-like receptor |
| TMEM16A | transmembrane member 16A |
| TNFα | tumor necrosis factor alpha |
| TRPM5 | transient receptor potential cation channel subfamily M member 5 |
| TUNEL | terminal deoxynucleotidyl transferase dUTP nick end labeling |
| VSP | variant surface protein |
| WD | working distance |
| Y-27632 | a ROCK-inhibitor |
| ZO-[number] | zonula occludens [number] |
| Ω | Ohm |

# 1. Introduction

## 1.1 The parasite *Giardia duodenalis*

*Giardia duodenalis*[1], initially described by van Leeuwenhoek in 1682, is a ubiquitous protozoan parasite of the small intestine of vertebrate species, including humans. It is responsible for one of the most common parasitic infections and can result in the diarrheal disease 'giardiasis' (Adam, 2001).

### 1.1.1 The biology of *Giardia* sp.

*Giardia* spp. belong to the order diplomonadida, which is characterized by the presence of two physiologically active and functionally equivalent nuclei, as well as eight flagella but no Golgi apparatus or classical mitochondria, which seem to became irrelevant and got lost as a consequence of its parasitic lifestyle (Adam, 2001; Tovar et al., 2003; Poxleitner et al., 2008; Faso & Hehl, 2011; Faso et al., 2013). They are microaerophilic organisms, not able to perform oxidative phosphorylation, but can tolerate low oxygen concentrations due to an antioxidant system (Tovar et al., 2003; Ankarklev et al., 2010; Mastronicola et al., 2015). Of note, the parasite is coating itself with variant-specific surface proteins (VSPs), which allows antigenic variation, thus immune evasion (Aggarwal & Nash, 1988; Müller et al., 1996; Nash, 1997; Morrison et al., 2007; Prucca et al., 2008).
*G. duodenalis* is considered to resemble a species complex of currently eight known distinct phylogenetic groups, referred to as assemblages (A-H), which differ regarding their host specificities (Table 1). Assemblage A and B have the broadest host spectrum and seem to be the only ones which can infect humans (Thompson & Monis, 2012; Heyworth, 2016). However, they share only 78% amino acid sequence homology in proteins and some authors suggest to consider them as two distinct species (Thompson & Monis, 2004; Monis et al., 2009; Jerlström-Hultqvist et al., 2010).

[1] also known as *Giardia lamblia* or *Giardia intestinalis*; here in short referred as *G. duodenalis*

Table 1: *Giardia* spp. and *G. duodenalis* assemblages

| Species | Assemblage | Known hosts |
|---|---|---|
| *G. agilis* | | Amphibians |
| *G. ardeae* | | Birds |
| *G. microti* | | Muskrats and voles |
| *G. muris* | | Rodents |
| *G. psittaci* | | Birds |
| *G. varani* | | Lizards |
| *G. duodenalis* | A | Numerous vertebrates including humans |
| | B | Numerous vertebrates including humans |
| | C | Dogs |
| | D | Dogs |
| | E | Hoofed animals |
| | F | Cats |
| | G | Mice, rats |
| | H | Seals |

Table according to Adam (2001) and Feng & Xiao (2011).

*Giardia* spp. have two different life stages: the dormant, infective cyst stage and the motile, vegetative trophozoite stage (Figure 1A). The 8-12 µm (long axis) oval-shaped cyst (Figure 1B) is usually taken up by the host via contaminated drinking water and initiates excystation in the acidic environment of the host's stomach into four trophozoites within 15 min (Bingham et al., 1979; Buchel et al., 1987; Ward et al., 1997; Hetsko et al., 1998; Bernander et al., 2001). The 12-15 µm (long axis) pear-shaped, flagellated trophozoites (Figure 1C) colonize the duodenum and upper jejunum of the host by using their ventral adhesive disc as a suction cup to adhere to the intestinal epithelium. There they replicate, parasitize the lumen by absorbing nutrients on transit and can cause disease (Adam, 2001; Ankarklev et al., 2010). Trophozoites which translocate further down the intestine will experience a shift in pH, bile salts concentrations and fatty acid composition, triggering the encystation process in which a 0,3-0,6 µm thick cyst wall consisting of N-acetylgalactosamine is produced around a duplicated but not separated trophozoite within 16 h. Those four-nucleated cysts are subsequently shed with the host's feces (Gillin et al., 1987; Schupp et al., 1988; Erlandsen et al., 1996; Lujan et al., 1996).

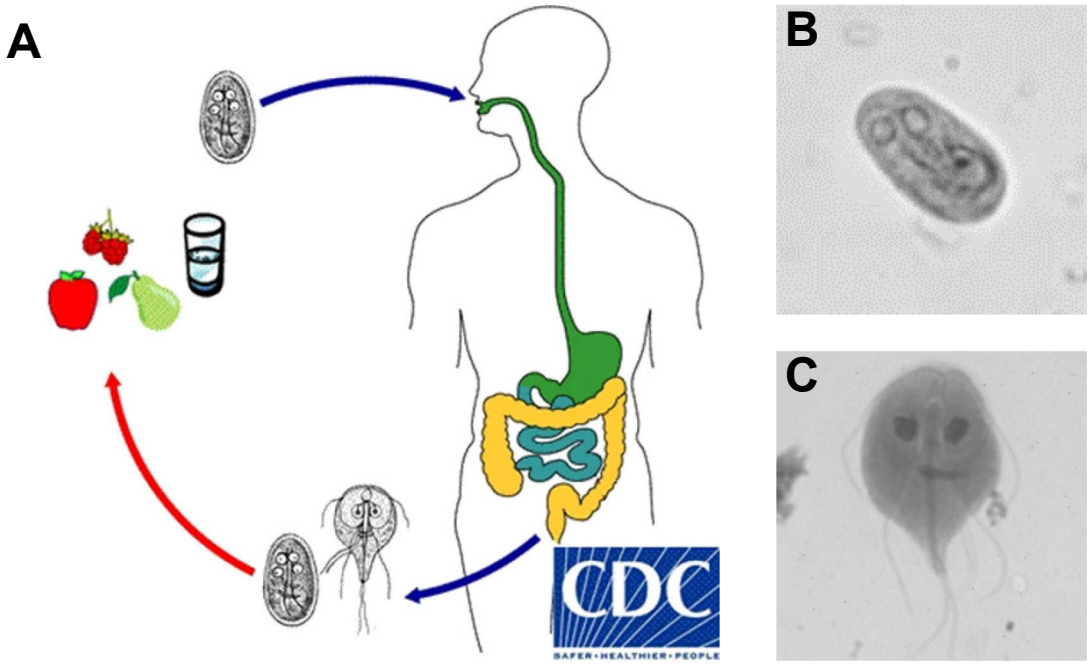


**Figure 1 Life cycle and stages of *G. duodenalis*.** Schematic life cycle and infection route of *G. duodenalis* (**A**), its infective cyst stage (**B**), and its motile and replicative trophozoite stage (**C**). Scheme and images modified from CDC DPDx database.

### 1.1.2 Giardiasis, the parasite's caused disease

Due to the fecal-oral route of infection, highest prevalences are reported for countries with poor access to higher sanitation standards. However, it is one of the most commonly reported parasitic infections in developed countries as well (Adam, 2001; Morrison et al., 2007). According to Ankarklev et al. (2010), 280 million symptomatic human infections per year are estimated and up to 5000 cases per year, approximately half of them travel-associated, are registered in Germany (Robert Koch-Institut: SurvStat@RKI 2.0). Young children after the breast-feeding period show the highest susceptibility (Goto et al., 2009; Ignatius et al., 2012; Abdel-Hafeez et al., 2013).

The infection dose can be as low as 10 cysts and first symptoms start usually between one and two weeks after infection (Rendtorff & Holt, 1954; Nash et al., 1987; Farthing, 1997). The symptomatology is highly variable in severity and manifestation with a variety of gastrointestinal complaints, like diarrhea (most prominent), abdominal pain (most common), steatorrhea, malabsorption, weight loss, nausea and vomiting and generally with a stronger clinical impact on children, which can result in growth retardation (Fraser et al., 2000; Adam, 2001; Ankarklev et al., 2010; Al-Mekhlafi et al., 2013; Bartelt et al., 2013). Additional factors known to influence the outcome, apart from age, are the host's nutritional status and immunocompetence (Farthing, 1997; Roxström-Lindquist et al., 2006). Furthermore, a possible correlation of *Giardia* infections

with chronic post-infectious sequelae such as irritable bowel disease (IBD) has attracted much attention in recent years (D'Anchino et al., 2002; Wensaas et al., 2012; Hanevik et al., 2014; Litleskare et al., 2015; Dormond et al., 2016; Halliez et al., 2016; Nakao et al., 2017). The infection itself is usually self-limiting and resolves spontaneously after two or three additional weeks but can also be treated with nitroimidazoles or benzimidazoles and their derivates (Paget et al., 1989; Edlind et al., 1990; Meloni et al., 1990; Chavez et al., 1992; Liu et al., 2000). However, it is not uncommon that giardiasis can become chronic and refractory to treatment (Robertson et al., 2010; Escobedo et al., 2014; Lalle & Hanevik, 2018).

Despite that, asymptomatic colonization is the more common course of infection (Rendtorff & Holt, 1954; Keystone et al., 1978; Nash et al., 1987; Ankarklev et al., 2010). The reasons for these fundamental differences in the consequences of infection are unclear (Adam, 2001; Troeger et al., 2007; Klotz & Aebischer, 2015; Tysnes & Robertson, 2015).

#### 1.1.2.1 Pathophysiology of giardiasis

Due to the various disease outcomes, the cause of giardiasis is considered to be multifactorial (Ankarklev et al., 2010; Stadelmann et al., 2012; Fisher et al., 2013). Table 2 lists pathomechanisms of *G. duodenalis* infections, described in the literature.

The major disease phenotypes can be clustered into two groups: the epithelial barrier dysfunction, characterized by disturbance of the tight junction complex and/or induction of apoptosis, and the malabsorption phenotype, including villus shortening, microvilli depletion, crypt hyperplasia, anion hypersecretion and impaired host digestive enzymes. Both groups can contribute to diarrhea.

However, insight into how exactly *G. duodenalis* causes those effects is only superficial at most. The parasite seems to degrade (Chin et al., 2002; Troeger et al., 2007; Chen et al., 2013) or dislocate (Teoh et al., 2000; Scott et al., 2002; Humen et al., 2011; Maia-Brigagao et al., 2012) tight junction proteins only upon attachment (Humen et al., 2011) or its bare presence (Teoh et al., 2000; Chin et al., 2002; Scott et al., 2002). Apoptosis occurs in some studies with the most commonly used isolate WB6 (Chavez et al., 1986; Panaro et al., 2007; Fisher et al., 2013), in other studies with the same isolate not (Chavez et al., 1986; Chin et al., 2002; Maia-Brigagao et al., 2012). However, apoptosis appears to be caspase-dependent (Chin et al., 2002; Panaro et al., 2007; Koh et al., 2013), albeit it could just be a consequence of junctional disruption (Frisch & Francis, 1994; Morrison et al., 2007; Lugo-Martínez et al., 2009). Regarding malabsorption, no mechanism of *G. duodenalis* is known to explain the phenotypes of villus atrophy, microvilli depletion or crypt hyperplasia. Reasons

or mechanisms for post-infectious afflictions are also still elusive (Klotz & Aebischer, 2015). Moreover, the symptomatology of giardiasis and celiac disease (or other intestinal anaphylaxes) are consimilar (Rubin et al., 1966; Curtis et al., 1990; Koot et al., 2009; Saurabh et al., 2017) and uncertainty still exists whether IBD is a possible consequence of *G. duodenalis* infection or its discomfort is just incorrectly attributed to a coincident asymptomatic colonization in some cases (Koot et al., 2009; Saurabh et al., 2017).

Several epidemiological studies had investigated functional correlates of giardiasis such as intestinal permeability (for barrier dysfunction) and growth retardation (for malabsorption) in different patient collectives suffering from *G. duodenalis* infection. Much like the mentioned *in vitro* or animal studies, inconsistent findings are common. Cross-sectional or longitudinal investigations, mostly on young children in their first couple of years of life and under poor living conditions, show sometimes increased gut permeability (Dagci et al., 2002; Goto et al., 2002; Kosek, 2017; Rogawski et al., 2017) or reduced body weight and height (Kosek, 2017; Rogawski et al., 2017), and sometimes - although using the same or comparable methods - not (Serrander et al., 1984; Di Campbell et al., 2004; Hollm-Delgado et al., 2008; Goto et al., 2009; Garzon et al., 2017). More confusingly, some studies observed even a negative correlation to severe diarrhea in highly endemic areas, suggesting protective features of *G. duodenalis* infections (Bilenko et al., 2004; Kotloff et al., 2013; Muhsen et al., 2014). Besides, basic permeability of the intestine shows a geographical distribution and studies, which associate increased permeability to *G. duodenalis*-infection, offer in many cases permeability ratios within those global geographical variances, rendering its sole impact on health questionable (Menzies et al., 1999). The observed inconsistencies and weak statistical significances might be a result of the high number of asymptomatic cases, which confounds the data, small sample/cohort sizes (Serrander et al., 1984; Dagci et al., 2002), intermittent cyst shedding concealing infection (Di Campbell et al., 2004; Goto et al., 2009), or other diseases and co-infections which are likely to be present in such cohorts under poor living conditions. Especially two retrospective studies, one of them analyzed 567 *Giardia*-positive cases from a broad patient cohort which underwent endoscopy due to unspecific gastrointestinal complaints (Oberhuber et al., 1997), the other one 32 *Giardia*-positive children from a tertiary pediatric gastroenterology center (Koot et al., 2009), found both only mild inflammation and partial villus atrophy in 3,7 % (Oberhuber et al.) and 3,1 % (Koot et al.) of the patients, concluding that it is highly advisable to take effort to exclude concomitant diseases.

Such findings raise the question whether or not *G. duodenalis* may be apathogenic in general and giardiasis a kind of overreaction of the host (allergic reaction, hypersensitivity, etc.) or an opportunistic pathogen, only virulent if there is an underlying host deficiency. Indeed, the status of *G. duodenalis* as a

pathogen was a controversy in the past (Stevens, 1982) and it was only as late as 1987 (Nash et al., 1987) - by fulfilling Koch's postulates - officially considered as a pathogen, although known for more than 300 years. Even today this discussion is occasionally started again by several authors, confronted with their negative or contradictory results (Bilenko et al., 2004; DuPont, 2013; Kotloff et al., 2013; Muhsen et al., 2014; Bartelt & Platts-Mills, 2016; Hanevik, 2016).

To summarize, *in vitro*, animal and epidemiological studies suggest that *G. duodenalis* can induce epithelial barrier dysfunction and histopathological changes resulting in malabsorption, but infection is predominantly inconspicuous. It is unknown why a fraction of hosts reacts to infection with symptoms characterized as giardiasis, while the majority does not. However, positive results show a high variability, are often inconsistent or not reproducible and sometimes even contradictory. The evidence is rather against *G. duodenalis* infection alone as being a clear cause of acute symptoms such as diarrhea.

Table 2: Pathomechanisms

| Pathophysiology | Model system | Reference |
|---|---|---|
| **Epithelial barrier dysfunction** | Human biopsies (chronic infected) | Troeger et al., 2007 |
| | Mice | Zhou et al., 2007 |
| | Gerbils | Hardin et al., 1997 |
| Tight junction disruption (e.g. ZO-1) | Human biopsies (chronic infected) | Troeger et al., 2007 |
| | immortalized cells | Teoh et al., 2000; Chin et al., 2002; Scott et al., 2002; Humen et al., 2011; Maia-Brigagao et al., 2012 |
| Apoptosis | Human biopsies (chronic infected) | Troeger et al., 2007 |
| | immortalized cells | Chin et al., 2002; Panaro et al., 2007; Fisher et al., 2013 |
| | Mice | Bartelt et al., 2013 |
| **Malabsorption** | Human biopsies (chronic infected) | Troeger et al., 2007 |
| | Gerbils | Buret et al., 1990, 1991 |
| Villus shortening/ atrophy | Mice | Williamson et al., 2000; Bartelt et al., 2013; Li et al., 2017 |
| | Gerbils | Buret et al., 1992; Araújo et al., 2008; Ventura et al., 2013 |
| | Rats | Erlandsen & Chase, 1974; Halliez et al., 2016 |
| | Goats | Koudela & Vitovec, 1998 |
| | Human biopsies | Oberhuber et al., 1997; Koot et al., 2009 |
| Microvilli depletion | Rats | Erlandsen & Chase, 1974 |
| | Gerbils | Buret et al., 1991; 1992 |
| Crypt hyperplasia | Mice | Bartelt et al., 2013; Li et al., 2017 |
| | Rats | Halliez et al., 2016 |
| | Gerbils | Buret et al., 1992; Araújo et al., 2008 |
| | Goats | Koudela & Vitovec, 1998 |
| | Human biopsies | Koot et al., 2009 |
| Anion hyper-secretion | Human biopsies (chronic infected) | Troeger et al., 2007 |
| | immortalized cells | Resta-Lenert et al., 2000 |
| | Mice | Gorowara et al., 1992, 1994 |
| Reduction of host digestive enzyme activities (e.g. disaccharidases) | Mice | Buret et al., 1990; Solaymani-Mohammadi & Singer, 2011; Keselman et al., 2016 |
| | Gerbils | Buret et al., 1991; Bénéré et al., 2012 |
| | Human biopsies | Singh et al., 2000 |
| **Inflammation (e.g. adaptive/ innate response)** | Mice | Jiménez et al., 2004; Andersen et al., 2006; Li et al., 2006; Li et al., 2007 |
| | Human biopsies | Oberhuber et al., 1997; Koot et al., 2009; Dizdar et al., 2018 |
| **Post-infectious sequalae (e.g. IBD)** | Humans (epidemiological) | D'Anchino et al., 2002; Carlson & Finger, 2004; Robertson et al., 2010; Wensaas et al., 2012; Hanevik et al., 2014; Litleskare et al., 2015; Dormond et al., 2016; Halliez et al., 2016; Nakao et al., 2017 |

## 1.2 The small intestinal epithelium

The surface of the small intestinal epithelium is with an average of 30 $m^2$ the largest body surface separating the inner environment from external disturbances (Helander & Fändriks, 2014). The main function is to digest and absorb nutrients and to pass them to the blood stream, whilst preventing the entrance of harmful agents.

### 1.2.1 Epithelial architecture and composition

The small intestinal epithelium is a polarized, non-ciliated, columnar monolayer which is attached to the lamina propria, a cell rich connective tissue, at the basement membrane. Together with the underlying thin layer of small muscles (muscularis mucosae) they form the mucosa, the innermost layer of the intestine (Allaire et al., 2018). The architecture of this epithelium is not flat. Its finger-shaped protrusions, known as villi, reach into the lumen to increase the absorptive surface area (Figure 2A). At the base of each villus are up to 10 invaginations, termed 'crypts of Lieberkühn' (in short 'crypts'), which harbor stem cells at their bottom and a highly proliferative transient amplifying zone (TA zone) to support the villus with a constant flow of new cells (Allaire et al., 2018). Therefore, the small intestinal epithelium has one of the highest regenerative capacities of all tissues and completely renews itself every 3-5 days (Sato et al., 2009; van der Flier & Clevers, 2009; Park et al., 2016). When cells reach the tip of a villus, they are detached from the monolayer, undergo anoikis[2] and are transported away by flushing (with mucus and chloride/CFTR-induced liquid secretion) and the flow of luminal contents (Johansson et al., 2013). By travelling up the crypts, cells mature and differentiate into several highly specialized cell types.

[2] Anoikis is the process of apoptosis due to contact deprivation as a result of cell detachment (Frisch & Francis, 1994).

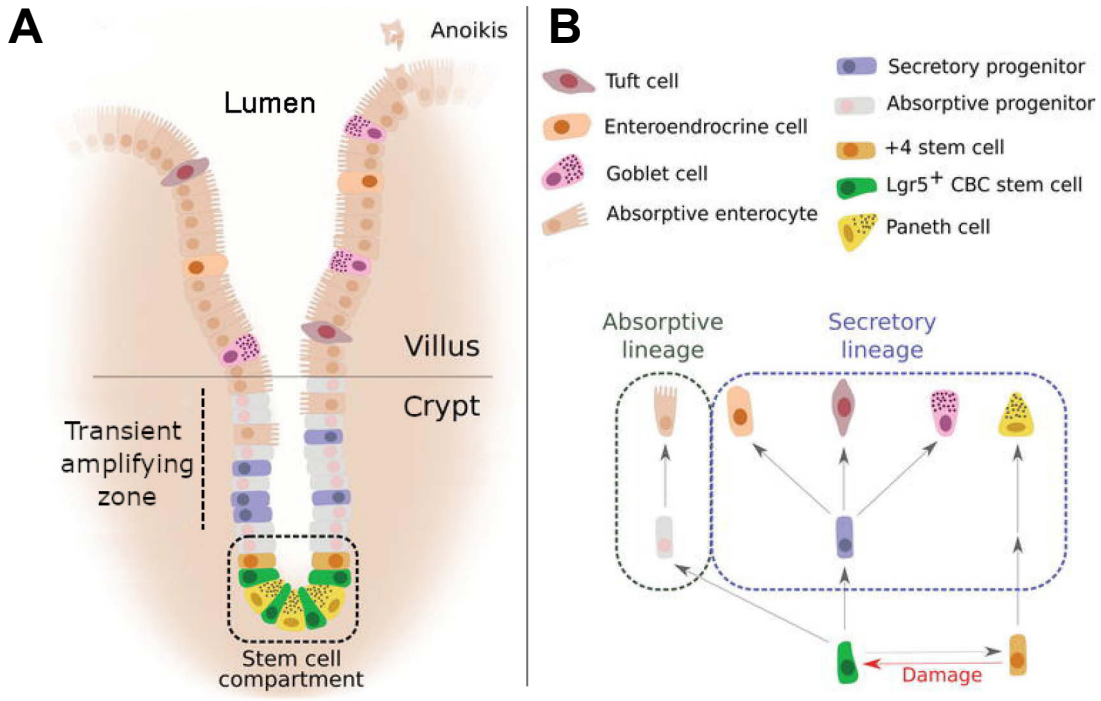


**Figure 2 Small intestinal epithelium and cell types.** Schematic representation of the small intestinal epithelium, showing crypt and villus region, including TA zone and stem cell containing crypt base (**A**), as well as cell types and their differentiation pathways (**B**). Image modified from (Gleizes et al., 2018 [CC BY 4.0]).

#### 1.2.1.1 Cell types and their function

Enterocytes (EC) represent the vast majority of epithelial cells. They are responsible for nutrient and water absorption but can also secrete antimicrobial peptides like β-defensins, cathelicidin, and Reg3-γ into the intestinal lumen, as well as immunoglobulins like IgA[3], which are prior absorbed from plasma cells at the basal side (Ogle et al., 2002; Hansen et al., 2006). Their apical membrane is densely filled with F-actin-supported membrane protrusions, known as microvilli, in a highly organized manner. This so-called brush border increases the absorptive surface area approximately nine-fold (Helander & Fändriks, 2014; Delacour et al., 2016). A network of acidic mucopolysaccharides and glycoproteins on the tips of the microvilli forms a glycocalyx which is not only full of digestive enzymes (Ugolev et al., 1977; Poley, 1988; Delacour et al., 2016), it also functions as a barrier by preventing the binding of microbes to membrane receptors (Frey et al., 1996; Pavlova et al., 2015), since enterocytes

[3] *Giardia* sp. secretes proteases to cleave IgA (Parenti, 1989), but antibodies do not seem to be required for parasite clearance anyway (Janoff et al., 1988; Singer & Nash, 2000; Zhou et al., 2007). The disruption of IgA, however, may have consequences for microbiota homeostasis, which could also be a cause for the disease.

are also the major target of numerous enteric pathogens (Gerbe et al., 2012; Lievin-Le Moal & Servin, 2013; Allaire et al., 2018).

Goblet cells (GCs) are scattered throughout the epithelium and produce and secrete large glycosylated proteins, Muc2, which is a gel-forming mucin and, besides water (>98%), main component of the mucus in the small intestine (Liévin-Le Moal & Servin, 2006; Gerbe et al., 2012; Johansson et al., 2013; Pelaseyed et al., 2014; Allaire et al., 2018). Mucin chains form polymers by cross-linking cysteine residues and together with the high level of glycosylation they are resistant to endogenous proteases. Muc2 is usually secreted at a baseline level but can also be rapidly released by pathogenic stimuli and cytokines (Il-22, IFNγ) via compound exocytosis[4] to protect the epithelium (Songhet et al., 2011; Johansson et al., 2013; Turner et al., 2013; Birchenough et al., 2015). In fact, GCs triggered by type 2 cytokines are very important in worm expulsion via RELMβ (Artis et al., 2004; Herbert et al., 2009). GCs also secrete other peptides like the tissue-protective trefoil factor 3 (Tff3), a mediator of epithelial maintenance and repair (Kindon et al., 1995; Mashimo et al., 1996; Taupin & Podolsky, 2003). Of note, it has been recently shown, that *Giardia* sp. can increase Tff3 expression which protects the epithelium in a co-infection setup (Manko et al., 2017). There is also evidence that goblet cells, like M cells, are involved in the antigen transfer from the lumen to basal dendritic cells (goblet cell associated antigen passages, GAP), which may promote oral tolerance[5] (McDole et al., 2012; Knoop et al., 2015).

Paneth cells (PCs) have with approximately two months the longest life span of all intestinal epithelial cells. Like stem cells, with which they are intercalated, PCs do not travel along the crypt-villus axis like the other cell types. Conversely, they translocate retrograde towards the crypt base (Gassler, 2017). There, PCs assume two tasks:

First, crypt and stem cell maintenance (Sato et al., 2011b). PCs regulate the 'stemness' of their adjacent stem cells by providing Wnt3a-, EGF-, R-spondin-1, notch-signaling, as well as lactate (Sato et al., 2011b; Gerbe et al., 2012, see also Figure 5).

Second, protection of the crypt base and microbiome-host homeostasis (Gassler, 2017). PCs are filled with granules containing several antimicrobial peptides, such as lysozyme, α-defensins, Reg3-β/γ, and PLA2, which are released by INF-γ-signaling or bacteria-sensitive TLR activation (Gassler, 2017; Allaire et al., 2018). Though they cannot directly react to protozoans (Ayabe et al., 2000), it has been shown that $CD4^+$ T cells, stimulated by *Toxoplasma gondii* to release

[4] Compound exocytosis is the plentiful fusion of vesicles with each other and with the plasma membrane (Pickett & Edwardson, 2006).

[5] Oral tolerance is the immunological non-responsiveness towards dietary antigens (Worbs et al., 2006; Tordesillas & Berin, 2018).

INF-γ, led to complete degranulation of PCs with their subsequent detachment and apoptosis (Raetz et al., 2013)[6]. Data from El-Shewy & Eid (2005) suggest another rather indirect mechanism by showing *Giardia muris* trophozoites, harboring peripheral bacterial endosymbionts, which were completely lysed in the crypts of mice, whereas trophozoites lacking those endosymbiotic bacteria had not activated PC degranulation.

Intestinal stem cells, positive for Lgr5 (Lgr5$^+$ ISCs), resides intimately connected to PCs at the crypt bottom (Barker et al., 2007), which has been termed the crypt base columnar (CBC) model (Cheng & Leblond, 1974). Usually 4-6 Lgr5$^+$ ISCs (or CBC cells) are in each crypt (Gassler, 2017). Those constantly cycling cells are responsible for the generation of all other cell types of the small intestine and their perpetual replenishment. However, the bulk of cells are produced in the crypt's TA zone, in which each cell undergoes 4-5 divisions within a very short period of 12 h (Marshman et al., 2002). Apart from the CBC model, lineage tracing indicated label-retaining cells at the +4 position relative to the crypt bottom (+4 LRCs), which are Lgr5$^-$ but may represent quiescent stem cells, hence termed the +4 LRC model (Potten et al., 1974; 1997; Li & Clevers, 2010). 2-4 of those +4 LRCs in a ring of 16 cells above the crypt base can be found on average and are suggested to translocate back to replace lost CBC stem cells in case of emergency (Li & Clevers, 2010; Muñoz et al., 2012).

Enteroendocrine cells (EECs) are chemosensory cells which can be found throughout the digestive tract with an abundance of roughly 1% of the epithelial cell population (Sternini et al., 2008; Gerbe et al., 2012). Stimuli from food or nutrients (monosaccharides, free amino/bile/fatty acids, peptides, etc.) trigger them to release hormones to regulate diverse mechanisms like food intake, gut peristalsis and insulin release (Gribble & Reimann, 2016). Moreover, they are also sensors of microbial metabolites and can activate mucosal immune responses (Worthington et al., 2018). EECs had been traditionally classified into numerous subpopulations according to their secreted peptide hormone, but recent insights from secretome studies indicated that EECs rather secrete an array of hormones in dependence of their location within the intestine, therefore challenging this dogma (Worthington et al., 2018).

Tuft cells (TCs), named because of their remarkable tuft of long microvilli, are a subset of enteroendocrine cells which gained a lot of attention recently (Grencis & Worthington, 2016). They can also be found in the epithelium of the lung and gall bladder, or in higher numbers in salivary/bile/pancreatic ducts (Sato, 2007; Gerbe et al., 2012) and therefore have been proposed to detect luminal pressure variations (Luciano & Reale, 1990). TCs are further characterized by a tubulovesicular system beneath the apical membrane (Sato et al., 2002), which

[6] Ironically, this was followed by bacterial dysbiosis due to the resulting lack of PCs.

could serve to rapidly change the apical surface area (Wattel & Geuze, 1978), glycocalyceal bodies of unknown function (Hoover et al., 2017), and lateral cytoplasmic projections (Sato et al., 2002). Furthermore, TCs show similarities with lingual bud cells, which are responsible for taste. It suggests that TCs could be involved in chemoreception as well (Gerbe et al., 2012). Two studies investigating helminth infections in mice had shown TC hyperplasia due to a feed-forward loop of Il-25 producing TCs, which stimulate innate lymphoid cells group 2 (ILC2s) to secrete Il-13, which in turn promotes further TC proliferation and GC hyperplasia in addition (McKenzie et al., 1998; Hasnain et al., 2013; Gerbe et al., 2016; Moltke et al., 2016). It has also been suggested by experiments with *Tritrichomonas muris* that TCs can detect protozoan parasites through the taste chemoreceptor TRPM5 as well (Howitt et al., 2016). Whether TCs can sense and react to *G. duodenalis* needs to be investigated.

Microfold cells (M cells) are located in Peyer's patches and are known to transcytose luminal antigens to the underlying gut-associated lymphoid tissue (GALT). This contributes to oral tolerance as well as mucosal immune surveillance (Neutra, 1998; Ohno, 2016; Lo, 2018). Their role in *G. duodenalis* infections is unknown.

#### 1.2.1.2 Cellular contacts and junctions

Cells establish contacts with their neighboring counterparts for multiple reasons, like barrier function, structural adherence and positioning within a tissue, and cellular communication. In order to serve those specific functions, several different contact sites and junctions can be found on cells.

The tight junction (TJ), also termed zonula occludens, forms a continuous lining along the apicolateral membrane of epithelial cells and is responsible for the barrier function by regulating the paracellular flux of ions and water (Suzuki, 2013). It consists, like all contact sites referenced in this section, of several multi-protein complexes (Figure 3).

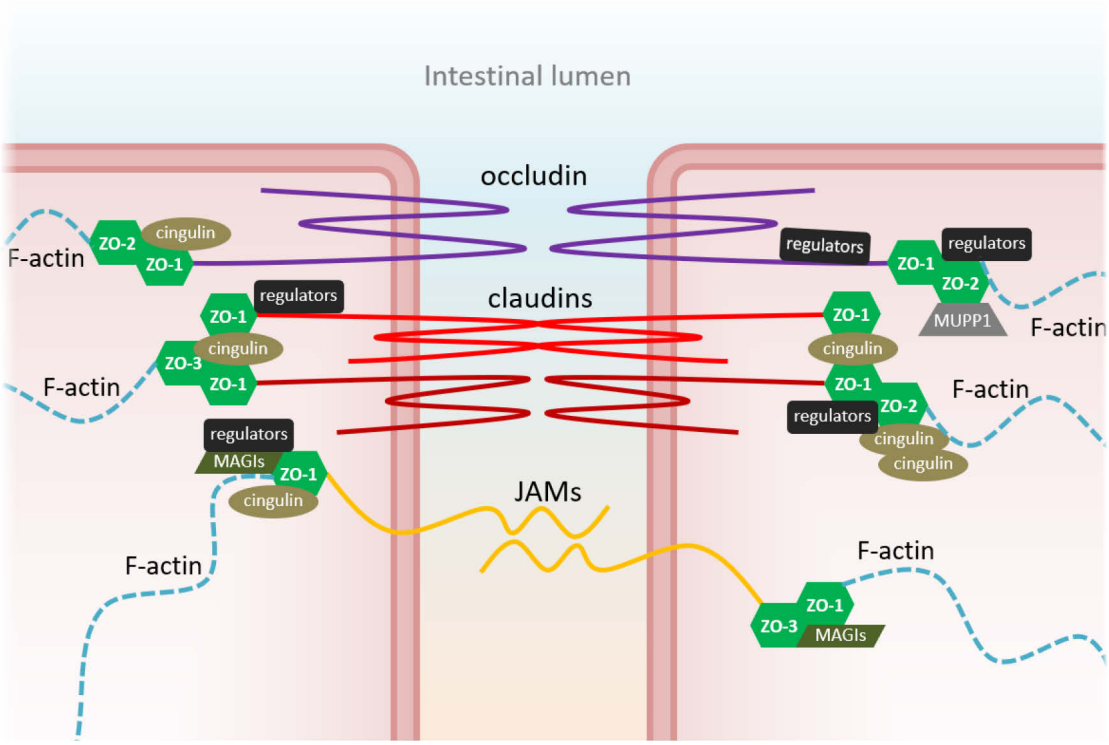


**Figure 3 The tight junction complex.** Schematic overview of the tight junction and a chosen fraction of its proteins. ZO-1 is the major adaptor protein, connecting the actual pore- or barrier-forming transmembrane proteins (like occludin, different claudins and JAMs) with the F-actin cytoskeleton and other scaffold proteins (like MUPP1, MAGIs, ZO-2/3) or regulatory proteins e.g. cingulin in multi-protein complexes.

On the extracellular side, the TJ is composed of transmembrane proteins like occludin, junctional adhesion molecules (JAMs), claudins, and tricellulin at tricellular TJ interfaces (Furuse et al., 1993; Furuse et al., 1998; Martìn-Padura et al., 1998; Ikenouchi et al., 2005; Krug et al., 2009; Mariano et al., 2011). Especially the tissue-specific claudin family, consisting of currently 24 known claudins in humans (Schneeberger & Lynch, 2004) is important for the regulation of permeability. For example, claudin-1 (cldn-1) has barrier-forming properties to prevent the passage of even smallest ions, whereas cldn-2 is a pore-forming protein, allowing the passage of certain small cations ($K^+$, $Na^+$) and water. The ionic selectivity is determined by the number and position of charged amino acids in the first extracellular loop (Krause et al., 2009). If required, claudins can be dynamically exchanged in response to an alternated luminal environment (Lu et al., 2013). For the intestine, relevant claudins are cldn-1, -3, -4, -5, -8, -9, -11, -14 (barrier forming) and cldn-2, -7, -12, -15 (pore-forming) (Suzuki, 2013).

On the intracellular side, the above-mentioned transmembrane proteins are anchored to zonula occludens proteins (ZO-1, -2, -3), which are scaffold proteins to perform the task of adapters by connecting to the F-actin cytoskeleton. They mediate TJ assembly as well (Suzuki, 2013).

The alteration of TJ permeability by modification of TJ proteins (TJPs) is closely

associated with intestinal health and disease. Several studies found TJ-degrading effects of *G. duodenalis* infections (Teoh et al., 2000; Chin et al., 2002; Scott et al., 2002; Troeger et al., 2007; Humen et al., 2011; Maia-Brigagao et al., 2012; Chen et al., 2013). However, others did not (Chavez et al., 1986; 1995; Hardin et al., 1997; Tysnes & Robertson, 2015; Kraft et al., 2017).

The adherens junction (AJ), also known as zonula adhaerens, is located below the TJ with the purpose of holding cells together and at place in the tissue but still offer possibilities of cellular rearrangements, thus serving a more structural function (Peglion et al., 2014; Takeichi, 2014; Yonemura, 2017).
On the extracellular side, proteins of the cadherin family, most prominently epithelial cadherin (E-cadherin), form strong $Ca^{+}$-dependent trans-dimers. Due to their chain-like segmentation (extracellular cadherin repeats) they can raster along their longitudinal axis, thus controlling the diameter of the paracellular space (Martinez-Rico et al., 2005; Halbleib & Nelson, 2006). Nectins are the second species of AJ transmembrane proteins. They function similar to cadherins but offer much weaker interaction and seem to be important for the establishment of apico-basolateral polarity (Campbell et al., 2017).
On the intracellular side, cytoplasmatic ends of cadherins and nectins bind to β-catenin and afadin, respectively, which in turn form a complex with α-catenin to establish association with the F-actin cytoskeleton. It could be recently shown that TJ and AJ also work together more closely than expected and α-catenin can even be connected to ZO-1 (Campbell et al., 2017; Yonemura, 2017). In regard to *G. duodenalis* infection, AJ did not show altered phenotypes (Humen et al., 2011) or only mild rearrangements at most (Maia-Brigagao et al., 2012).

Gap junctions (GJ), seldomly also macula communicans, directly connect the cytoplasm of adjacent cells via hemichannels, formed by connexins, to allow exchange of metabolites, nutrients, and second messengers, thus enabling cell-cell communication. They can be opened or closed using membrane potentials, calcium concentration, pH, phosphorylation, and protein interactions and can be selective for direction and molecule charge and size. GJs cluster as patches along the lateral side below the AJ (Nielsen et al., 2012).

Desmosomes, or macula adhaerens, combine the functions of AJs and GJs and are scattered as patches along the lateral side with higher numbers in the lower/basal half of the cell. They are using desmogleins and desmocollins, both members of the cadherin family, to establish strong $Ca^{+}$-dependent bonds to withstand mechanical stress, which is the reason desmosomes can predominantly be found in epithelial tissues. However, in contrast to AJs, they are anchored to intermediate filaments, instead of F-actin (Kowalczyk & Green, 2013; Stahley & Kowalczyk, 2015).
The role of desmosomes in cell signaling is complex and poorly understood.

They can bind and release transcription factors (TFs) and signal cascade proteins like β-catenin, PI3K/Akt, MAPK, STAT3, and NFκB, but also their structural proteins like plakoglobin, desmoplakin, and plakophilin can exert signal functions, important for proliferation, differentiation, development, and apoptosis (Thomason et al., 2010). The desmosomal proteins desmocollin-2/3 showed mild rearrangements in one study under *G. duodenalis* infection stress (Maia-Brigagao et al., 2012).

Focal adhesions (FAs) mediate cell-matrix contacts, therefore only present on the basal membrane. They anchor the cell via F-actin-associated integrins to collagen IV, fibronectin, laminin and other extracellular matrix (ECM) proteins of the basal lamina (Burridge, 2017). FAs resemble the basal equivalent of desmosomes and, like them, are important for signal transduction (Kim et al., 2011).

### 1.2.2 Epithelial barrier dysfunction and diarrhea

The disruption of the TJ complex or ablation of the epithelial layer, and therefore loss of barrier function, can lead to activation of mucosal immune responses by luminal antigens or bacterial infiltration as well as malabsorption and diarrhea due to the inability to create and maintain ionic gradients driving nutrient uptake (Nusrat et al., 2000; Farhadi et al., 2003; Clayburgh et al., 2004; Turner, 2009). The acute symptomatology of *G. duodenalis* infections, foremost diarrhea, has been linked to such mechanisms (Buret, 2007; Ankarklev et al., 2010). However, barrier dysfunction alone is most likely not sufficient to cause significant diarrhea (Teshima & Meddings, 2008; Camilleri et al., 2017) because of the massive reabsorption potential of the colon (Harris & Shields, 1970). Therefore, other mechanisms may contribute to the observed diarrhea in acute giardiasis. Impaired disaccharidase activity[7] (Buret et al., 1990; Singh et al., 2000; Solaymani-Mohammadi & Singer, 2011; Bénéré et al., 2012; Keselman et al., 2016), increased anion secretion[8] (Gorowara et al., 1992, 1994; Resta-Lenert et al., 2000; Troeger et al., 2007), and mucosal inflammation[9] (Oberhuber et al., 1997; Jiménez et al., 2004; Andersen et al., 2006; Li et al., 2006; Koot et al., 2009; Dizdar et al., 2018) have also been linked to diarrheic giardiasis. And much is unknown about other, more neglected causes of diarrhea like increased

[7] Sugars are not taken up and stay in the digestive system. They are subsequently fermented by bacteria causing abdominal discomfort, most prominently known is lactose intolerance (Fassio et al., 2018). High sugar concentrations can also lead to osmotic diarrhea (Gericke et al., 2016).
[8] High luminal anion amounts draw cations and therewith water from the epithelium into the lumen, leading to watery diarrhea (Thiagarajah et al., 2015).
[9] Barrier-disturbing immune responses like MLCK-activation (W. V. Graham et al., 2019) or epithelial collateral damage from e.g. mast cell activation (Albert-Bayo et al., 2019).

intestinal motility, malign hormone signaling or an altered microbiome (Allain et al., 2017; Camilleri et al., 2017). It must be considered that the etiology of diarrhea is manifold and complex and barrier dysfunction alone may not be a robust functional correlate for diarrhea, despite being used as proxy in many studies as well as this work.

## 1.3 Epithelial *in vitro* model systems

Epidemiological approaches are, as mentioned earlier (1.1.2.1), prone to confounders and concomitant diseases and can only be investigated by proxy and mostly non-invasive techniques. Some of those limitations are true for animal trials as well and, on top of it, mice infected with *G. duodenalis* cannot reproduce the characteristics of human giardiasis[10], rendering also animals a suboptimal model. Biopsies or other *ex vivo* explants are decaying material thus hard to maintain over the course of several days. A primary culture, which preserves epithelial *in vivo* characteristics is not possible. Standardization is also problematic due to individual patient variables, exact probing location and sample quality, and other circumstances (duration of the procedure, interferences of remaining microbiota, composition and activation status of immune cells, etc.).
To overcome the difficulties of such high-variable models, much simpler *in vitro* approaches exist. Although limited to carcinoma-derived cell lines with their degenerated characteristics compared to *in vivo* counterparts, these systems can offer less confounders, better comparability, standardization and reproducibility, leading ultimately to more robust results (Liévin-Le Moal, 2013). Indeed, great achievements have been made with such *in vitro* systems and several gastrointestinal pathogens like certain bacteria and their products/toxins/proteases (Malago et al., 2003; Fajdiga et al., 2006; Rees et al., 2008; Liu et al., 2012; Anderson et al., 2013; Fiorentino et al., 2013) as well as parasitic protozoans like *Entamoeba histolytica*, *Cryptosporidium parvum*, or *Blastocystis* sp. (Li et al., 1994; Leroy et al., 2000; Buret et al., 2003; Betanzos et al., 2014; Wu et al., 2014). Consequently, those systems were also adapted for *Giardia* sp. research and most investigations concerning the parasite-induced barrier dysfunction have been made *in vitro* (Buret, 2007; Ankarklev et al., 2010). One of the most commonly used *in vitro* models is the Caco-2 cell line in the transwell-filter system.

[10] *G. muris* on the other side can infect mice in a way which results in diarrhea. However, *G. muris* - which cannot infect humans - differs much from *G. duodenalis*, hence questioning comparability (Chavez et al., 1986; 1995; Troeger et al., 2007; Zhou et al., 2007; Fisher et al., 2013; Klotz & Aebischer, 2015).

### 1.3.1 The Caco-2 cell line

To this day, no human small intestinal cell line is available. However, studies on human colorectal adenocarcinoma derived cell lines, established in the 1970s for cancer research and treatment (Fogh et al., 1977), showed that one of those cell lines, Caco-2, possess the ability to spontaneously differentiate under long-term culture conditions, featuring several morphological and biochemical characteristics[11] of small intestinal ECs (Pinto et al., 1983), though developing some colonic properties as well (Engle et al., 1998). Therefore, numerous studies took advantage of Caco-2 as small intestinal-like model system since the 1990s to investigate nutrient/toxin/drug absorption (Artursson, 1990; Caloni et al., 2002; Jochems et al., 2018), barrier function (Hidalgo et al., 1989), pathogen infection (Lievin-Le Moal & Servin, 2013), and lipid transport (Nauli & Whittimore, 2015), to name only a few[12]. Due to its popularity and also its heterogenous character - individual Caco-2 cells vary in size, microvilli formation and also biochemical properties (Katelaris et al., 1995; Sambuy et al., 2005) - several clonal populations were created to serve specific needs. Most commonly used is Caco-2/TC7, simply a clone of the parental line of the 198$^{th}$ passage (Chantret et al., 1994). This work, however, uses mainly the Caco-2 bbe population, which is more homogenous than its parental line and features increased brush border enzyme activity (Peterson & Mooseker, 1992), resembling the small intestinal epithelium closer and is therefore even considered to represent the small intestinal epithelium best (Fisher et al., 2013; Lievin-Le Moal & Servin, 2013).

Caco-2 should not be grown (apart from regular culture) on plain culture surfaces (Sambuy et al., 2005; Srinivasan et al., 2015). Instead, the use of a transwell-filter system to grow Caco-2 monolayers on porous membranes is recommended, since it facilitates differentiation and polarization, avoids blister or dome formation or other peculiarities (Appx. 26) and allows (together with a simple electrode and Volt-Ohm meter) the measurement of trans-epithelial electric resistance (TEER) values (Figure 4), which are an indicator for paracellular permeability or monolayer injury thus barrier dysfunction (Sambuy et al., 2005; Srinivasan et al., 2015).

[11] Cylindrical, polarized monolayers with microvilli; TJs, hydrolase activity similar to fetal ileum (Pinto et al., 1983; Sambuy et al., 2005).

[12] Pubmed database lists under the search term “Caco-2” to date 13785 entries.

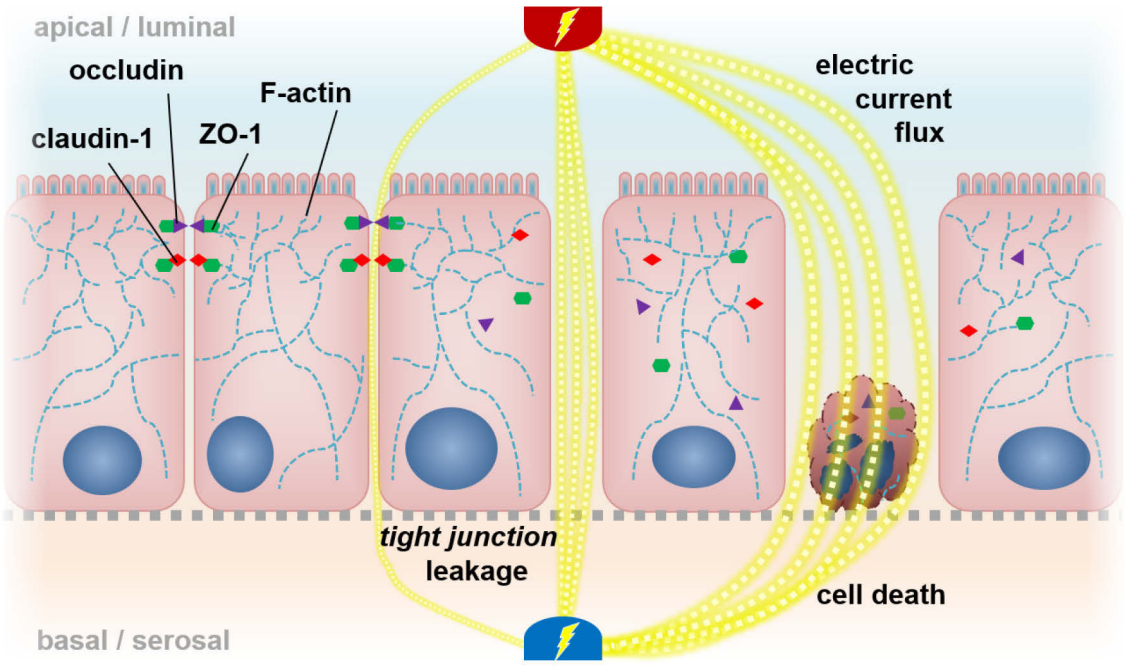


**Figure 4 Transwell-filter system and TEER measurement.** Schematic representation of the transwell-filter system. Cells grow on a permeable filter membrane, forming a basal and luminal compartment. Using a (chop stick) electrode, electric current can be conducted through this cell monolayer. A decrease in electric resistance indicates barrier dysfunction.

### 1.3.2 Organoid technology

The seminal work of Sato et al. (2009) from the Clevers group showed that murine Lgr5⁺ ISCs, if cultured under the right conditions, can undergo replication and differentiation to establish 3-dimensional self-organizing tissue structures with villus- and crypt-like domains as well as different cell types, resembling morphological and functional miniature “organs” (so-called organoids) of the small intestine (Sato et al., 2009). For the first time, a stable primary culture (of biopsy-derived ISCs), but which redevelops its small intestinal epithelial characteristics upon differentiation instead of maintaining its original conformation, has been achieved for the murine small intestine. A bit later, this system was adapted to model the human small intestine and colon (Sato et al., 2011a; Spence et al., 2011), as well as other tissues to mimic stomach (McCracken et al., 2014), pancreas (Boj et al., 2015), prostate (Gao et al., 2014; Karthaus et al., 2014), kidney (Takasato et al., 2014) the complex architecture of the liver (Huch et al., 2013; Takebe et al., 2013) and even the brain (Lancaster et al., 2013).

The benefits of organoid cultures are manifold (Huch et al., 2017). Unlike biopsy explants, they can undergo considerable - theoretically unlimited - expansion

since the Hayflick limit[13] can be bypassed because active ISCs are still present (Sato et al., 2011a). In contrast to carcinoma cells is their genome intact (or rather not altered by procedure) and they retain their genomic stability over time, since DNA repair processes are still functional (Sato et al., 2011a; Huch et al., 2015). And where animal models can only offer end-point results or secondary (proxy) data, organoids are not a black box and are amenable to real-time imaging and other approaches for direct manipulation and observation. With those features, organoids are poised to fill the gap between traditional cell culture and animal models.

For *Giardia* research specifically, organoids offer an environment closer to the *in vivo* condition, the ability to investigate the parasite's impact on material derived from patients with different disease manifestations or certain phenotypes to study host factors, the ease of genetic manipulation since theoretically a single ISC can be a bottleneck to start a new organoid culture, or may even enable the culturing of *Giardia* sp. isolates[14], which are currently not manageable to cultivate *in vitro*, in an organoid co-culture system (Klotz et al., 2012). However, problematic may be the 3D configuration, since the intestinal lumen - the site of *G. duodenalis* infection - is a compartment within the organoid structure and therefore hard to reach. A 2D organoid system would be more preferable.

[13] The theory that somatic cells can only undergo a certain amount of divisions until they reach a state of senescence, e.g. by shortening of telomers. Stem cells, however, are not affected by this aging process (Hayflick, 1979).

[14] Current research is biased towards easy to culture isolates with unknown significance to reflect the real-world situation (Smith et al., 1982b; Klotz et al., 2012).

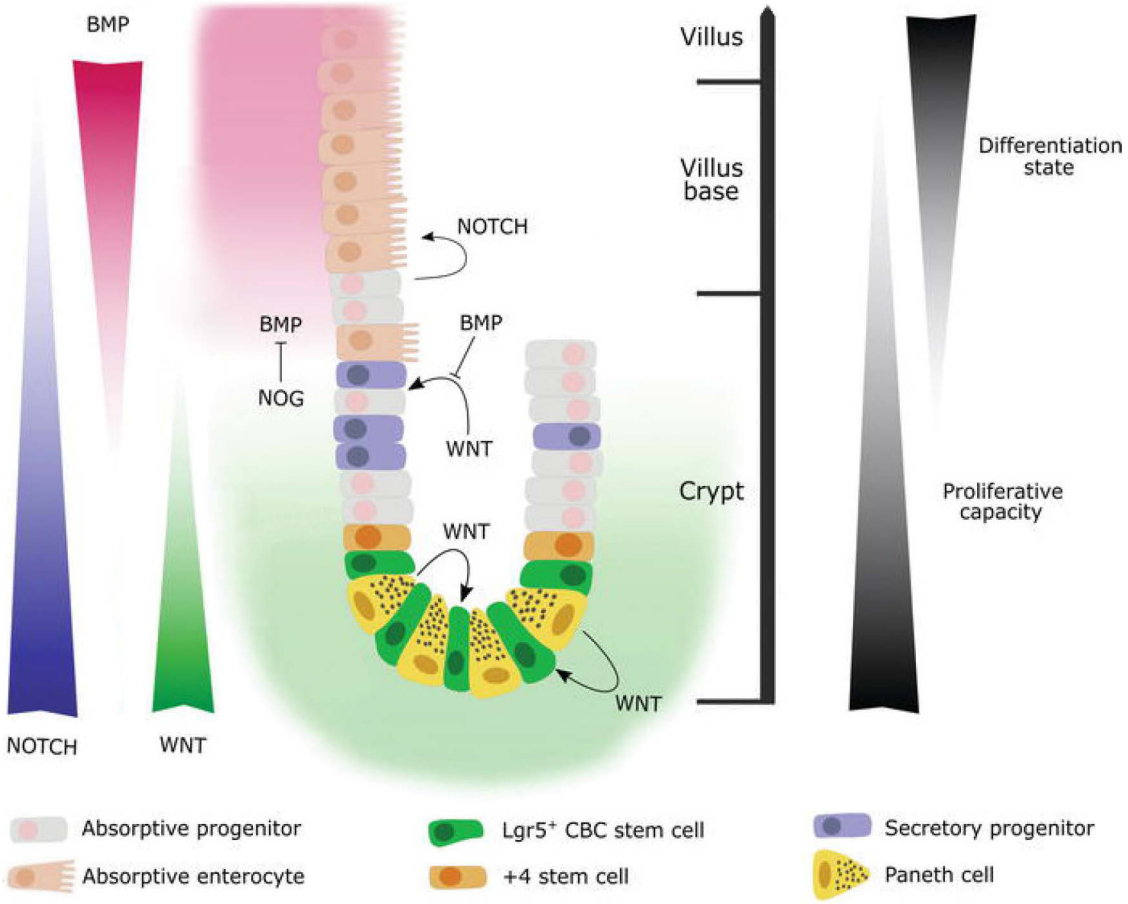


**Figure 5 Signaling along the crypt-villus axis.** Schematic signal environment and gradients from the crypt base to the villus. PCs regulate ISCs by Wnt secretion and lateral inhibition of notch. BMP signaling increases and blocks Wnt-signals towards the villus because of decreased concentration of BMP-inhibitor noggin, leading to differentiation. Image modified from (Gleizes et al., 2018 [CC BY 4.0]).

Small intestinal organoid cultures mimic the signaling along the crypt-villus axis (Figure 5), by artificially providing a (structural- but more importantly basal signaling-supporting) extracellular matrix mixture (Matrigel®), and a strong Wnt3A-signal to support and maintain ISC growth (Sato et al., 2009). Additionally, supplemented R-spondin-1 augments Wnt3A-signaling by binding to the Wnt-receptor complex (Lrp5/6/frizzled) and supplemented noggin inhibits BMP-signals by snatching away BMP which would otherwise prevent crypt formation (Sato & Clevers, 2013). Although PCs regulate ISCs (as mentioned under 1.2.1.1), such supplementation is required since underlying mesenchymal cells are absent is those purely epithelial cultures (Sato et al., 2009). The gradients are non-existent in the beginning of the culture but seem to establish themselves, as evidently shown by organoid morphology (Sato et al., 2009).

## 1.4 Aim of this work

The literature on the pathology of *G. duodenalis* infections is often inconsistent or contradictory. In order to gain more insight and reliable results, a robust *in vitro* infection model may offer advantages over the weaknesses of epidemiological approaches with this specific pathogen, as mentioned before. Therefore, the two most promising *in vitro* model systems to simulate the human small intestinal epithelium should be assessed in regard to their response to *G. duodenalis* infections:
The Caco-2 system, which has been used by studies before to indicate *G. duodenalis*-induced malign epithelial alterations, although with mixed results. And a human small intestinal organoid-based model, which, as a genetically unaltered primary culture, may allow more solid findings than traditional cell lines or *ex vivo* approaches. However, a suitable organoid-based model system needs to be established first by this work.
TEER and therefore barrier (dys)function, as proposed surrogate parameter for the acute diarrheic manifestation of giardiasis, should be used similarly to published studies. Since epithelial barrier properties are determined by tight junction, as well as cellular integrity, more detailed investigations of such junctional complexes and cell death could help to generate more hypotheses about the parasite's still unclear pathomechanisms.

Summarizing, the aims of this work are (1) replicating or refuting published contradictory findings regarding *G. duodenalis*-induced barrier dysfunction on Caco-2, (2) the establishment of a human organoid-based *in vitro* model system to study *G. duodenalis* infections, (3) its comparison to the Caco-2 model.

# 2. Results

## 2.1 Caco-2 model system

The Caco-2 transwell system is well established in the literature and was used in many studies to investigate *G. duodenalis* infections (Kraft et al., 2017). Therefore, this model was adapted in this work as well. Experiments were predominantly conducted on the Caco-2 bbe subpopulation, which is more homogenous than other subpopulations or the parental cell line (Sambuy et al., 2005; Lievin-Le Moal & Servin, 2013; Srinivasan et al., 2015).

### 2.1.1 Characterization of the Caco-2 model system

As mentioned before (1.3.1), Caco-2 cells artificially differentiate into enterocyte-like cells after 14-21 days of confluent incubation. By seeding high numbers (100.000 cells) per 0.6 $cm^2$ transwell-filter, it is assumed that each cell statistically divides only once to achieve a confluent monolayer, hence accelerating this process. TEER measurements were conducted to surveil the monolayer formation and its differentiation (Figure 6).

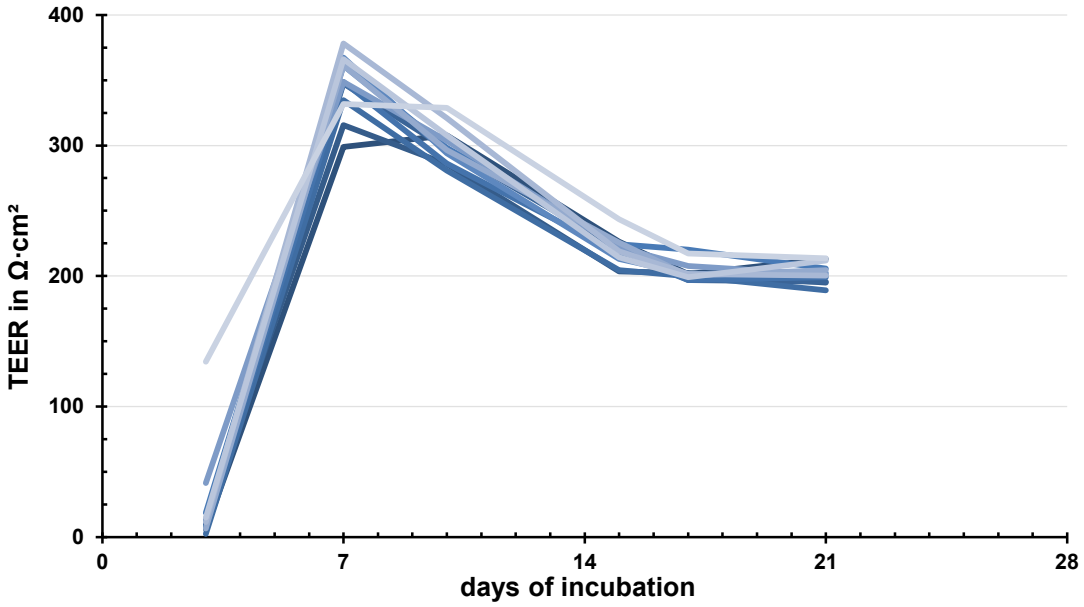


**Figure 6 Monolayer formation and differentiation of Caco-2.** Development of absolute TEER changes of 12 individual Caco-2 bbe monolayers, are shown with measurements, taken right before medium exchanges as a matter of routine at day 3, 7, 10, 15, 17 and 21 after seeding of 100.000 cells into transwell filters. After a steep increase in TEER when reaching confluence, which is referred in the literature as "peak resistance", TEER of monolayers normalized in the subsequent days until reaching a plateau phase. To that time point, Caco-2 cells are regarded in the literature as fully differentiated. Conducted experiments started at day 22 after seeding.

It is described in the literature (Sambuy et al., 2005; Srinivasan et al., 2015) that Caco-2 monolayers reach highest electric resistance values after 7-10 days and show stable resistance after 2 weeks, which indeed was the case.

Throughout this work, the monolayer development was routinely monitored at the single filter level by using TEER measurements. Of note, with Caco-2's increasing passage numbers, the basic TEER increases in a linear manner after approximately 36 passages (Figure 7), which has been also observed with a highly similar course in other studies (Lu et al., 1996; Briske-Anderson et al., 1997; Yu et al., 1997).

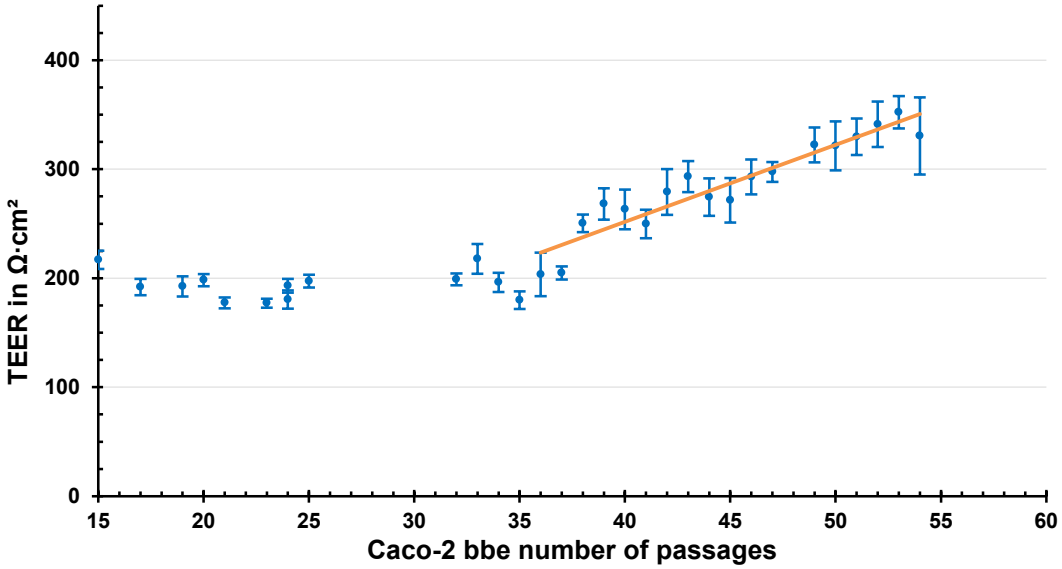


**Figure 7 Basic TEER rise with passages.** TEER values of Caco-2 bbe monolayers after 21-days of differentiation before experimental start are shown. After 37 (weekly) passages, monolayers tend to increase their basic TEER with every further passage in an apparent linear manner ($R^2$=0.89). Each data point indicates mean and SD of 12 monolayers. Linear regression is shown in orange.

To verify the differentiation further, an assay to investigate the activity of intestinal alkaline phosphatase (ALPi), which is assumed to be more expressed in differentiated enterocytes, was tested with an pNPP/pNP assay. ALPi hydrolyses the phosphate-residue of *para*-nitrophenylphosphate (pNPP). The converted *para*-nitrophenol (pNP) can be used as a measurement to quantify pNP and therefore ALPi activity, which corresponds to the ALPi amount, bound to the apical membrane. As presented below (Figure 8), weekly measurements of Caco-2 monolayers indicated a peak in ALPi activity/amount after 21 days. Those findings are in line with other studies (Zeller et al., 2015).

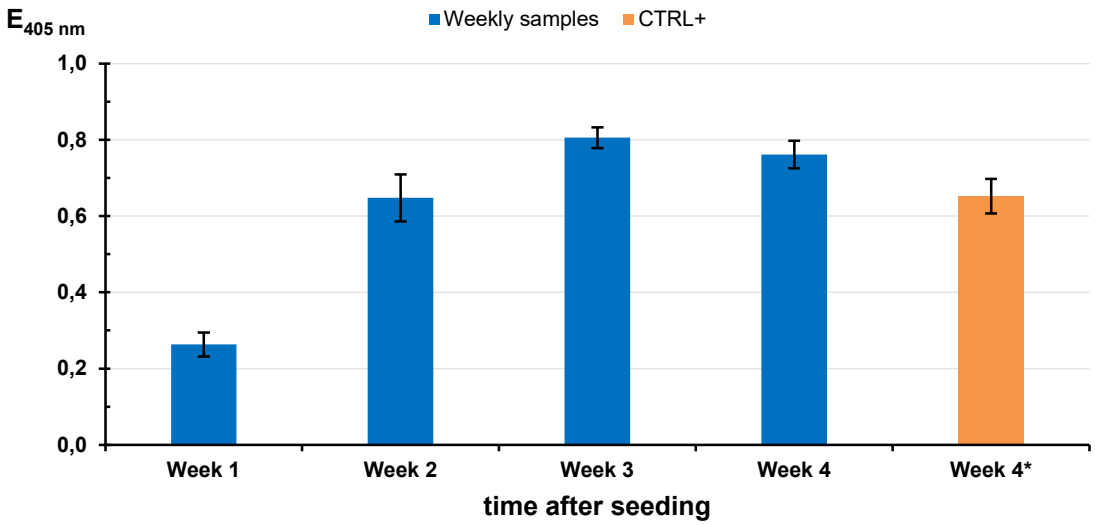


**Figure 8 Intestinal alkaline phosphatase activity assay.** The substrate pNPP was dephosphorylated by ALPi to pNP, whose absorption can be measured at 405 nm. Increased signals suggest higher ALPi activity, which is a differentiation marker for Caco-2 cells. Monolayers were tested weekly under 10 min incubation with pNPP. CTRL+ shows samples from monolayers by the end of week 4 from prior experiments. ALPi activities constantly increased with time until 3 weeks, which is considered the usual time span Caco-2 cells need to differentiate. Afterwards, a plateau phase is reached. Error bars represent SD, n=3.

Concluding, the Caco-2 model in this work offered a behavior like suggested by literature. As generally proposed in the scientific community, Caco-2 (infection) experiments were conducted at day 22 after seeding.

### 2.1.2 Epithelial barrier function experiments of *G. duodenalis* infected Caco-2 monolayers

TEER-measurements (Figure 4), as a reliable method to asses barrier integrity, were used as the primary readout for *G. duodenalis* infection experiments of 22-day Caco-2 monolayers.

#### 2.1.2.1 No TEER decreases with different parasite loads observable

The effect of *G. duodenalis* isolate WB6, which has been used widely in the literature in similar studies, on Caco-2 bbe as well as its parental cell line were investigated using the different infection loads of MOI 1, 10 and 100 (Figure 9). A MOI of 1 represents 200.000 trophozoites in this system and complete coverage of the epithelial cell layer by the parasites can theoretically[15] be assumed by MOIs past 3. Monolayers of both Caco-2 lines did not led to a decrease in TEER, and therewith barrier dysfunction, rather a dose-dependent increase in electric resistance values was observed (see also Appx. 23). For subsequent experiments, high parasite loads of MOI 20 were used as standard to prevent false negative evaluations due to low pathological impact.

[15] Trophozoite surface area (2D, ventral) approximated $1 \cdot 10^{-8}$ nm$^2$ using microscopic image analysis with Zen blue software. According to a transwell-filter area of 0.6 cm$^2$, $6 \cdot 10^5$ attached trophozoites are required to cover the surface area, resembling MOI 3. Of note, trophozoites attach rapidly to surface areas like culture dish plastic or cell layers (e.g. reaching complete surface coverage within one minute using MOI 10 loads).

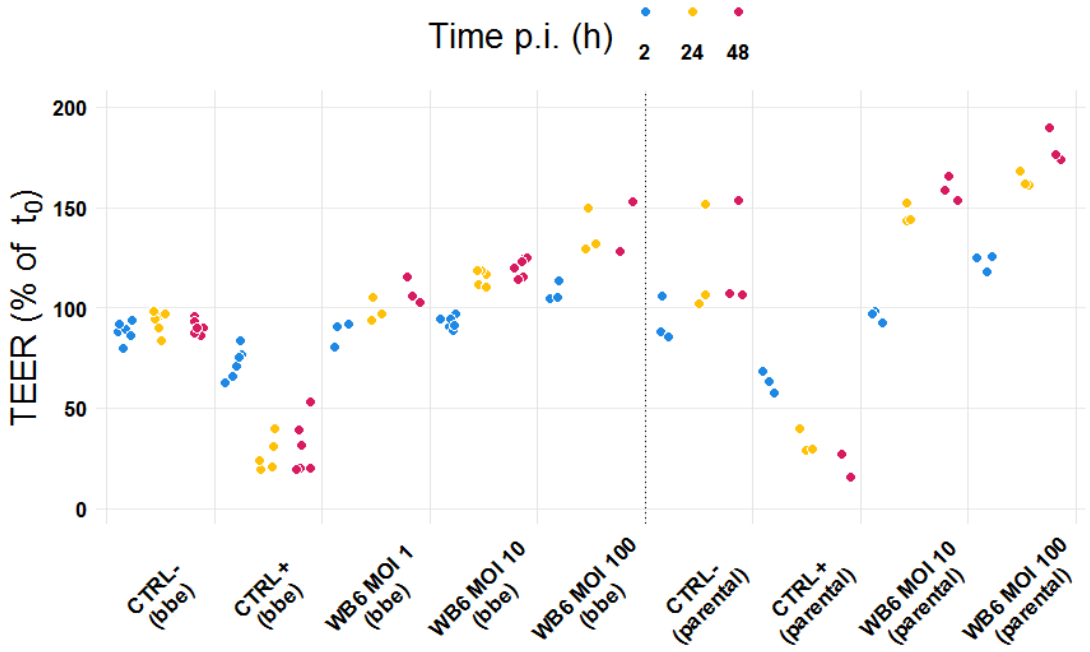


**Figure 9 Infection load dependency of TEER.** TEER changes of Caco-2 bbe and Caco-2 parental line monolayers, normalized to measurements before infection, are shown when infected with MOIs ranging from 1-100, as well as uninfected (CTRL-) and treated with apoptosis-inducing agent staurosporine at 0.5 (bbe) and 1 (parental) µM (CTRL+) for up to 48 h. No *Giardia*-linked TEER decreases were detectable. Data points represent individual monolayers, n=3-6. Time after infection is color coded. Absolute TEER was 204.3 Ω·cm$^2$ (SD 15.1 Ω·cm$^2$) for bbe, and 282.6 Ω·cm$^2$ (SD 31.1 Ω·cm$^2$) for parental Caco-2 at $t_0$. Appx. 1 contains relevant probability values (Tukey post-hoc test).

2.1.2.2 Caco-2 tight junctions did not show altered phenotype upon infection

In order to study proposed pathological effects like disruption or delocalization of the tight junctions (Table 2), immunofluorescence assays (IFAs) of several TJPs were conducted (Figure 10). None of the infection conditions suggested, like the TEER experiments indicated, any degrading or delocalizing effects of the investigated TJPs.

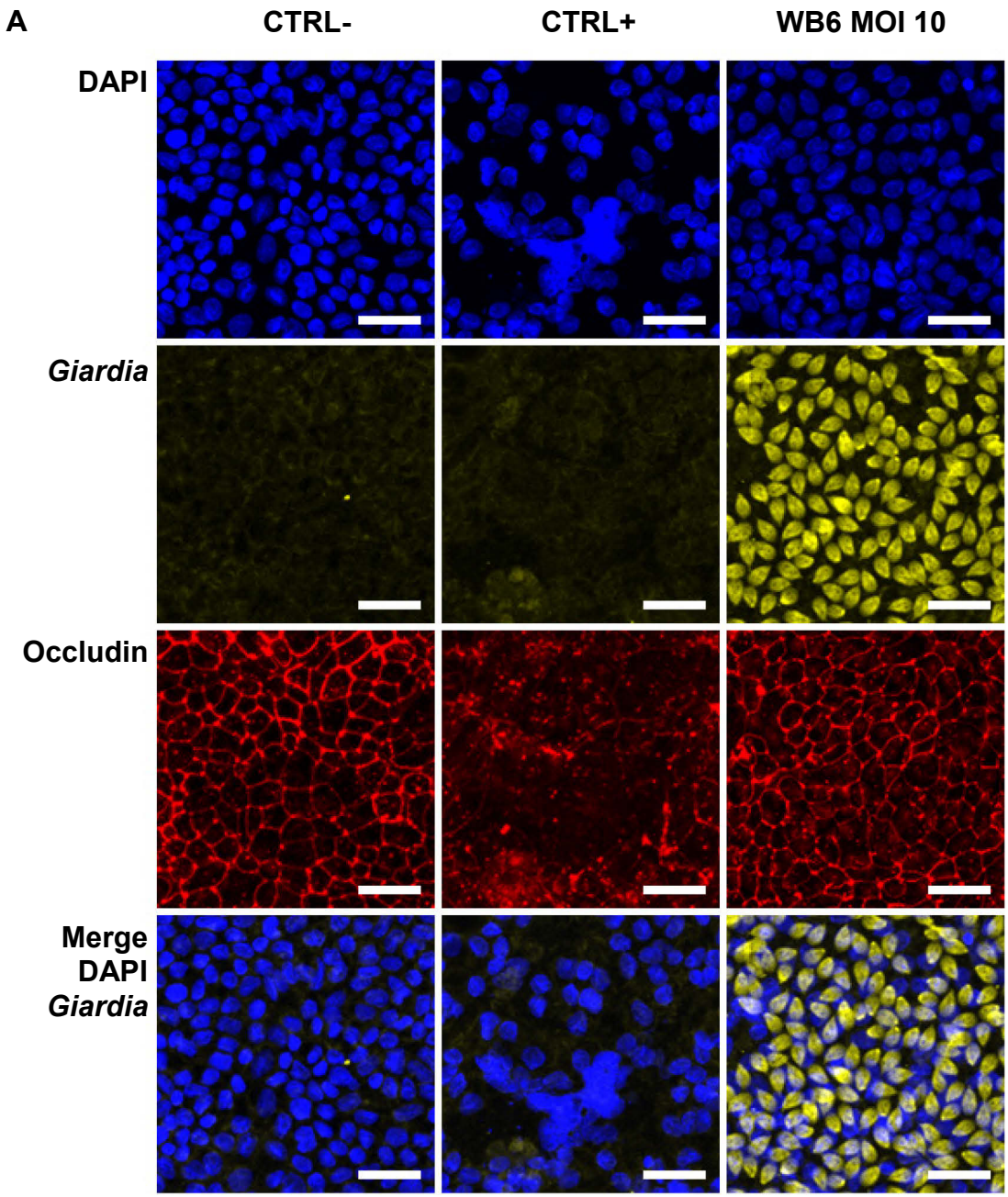

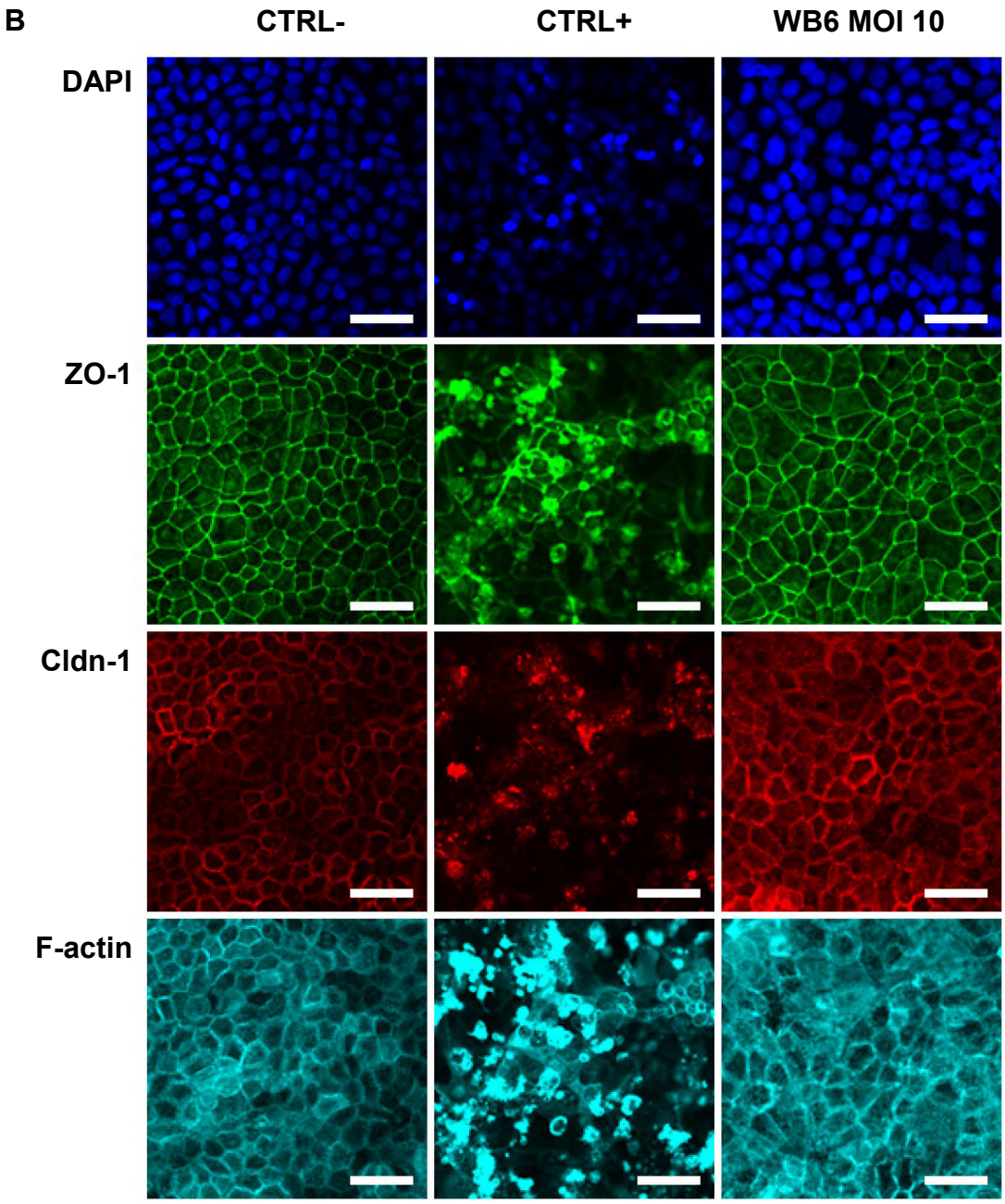


**Figure 10 Tight junctions remained inconspicuous during *G. duodenalis* infection.** (**A**) Micrographs depict tight junction protein occludin (red) and trophozoites (yellow) in Caco-2 bbe monolayer after 24 h. (**B**) Micrographs depict tight junction proteins ZO-1 (green), claudin-1 (red), and F-actin cytoskeleton (cyan) after 72 h. Nuclear staining with DAPI is shown in blue. MOI 10 infections of *G. duodenalis* isolate WB6 were compared to uninfected controls (CTRL−) and 1 µM staurosporine controls (CTRL+), inducing apoptosis.
Tight junction-associated proteins showed typical reticule structures, whereas F-actin cytoskeleton was more diffuse. No observable changes in any of the examined proteins as a result of *Giardia*-infection were detectable, also with higher MOIs (not shown). Methanol precipitation was used to preserve trophozoites *in situ*. Scale bars indicate 40 µm. Representative micrographs, n=3.

#### 2.1.2.3 Influence of parasite attachment on TEER

Attached trophozoites might increase TEER by physically inhibiting the electric current flow through the monolayer. To exclude this, trophozoites were removed from (or inhibited to attach to) the Caco-2 monolayers by using the potent *Giardia* sp. detachment reagent formononetin, which paralyzes trophozoites immediately without affecting their viability (Fisher et al., 2013). Two different *G. duodenalis* isolates (NF and S2, both assemblage A; see also 2.1.2.6) were used additionally to WB6.

Figure 11A shows difference between infected or sham-treated uninfected monolayers on TEER after formononetin addition, although >95% of trophozoites were removed (not shown). Rather the measurement itself, the pipetting and mixing step and temperature influenced electric resistance more than the chemical compound or the subsequent *Giardia*-detachment. Also, the trophozoite-driven increase in TEER seemed independent of trophozoite attachment. However, if attachment was prevented directly from start, TEER increase was slightly diminished (Figure 11B) and reached only mild statistical significance ($p < 0.05$) after 24 h. Though, this can be a side effect of formononetin, since it is speculated that it inhibits the parasite's microtubule function or associated motor-proteins, which may lead to complications in its metabolism, influencing TEER indirectly by altered trophozoite activity.

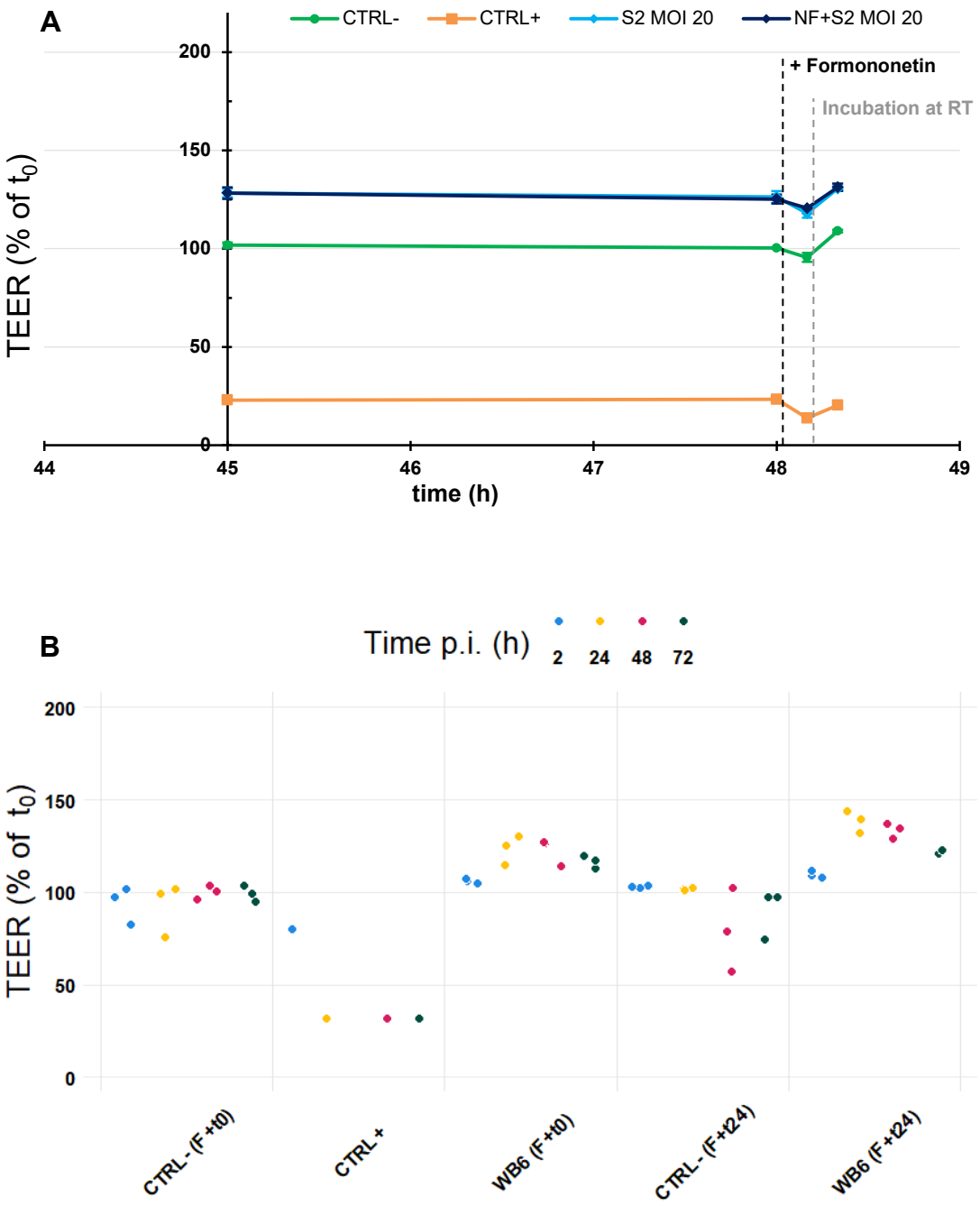


**Figure 11 No attachment-dependent influence on TEER.** TEER changes of Caco-2 bbe monolayers, normalized to measurements before infection, are shown when infected with assemblage A trophozoites (MOI 20) and treated with 20 µM *Giardia* sp. detachment reagent formononetin (F+). (**A**) NF+S2 is a mixture of NF and S2 assemblage A isolates (used to exclude potential synergistic effects) and was sham treated after 48 h for 10 min at 37°C and additional 10 min at RT. Data lines indicate means of 3 individual monolayers per condition, error bars represent SD. (**B**) Formononetin treatment right after beginning (F+t0) or after 24 h (F+t24) is shown. CTRL+ was 1 µM staurosporine. Data points represent individual monolayers, n=1-3. Time after infection is color coded. Absolute TEER was 330.4 Ω·cm² (SD 35.5 Ω·cm²) at $t_0$. Appx. 2 contains relevant probability values (Tukey post-hoc test).
Formononetin treatment had no significant influence on TEER (**A**, **B**), trophozoites were still able to increase TEER despite attachment-inhibition (**B**) and monolayers with increased TEER indicated no regression to levels before infection after trophozoite detachment (**A**, **B**).

### 2.1.2.4 TEER increase is dependent on vital trophozoites

In an additional attempt to investigate the unexpected TEER increase of infected Caco-2 monolayers, trophozoite lysates (produced via French press or sonication), trophozoite debris (produced by heat-inactivation) and secreted trophozoite products (previously collected apical medium supernatants of infected Caco-2 monolayers) were compared (Figure 12). None of those conditions led to an increased TEER comparable to vital trophozoites.

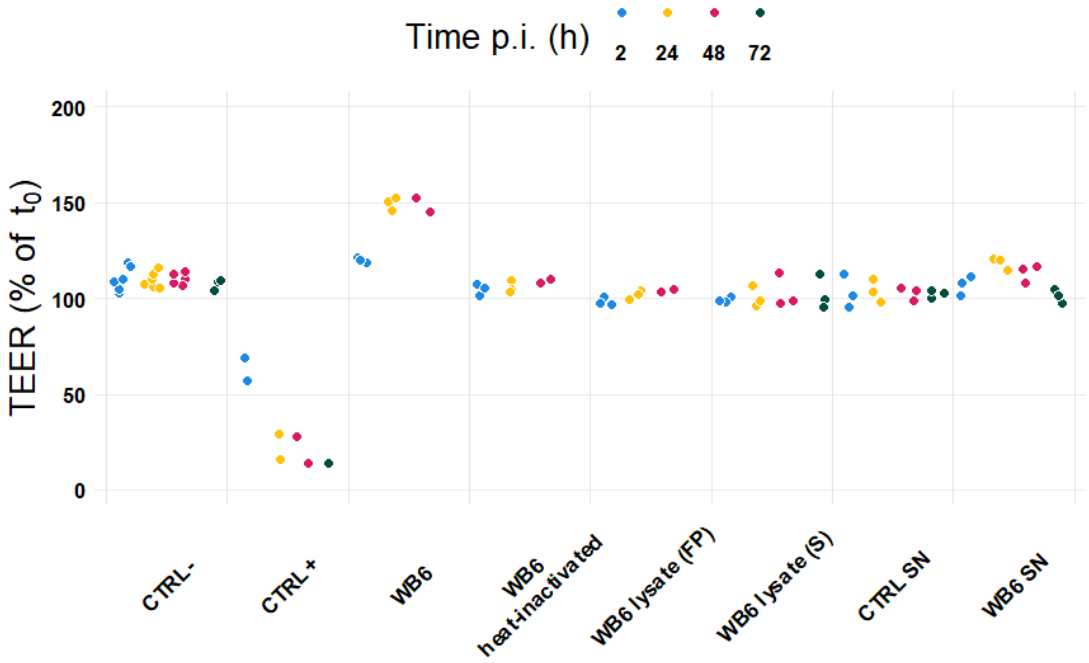


**Figure 12 Only vital trophozoites led to TEER increases.** TEER changes of Caco-2 bbe monolayers, normalized to measurements before infection, are shown when infected with vital WB6, or dead but intact (heat-inactivated) trophozoites, and trophozoite lysates made by French Press (FP) or sonication (S) all corresponding to MOI 20, as well as spent medium (filtered supernatants, SN) from the apical compartments from uninfected or WB6 MOI 100 conditions of prior experiments). CTRL+ was 1 µM staurosporine. Only vital trophozoites significantly increased TEER after 24 h. No TEER decreases were detected. Data points represent individual monolayers, n=2-6. Time after infection is color coded. Absolute TEER was 284.5 Ω·cm$^2$ (SD 20.4 Ω·cm$^2$) at $t_0$. Appx. 3 contains relevant probability values (Tukey post-hoc test).

Summarizing, the TEER increase is dependent on vital trophozoites without the requirement of attachment, excluding physical blocking of electric current fluxes by attached trophozoites as the cause of the TEER increase.

### 2.1.2.5 Vitality of *G. duodenalis* in the Caco-2 setup

In order to exclude a decreased parasite survival as cause for the apparent lack of epithelial barrier dysfunction, two methods to investigate trophozoite viability (survival by dye exclusion and reproduction assay) were performed (Figure 13). As expected, survival rates slowly decreased and were more than halved after 72 h. However, due to the high parasite load (MOI 20), this leaves enough parasites alive to be comparable to highest used loads (MOI 8) in the literature (Humen et al., 2011) even at the end of experiments. To investigate the reproductive success, the minimal number of trophozoites, capable to start a new growth culture, was assessed. The curve recapitulates the shape of the plotted survival data, confirming the expected link between both.

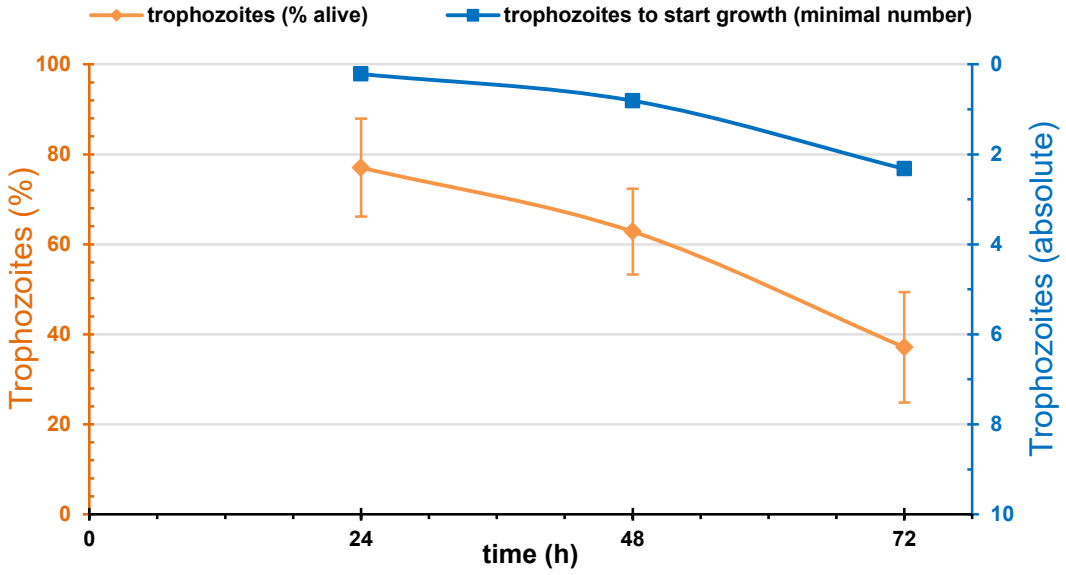


**Figure 13 Trophozoite viability on Caco-2 did not change significantly within 48 h.** Changes in trophozoite survival (orange), and the minimal number to initiate culture growth (blue, secondary axis, reverse) are shown in relation to time after Caco-2 monolayer infection with WB6 (MOI 20). For survival (dye exclusion), more than 20 trophozoites were counted per time point and per n, n=3, error bars represent SD. Appx. 4 contains relevant probability values (Tukey post-hoc test).

### 2.1.2.6 Effect of different *G. duodenalis* isolates

The *G. duodenalis* isolate WB6, which was used widely in previous studies as well as in this work, was originally derived from a symptomatic, treatment-refractory 29-year old male in Afghanistan (Smith et al., 1982a). However, other isolates exist, several claimed to be highly pathogenic as well. Therefore, different isolates of four assemblages were tested to examine if they induce barrier dysfunction or elicit different TEER values on Caco-2 monolayers. The isolates NF (from sampled water during a *G. duodenalis* outbreak in

Newfoundland, Teoh et al., 2000) and S2 (isolated from a sheep, Buret et al., 1990), belong together with WB6 to assemblage AI, and were described as highly pathogenic, likewise the assemblage B isolate GS/M-H7 (GS), sampled in Alaska's wilderness (Nash et al., 1985). P15/E (isolated from a piglet in Czech Republic, Koudela et al., 1991), on the contrary, is the only isolate apathogenic to humans, since it belongs to assemblage E, which members can only infect hoofed animals. Additionally, several isolates from the RKI's *G. duodenalis* biobank (all taken from symptomatic human patients), mainly belonging to assemblage B, since it offers the most isolate heterogeneity amongst all assemblages, were used as well (Figure 14). Apart from a consistent increase in TEER, neither, a significant difference between isolates, nor between assemblages was found. Therewith, a putative loss of virulence of isolate WB6 due to long term axenic culture as an explanation for the absence of barrier leakage was excluded.

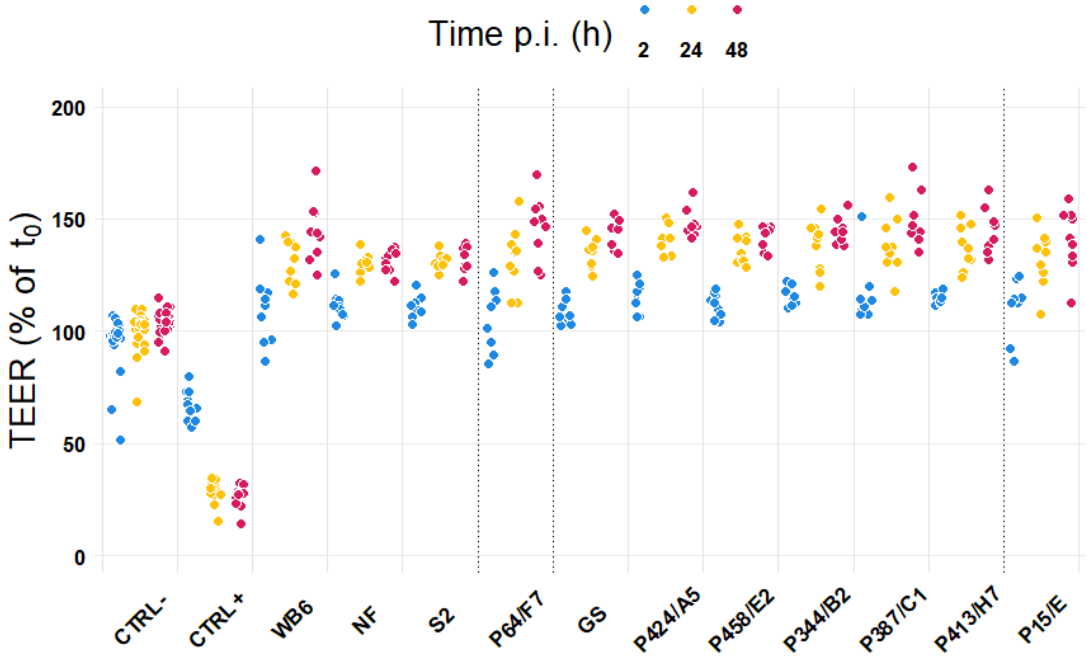


**Figure 14 Different *G. duodenalis* isolates.** TEER changes of Caco-2 bbe monolayers, normalized to measurements before infection, are shown when infected with 11 different *G. duodenalis* isolates (all MOI 20), including 5 reference strains WB6, NF, S2 (assemblage AI), GS (assemblage B), P15/E (assemblage E) and 6 newly established clinical isolates consisting of P64/F7 (assemblage AII), and 5 assemblage B isolates (P424/A5, P458/E2, P344/B2, P387/C1, P413/H7). CTRL+ was 1 µM staurosporine. No evidence for parasite-induced decreases in TEER was found, all isolates increased TEER with very strong significance ($p < 0.0001$). Also, TEER did not differ between isolates or assemblages. Data points represent individual monolayers, n=9-18. Time after infection is color coded. Darker lines separate assemblages. Absolute TEER was 257.6 $\Omega \cdot cm^2$ (SD 54.2 $\Omega \cdot cm^2$) at $t_0$. Appx. 5 contains relevant probability values (Tukey post-hoc test).

### 2.1.2.7 No barrier dysfunction using premature/FBS-free Caco-2 monolayers

Due to the use of lesser differentiated Caco-2 monolayers in some studies (Teoh et al., 2000; Buret et al., 2002; Chin et al., 2002; Humen et al., 2011), monolayers were used for experiments already after 7 days instead of the usual 21-day period. Additionally, the impact of FBS was investigated, since it is known to contain several anti-apoptotic factors (Zoellner et al., 1996), which may counteract and obscure possible apoptosis-inducing parasite factors (Figure 15). The data suggests that neither 7-day monolayers, nor absence of FBS result in barrier dysfunction.

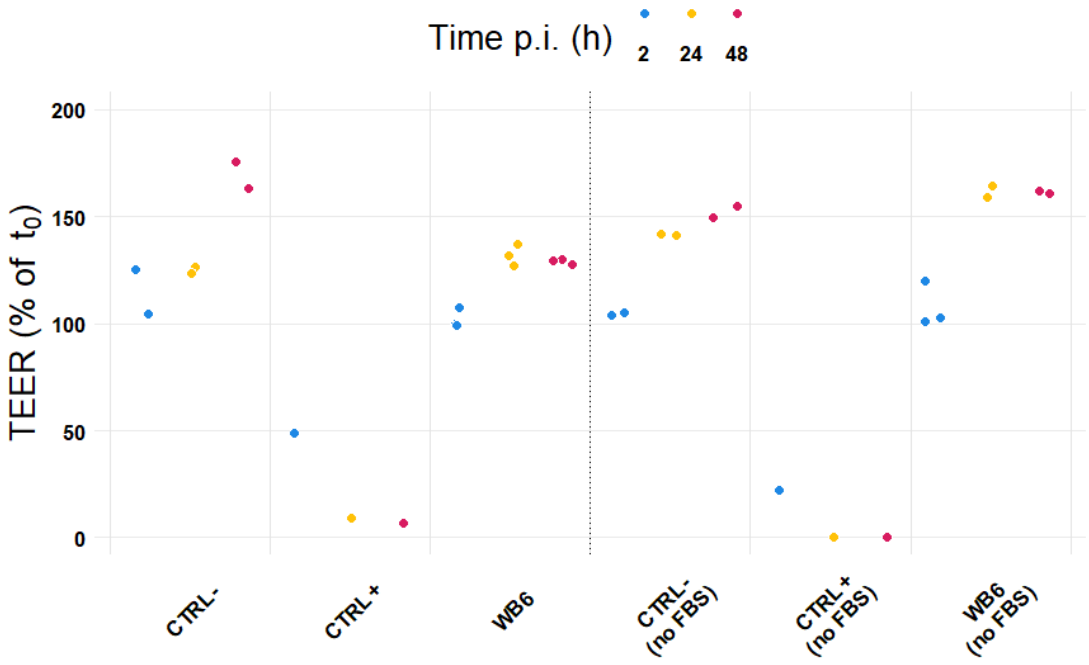


**Figure 15 FBS removal and infection of 7-day-monolayers did not led to TEER decrease.** TEER changes of Caco-2 bbe monolayers, normalized to measurements before infection, are shown after just 7 days of incubation instead of the usual 21 days. Neither, infection of not fully differentiated monolayers nor withdrawal of FBS led to barrier dysfunction. CTRL+ was 1 µM staurosporine. Data points represent individual monolayers, n=1-2. Time after infection is color coded. Absolute TEER was 416.4 Ω·cm$^2$ (SD 154.2 Ω·cm$^2$) at $t_0$. Due to high TEER variances of 7-day monolayers and ongoing TEER increase to peak resistance (see also Figure 6), statistical hypothesis testing was underpowered to investigate differences in TEER increases and therefore not conducted. The main hypothesis of barrier dysfunction (as purpose of this experiment) had to be rejected anyway.

### 2.1.2.8 No impact of different glucose concentrations on TEER

It has been shown that the sodium-dependent glucose cotransporter (SGLT)-1 can exert anti-apoptotic effects under high glucose conditions (Yu et al., 2005; 2008). With regard to the 25 mM glucose concentration in regular Caco-2 DMEM (considered as high), it may also obscure apoptosis and therefore barrier dysfunction, similar to what was hypothesized about FBS under 2.1.2.7. Low glucose conditions, however, did not led to *Giardia*-induced barrier dysfunction (Figure 16).

There is also a study, which published that the contrary, hyperglycemia, can lead to intestinal barrier disruption and altered cellular junctions via the other important glucose transporter (GLUT2) by transcriptional reprogramming of epithelial cells (Thaiss et al., 2018). Taken this into consideration, an even higher glucose concentration (50 mM), such as suggested by Thaiss et al., was used (Figure 16). Again, no barrier dysfunction was observable.

Summarizing, glucose concentration had no effect on TEER in this Caco-2 monolayer setup.

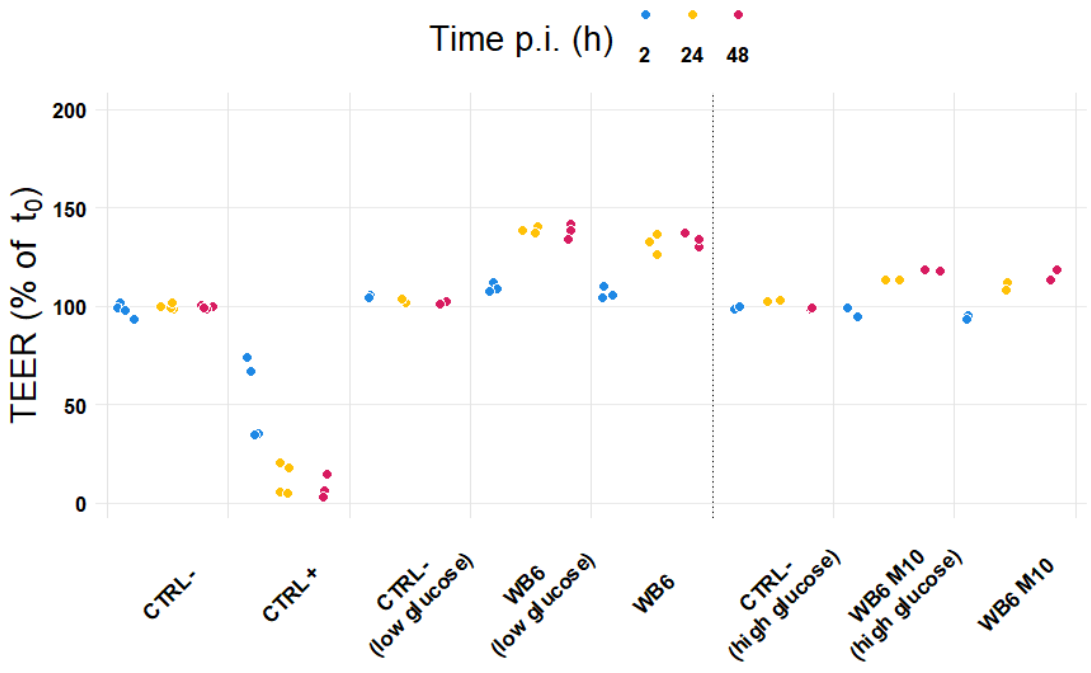


**Figure 16 Glucose-concentrations had no influence on TEER of Caco-2 monolayers.** TEER changes of Caco-2 bbe monolayers, normalized to measurements before infection, are shown when infected with WB6 (MOI 20) under low glucose (5 mM + 20 mM D-mannitol for osmotic balance) and standard glucose (25 mM), as well as WB6 (MOI 10) under high (50 mM) and standard glucose conditions. Lower MOIs in high glucose conditions were still more than sufficient to completely cover the monolayer with trophozoites (see 2.1.2.1) but consumed less glucose and therefore prolonged the high glucose environment. CTRL+ was 1 µM staurosporine. No significant differences in TEER regarding glucose concentrations of infected or uninfected monolayers were detectable. Data points represent individual monolayers, n=2-3. Time after infection is color coded. Absolute TEER was 246.4 $\Omega \cdot cm^2$ (SD 41.1 $\Omega \cdot cm^2$) at $t_0$. Appx. 8 contains relevant probability values (Tukey post-hoc test).

### 2.1.2.9 TEER effects of *Giardia* sp. medium TYI-S-33 on Caco-2 monolayers

Although sufficient numbers of *G. duodenalis* were alive to cover the Caco-2 monolayers (2.1.2.5, also 2.1.2.2), they may lack a critical component of the medium to trigger their virulence. Therefore, TYI-S-33 medium (Keister, 1983) was added to the apical compartment of the monolayers, since it was developed to mimic the human small intestinal fluid and is also used to cultivate *Giardia* sp. axenically. Infected Caco-2 monolayers with TYI-S-33 dropped down to their initial TEER values at 24 h and were collapsed at 33 h after infection. But uninfected TYI-S-33 monolayers were also collapsed at 33 h, which was experienced by others (Chavez et al., 1986) as well (Figure 17). By titrating different concentrations of TYI-S-33 to find a dilution which offered stable TEER values (not shown), a 50% TYI-S-33/Caco-2-DMEM concentration emerged as a solid compromise between monolayer stability and most possible TYI-S-33 amount within a 72-h-period. However, if also infected with *G. duodenalis*, TEER of Caco-2 monolayers increased even more (Figure 17) without monolayer collapse.

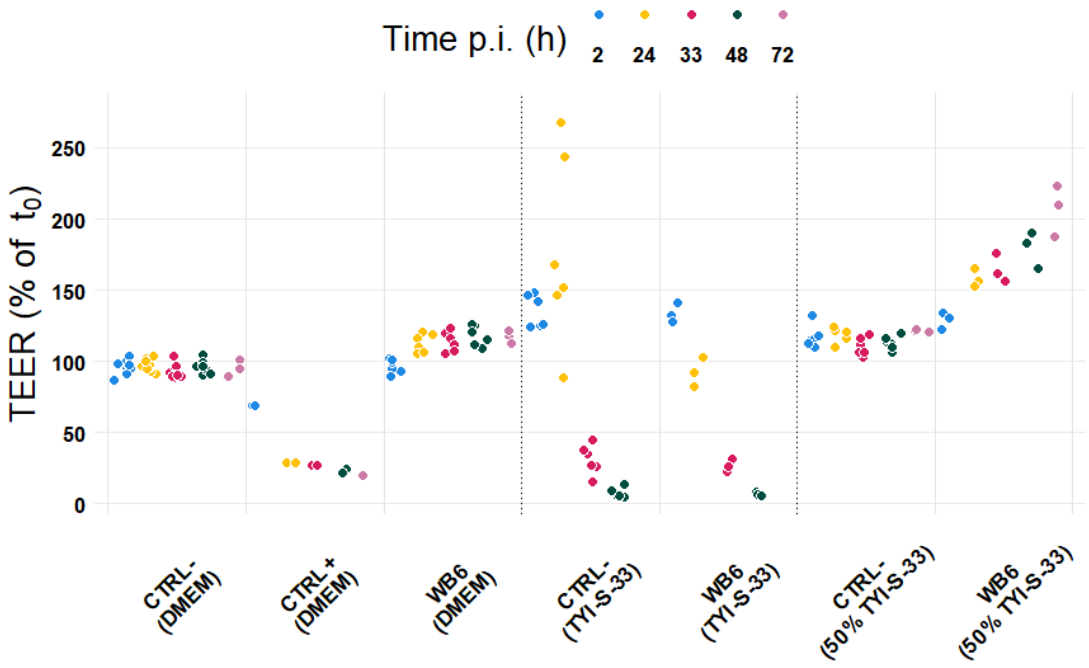


**Figure 17 Partial TYI-S-33 substitution does not enable *G. duodenalis* to decrease TEER.** TEER changes of Caco-2 bbe monolayers, normalized to measurements before infection, are shown when infected with WB6 (MOI 20) under complete and 50% apical substitution of DMEM with TYI-S-33 medium. CTRL+ was 1 µM staurosporine. TEER increases with 100% TYI-S-33 alone, but monolayers were collapsed at 33 h, irrespective of their infection status. A 50% TYI-S-33 substitution led to an elevated but stable TEER up to 72 h, which rose almost in a linear manner in the presence of WB6. Data points represent individual monolayers, n=2-6. Time after infection is color coded. Absolute TEER was 188.2 Ω·cm$^2$ (SD 11.2 Ω·cm$^2$) at $t_0$. Appx. 6 contains relevant probability values (Tukey post-hoc test).

#### 2.1.2.10 No parasite-induced TEER decrease under oxygen-deprivation

Given the microaerophilic nature of *G. duodenalis*, it can be speculated that the normal atmospheric oxygen content may inhibit the parasite's virulence. In order to test this hypothesis, aerobic (standard incubation) and oxygen-deprived (sealed jars with oxygen-consuming sachets) conditions were compared (Figure 18).

An increase in TEER in oxygen-deprived conditions was observable, which was more pronounced if monolayers were also infected with the parasite. However, no collapse of the barrier function within the 72-h-period was observed. After three additional days, all cultivated monolayers under oxygen-deprivation were destroyed, irrespective of infection status as a result of hypoxia.

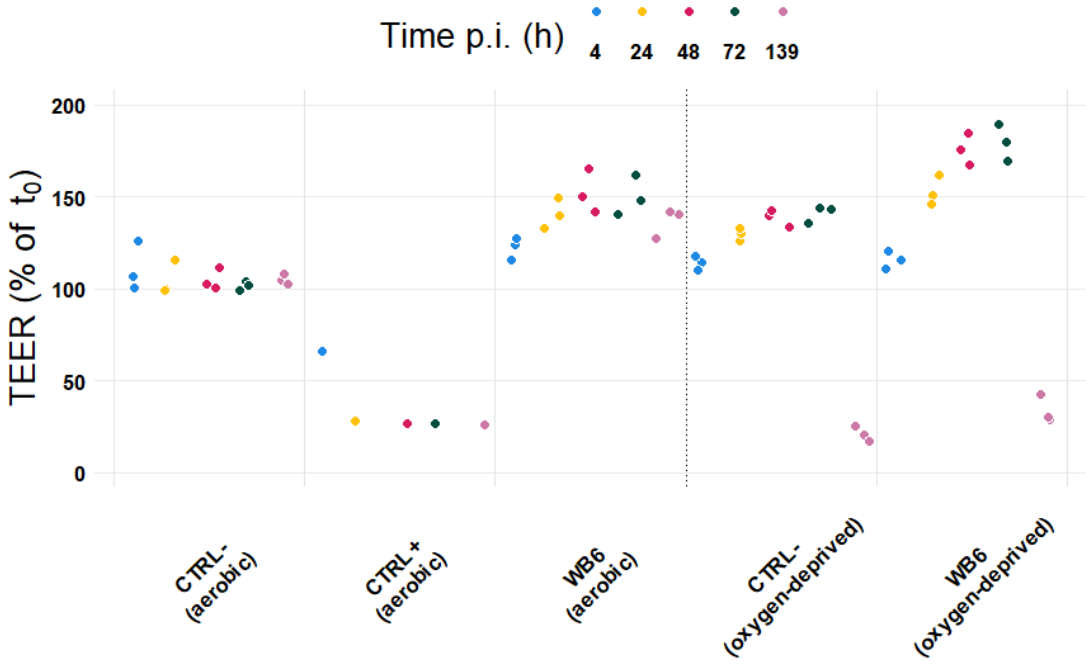


**Figure 18 $O_2$-deprivation did not lead to parasite-induced barrier collapse.** TEER changes of Caco-2 bbe monolayers, normalized to measurements before infection, are shown when infected with WB6 (MOI 20) under normal aerobic and oxygen-deprived conditions. CTRL+ was 1 µM staurosporine. No TEER decreases were detectable within 72 h. Generally, TEER increased under oxygen-deprived conditions, even more if also infected. Lack of oxygen led eventually to monolayer collapse. Data points represent individual monolayers, n=1-3. Time after infection is color coded. Absolute TEER was 185.3 Ω·cm$^2$ (SD 8.0 Ω·cm$^2$) at $t_0$. Appx. 7 contains relevant probability values (Tukey post-hoc test).

#### 2.1.2.11 No effect of GLV-infected parasites on TEER of Caco-2 monolayers

Viral infections occur in protozoans as well. It is known, for example, that the *Leishmania*-specific RNA virus "Leishmania RNA virus-1" (LRV1) affects the severity of leishmaniasis by accelerating transition from cutaneous to mucocutaneous leishmaniasis caused by the Viannia subgenus, endemic to South America (Ives et al., 2011). Depending on the expression of a specific surface receptor (Miller et al., 1988; Sepp et al., 1994), *G. duodenalis* can be infected by a related virus (also family of *Totiviridae*), the *Giardia lamblia* virus (GLV), a double-stranded RNA virus of 7 kb genomic size (Wang & Wang, 1986; Janssen et al., 2015). It could represent a factor that increases *Giardia* spp. virulence, like LRV1 for *Leishmania Viannia* spp. However, regarding TEER, no differences between GLV-infected or uninfected WB6 and GS *G. duodenalis* isolates were found (Figure 19). This also confirms the observations of earlier studies, showing no correlation regarding GLV infection of *Giardia* isolates to symptomatic or asymptomatic patients (Jonckheere & Gordts, 1987).

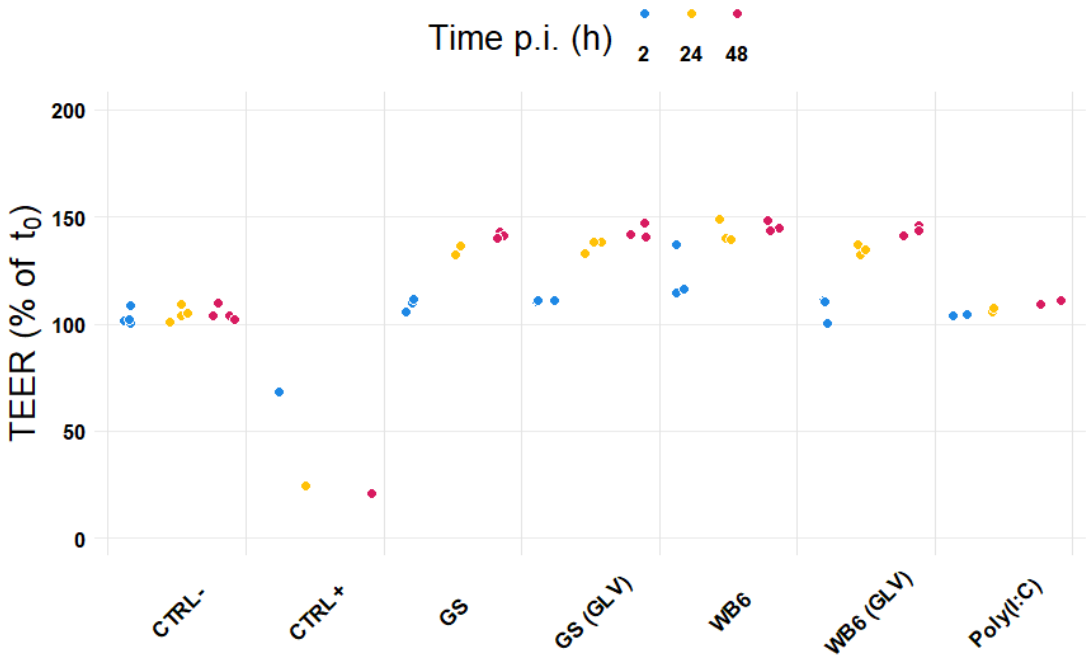


**Figure 19 Giardia virus-containing parasites did not indicate different TEER values.** TEER changes of Caco-2 bbe monolayers, normalized to measurements before infection, are shown when infected with GLV-positive and negative WB6 and GS trophozoites (MOI 20). Poly(I:C) (10 mg/ml) served as control for dsRNA-viruses. CTRL+ was 1 µM staurosporine. No significant differences in TEER regarding GLV presence were detectable. Of note, none of the isolates shown in Figure 14 was infected with GLV. Data points represent individual monolayers, n=1-4. Time after infection is color coded. Absolute TEER was 245.5 $\Omega \cdot cm^2$ (SD 15.4 $\Omega \cdot cm^2$) at $t_0$. Appx. 9 contains relevant probability values (Tukey post-hoc test).

#### 2.1.2.12 FITC-dextran permeability recapitulates TEER

Apart from TEER, macro-molecular permeability assays can be used to probe not only paracellular leakage but also absorption and subsequent trans-cellular transport of biomolecules, which are key functions of small intestinal epithelia (Kiela & Ghishan, 2016). Therefore, molecule-based permeability assays can deliver conclusions about barrier (dys)function in a broader sense. In several *in vitro* studies, labeled sugar compounds like fluorescein isothiocyanate (FITC)-conjugated dextran, was used successfully to assess *Giardia*-induced paracellular permeability (Buret et al., 2002; Chin et al., 2002; Scott et al., 2002). Figure 20 shows FITC-dextran (3000 MW) permeabilities of several conditions used in TEER experiments, with highly similar results. Only the staurosporine control, which consistently reduced barrier function due to heavy apoptosis, indicated increased apical to basal flux of FITC-dextran. Like TEER indicated, other conditions did not show increased permeability (Figure 20). Permeability values of intact or impaired monolayers were in line with published data (Buret et al., 2002; Chin et al., 2002).

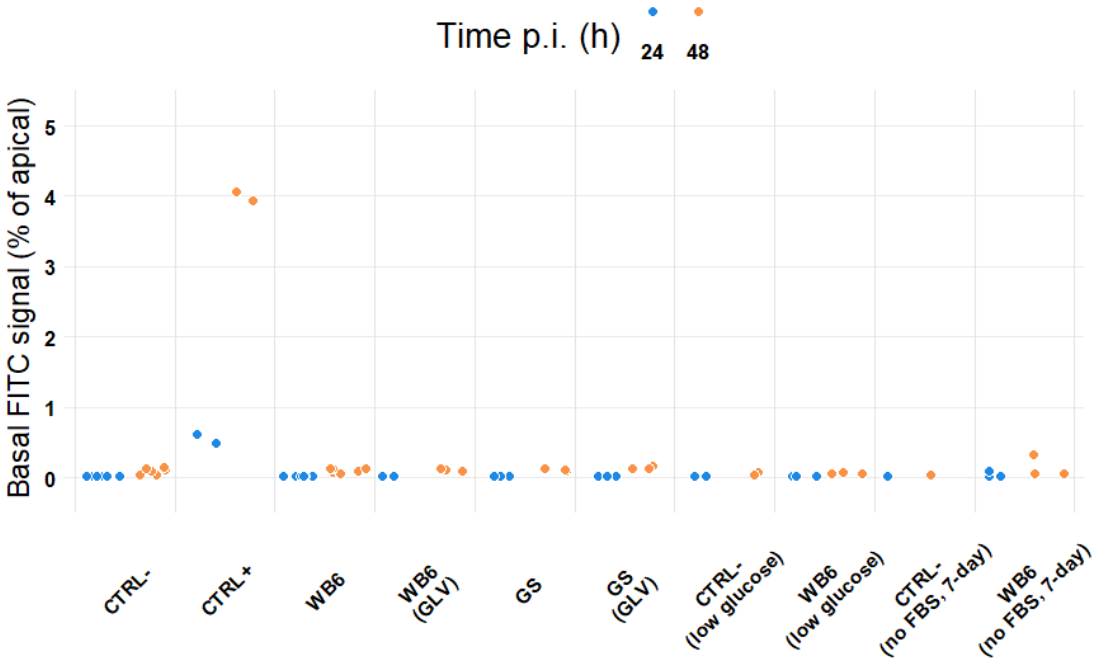


**Figure 20 FITC-dextran permeabilities corroborate TEER data.** Flow-through of FITC-dextran (3000 MW) to the basal compartment has been measured after 2 h of apical incubation at 24 h p.i. (blue) or additional 24 h (orange) and expressed as percentage of the apical signal. Selected conditions of several experiments are shown. Data corresponded to TEER values, showing only significantly increased permeability of monolayers incubated with 1 µM staurosporine. Data points represent individual monolayers, n=2-6. Appx. 10 contains relevant probability values (Tukey post-hoc test). Appx. 29 shows additional assay data.

### 2.1.3 Cytokine response of *G. duodenalis* infected Caco-2 monolayers

Because of the absent evidence of any barrier impairing effects of *G. duodenalis* infections under various conditions used in this Caco-2 setup, the apparent asymptomatic outcome was further investigated on the cytokine level. A study in 2005 used micro-array analysis of *G. duodenalis*-infected Caco-2 cells during the first 18 h and showed an increase in CCL20, CCL2, and CXCL1/2 mRNA abundances among others (Roxström-Lindquist et al., 2005). In an attempt to corroborate those findings on protein level, an ELISA-based multiplex approach (Luminex® assay) was conducted, which additionally included other cytokines, likely to be regulated under *Giardia*-infection stress. The collected data suggested neither, dose-dependent cytokine responses of Caco-2 towards different infection loads, nor responses towards various *G. duodenalis* isolates. Only CCL20 abundances could be measured within the limit of detection (Figure 21). All other investigated cytokines (CCL2, CXCL1, CXCL2, Il-8, TNFα, and GM-CSF) were below detection limits (Appx. 11).

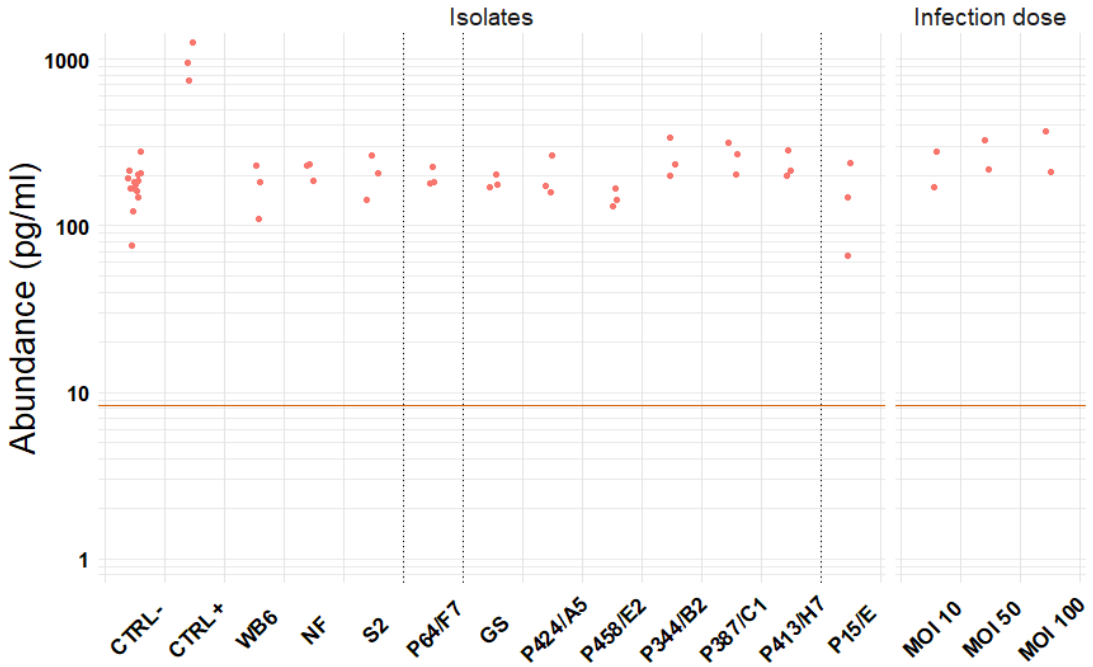


**Figure 21 CCL20 abundance.** CCl20 levels of Caco-2 bbe monolayers, infected with 11 different *G. duodenalis* isolates (all MOI 20), including 5 reference strains WB6, NF, S2 (assemblage AI), GS (assemblage B), P15/E (assemblage E) and 6 newly established clinical isolates consisting of P64/F7 (assemblage AII), and 5 assemblage B isolates (P424/A5, P458/E2, P344/B2, P387/C1, P413/H7), as well as additional MOIs (10, 50, and 100) of WB6 were compared using basal supernatants collected after 72 h of the conducted TEER experiments (see Figure 14) with the Luminex® technology. CTRL+ was 1 µM staurosporine. Colored horizontal line indicates limit of detection. Data points represent pooled basal supernatant samples of 3 individual monolayers, n=3-14. Darker lines separate assemblages. Appx. 12 contains relevant probability values (Tukey post-hoc test).

## 2.2 Organoid-derived monolayer (ODM) model system

The Caco-2 model, as an old and degenerated carcinoma-derived cell line may not reproduce the *in vivo* small intestinal epithelium to a degree which allows the obtainment of reliable results, consistent between studies. This may also be an explanation for contradicting literature. Despite its broad usage in the field, the limitations of Caco-2 are known (Sambuy et al., 2005; Sun et al., 2008).
The highly progressing field of stem-cell derived primary cell cultures based on organoids, which usefulness and superiority over conventional cell lines becoming more and more apparent (Huch et al., 2017), may offer, as a potentially infinite primary cell system, a much more *in vivo*-like model. Therefore, it was assumed that organoids may indicate the described pathological effects of *G. duodenalis*, which were not found with the Caco-2 model.

### 2.2.1 Establishment of the ODM model system

By extracting crypts from duodenal biopsy samples of patients who underwent routine screenings, starting material was gained for human small intestinal organoid cultures (4.2.1.5).

#### 2.2.1.1 Culturing of human small intestinal organoids

Based on published protocols, human small intestinal organoid culturing was successfully achieved with a phenotype resembling the descriptions of published data from the lab of H. Clevers (Sato et al., 2009; 2011a; 2011b; 2013) and others (Mahe et al., 2013; Miyoshi & Stappenbeck, 2013), as depicted in Figure 22 (left). It is worth to mention that in this work all organoid data presented is based on isolate CBF1, which was derived from a 30 years old male patient with - regarding the intestine - a healthy phenotype.

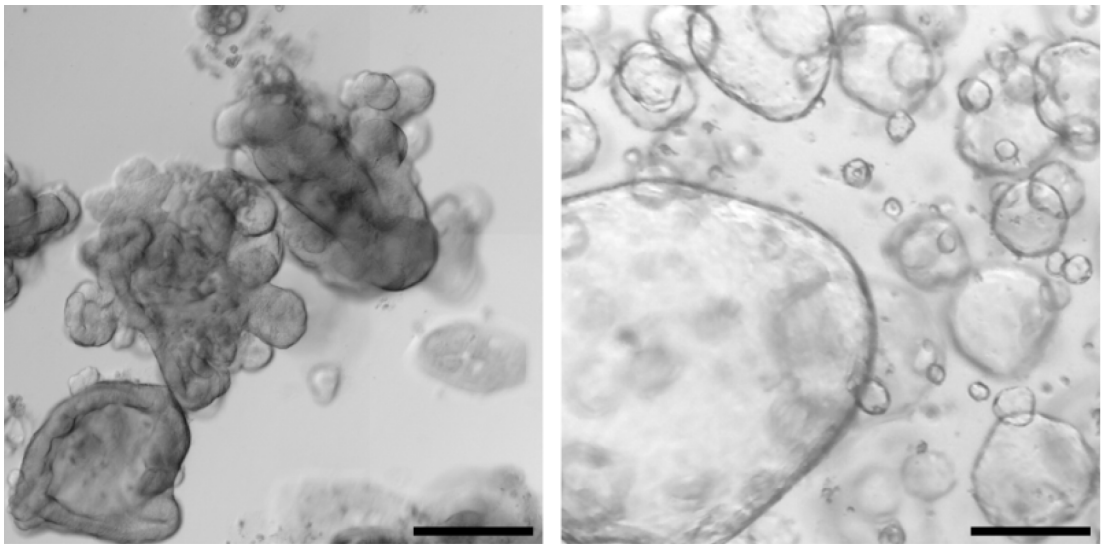

**Figure 22 Traditional organoid versus spheroid culture.** The classical small intestinal organoid culture according to Sato et al., 2009 was reproduced by following published protocols (left). However, in order to increase yield, a new culture medium mix (see medium "SM") has been developed to raise the number of stem cells. This led to formation of large, multicellular and undifferentiated spheres, called spheroids, which indeed increased proliferation rate of those cultures. Scale bars indicate 200 µm, bright field images.

Traditional organoid cultures suffer two disadvantages, relevant for this work. First, their growth is slow compared to cancer-derived cell lines. Second, they are hard to infect reproducibly, not only because they vary strongly in size and shape, but also due to their embedding in Matrigel® and the need to puncture them in order to release parasites in their inner compartment through a syringe, which is either, too large to prevent significant interference of the procedure or too small, clogging its narrow channel with trophozoites. To overcome those problems, organoid culturing in a 2-dimensional system, preferably the transwell-setup, was set as objective. Since this approach required a large amount of cell material, efforts were taken to increase the organoids' growth rate. The medium was modified (from composition suggested by Sato et al., 2011a to a new mix "SM", 4.1.3.3) to further boost Wnt-, R-spondin- and Noggin-signaling in order to increase ISC numbers by inhibiting their differentiation more rigorously. This led to putative stem cell-only cultures, offering a phenotype of large (up to 1 mm in diameter), thin-walled spheres, consisting of hundreds of undifferentiated cells (Figure 22, right), which are known as spheroids (McCracken et al., 2011; Spence et al., 2011; Miyoshi & Stappenbeck, 2013; Mustata et al., 2013). The spheroid culturing allowed doubling of cell mass by every passage (two times a week), providing the necessary turnover to shift to monolayer generation. In comparison, traditional culturing allowed a doubling every two weeks (lab observation, no data to show).

2.2.1.2 (Re)Differentiation of spheroids

In order to investigate *G. duodenalis* infections not only on stem cells, but in a setup, which contained differentiated cells (e.g. ECs), a second medium was required (with fewer or without differentiation inhibitors) to initiate this differentiation. Therefore, different mediums or strategies were investigated to gain differentiated cells, by observing cell-thickening (a consequence of polarization) or organoid-budding (the traditional organoid phenotype) as qualitative readout (Figure 23).

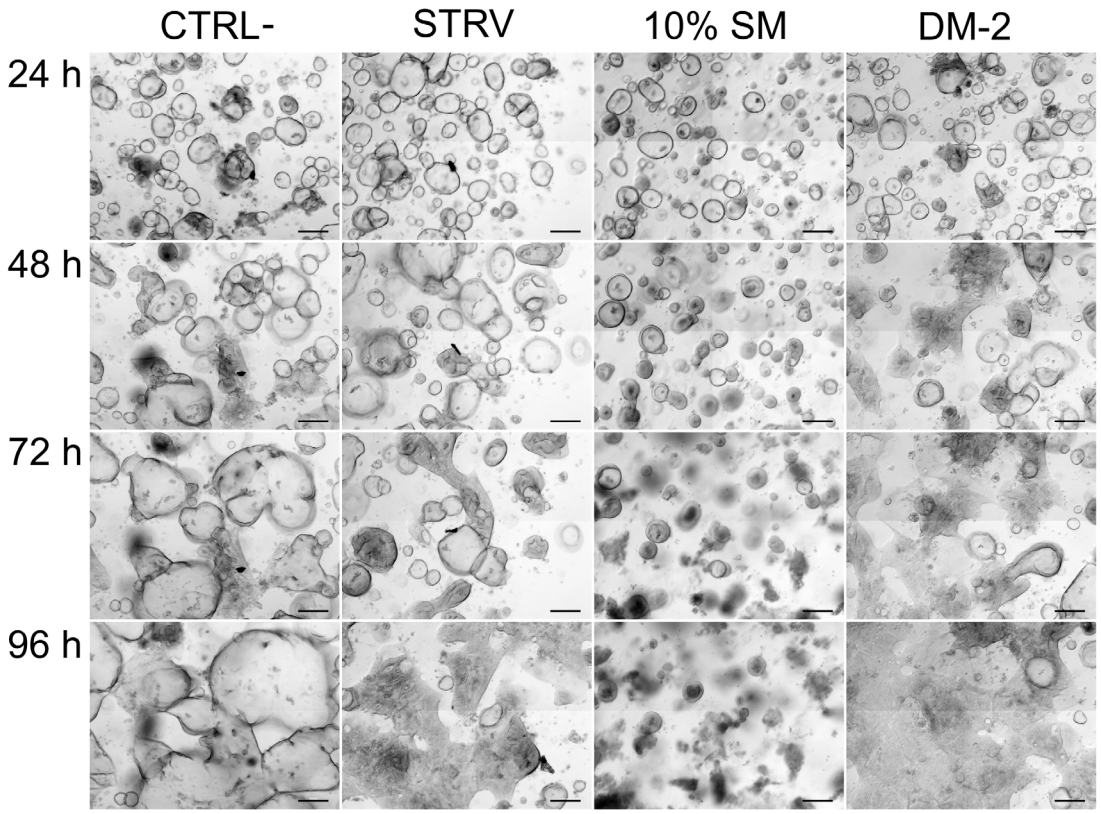


**Figure 23 Comparison of chosen differentiation attempts.** Different medium conditions were assessed for up to 96 h, with medium exchanges every 48 h, except STRV, which was a starvation condition. CTRL- resembled regular spheroid culturing, but without intermittent passaging. For induction of differentiation, a dilution of regular spheroid medium down to 10% (10% SM) and with differentiation mix 2 (DM-2, DM-1 not shown) was investigated. DM-2 offered the earliest signs of differentiation and cells remained vital and even formed multiple layers within the Matrigel®. 10% SM also offered indicators of differentiation but stagnated in growth, lost cell viability, and loss of culture. Scale bars indicate 200 µm, observed areas were fixed locations, n=2.

Without passaging, spheroids fused together to even larger structures, but kept their undifferentiated state, as expected. Diluting the spheroid medium mix (SM) to 10%, as a simple reduction in growth factor signaling, led to cell death if not supplemented with serum (not shown), as done by others with up to 20%

serum levels (Moon et al., 2014; Takahashi et al., 2018; Teal et al., 2018). Addition of serum, however, was preferred to be avoided. DM-2, on the contrary, a mixture of reduced levels of noggin, without R-spondin-3 (but still R-spondin-1), and without the inhibitors of TGF-β (A83-01) and p38 MAPK (SB202190) compared to SM (similar to suggestions by Sato et al., 2011a but modified according to findings of VanDussen et al., 2015 and Miyoshi et al., 2017), led to earliest signs of differentiation and organoids were still vital at the end of the experiment. Furthermore, formation of cell layers was observed, which also suggested cell differentiation/polarization. As a side note, DM-1 (with TGF-β-inhibitor A83-01) offered similar but overall milder effects (not shown). The starvation condition, as an assumed positive control, also formed cell-layers but most likely due to growth factor consumption-related differentiation. However, the use of starvation as a technique was considered to be incompatible with confluent monolayer generation.

#### 2.2.1.3 Generation of monolayers (ODMs)

By achieving highly proliferating spheroid cultures (2.2.1.1) as well as differentiation medium (2.2.1.2), experiments to obtain ODMs in the transwell system were conducted. In contrast to Caco-2 cells, a coating step to facilitate attachment of the cells was required (Figure 24). Both, 10% Matrigel®, and 0,01% collagen coatings worked comparably, leading to confluent monolayer growth. For all subsequent coatings, Matrigel® was chosen[16], due to its usage in the 3D organoid/spheroid culture and its composition, which includes several other basement membrane proteins like laminin, fibronectin, etc., thus better resembling *in vivo* conditions. Both coatings offered 3D-organoid-like structures, which appeared to be grown into the monolayers. Such structures correlated with insufficient organoid dissociation during seeding and flattened with passing time. Hence, for subsequent experiments, spheroids were more vigorously mechanically destroyed with shear forces of 200-µl pipet tips to achieve cell clumps consisting of less than 10 cells and also treated with ROCK-inhibitor to prevent apoptosis via anoikis during the seeding step. Furthermore, medium was exchanged every other day to remove debris.

[16] However, Matrigel® must be used with caution since it contains gentamicin, which does not influence *G duodenalis*, but will interfere with many bacterial infection setups if used in the same way.

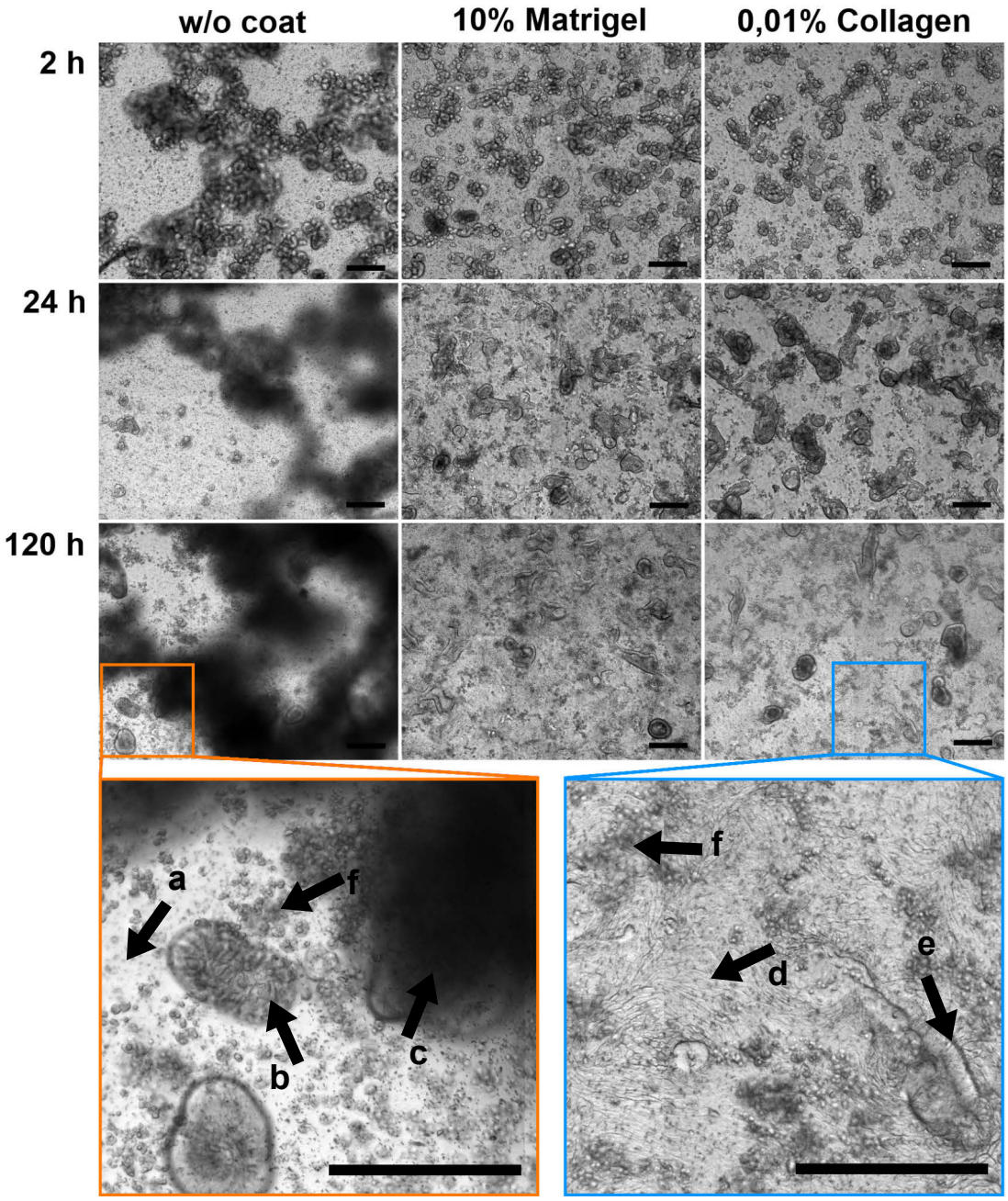


**Figure 24 Monolayer generation required surface coating.** Images show differences in cellular attachment after 10% Matrigel® and 0,01% collagen coating, as well as no coating at all, up to 5 days after seeding on translucent PET-transwell-filters. Magnified image sections at the bottom include indication arrows, showing blank filter surface without attached cells (a), unattached but settled organoids (b), and unattached free-floating organoids without coating (c), and a confluent cell monolayer (d). If organoids were not dissociated vigorously enough, structures, suggesting organoids grown into the monolayer, appeared more often (e). Cellular debris (f) was present on all conditions. Scale bars indicate 200 µm, representative bright field images, n=2.

### 2.2.2 Characterization of the ODM model system

After optimization, as described in the previous section, confluent ODMs could be generated very reliable and maintained with a stable phenotype (Figure 25). By a number of experiments, ODMs were characterized to evaluate their benefits over Caco-2.

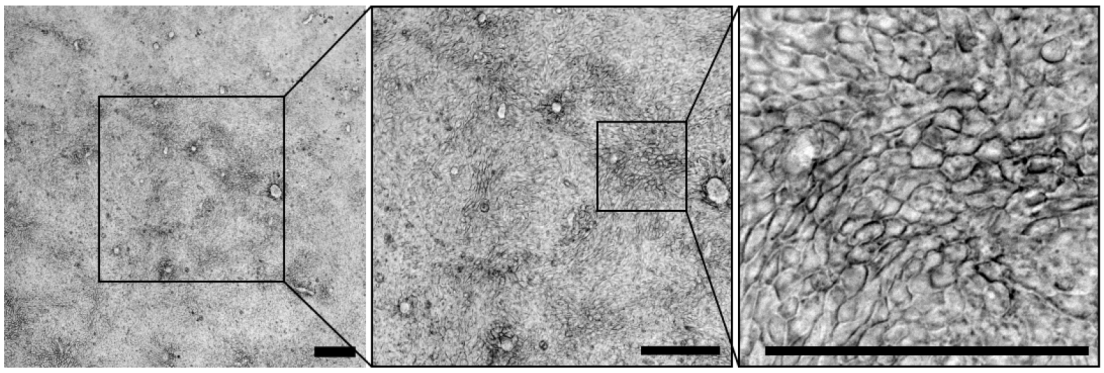

**Figure 25 Optimized ODM.** Images show transmitted-light bright field magnifications of a regular ODM 11 days after seeding. Optimization of cell dissociation led to flatter monolayers, more homogenous in appearance. Scale bars indicate 200 µm, representative images, n=5.

#### 2.2.2.1 ODMs offered strong polarization and brush border formation

One of the first characteristics to investigate was the polarization, because it is also a marker for differentiation to a certain degree and important to correctly mimic luminal infections, as well as barrier function in general (Figure 26). In contrast to Caco-2, in which F-actin signals form diffuse clouds throughout the cytosol (compare to Figure 10), ODMs offer a high degree of polarization. Moreover, details such as stress fibers are visible and even the presence of microvilli (which are built by long, clustered actin filaments) can be assumed.

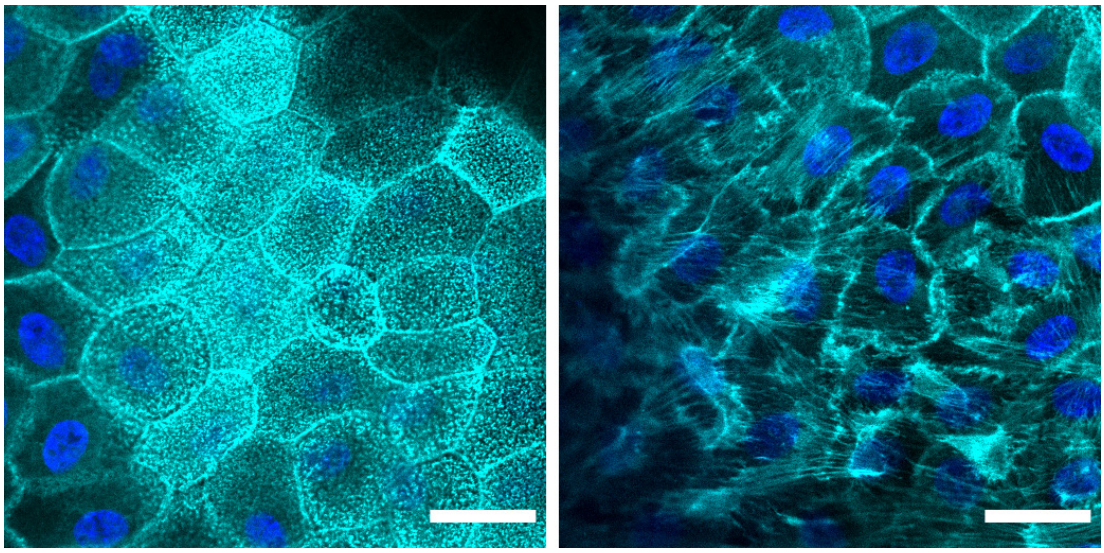

**Figure 26 F-actin signal distribution indicated ODM polarization.** Micrographs depict F-actin staining (cyan) on the apical (left) and basal (right) side of the same ODM section. Nuclei (DAPI) in dark blue. F-actin appeared as a granular signal on the top of the cells, which is an indicator of microvilli. On the basal side it forms stress fibers, which are known to be anchored to focal adhesion complexes at the base membrane. See also Figure 30. Scale bars indicate 20 µm. Representative micrographs, n > 20.

In order to validate the assumption of microvilli present in ODMs (as suggested by F-actin signals in the polarization experiments) scanning electron microscopy (SEM, Figure 27) and villin-stainings were conducted (Figure 28).

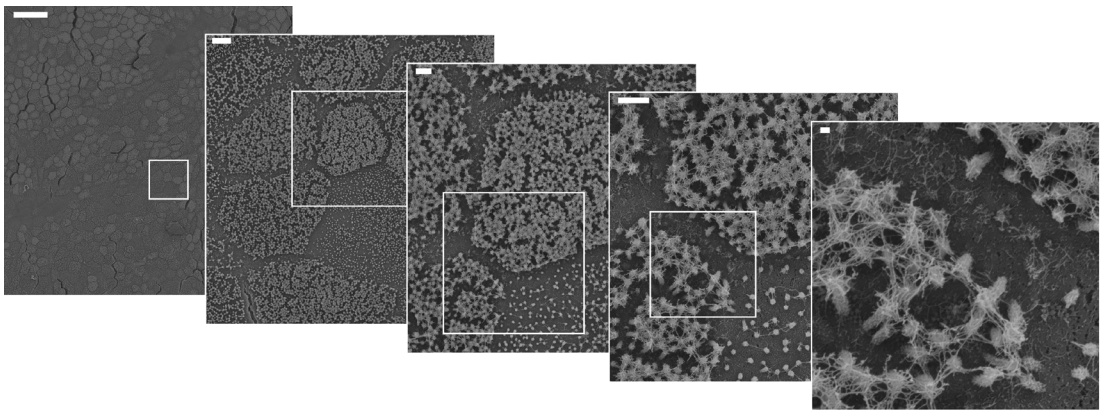

**Figure 27 SEM of ODM surface.** Micrographs of a single ODM section are sorted from left to right with increasing magnification with scale bars indicating 10 µm, 3 µm, 1 µm, 1 µm, and 100 nm. Microvilli were observed with varying degree on top of the cells, giving the monolayer surface a mosaic-like pattern, which could also be seen in the F-actin- and villin-stainings (Figure 28 and 30). With the highest magnification (very right) a fine web of fibers on the top of the microvilli can be observed, the glycocalyx. Fissures (very left, black lines) were artifacts of monolayer preparation for SEM imaging. SEM images taken by G. Holland (RKI ZBS4). Representative micrographs, n=4.

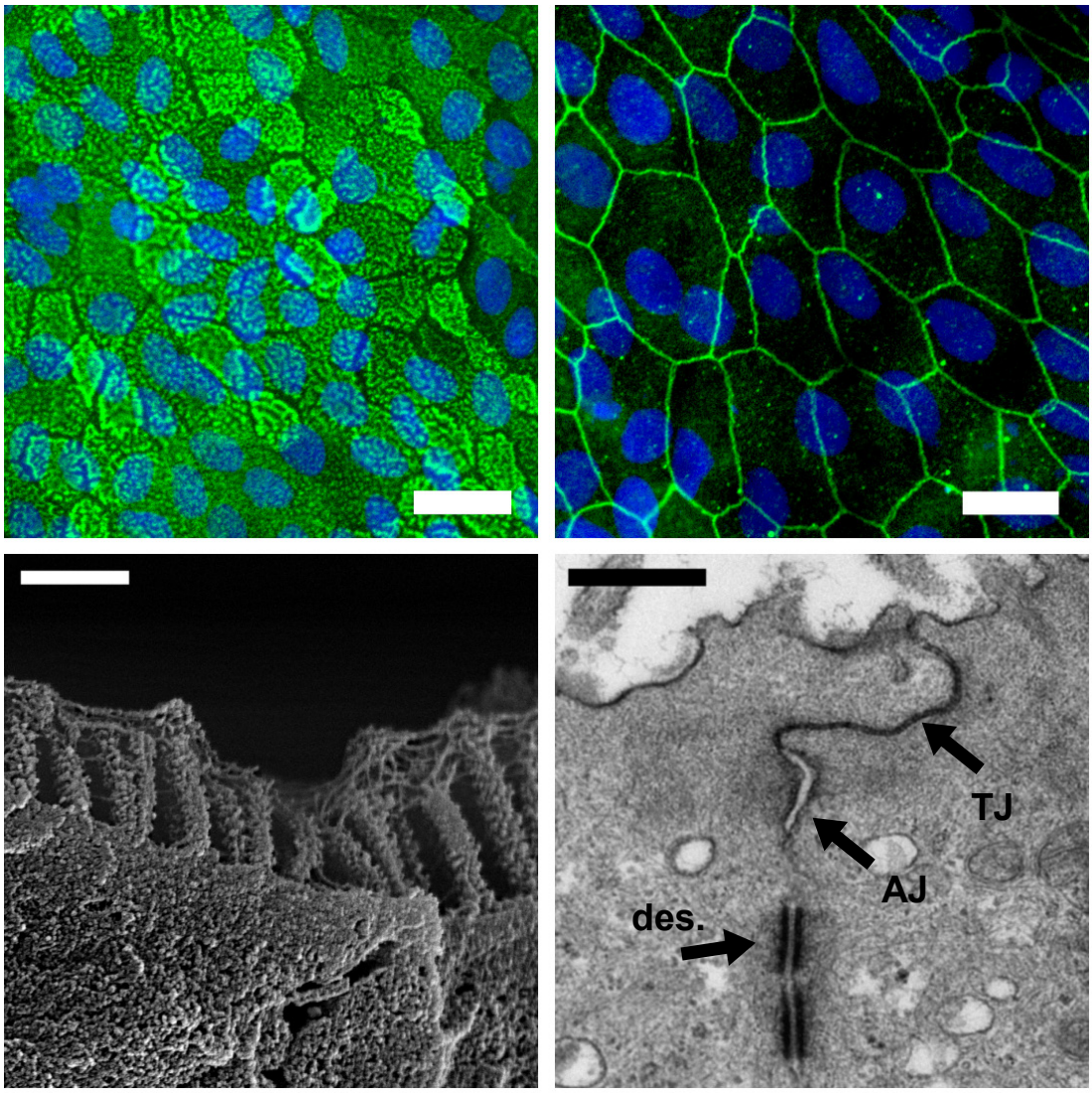


**Figure 28 Brush border and cellular contacts of ODMs.** Top left micrograph shows microvilli by staining of villin, which associates with F-actin bundles within the tips of microvilli. Bottom left SEM micrograph shows lateral fraction of the brush border with microvilli and the glycocalyx as highly branched network on their tips. The top right micrograph shows the tight junction network on the apical side, by staining the major scaffold-protein ZO-1 as surrogate. Stainings of cldn-1, -2 and occludin were comparable (see also Figure 49). Bottom right transmission electron microscopy (TEM) micrograph shows the apicolateral contact site of two adjacent cells. The solid, dark, curved line is the zonulae occludens (tight junction), directly followed at the lower end by a wider rift, zonula adhaerens (adherens junction), with slightly dark fibers spreading both sides (F-actin anchoring). Further down are two desmosomes, which can be found in high numbers along the basolateral membrane, as usual in epithelial tissues. Scale bars indicate 50 µm (villin) and 20 µm (ZO-1) for IFAs, 500 nm for EM. SEM/TEM images taken by G. Holland (RKI ZBS4). Representative micrographs, n=4.

According to EM and IFA data (Figure 27 and 28), ODMs not only developed microvilli, which were not significantly present in the previous Caco-2 experiments, but also a glycocalyx to an extent comparable with the *in vivo* condition (Frey et al., 1996; Giannasca et al., 1996). Of note, cells varied in their degree of microvilli formation as well as glycocalyx thickness. Regarding their cellular contacts, ODMs concordantly mimicked small intestinal epithelial tissue. All tested tight junction proteins (ZO-1, occludin, cldn-1, cldn-2; see also Figure 49) were present, and described contact sites (1.2.1.2) were found in electron microscopy (Figure 28). Additional TEER experiments one week after seeding (Figure 29) showed tight monolayers with comparable values (mean 195 $\Omega cm^2$, SD 45.8 $\Omega cm^2$) to Caco-2 (mean 198 $\Omega cm^2$, SD 20.0 $\Omega cm^2$, before passage number related increase; Figure 7), as well as ODMs generated by others (mean 198 $\Omega cm^2$) in parallel (Kozuka et al., 2017). However, the variation is higher than experienced with Caco-2 monolayers, most likely due to inherently higher variability of seeding technique (number of cells pooled from 3D cultures, degree of organoid disruption and differentiation, etc.).

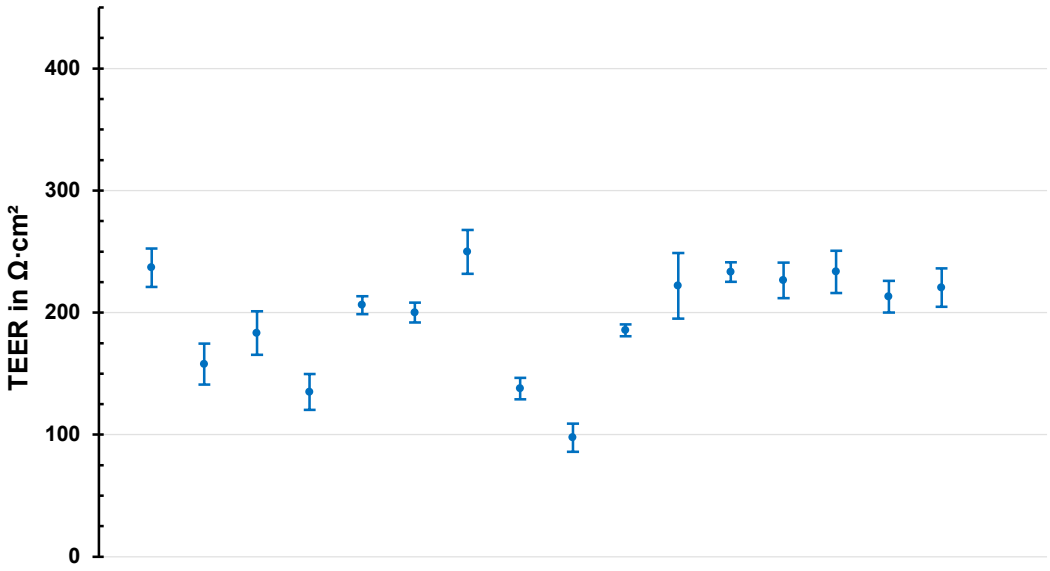


**Figure 29 Basic TEER of ODMs varied around 196 Ω·cm².** TEER values of ODMs 8 days after seeding on transwell-filters are shown. Mean values were comparable to Caco-2 data, however variation was higher. Each data point indicates mean and SD of 8-12 monolayers.

#### 2.2.2.2 Maturation of ODMs

To investigate temporal course of ODM differentiation, three time points were compared. Infection experiments with *G. duodenalis* were usually started on day 8 after seeding. In order to classify the degree of differentiation, an earlier time point has been chosen (3 days, just reached confluence) and a later time point after two weeks (Figure 30). Even the youngest ODMs offered microvilli and glycocalyx, not significantly different to the other time points. But the cells grew from a cubic to a more elongated, columnar shape with time (Figure 30 and 31).

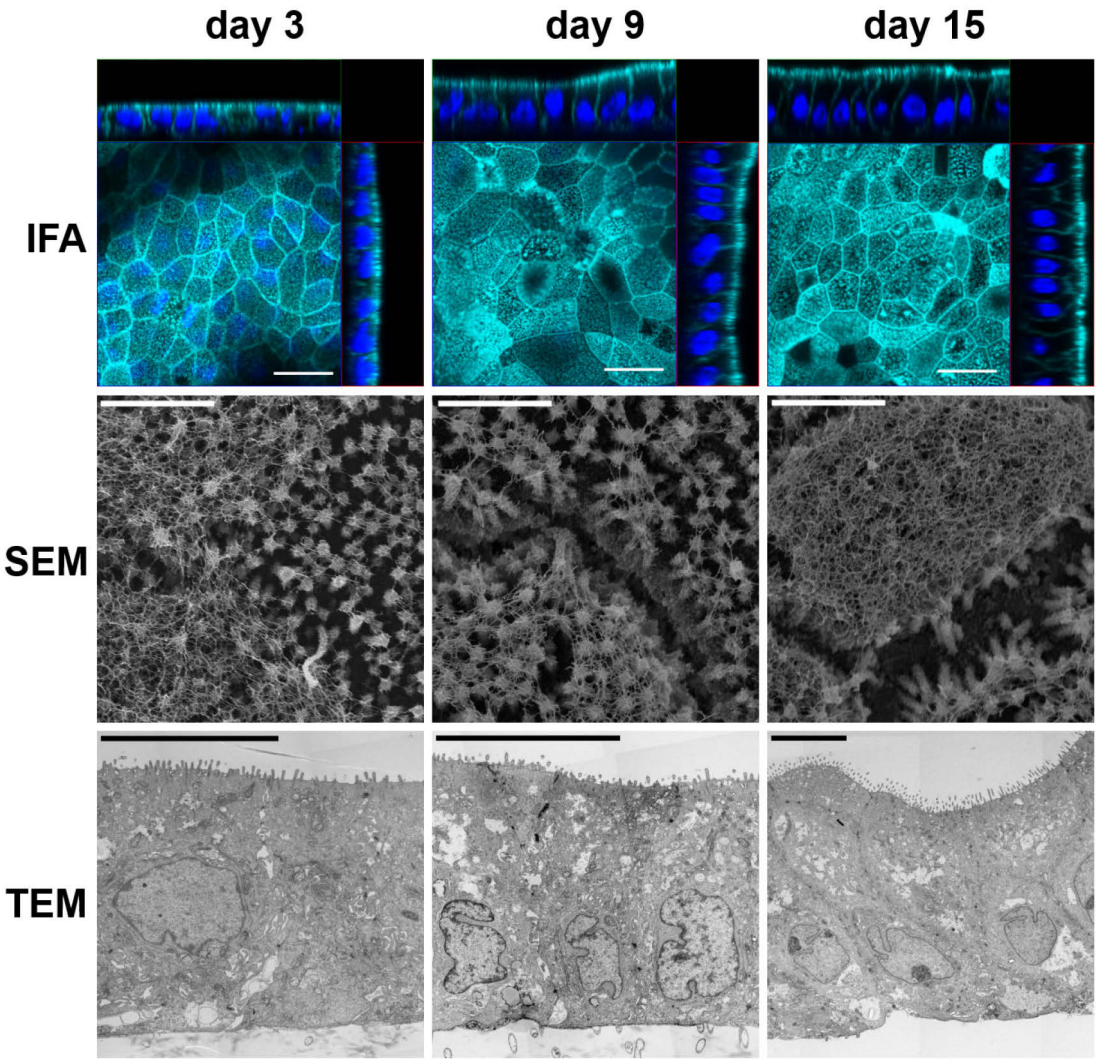


**Figure 30 Temporal development of ODMs.** Top row shows F-actin-stainings of ODMs, middle row SEM micrographs with focus on tricellular junctions, bottom row TEM lateral sections, all after 3 days (confluence reached), 9 days (within the usual scheduled infection period), and 15 days (for comparison). Microvilli as well as glycocalyx were present already after 3 days without significantly changing thereafter. The variation between cells was higher than between time points. However, thickness of ODMs increased with time (best seen in orthogonal IFA projections). Occasionally, on some areas the monolayer made a transition into a pseudo-stratified epithelium, as observable in the micrograph showing TEM after 15 days. Scale bars are 20 µm for IFA, 2 µm for SEM, and 10 µm for TEM. SEM/TEM images taken by G. Holland (RKI ZBS4). Representative micrographs, n=2.

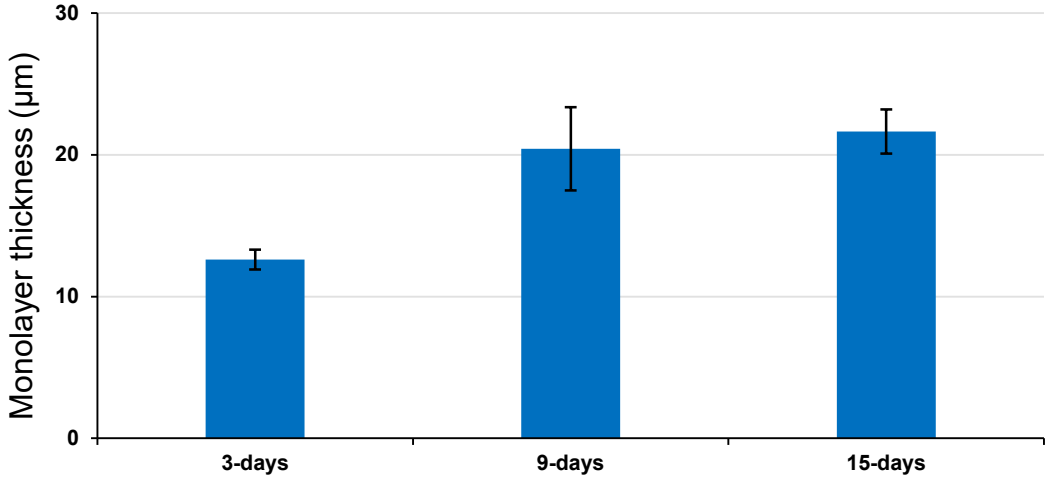


**Figure 31 Thickness of ODMs increased with time.** Height of monolayers after 3, 9, and 15 days of incubation after cell seeding is shown. After 9 days, ODM cells were significantly ($p < 0.05$) longer (apical to basal length) than on day 3. Prolonged incubation up to 15 days did not indicated a further increase. With passing time, monolayer thickness increases. Data derived from measurements of z-stack IFA micrographs using Zen software. Random spots of 3 independent monolayers per condition were measured. Error bars represent SD, n=3. Appx. 13 contains relevant probability values (Tukey post-hoc test).

Infection experiments were conducted at 8 days after, since 3-day ODM-cells, although also offering microvilli and glycocalyx, were more cubic, which contrasted to the typical cylindrical cell shape of the highly prismatic duodenal epithelium *in vivo*. Day-15 ODMs, on the other hand, were considered unnecessary, since the epithelium exchanges itself every 3-5 days (Sato et al., 2009; van der Flier & Clevers, 2009; Park et al., 2016). Therefore, an extended period does not necessarily represent the *in vivo* condition better. Other authors propose the range of 5-7 days to achieve characteristics similar to freshly isolated biopsies (Kozuka et al., 2017).

### 2.2.2.3 Mucus detection on ODMs

To detect a potential mucus layer on the surface of ODMs, histochemical stainings were conducted. The blue staining of a fine apical layer suggested the presence of acidic glycoproteins, which could represent mucins but also the glycocalyx (Figure 32).

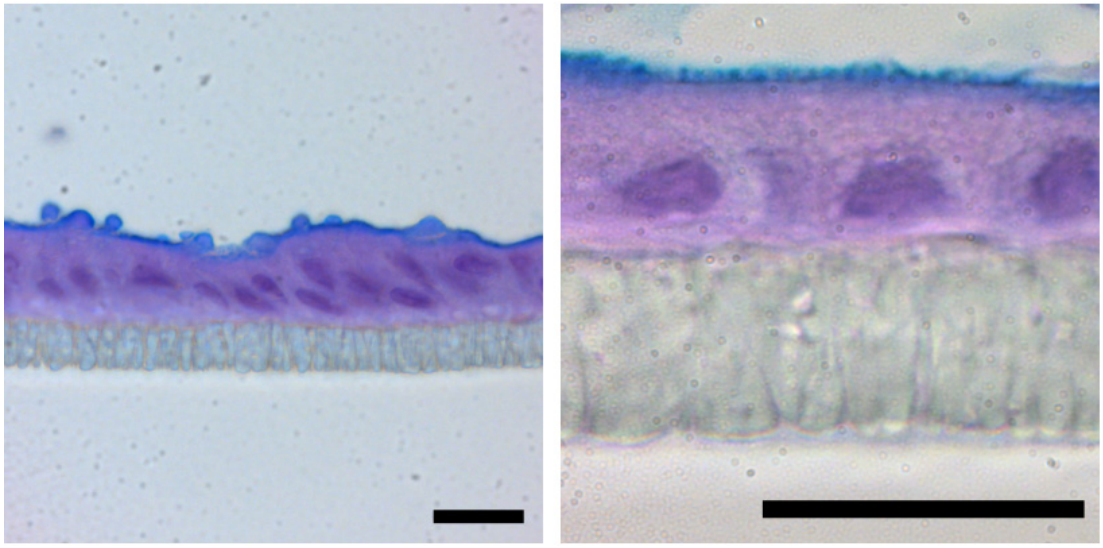

**Figure 32 Histochemistry (Alcian blue/PAS) on ODMs.** Bright field microscopic images show lateral ODM sections, stained with Alcian blue (blue), periodic acid–Schiff (PAS, violet) and nuclei (dark violet). PAS is used to visualize glycoproteins such as mucins. Alcian blue stains especially acidic polysaccharides of mucus. The combination of both is usually used to make mucus visible. Whereas PAS stained whole cells homogenously, Alcian blue seemed to be specific for the apical membrane area. Scale bars indicate 20 µm. Representative images, n=3.

#### 2.2.2.4 Cellular composition of ODMs

Another advantage of organoid-based systems over conventional cell lines is that they can generate different cell types (Sato & Clevers, 2013). Therefore, IFA experiments have been conducted to investigate ODMs with regard to their cellular composition (Figure 33). However, antibodies labeling intestinal alkaline phosphatase (ALPi, marker for ECs) and LGR5 (marker for LGR5$^+$ ISCs) offered background-like signals, which could suggest immature ECs or simply unspecific antibody binding.

To label GCs, three different anti-Muc2 antibodies were investigated (all without signals, Appx. 14), as well as an anti-ClCa-1 antibody, which performed well on murine duodenal biopsy sections (Appx. 14) but also delivered no signals on ODMs, suggesting no presence of GCs. This was also supported by the lack of GC phenotypes in EM.

A diagnostic anti-lysozyme antibody (marker for PCs), also working reliably on murine duodenal sections (Appx. 14), labeled single cells on ODMs with different intensity, reaching form cells without any signal to cells with very high intensity levels, often directly adjacent and therefore unlikely to represent signal artifacts. However, many cells offered also signal intensities between those extremes, suggesting a state of "semi"-differentiation or up-taking of available lysozyme.

ChrA was used as a marker for EECs, which worked appropriate on murine duodenal sections (Appx. 14). However, ChrA signals were never found on ODMs. Also, EM imaging suggested that EECs do not seem to exist in ODMs.

For TCs, the situation of finding a marker is difficult. A number of proteins can be used but all of them do not label all kinds of TCs, but different subpopulations of EECs, making an intersection of several positive marker proteins necessary to properly evaluate TC presence (Gerbe et al., 2012; Middelhoff et al., 2017). However, this effort was not taken, due to probably low TCs numbers – and therefore questioning relevance – on ODMs. Instead, the microtubule-linked protein kinase doublecortin-like kinase 1 DCLK-1 (formerly Dcamkl-1) as probably the most specific marker was chosen. There was no received signal on murine duodenal biopsies (Appx. 14), but a low number of cells (approximately 0.03%) were cytosolically stained on ODMs. Those may be true results regarding the marker, however it cannot be stated that those cells really represent TCs for reasons mentioned above. Also, their low numbers (lower than *in vivo* by two orders of magnitude) rendered them insignificant for this more barrier-related work.

Taken together, it was considered that ODMs mainly consisted of an immature form of ECs and a hard-to-define proportion of PCs. Presence of GCs was excluded. However, this assessment requires further experiments beyond the scope of this work.

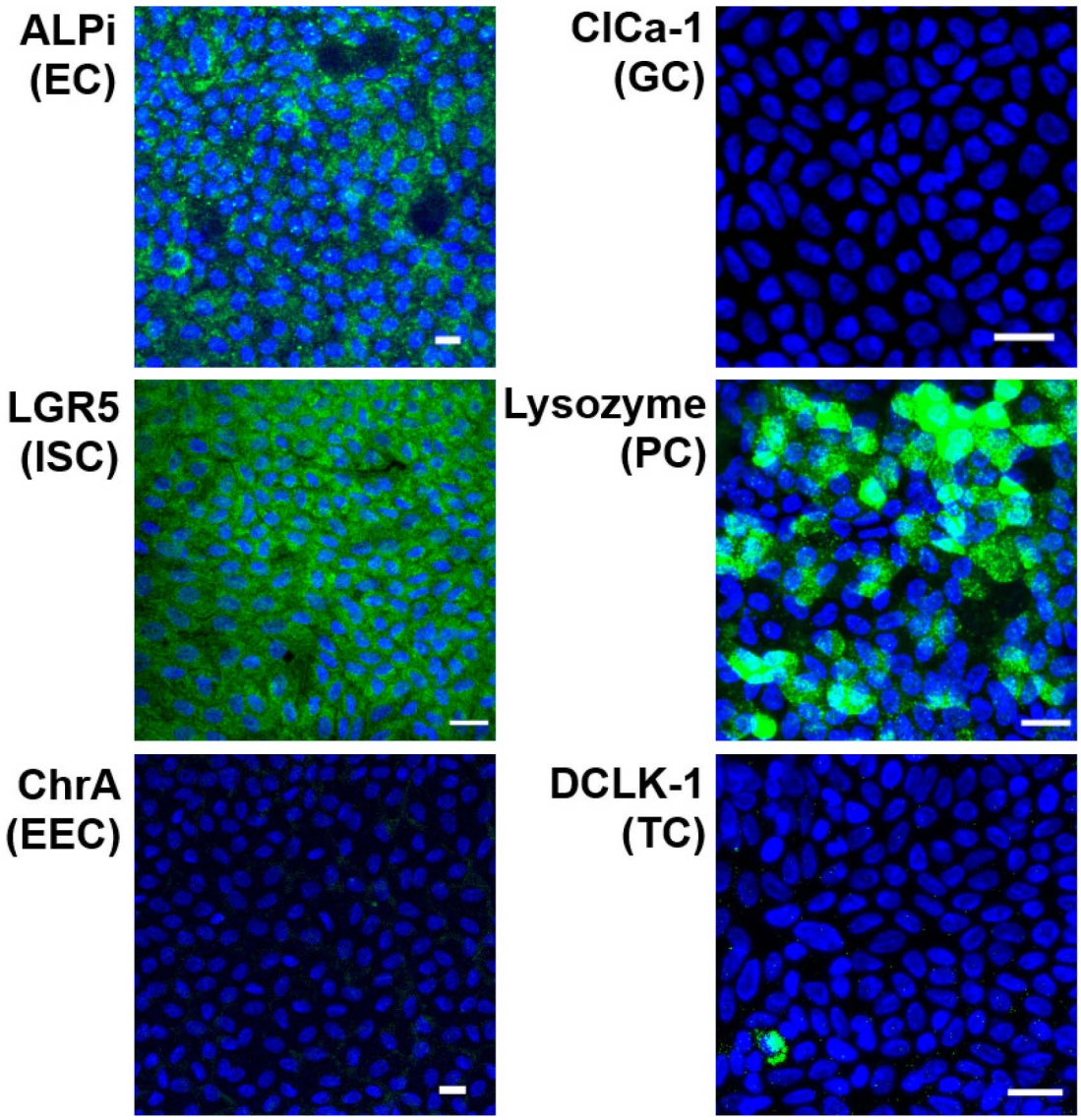


**Figure 33 Markers for different epithelial cell types.** IFA micrographs depict different protein markers (green) on ODMs to distinguish specific cell types. Nuclei (DAPI) in blue. **ALPi** (intestinal alkaline phosphatase) as a marker for ECs offered low background-like signals on ODMs but was also underperforming in the validation on murine duodenal sections. For GCs, **ClCa-1** (a channel-protein which is heavily secreted into the mucus by GCs), worked well in validation but almost no ClCa-1 signals were found on ODMs. **LGR5** as the marker for LGR5$^{+}$ ISCs stained every cell in ODMs but statistically too less in the validation. **Lysozyme**, labeling PCs, was used and performed well in murine organoids and murine duodenal sections. On ODMs, it stained a fraction of cells with different intensities. **ChrA** (C-20), an EEC marker, showed likely signals in the validation, but not on ODMs, suggesting no presence of EECs. **DCLK-1**, a partial marker for TCs, showed no signals in the validation, but the cytosol of very few cells on ODMs. Scale bars indicate 20 µm. Representative micrographs, n=2-8.

### 2.2.3 Effect of *G. duodenalis* on ODM barrier integrity

With ODMs, as a new *in vitro* model system, *G. duodenalis* infections were conducted similar to previous experiments on Caco-2. Initial TEER experiments indicated comparable results to the Caco-2 model (Figure 34). Concluding, the absence of *G. duodenalis*-induced barrier dysfunction pathology cannot be explained by putative inadequate features of Caco-2 (due to its carcinoma lineage). Therefore, the hypothesis that a trigger is required to initiate parasite virulence was investigated on ODMs as well.

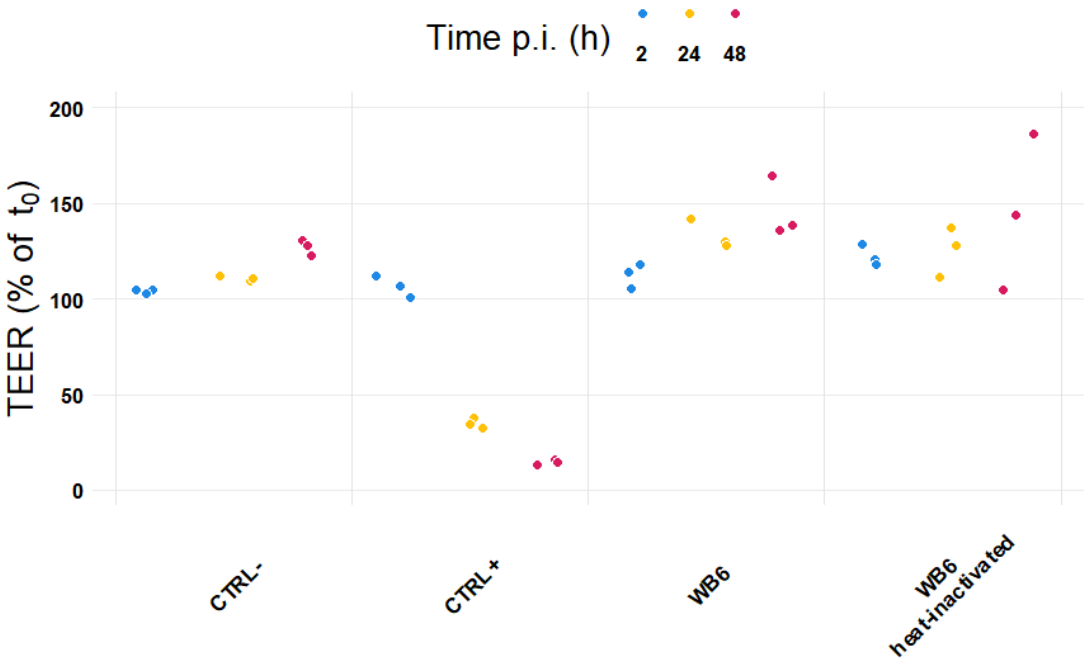


**Figure 34 ODM-infection with *G. duodenalis* did not show differences to Caco-2 model.** TEER changes of ODM CBF1 monolayers, normalized to measurements before infection, are shown when infected with WB6 (MOI 20). CTRL+ was 1 µM staurosporine. Overall TEER pattern is not different to the Caco-2 experiments. Data points represent individual monolayers, n=3. Time after infection is color coded. Absolute TEER was 157.8 Ω·cm$^2$ (SD 17.5 Ω·cm$^2$) at $t_0$. Appx. 15 contains relevant probability values (Tukey post-hoc test).

### 2.2.3.1 High glucose conditions did not decrease TEER of infected ODMs

The influence of high levels of glucose has been investigated on ODMs as a final approach to reproduce barrier dysfunction as claimed by Thaiss *et al*. and to examine whether it could influence the outcome of infected ODMs (Figure 35). Obtained ODM TEER data was not different from Caco-2. Also, IFAs were conducted to search for the phenotypes proposed by Thaiss *et al*. (2018), without finding them either (not shown).

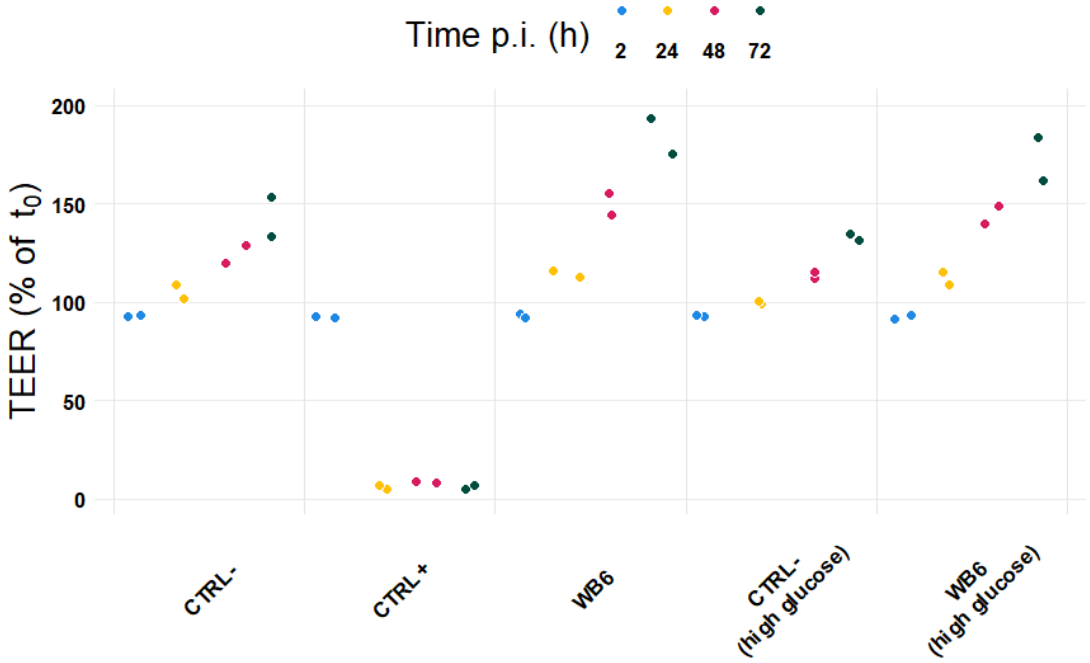


**Figure 35 (Infected) ODMs did not show reduced TEER due to high glucose amounts.** TEER changes of ODM CBF1 monolayers, normalized to measurements before infection, are shown when infected with WB6 (MOI 10) under standard glucose (25 mM) and high glucose (50 mM) conditions. Experimental setup was comparable to Figure 16. CTRL+ was 2 µM staurosporine. Data followed the same course as on Caco-2 monolayers. Data points represent individual monolayers, n=2. Time after infection is color coded. Absolute TEER was 252.5 Ω·cm$^2$ (SD 19.4 Ω·cm$^2$) at $t_0$. Appx. 16 contains relevant probability values (Tukey post-hoc test).

### 2.2.3.2 TYI-S-33 medium led to barrier dysfunction of infected ODMs only

Due to the characteristics of TYI-S-33 as being an artificial replacement of the luminal environment of the small intestine (as mentioned before; 2.1.2.9), the apical substitution of this medium was investigated again. Preceding experiments with TYI-S-33 on ODMs suggested – in strong contrast to Caco-2 monolayers – that this medium is tolerated for at least four days (data not shown). Therefore, this condition was subsequently tested in an infection setup (Figure 36). For the first time, a consistent barrier dysfunction effect was observed, indicated by decreasing TEER, reaching minimal electric resistance after 48 h. With standard DMEM (Caco-2 composition), infected ODMs indicated reduced TEER after 72 h to a level comparable to pre-infection. However, in contrast to the TYI-S-33 related decline, this was not consistent and could not be reproduced in other experiments.

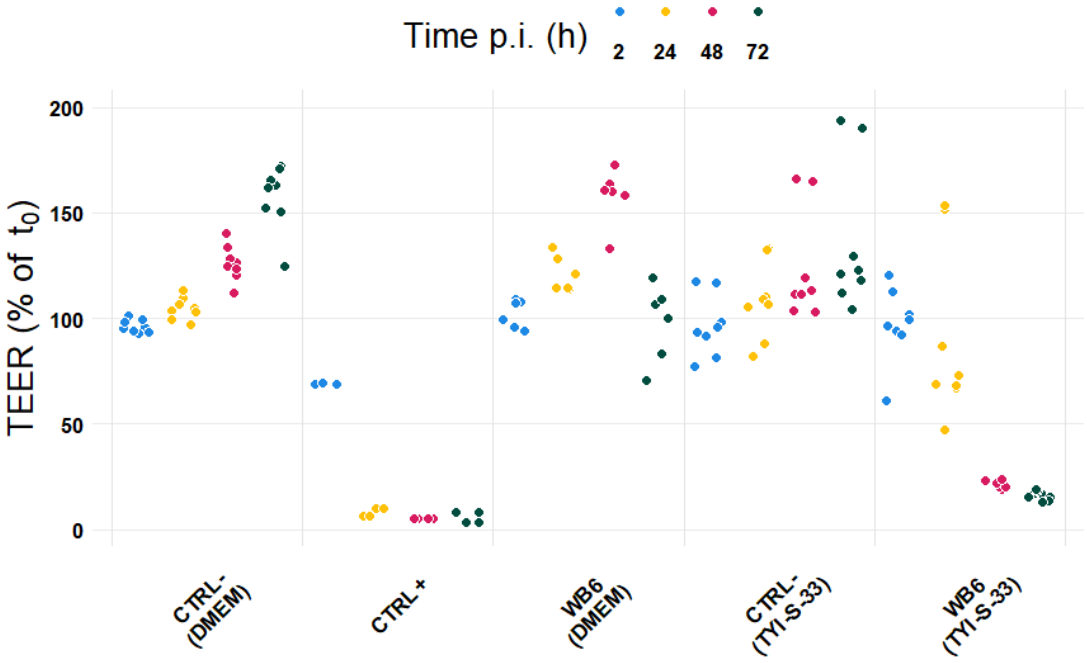


**Figure 36 TYI-S-33 enabled *G. duodenalis* to induce barrier dysfunction on ODMs.** TEER changes of ODM CBF1 monolayers, normalized to measurements before infection, are shown when infected with WB6 (MOI 10) under complete apical substitution of DMEM with TYI-S-33 medium, comparable to previous Caco-2 experiment (Figure 17). CTRL+ was 2 µM staurosporine. TEER decreased if ODMs were infected with *G. duodenalis* and TYI-S-33 medium in the apical compartment until complete barrier breakdown by 48 h. Data points represent individual monolayers, n=4-8. Time after infection is color coded. Absolute TEER was 215.9 Ω·cm$^2$ (SD 18.6 Ω·cm$^2$) at $t_0$. Appx. 17 contains relevant probability values (Tukey post-hoc test).

The barrier disruption suggested by TEER, was visualized using IFAs (Figure 37). Large-scale destruction of the epithelial layer was observable. Cells appeared to be rounded off and attached to each other only punctually, presumably at junction sites like desmosomes. The tight junction, moreover the complete brush border including microvilli, seemed to be lost. Nuclei showed a phenotype of highly condensed chromatin, which accumulated in the peripheral regions near the nuclear envelope and could represent some form of oncosis[17] (Majno & Joris, 1995). In contrast, staurosporine offered the typical cell- and nuclei-shrinkage, pyknosis, and karyorrhexis which are characteristic for apoptosis[18] (Elmore, 2007). The most interesting observation, however, was the appearance of considerable amounts of ClCa-1-positive cells, which could suggest the emergence of GCs.

[17] Oncosis is a form of hypoxia-induced/ischemic cell death accompanied by cellular and organelle swelling, membrane blebbing, and increased permeability (Majno & Joris, 1995).

[18] Incidentally, the original term for apoptosis was “shrinkage necrosis” (Kerr, 1971).

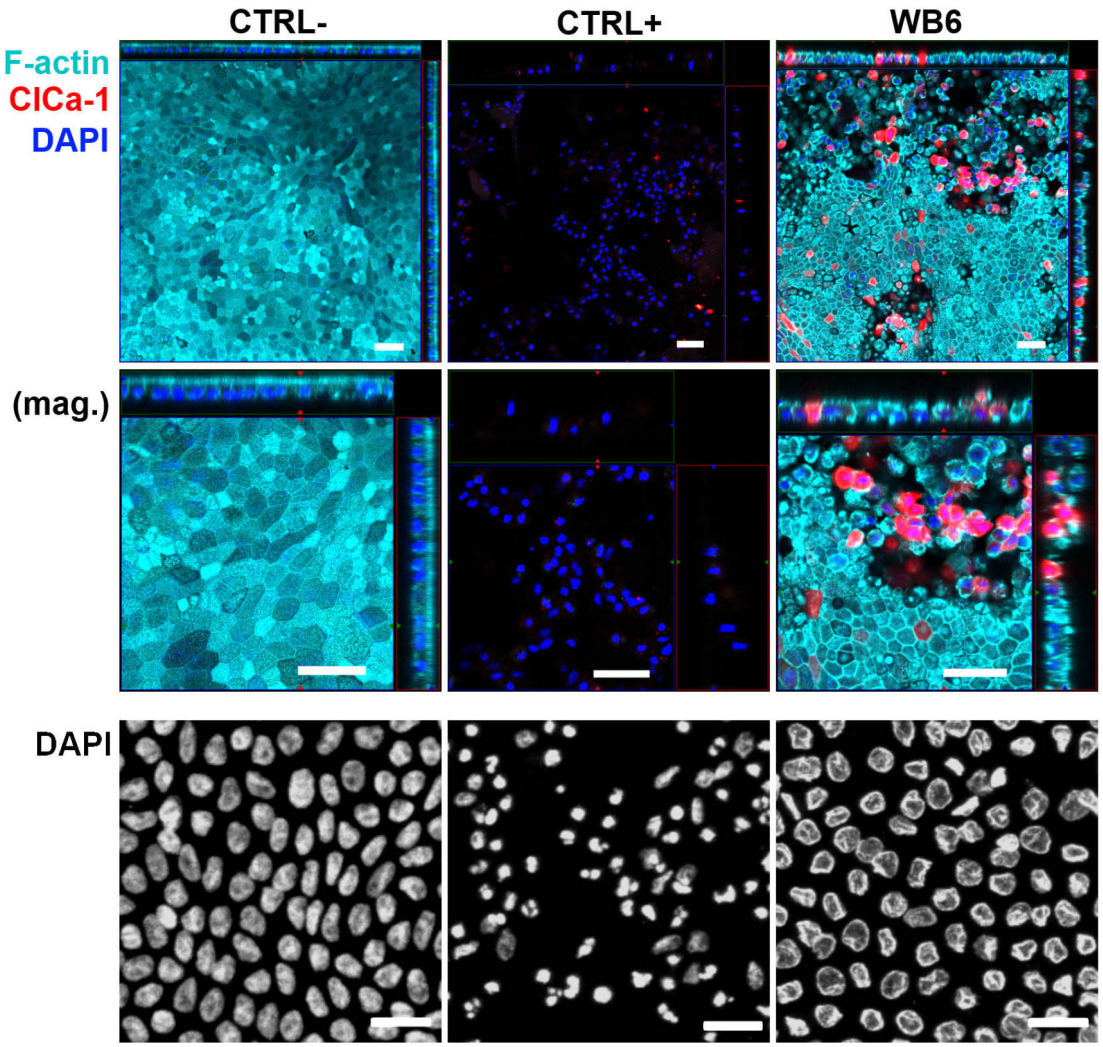


**Figure 37 ODM destruction, ClCa-1 and „hollow" nuclei phenotype.** Micrographs depict WB6-infected and uninfected ODMs. F-actin (cyan), ClCa-1 (red) and DAPI (dark blue, as well as white for better visualization in the bottom panel). Staurosporine (CTRL+) offered large areas without cells, and nuclei were shrinked and disintegrated. A WB6-infection after 72 h also showed areas of large monolayer destruction, however nuclei are not shrinked but offered a high degree of chromatin-condensation in the nuclear periphery, giving them a "hollow" appearance in IFAs. F-actin cytoskeleton was apparently completely disintegrated in the 2 mM staurosporine conditions and under *G. duodenalis* infection stress the clear brush border disappeared (compare lateral projections in the magnified (mag.) micrographs). Of note, many cells are positive for the GC-marker ClCa-1 in the infection conditions. Scale bars indicate 50 µm (top panel) and 20 µm (nuclei staining). Representative micrographs, n > 10.

Barrier dysfunction by monolayer destruction as well as loss of brush border features and the appearance of ClCa-1$^+$ cells were all linked to the usage of luminal mock medium TYI-S-33 (Figure 38). Therefore, all following experiments used apical TYI-S-33 substitution and differentiation medium DM-2 in the basal compartment of the transwell-filter systems.

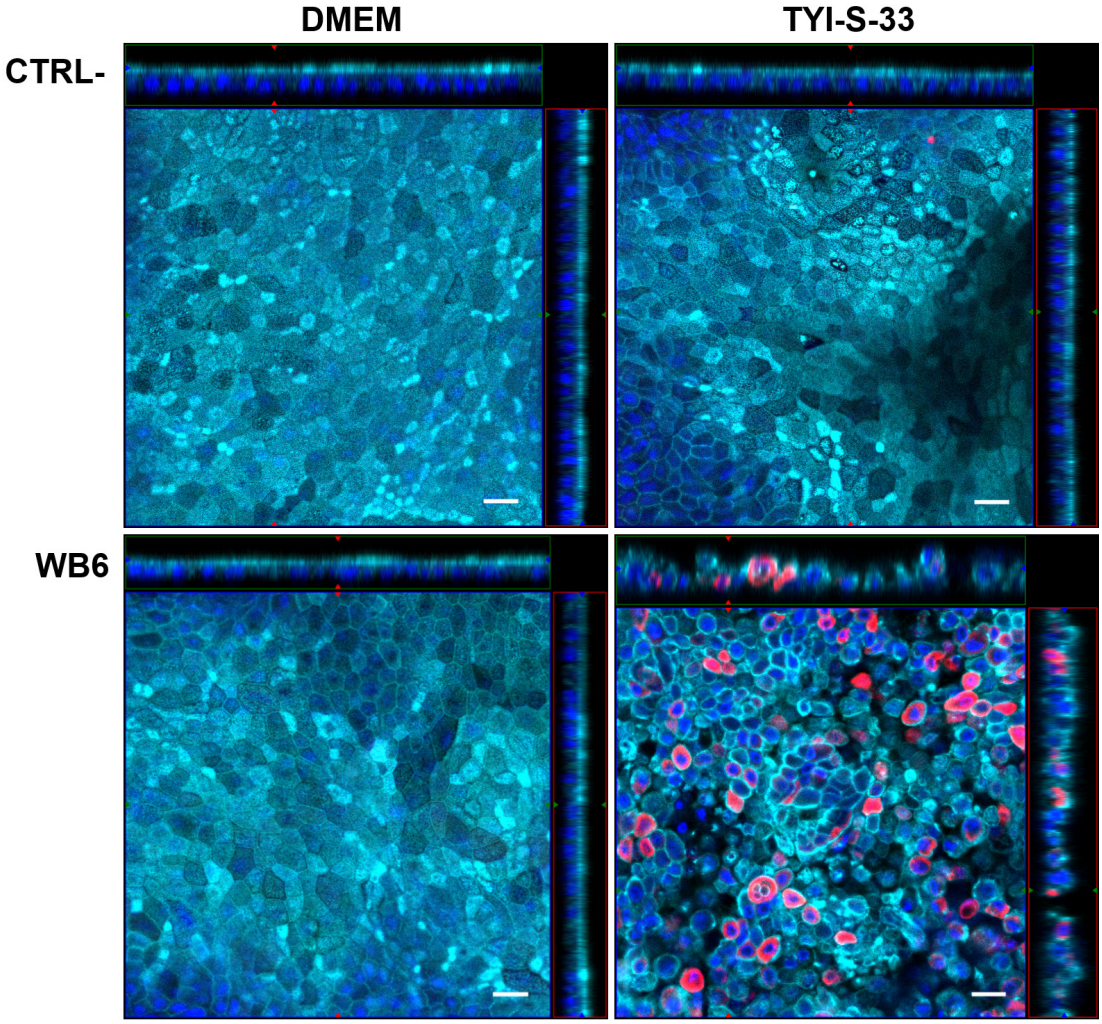


**Figure 38 Comparison of (infected) ODMs with apical DMEM or TYI-S-33.** Micrographs showing F-actin and ClCa-1 staining of infected and uninfected CBF1 ODMs with apical DMEM or TYI-S-33 medium. The basal compartments contained regular differentiation medium DM-2 (also in all other experiments). Only *G. duodenalis*-infections in the presence of TYI-S-33 led to monolayer destruction and ClCa-1 signals. Scale bars indicate 20 µm. Representative micrographs, n=3.

### 2.2.3.3 TEER decrease was reproducible with different *G. duodenalis* isolates

In order to investigate whether other *G. duodenalis* assemblages can induce barrier dysfunction in this new system, the comparative experiment on Caco-2 (2.1.2.6) has been partially repeated on ODMs with one representative isolate for every assemblage used before (Figure 39). All tested isolates led to monolayer destruction, even the cattle-specific P15/E. Therefore, the observed barrier dysfunction may be a general pathomechanism for *G. duodenalis* or even *Giardia* sp. parasites.

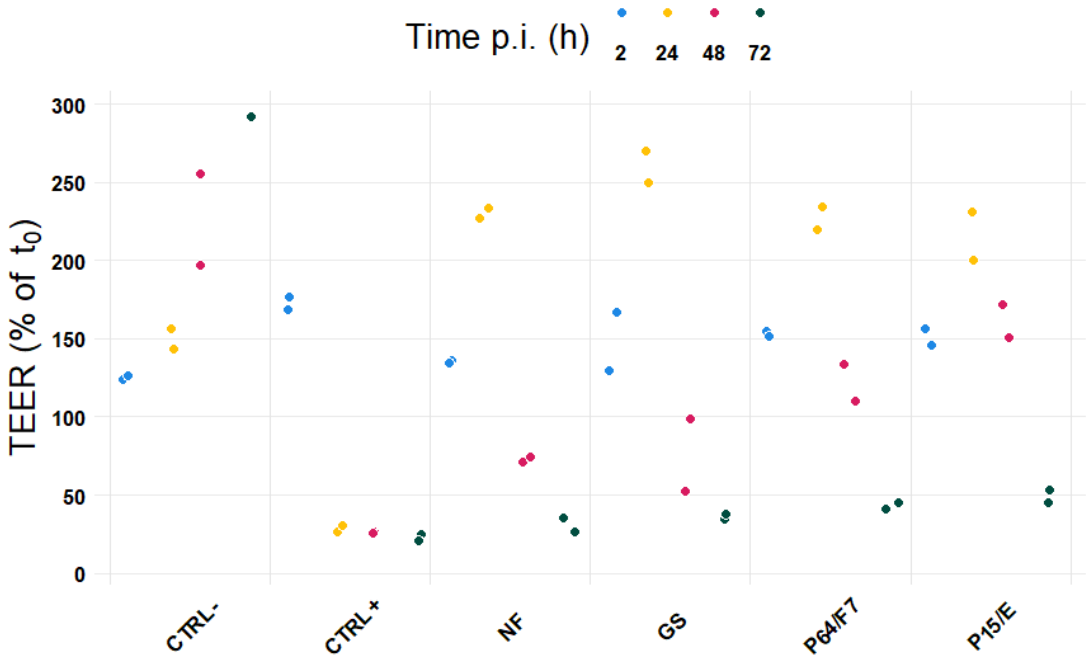


**Figure 39 *G. duodenalis* assemblage AI, AII, B, and E induced barrier dysfunction on ODMs.** TEER changes of ODM CBF1 monolayers, normalized to measurements before infection, are shown when infected with NF (assemblage. AI), P64/F7 (assemblage AII), GS/H7 (assemblage B), and P15/E (assemblage E) all in MOI 10. CTRL+ was 2 µM staurosporine. All tested isolates eventually led to a complete monolayer destruction. Of note, the uninfected control (CTRL-) showed a relatively high increase in TEER, which can be explained by low basic TEER values in the beginning. Data points represent individual monolayers, n=2. Time after infection is color coded. Absolute TEER was 97.6 $\Omega \cdot cm^2$ (SD 12.1 $\Omega \cdot cm^2$) at $t_0$. Appx. 18 contains relevant probability values (Tukey post-hoc test).

### 2.2.3.4 Parasite-induced TEER decrease was dose-dependent

To investigate a dose-dependency of the observed phenotypes, different MOIs of WB6 were compared (Figure 40). Lower infection levels with non-confluent attachment led to a milder TEER decline, however it could indicate both, a delayed effect or a response of lower magnitude. Regarding the confluent and over-confluent parasite loads, which led to simultaneous barrier breakdown with an almost identical pattern, suggests the attachment itself is a cause of, or connected to, the pathology. Therefore, the harmful effects on the epithelial barrier may start at the same time (independent of MOI) but concern only cells which are directly in contact with the parasite.

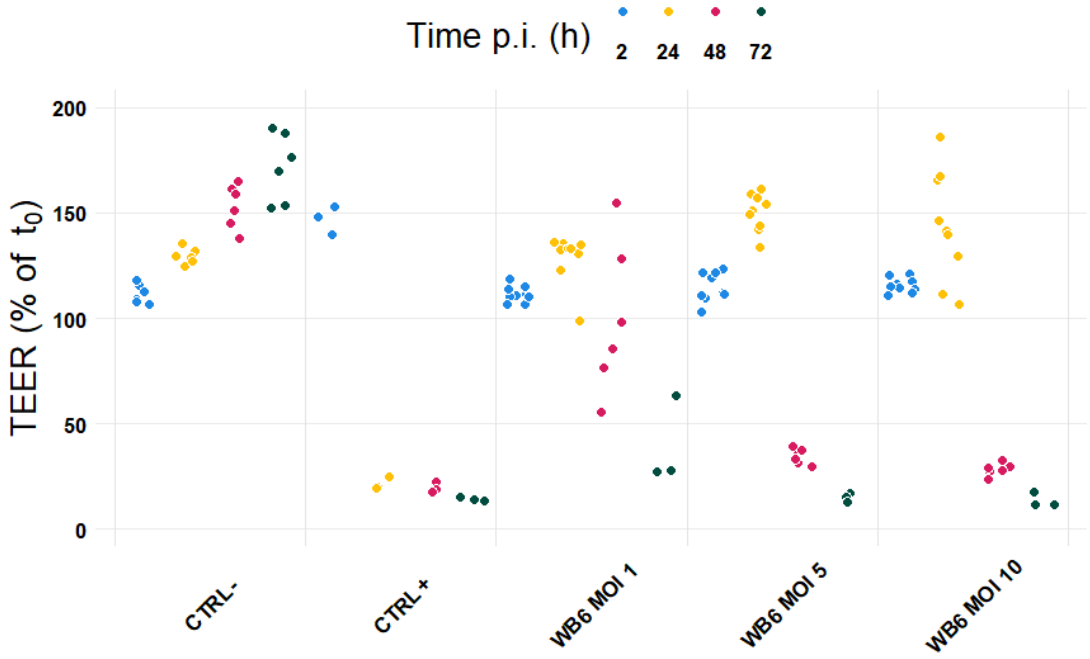


**Figure 40 Infection load dependency on ODMs.** TEER changes of ODM CBF1 monolayers, normalized to measurements before infection, are shown when infected with WB6 loads of MOI 1 (non-confluent attachment), MOI 5 (confluently attached layer of trophozoites), and MOI 10 (over-confluence). CTRL+ was 2 µM staurosporine. The TEER decline of both conditions with confluently attached trophozoites appeared to develop synchronously, indicating that direct *G. duodenalis* attachment is connected to barrier dysfunction rather than dose-related factors. MOI 1 featured a less pronounced impact on TEER but also led to barrier collapse eventually. Data points represent individual monolayers, n=3-9 (monolayers were sequentially removed for other analysis). Time after infection is color coded. Absolute TEER was 213.6 Ω·cm$^2$ (SD 26.6 Ω·cm$^2$) at $t_0$. Appx. 19 contains relevant probability values (Tukey post-hoc test).

### 2.2.3.5 Trophozoite vitality on ODMs

Due to the new luminal mock medium TYI-S-33, it is possible that *G. duodenalis* may offer now pathogenic effects due to increased viability. Indeed, the absence of almost any readings of dead trophozoites, up to 72 h, was observed (Figure 41). However, regarding that even Caco-2 DMEM conditions, less favorable for the parasite, did not significantly impacted trophozoite vitality within 48 h (Figure 13), a period in which barrier dysfunction took place in the TYI-S-33 ODM system, it is unlikely that diminished parasite survival can explain the absence of barrier impairment with the use of DMEM. It rather suggests that TYI-S-33 medium contains some sort of virulence-trigger, already hypothesized under section 2.1.2.9.

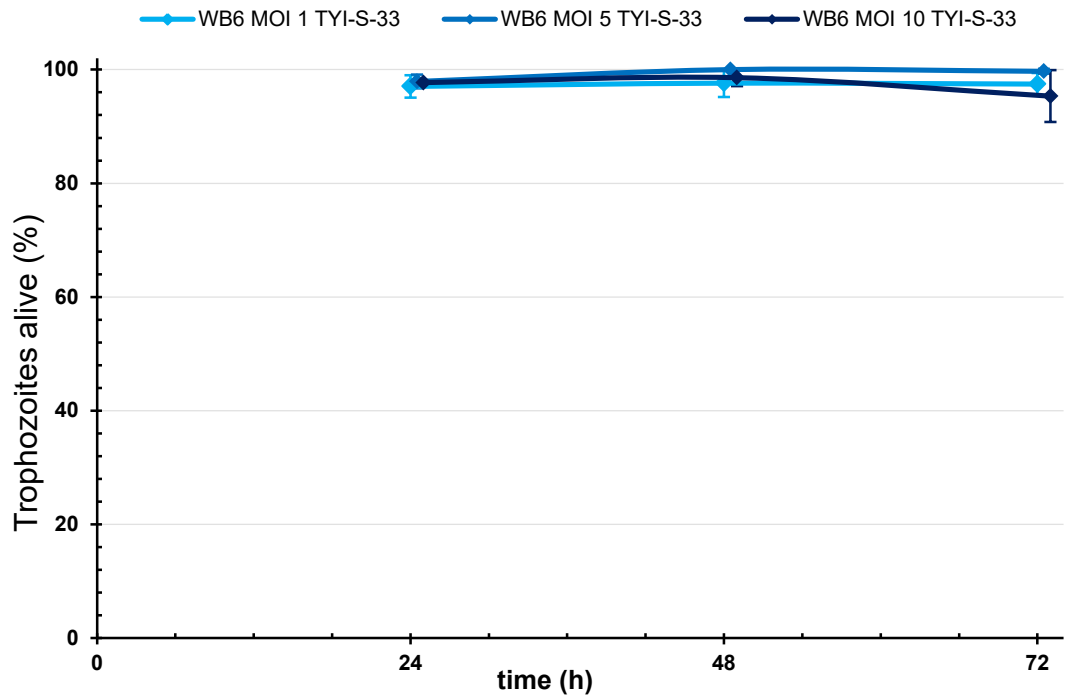


**Figure 41 Trophozoite viability with the new system.** Relative changes in WB6 viability (dye exclusion) of different parasite loads in the new model system (ODMs + apical TYI-S-33) were compared. Trophozoites kept their vitality with the new system until end of observation. More than 30 trophozoites were counted per condition and per n, n=3, error bars represent SD. Appx. 20 contains relevant probability values (Tukey post-hoc test).

### 2.2.3.6 Quantification of ODM cell death using TUNEL

As evidently in previously shown IFAs (Figure 37 and 38), severe monolayer destruction was taking place on *G. duodenalis* infected ODMs. This could be either, caused by cell death directly or by detachment of cells from the monolayer (and maybe secondary induced cell death e.g. anoikis afterwards). To investigate the extent of cell death, terminal deoxynucleotidyl transferase dUTP nick end labeling (TUNEL), a marker for apoptosis - although other kinds of cell death may be detected as well (Grasl-Kraupp et al., 1995; Torres et al., 1997) - was used (Figure 42).

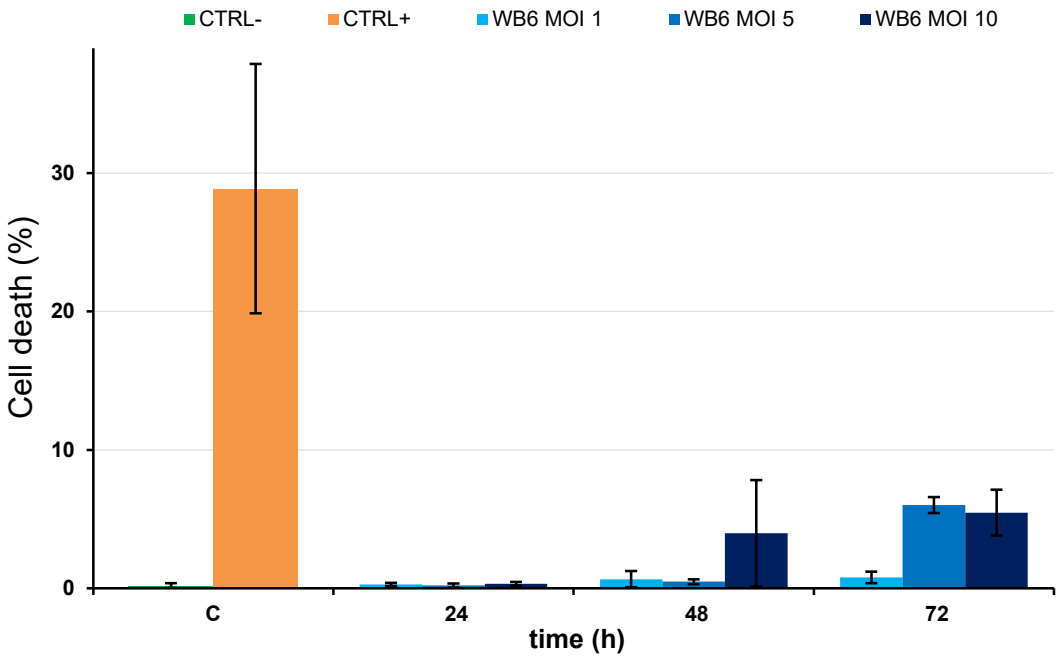


**Figure 42 *G. duodenalis*-induced cell death of ODMs, detectable by TUNEL.** Percentages of dead cells (TUNEL positive) were automatically counted and calculated from IFA micrographs. The effect of different MOIs (1, 5, 10) was compared up to 72 h. Controls were investigated after 72 h. An infection load of MOI 10 led to a significant ($p < 0,05$) increase in cell death after 48 h. The lower dose of MOI 5 only after additional 24 h ($p < 0,001$). Apoptosis-control with 2 µM staurosporine (CTRL+) can be considered as ~100% dead, however bar indicates only ~30%, which may be due to interference of advanced karyorrhexis with automated counting. Error bars represent SD, n=3. Appx. 21 contains relevant probability values (Tukey post-hoc test).

Interestingly, TUNEL$^+$ cells were counted in rather low numbers, indicating a cell death rate of only 6%. This is surprising regarding the striking phenotype of infected monolayers, however in line with other observations on human duodenal biopsies of chronically infected patients for example, which showed just 1,5% TUNEL$^+$ cells (Troeger et al., 2007). Therefore, apoptosis may not be the driving factor for the observed destruction.

### 2.2.3.7 Quantification of ClCa-1-induction

Another observation was the emergence of intense ClCa-1 signals in *Giardia*-infected conditions, whereas uninfected ODMs virtually lack those signals (Figure 37, 38, and 44). It is of particular interest because ClCa-1 is a reliable marker for mucin-producing cells in lung and intestine, specific GCs (Gruber et al., 1998; Gibson et al., 2005). Moreover, it has also been established as an Il-13-controlled key regulator of metaplasia towards mucin-producing cells (Alevy et al., 2012). This suggests that ODM cells in this work, which are assumed to consist mainly of (immature) ECs, could transform (metaplasia), or possibly residual ISCs could differentiate into GCs due to interaction with *G. duodenalis*.

A quantification of ClCa-1 signals is shown below (Figure 43). ClCa-1⁺ cells rise with time and trophozoite load up to ~16% in a pattern which slightly resembles the TUNEL signal data (Figure 42), which could indicate a connection. However, ClCa-1 signals do only occasionally overlap with TUNEL signals in an apparent random manner (Figure 44).

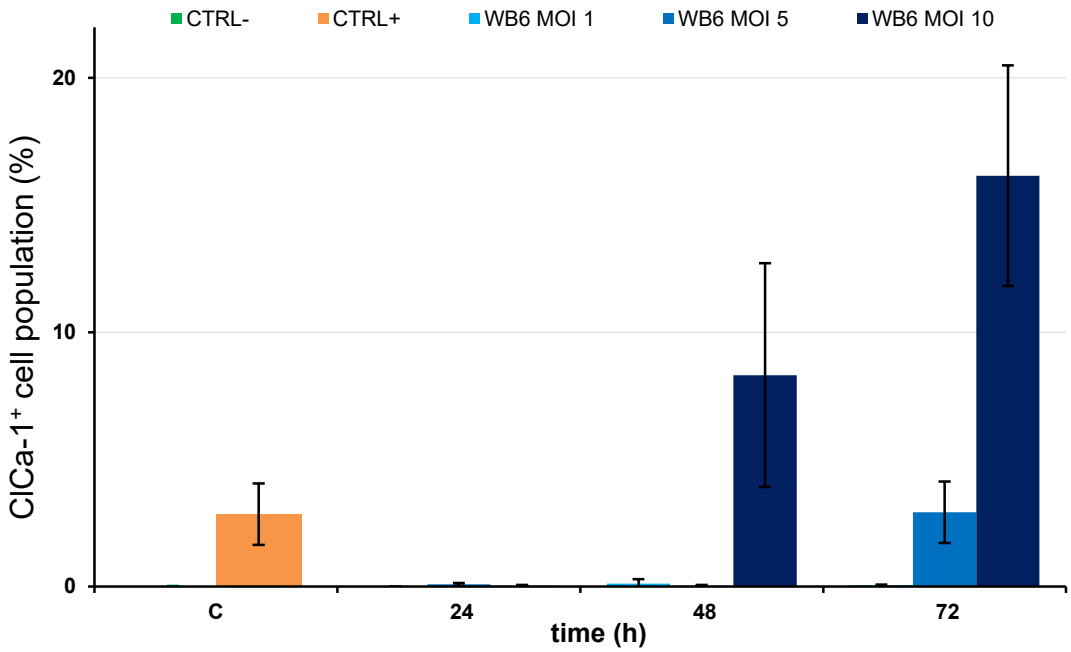


**Figure 43 *G. duodenalis*-induced ClCa-1 signal counts increased with severity of infection.** Percentages of ClCa-1⁺ cells were automatically counted and calculated from IFA micrographs. The effect of different MOIs (1, 5, 10) were compared up to 72 h. Controls (CTRL- and CTRL+) were investigated after 72 h. After 48 h an infection load of MOI 10 led to a significant ($p < 0{,}001$) increase in ClCa-1 signals, which further increased up to 16,2% after 72 h ($p < 0{,}001$). The lower dose of MOI 5 offered significant ClCa-1 signals after 72 h ($p < 0{,}001$). With the lowest infection load (MOI 1) no increase was observed. 2 µM staurosporine control (CTRL+) also offered some ClCa-1 signal counts, however, those were automatically included by the searching algorithm and may represent artifacts or background noise. CTRL- not plottable due to complete absence of ClCa-1 signals. Error bars represent SD, n=3-6. Appx. 22 contains relevant probability values (Tukey post-hoc test).

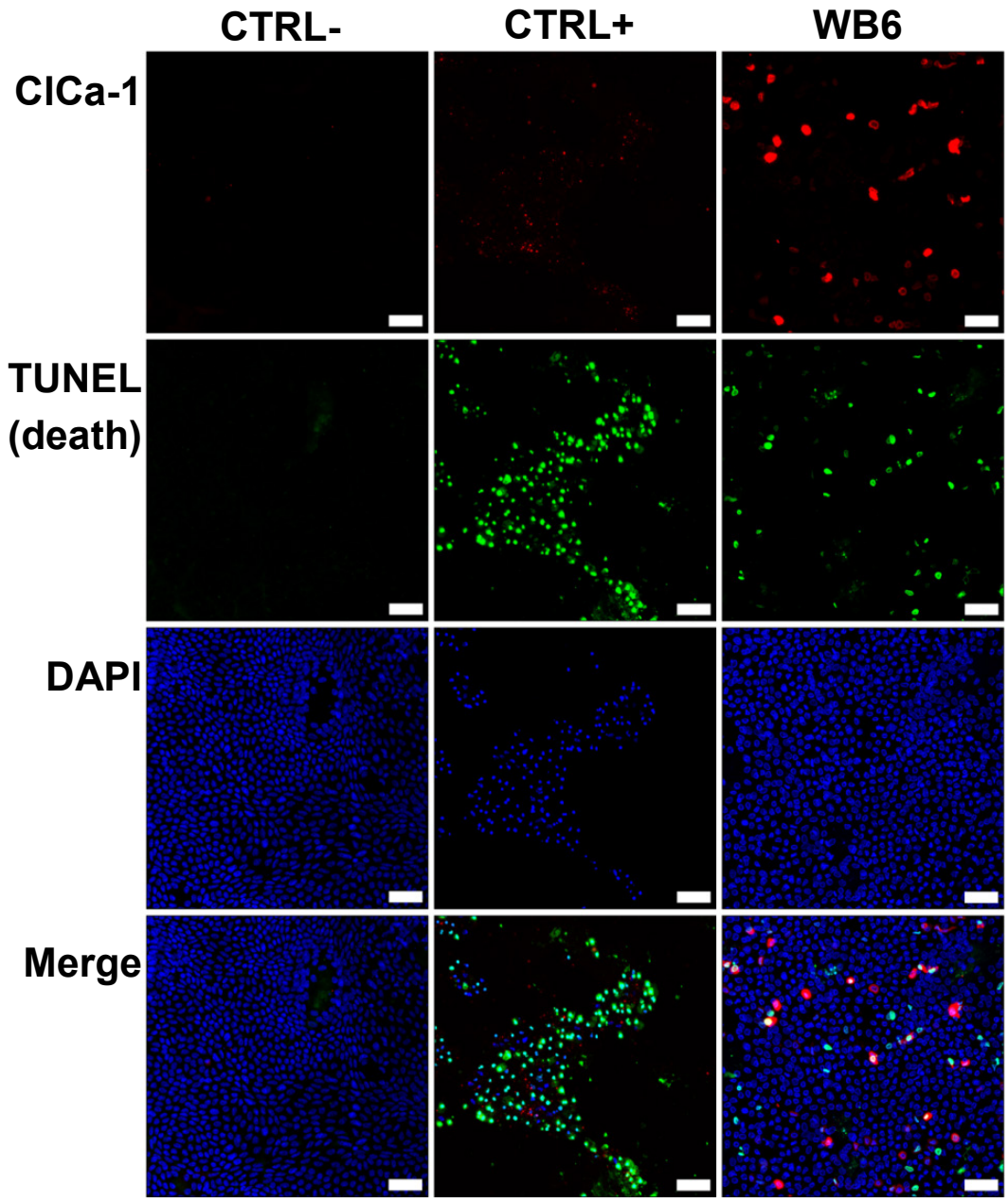


**Figure 44 TUNEL staining of *G. duodenalis*-infected ODMs.** Example micrographs of WB6-infected (MOI 10) and uninfected ODMs are shown. Marker for cell death (TUNEL) is colored in green, marker for GCs (ClCa-1) in red. TUNEL and ClCa-1 signals overlap only occasionally, suggesting no link between them. Scale bars indicate 50 µm. Representative micrographs, n=3

### 2.2.3.8 ClCa-1-induction was not connected to plain epithelial damage

Because of the hypothesized (but not directly cell-level-based) connection between emerging ClCa-1 and TUNEL signals in the previous section (2.2.3.7), it was speculated that monolayer injuries could trigger a damage response, leading to increased GC-numbers (ClCa-1$^+$) to enhance regeneration and protection of the mucosa. In order to test this hypothesis, a scratch assay was conducted by using small pipette-tips to physically damage ODMs (Figure 45).

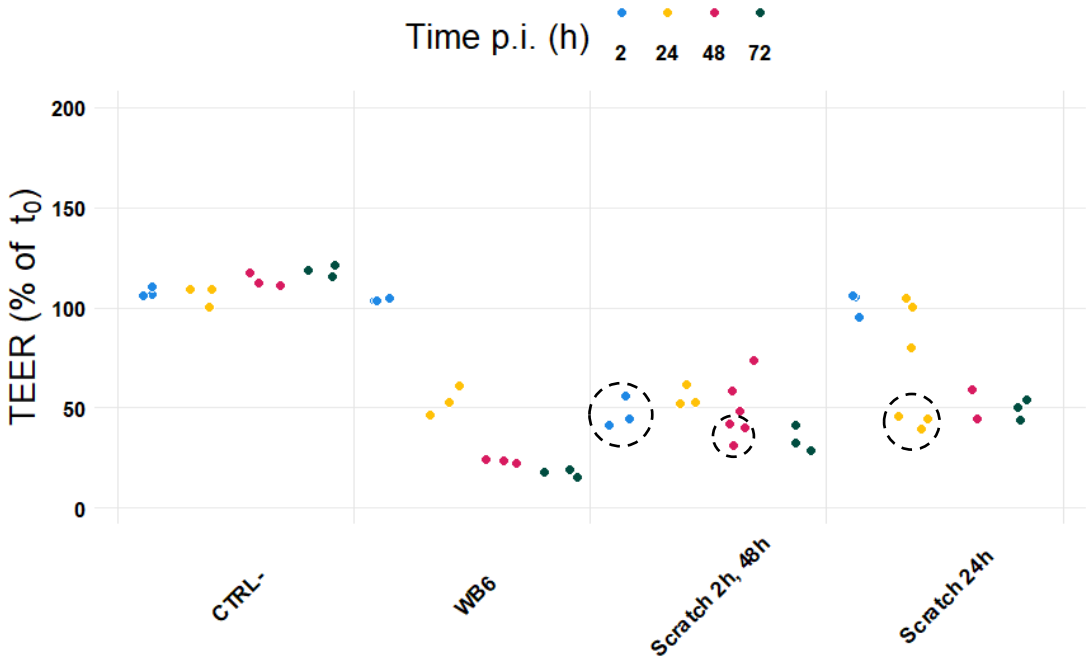


**Figure 45 Scratch assay damaged monolayers, resulting in decreased TEER.** TEER changes of ODM CBF1 monolayers, normalized to measurements before infection /scratch, are shown. CTRL+ was WB6 (MOI 10). Monolayers were scratched with 10 µl tips two times (after 2 and 48 h) or once (after 24 h), to ensure sufficient time and damage-intensity to induce potential GC generation. Clear TEER declines were observed after each scratching procedure (respective measurements indicated by dashed circles). Data points represent individual monolayers, n=3. Time after infection is color coded. Absolute TEER was 226.4 Ω·cm$^2$ (SD 15.2 Ω·cm$^2$) at $t_0$.

Scratching procedures were successful, however, by observing IFAs (Figure 46) no cells with increased ClCa-1 signals were found in the vicinity of the scratches. This suggests that GC metaplasia - or at least ClCa-1 expression - is not a secondary effect of epithelial damage.

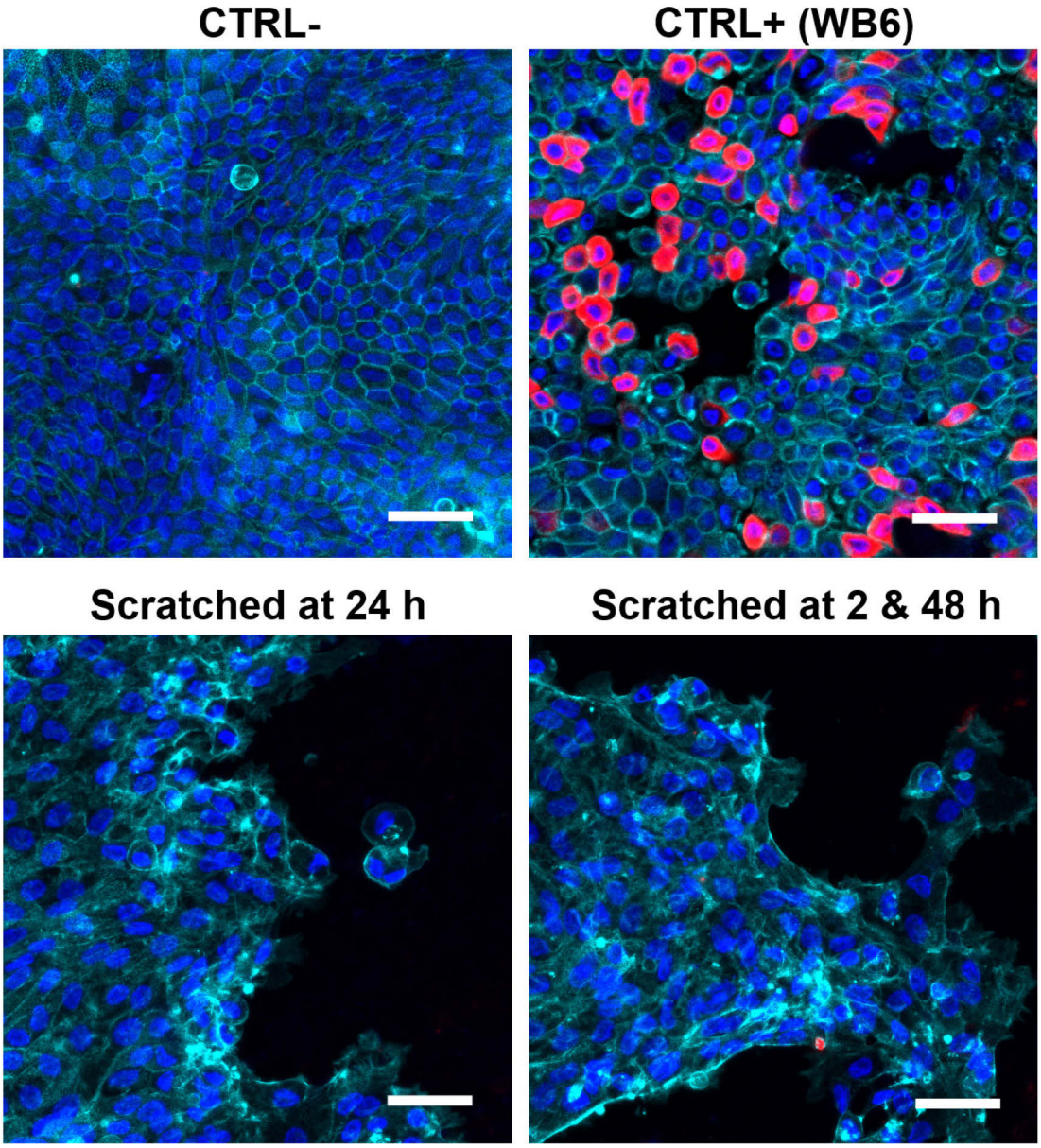


**Figure 46 No ClCa-1 inductions of scratched monolayers.** Micrographs showing F-actin and ClCa-1 staining of WB6-infected (CTRL+) and uninfected but scratched CBF1 ODMs after 72 h. ClCa-1 signals appear specific to *Giardia*-infections and are not detected at the edges of scratches. Scale bars indicate 50 µm. Representative micrographs, n=3.

### 2.2.3.9 Histological assessment of infected ODMs

Histochemical stainings, like previously described (Figure 32), were conducted, especially with the objective to find GCs, as suggested by ClCa-1 signals. Figure 47 shows *Giardia*-infection-specific cellular phenotypes, which are in line with lateral projections of IFAs shown before (Figure 37 and 38). Such are loss of microvilli, loss of cellular contacts, deformation, and the "hollow" nuclei phenotype. GCs could not be identified with neither, Alcian blue nor PAS stainings. However, it cannot be excluded that apparent cellular deformations prevented GC recognition.

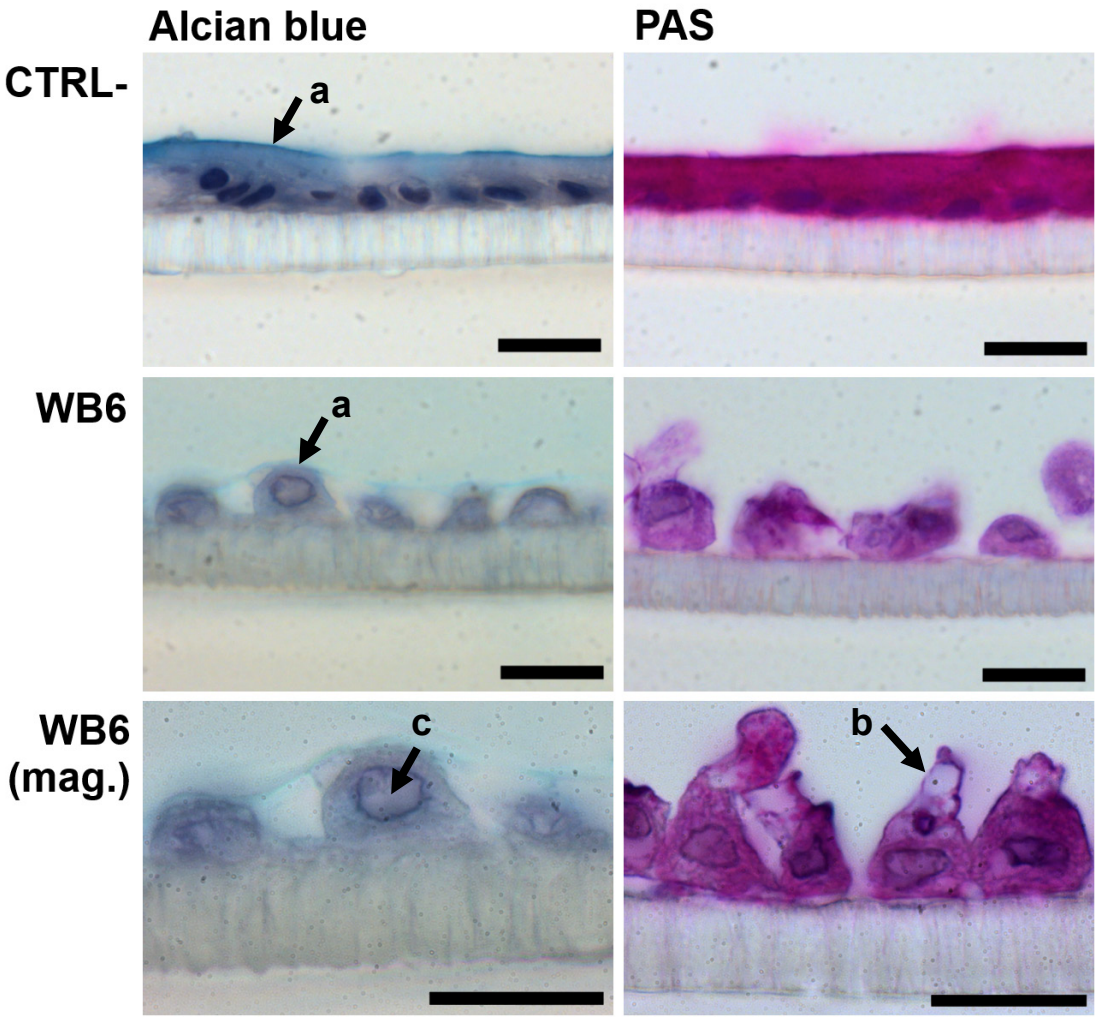


**Figure 47 Infected ODMs indicated loss of cellular contact sites and cellular organization.** Bright field microscopic images show lateral ODM sections, stained with Alcian blue (left), PAS (right) and DAPI (dark blue) after 72 h with or without WB6 MOI 10 infection. Observable was the loss of microvilli at the brush border (solid dark-blue line (a) of Alcian blue diminishes in infected conditions). Cells of infected ODMs possessed an excessive amount of apical membrane (b), probably because of membrane expansion due to loss of microvilli organization. Cells lost contact to their cellular neighbors as well. The distinct condensation of chromatin (c) was also observed as peripheral dark line on the nuclear envelope in infected conditions, which was in strong contrast to the whole homogenous staining of nuclei in the controls. 2 µM staurosporine (CTRL+) not shown, due to massive cell loss, probably increased by histochemical staining procedures. Scale bars indicate 20 µm. Representative images, n=3.

### 2.2.3.10 EM imaging of infected ODMs

To observe histological changes in more detail, TEM images were taken from infected and uninfected ODMs (Figure 48). All pathological phenotypes shown with bright field microscopy (Figure 47) can be found in TEM micrographs as well. Moreover, degradation of TJs and desmosomes suggests that cellular detachment is an induced (perhaps regulated) process. However, interference of necrotic processes cannot be excluded.

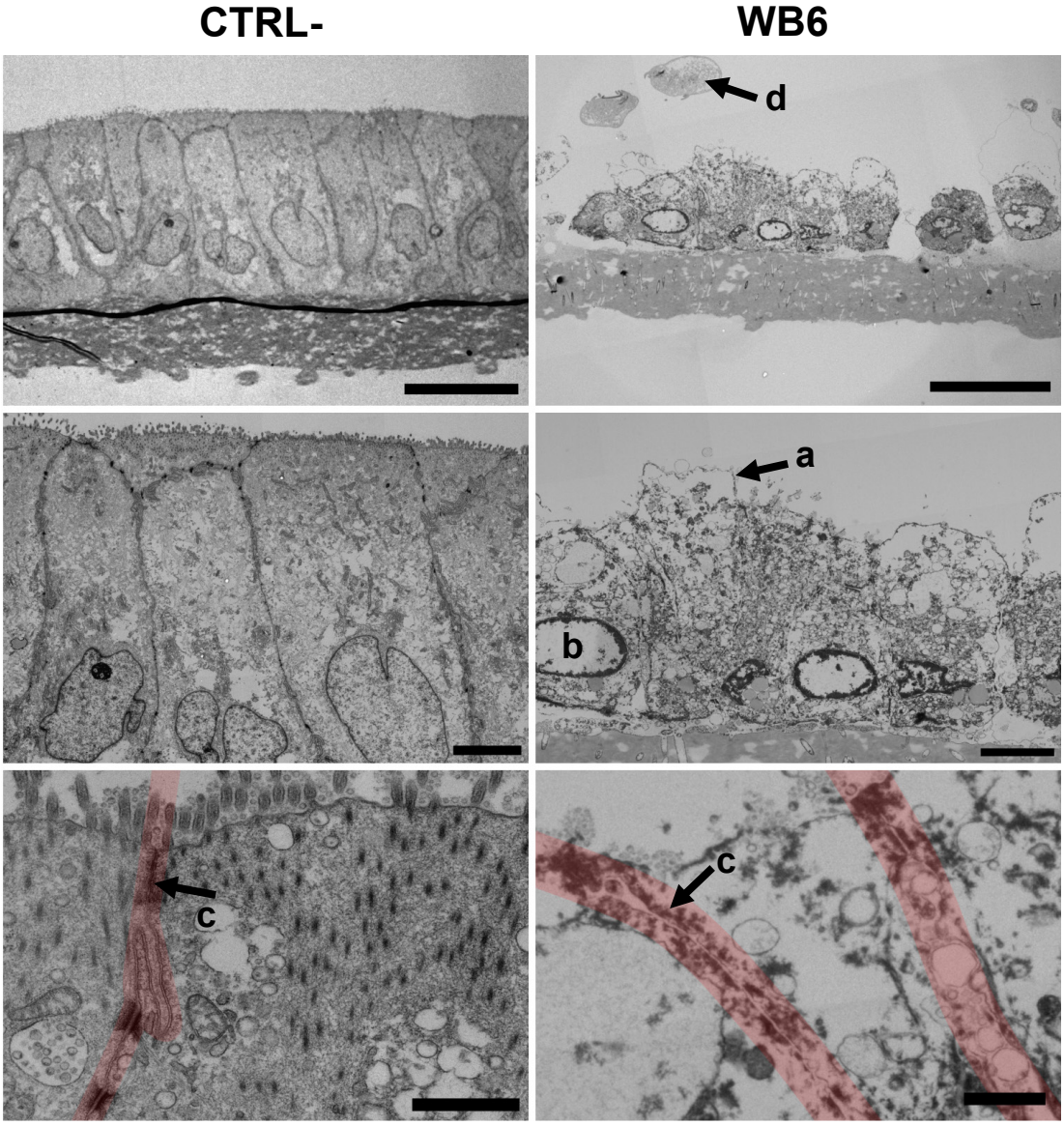


**Figure 48 TEM imaging of *Giardia*-infected ODMs suggested loss of TJ integrity.** TEM micrographs show ODMs after 72 h of WB6 MOI 10 infection and uninfected controls. With highest magnification, lateral membranes with cellular contacts are highlighted in faint red. Infections show a rather necrotic phenotype. Loss of microvilli, redundant apical membrane surface area (a), "hollow" (peripherally condensed) nuclei (b), and degradation of cellular contact sites (c) could be observed. Two trophozoites can also be seen (d). Scale bars indicate 20 µm (top panel), 5 µm (center panel), and 1 µm (bottom panel). Representative micrographs, n=3.

#### 2.2.3.11 Effects on ODM's tight junction complex

Since experiments of the previous sections suggested barrier dysfunction by tight junction impairment, IFAs were conducted similar to the Caco-2 experiments (Figure 10), on ODMs (Figure 49 and 50).

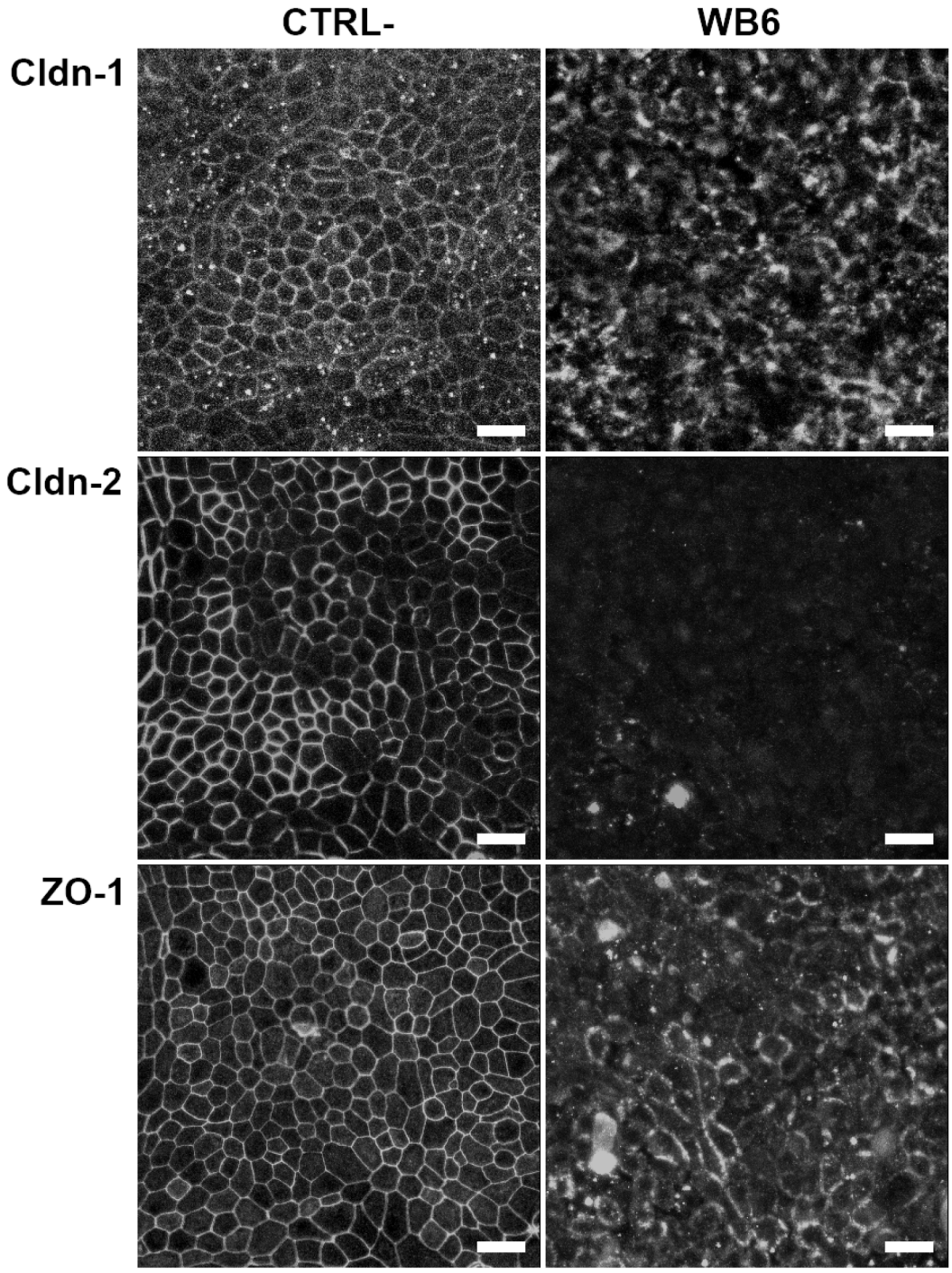


**Figure 49 Different TJPs of infected ODMs were differently affected.** Micrographs show uninfected and WB6 MOI 10 infected ODMs after 72 h with different TJPs. All TJPs showed the expected network-like pattern in the controls, however cldn-1 also appeared aggregated within the cytosol of some cells, which could indicate its presence in or at the aggresome or other cytoplasmic bodies. Interestingly, all three TJPs seemed to be differently affected by *Giardia*-infection. Whereas cldn-1 seemed to delocalize, cldn-2 disappeared almost completely, and ZO-1 offered an heterogenous disassembly from the TJs in which cells were differently affected. Scale bars indicate 20 µm. Representative micrographs, n=3.

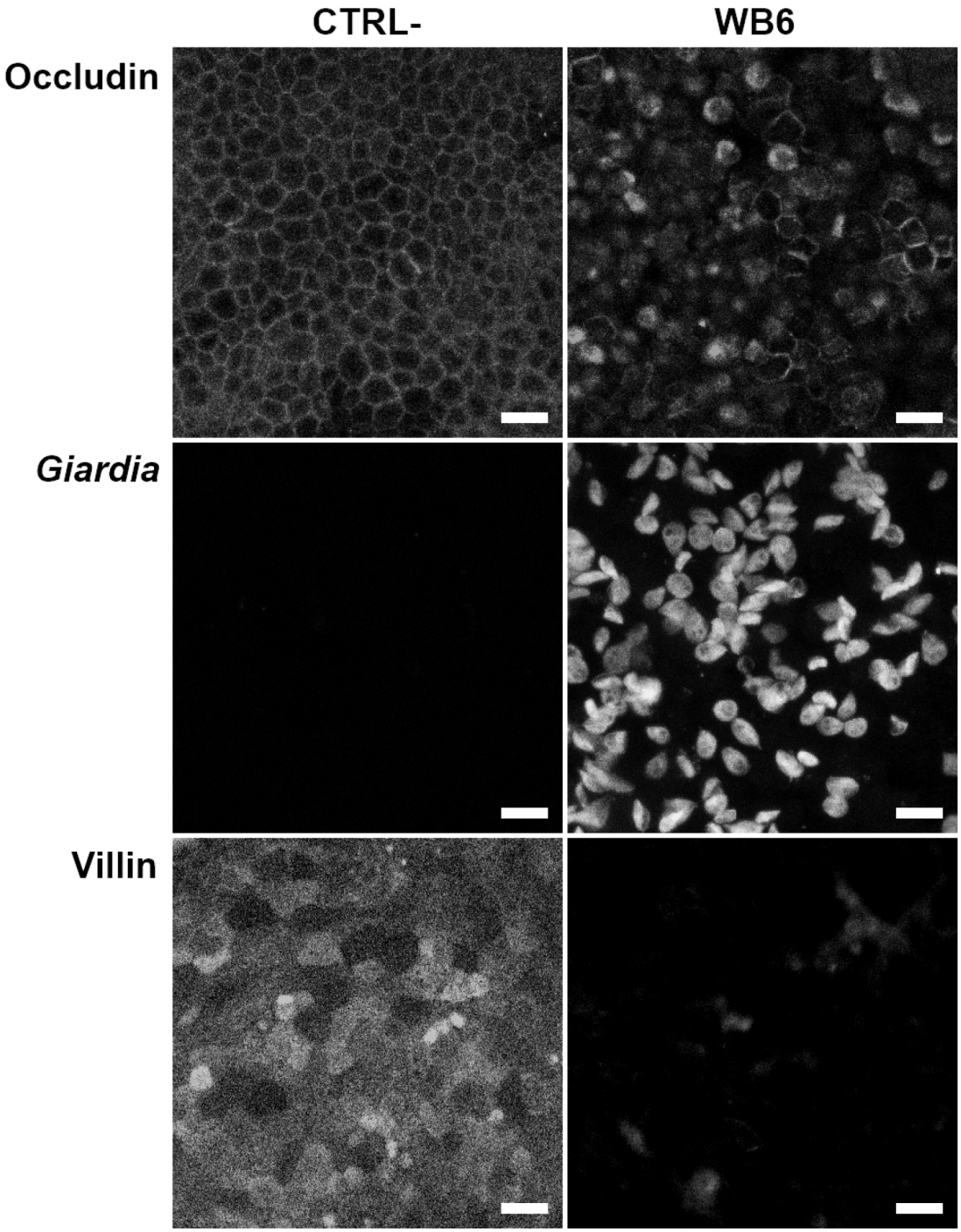


**Figure 50 Loss of villin signal indicated microvilli depletion.** Micrographs show uninfected and WB6 MOI 10 infected ODMs after 72 h. The TJP occludin, *G. duodenalis* trophozoites and the microvilli-specific protein villin are shown. Occludin was degraded or drawn from the membranes into the cytosol. Microvilli, as indicated by villin, disappeared (as also shown with F-actin, histochemistry or EM in previous sections). Scale bars indicate 20 µm. Representative micrographs, n=3.

Due to differently impacted TJPs, it can be assumed that those delocalization or degradation effects are at least in part regulated processes and not only a consequence of putative parasite-induced tissue damage.

### 2.2.3.12 ODM permeability, ion selectivity and transporter activity

Further permeability experiments were conducted at the Charité CBF together with Dr. Susanne M. Krug in a setup of Ussing chambers. TEER and permeability was validated (Figure 51), showing same parasite load- and exposition time-dependency as previous experiments (Figure 40 and others).

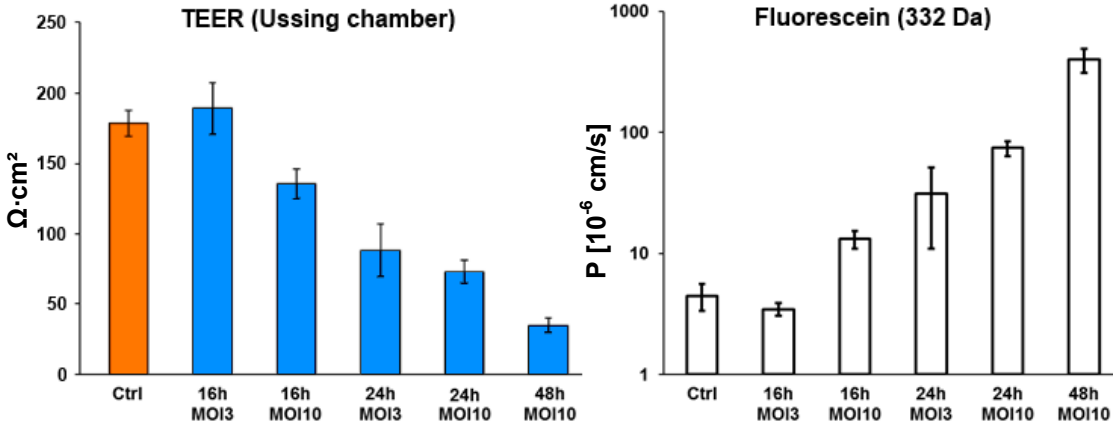


**Figure 51 Fluorescein permeabilities of infected ODMs recapitulates TEER data.** TEER changes of ODM CBF1 monolayers in Ussing chambers are shown in absolute numbers when infected with WB6 (MOI 3 and 10) as well as their paracellular leakage flux of fluorescein (log scale; calculated from samples taken every 10 min for a period of 40 min). TEER values were in line with previous chop-stick measurements and fluorescein fluxes recapitulated closely electric resistance measurements. Data provided by Dr. Susanne M. Krug. Error bars represent SD, n=3 (infections), 9 (Ctrl).

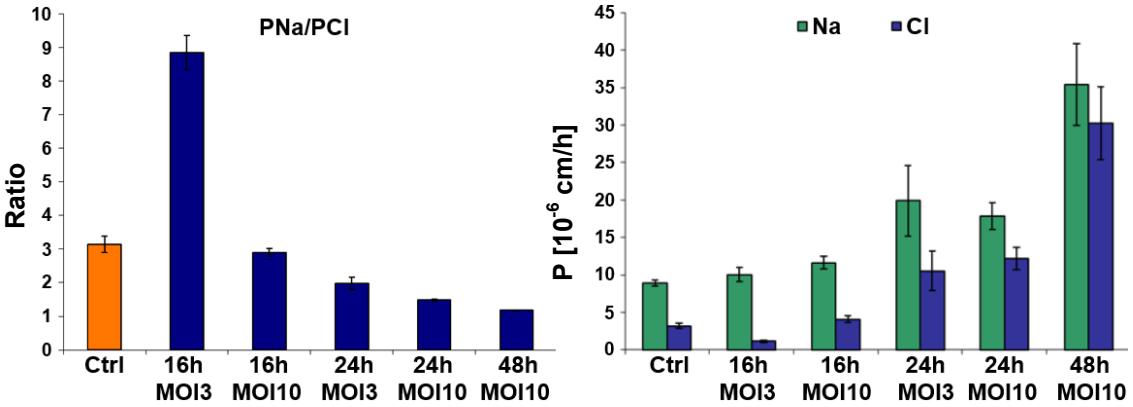


**Figure 52 Ionic permeabilities increased, selectivity decreased in relation to infection.** Ionic permeabilities (calculated from dilution potentials) of $Na^+$ and $Cl^-$ ions are plotted as ratio as well as directly. Interestingly, at MOI 3 for 16 h (before barrier breakdown could be measured), ODMs limited the passage of $Cl^-$ almost 3-times more than their uninfected counterparts, while $Na^+$ permeability remained unaffected. As barrier dysfunction started to take place, both anion and cation permeabilities increased and ionic selectivity decreased. Data provided by Dr. Susanne M. Krug. Error bars represent SD, n=3 (infections), 9 (Ctrl).

The increased ionic selectivity of infected, but not yet leaking ODMs (Figure 52), suggests a *Giardia*-induced change on ODMs leading to lesser anion permeability. If malign or on purpose is unknown.

By investigating short-circuit current ($I_{SC}$; not to be confused with ISC – intestinal stem cells), net ion transport can be measured. By stimulating or inhibiting certain ionic transporters, conclusions regarding their respective activity can be drawn (Figure 53). Like suggested by the previous experiments, altered ionic transport between uninfected, infected but intact, and infected and dysfunctional epithelial barriers could be observed, indicated by differences in basal $I_{SC}$. With ongoing stress of infection, ionic transporters became less responsive (reduced anion secretion) or in their activity ineffective due to loss of ionic gradients (e.g. NKCC) as a consequence of barrier leakage.

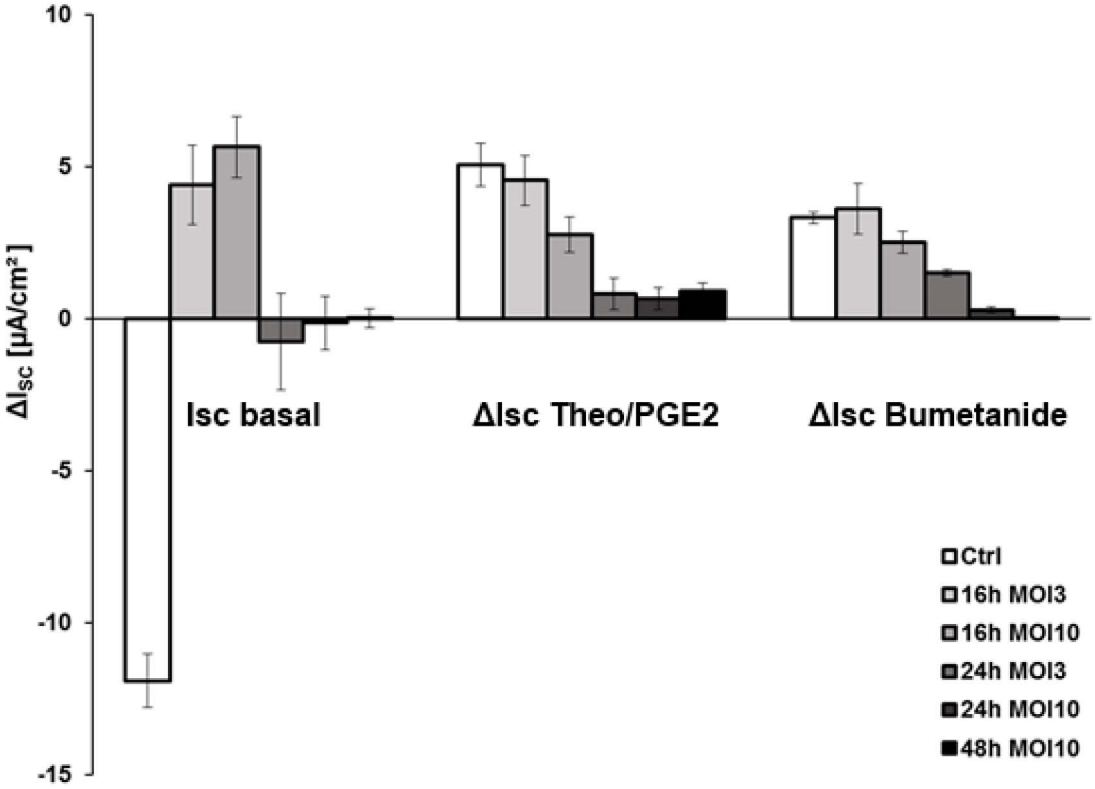


**Figure 53 $I_{SC}$ and ionic transporter function altered in *Giardia*-infected ODMs.** Basal as well as differential $I_{SC}$ values of WB6-infected and uninfected ODMs are shown. Theophylline/PGE2 stimulates anion secretion, bumetanide blocks Na-K-Cl cotransporter (NKCC). Basal $I_{SC}$ was different for infected ODMs, indicating altered ionic transport, which changed again by barrier breakdown, as also suggested previously (Figure 52). $Cl^-$-secretion by Theophylline/PGE2 stimulation was decreased with infection-stress in a dose/time-dependent manner. NKCC inhibition by bumetanide showed a similar pattern, indicating loss of $Na^+$-gradients. Data provided by Dr. Susanne M. Krug. Error bars represent SD, n=3 (infections), 9 (Ctrl).

# 3. Discussion

This work shows the absence of the acute symptomatic giardiasis phenotype of barrier dysfunction in the Caco-2 model system. By switching to an organoid-based primary culture model system the barrier dysfunction could be reproduced. Moreover, subtle effects like increased ClCa-1 expression, which could suggest the emergence of goblet cells, were found as well. Also, microvilli depletion, belonging to the malabsorption phenotype, which may even occur under inconspicuous colonization, was observed in the new model.

## 3.1 The irresponsiveness of the Caco-2 model towards *G. duodenalis* and the inconsistency between studies

The findings in this work (2.1.2-3) suggest no epithelial barrier compromising effects of diverse *G. duodenalis* isolates derived from stool samples of acute symptomatic patients, in the Caco-2 model used herein, which is in line with data of some previous studies (Chavez et al., 1986; 1995; Tysnes & Robertson, 2015), but is contradictory to others (Teoh et al., 2000; Humen et al., 2011; Maia-Brigagao et al., 2012). This discrepancy, which exists not only between *in vitro* studies on the Caco-2 model but seems also to be a general problem in any study type investigating *G. duodenalis* (as pointed out in section 1.1.2.1), may lead to the idea that *G. duodenalis*-infection alone is insufficient to cause the acute symptomatology of barrier dysfunction and additional factors are required, as also proposed by others (Bartelt & Sartor, 2015). Since several *in vitro* studies described barrier dysfunction phenotypes in their setups, it is possible that they included - wittingly or unwittingly - such (an) elusive factor(s) in their setups, which justifies a deeper analysis.

One factor is parasite load, which ranges from MOI 0,5 to 8 between and even within studies (Humen et al., 2011). In this work, the wide range of four orders of magnitude from MOI 0,1 (not shown) to very high parasite numbers such as MOI 100 (2.1.2.1-2) was used. No barrier dysfunction has been observed with TEER and TJ integrity as proxy. As the ODM model shows, a MOI of 1 is sufficient to induce notable barrier dysfunction within 72 h (2.2.3.4). Therefore, it seems unlikely that a kind of threshold in parasite load needs to be passed to manifest the barrier dysfunction phenotype in the Caco-2 model. There was, however, a consistent dose-dependent increase in TEER present, which offered a saturation effect past MOI 50 (Appx. 23). Such increase has been also described by others (Chavez et al., 1995).

To explain the TEER-increase, it was hypothesized that trophozoites' physical attachment could function as an ‘electric resistor’ by blocking electric current fluxes at the top of pores and channels of the epithelial monolayer, which was also speculated by others (Chavez et al., 1995; Teoh et al., 2000; Chin et al., 2002; Scott et al., 2002; Tysnes & Robertson, 2015). However, by using formononetin, an isoflavone and phytoestrogen of leguminous plants which can paralyze and remove trophozoites almost instantly without affecting their viability, presumably by interfering with microtubules or their associated motor proteins (Fisher et al., 2013), was not able to normalize increased TEER values, though treatment right at start of infections (to prevent even initial attachment) seemed to slightly reduce the effect’s magnitude (2.1.2.3). It cannot be excluded that this minor effect is due to potential interference of formononetin with the metabolism of the trophozoites (e.g. potentially affected intracellular substrate transport) and therefore not directly associated with detachment or attachment-prevention alone. Concluding, the cause of the increase in TEER is connected to trophozoites but is not due to physical obstruction of the electric flux caused by attachment of parasites to the monolayer. The increase itself may be a protective reaction of the host cells by enhancing tight junctional barrier properties e.g. by substituting pore-forming claudins with barrier forming proteins like claudin-1. Although not observable on Caco-2, ODM experiments suggested claudin-2 (pore-forming) to be the least abundant investigated TJP upon infection (2.2.3.11).

Artifacts introduced by treatment or measuring procedures could contribute to the inconsistent or conflicting results between studies as well. Several studies washed intensively Caco-2 monolayers with ice cold PBS to remove parasites (like done traditionally in axenic *in vitro* culture) and subsequently measured TEER (Teoh et al., 2000; Scott et al., 2002; Maia-Brigagao et al., 2012). The ice-cold shock can induce changes in the epithelial monolayer like cytoskeletal rearrangements and triggering of signal cascades (Fujita, 1999) or even direct damage (Fisher et al., 2013), especially with standard PBS (without $MgCl_2$ and $CaCl_2$) which depletes necessary ionic substrates for TJP integrity. Also, TEER measurement itself is temperature-dependent (Blume et al., 2010; Srinivasan et al., 2015). Own experiments also suggest the introduction of generally elevated TEER values with very high variances after ice-cold PBS washing steps, which took several hours to normalize (Appx. 25). Therefore, washing steps were not conducted in this work prior TEER measurements, only formononetin-treatment in some experiments. Studies which include cold washing procedures should be interpreted carefully as also suggested elsewhere (Fisher et al., 2013).

Other experimental setups tried to circumvent this issue by using sonicated lysates or trophozoite-conditioned medium but produced contradictory results as well. Caco-2 monolayers were shown to reduce their TEERs when exposed to,

for example, NF or S2 lysates after 24 h (Teoh et al., 2000). This could be explained by factors like proteases or other degradative enzymes from trophozoites intracellular compartments e.g. microvesicles (Evans-Osses et al., 2017), released by sonication or other lysis techniques (Buret, 2007; Cotton et al., 2011; 2014; Bhargava et al., 2015). In contrast, WB6 lysates and heat-inactivated trophozoites in this work, did not influence Caco-2 monolayers' TEER (2.1.2.4). TEER values of spent medium also did not differ from controls in this work (2.1.2.4), which is partially in line with findings of Humen et al. (2011), who noted that TEER decreases could not be triggered by spent medium. Those contradictory results could indicate that *G. duodenalis* trophozoites produce and release potential barrier-influencing effectors only under certain conditions or in response to a trigger factor, which was present in some studies but in others not.

The parasite itself can contribute to different experimental outcomes, since *Giardia* sp. isolates, especially regarding the heterogenous assemblage B, differ to each other, as also indicated by their various host preferences. Table 3 shows an overview of different isolates used in this and other works. Many studies, like this work as well, conducted experiments with WB6 (assemblage A) trophozoites. However, even with this isolate alone, results are contradictory. Surprisingly, all tested isolates in this work on Caco-2 monolayers offered the same non-barrier-compromising course regarding TEER (2.1.2.6). On ODMs, the final result of total barrier dysfunction after 72 h latest, was the same for all tested isolates, including non-human infecting P15/E, as well. It can still be hypothesized that different isolates lead to a different or differently severe outcome of the infection, however, the basically same behavior of all tested isolates within each model system suggest that the absence of pathological effects in the Caco-2 model is not due to isolate-related differences between studies.

Table 3: *Giardia* sp. isolates used in barrier-function *in vitro* or *ex vivo* studies

| Assemblage | *Giardia* sp. isolate | Used in study |
|---|---|---|
| A (AI or unspecified sub-assemblage) | NF | *; Teoh et al., 2000; Chin et al., 2002 |
| | PB | Chin et al., 2002 |
| | Portland-1 | Chavez et al., 1986 |
| | R-2 | Tysnes & Robertson, 2015 |
| | S2 | *; Hardin et al., 1997; Teoh et al., 2000; Buret et al., 2002; Chin et al., 2002; Scott et al., 2002 |
| | WB1267 | Humen et al., 2011 |
| | WB6 | *; Chavez et al., 1986; Chin et al., 2002; Humen et al., 2011; Maia-Brigagao et al., 2012; Tysnes & Robertson, 2015 |
| AII | P64/F7 | * |
| B | P344/B2 | * |
| | P387/C1 | * |
| | P413/H7 | * |
| | P424/A5 | * |
| | P458/E2 | * |
| | GS | *; Zhou et al., 2007; Humen et al., 2011; Chen et al., 2013 |
| E | P15/E | * |
| unknown | 10 clinical isolates | Chavez et al., 1995 |
| | 13 clinical isolates | Troeger et al., 2007 |

*used in this work

The fact that all tested isolates performed similar in the Caco-2 model suggests that the presence or absence of the hypothesized factor or environmental condition affects all isolates likewise or even *G. duodenalis* or *Giardia* sp. in general. To exclude decreased trophozoite viability or even death before pathogenic mechanisms come to effect, life/death- and reproduction-assays were conducted with the conclusion that enough parasites are alive to completely cover the Caco-2 monolayers under given conditions up to 72 h (2.1.2.5). Most studies describe pathological effects within 48 h (Teoh et al., 2000; Chin et al., 2002), at 24 h (Buret et al., 2002; Humen et al., 2011; Tysnes & Robertson, 2015), or even as early as 2 h post infection (Scott et al., 2002; Zhou et al., 2007; Maia-Brigagao et al., 2012). Unfortunately, they do not make statements concerning trophozoite viability in their setups. With regard to those parasite exposition times and the vitality data of *G. duodenalis* in this work, it can be concluded that insufficient parasite vitality is not responsible for the lack of pathological effects with Caco-2, although survival of trophozoites in TYI-S-33, as used in the ODM system, is indeed better and not negatively affected even at later stages (2.2.3.5).

The medium composition seems to be a key parameter in *Giardia*-infection experiments, as clearly evidenced by the ODM model in this work (2.2.3.2). However, other authors, describing barrier breakdown, only used DMEM for Giardia-Caco-2-interaction (Teoh et al., 2000; Buret et al., 2002; Chin et al., 2002; Humen et al., 2011; Maia-Brigagao et al., 2012). Any kind of potential supplements to this were not mentioned in any study. It is confusing that

TYI-S-33 seems to be the responsible factor to induce barrier dysfunction in the ODM system but is not a requirement in other Caco-2 studies. Unfortunately, TYI-S-33 medium cannot be tested with the Caco-2 model because it has devastating effects on such monolayers (2.1.2.9) – as also remarked by others (Chavez et al., 1986). It can be speculated that ODMs, as genetically intact primary cultures can cope with this stressful medium better than the colorectal cancer-derived Caco-2 cells. TYI-S-33, designed to mimic intestinal luminal fluid to allow axenic *E. histolytica* and later *G. duodenalis* cultivation (Diamond et al., 1978), contains besides usual basic medium ingredients like salts, sugars, proteins (peptone), and serum (10% FBS) also bile acids and cysteine (Keister, 1983). Especially the high amount of cysteine (16,5 mM; compared to 0,2 mM in DMEM or ~0,1 mM in human serum)[19], used to bind reactive oxygen species (ROS) due to its antioxidative properties, may represent the problematic ingredient for Caco-2 cells. Since the reductive potential *in vivo* is balanced by high amounts of glutathione (GSH/GSSG ratio; Schafer & Buettner, 2001) and not its precursor cysteine (cystine/cysteine ratio), glutathione may offer a better alternative to establish an environment free of oxidative stress. This should be tested in future works.

Another method to prevent or decrease oxidative stress is to use oxygen-deprived incubation conditions. Most effectively would be the usage of the two compartments with an anaerobic environment on the apical side, mimicking the luminal situation and supporting the parasite, and tissue-physiological oxygen conditions at the basal area to support the epithelial monolayer. However, this is a challenging setup which requires customized apparatuses beyond the scope of this work. Instead, experiments with general oxygen-deprivation were conducted, but no pathological effects within the expected time frame (2.1.2.10) were found. Monolayers collapsed eventually at later time points due to hypoxia. This suggests that oxidative stress is not the factor which prevents parasite virulence in the Caco-2 model. Furthermore, none of the mentioned studies used anaerobic or microaerobic incubation conditions. Interestingly, oxygen-deprived monolayers react with increased TEER values. It could be speculated that this is also a possible explanation for the consistent dose-dependent but saturatable TEER increase measured on *Giardia*-infected monolayers, because *G. duodenalis* is known to scavenge oxygen to a certain degree (Lloyd et al., 2000; Tovar et al., 2003; Ma'ayeh et al., 2015; Mastronicola et al., 2015).

Since described pathological effects for *Giardia*-infections, like apoptosis, could be masked by anti-apoptotic factors or apoptosis inhibitors, which are known

[19] Cysteine is known to become toxic to mammalian cells in concentrations exceeding serum levels (Janáky et al., 2000).

serum components (Zoellner et al., 1996), medium with and without 10% FBS was compared in infection experiments. However, results indicated no difference in outcome (2.1.2.7). Authors who described pathological effects with *G. duodenalis* used 5% FBS (Teoh et al., 2000; Buret et al., 2002; Chin et al., 2002), 10% FBS (Maia-Brigagao et al., 2012), or no FBS at all (Humen et al., 2011), suggesting no significant or at least no decisive influence of FBS in *G. duodenalis in vitro* infections.

Another apoptosis-masking effect could be initiated by the sodium-dependent glucose cotransporter (SGLT)-1, which has been shown to inhibit apoptosis in Caco-2 cells under high glucose conditions such as present in standard DMEM (Yu et al., 2005; 2008). However, this scenario is unlikely to took effect if the parental Caco-2 line was used, like in most studies on Caco-2 (Teoh et al., 2000; Humen et al., 2011; Maia-Brigagao et al., 2012; Tysnes & Robertson, 2015), because this parental line does not express SGLT-1 in relevant amounts in contrast to the bbe subpopulation (Turner et al., 1996; Yu et al., 2008; Steffansen et al., 2017). Moreover, data of the Caco-2 bbe line in this work show with low glucose conditions, comparable to Yu et al., not significantly different TEER values when compared with cultures using normal DMEM (2.1.2.8). Therefore, effects of anti-apoptotic SGLT-1 activity are also not the reason for negative outcomes in this work's Caco-2 model but could be a confounder in other studies.
According to Thaiss et al. (2018), hyperglycemia can induce barrier dysfunction by transcriptional reprogramming via another important glucose transporter (GLUT2). In an attempt to investigate whether or not an overshoot of glucose could be decisive for *G. duodenalis* to enable its virulence, or glucose-stressed epithelium more susceptible for barrier leakage, very high glucose conditions (in levels only found in comatose diabetes patients) - as suggested by Thaiss et al. - were tested. However, no significant differences in outcome were found (2.1.2.8). It should be noted that other aspects of the study from Thaiss et al., like their assumption of GLUT2 as being responsible for the effects in their Caco-2 experiments can be questioned, since GLUT2 is usually not yet expressed in the 7-day old Caco-2 cells they used (Mahraoui et al., 1994; Mesonero et al., 1994; Baron-Delage et al., 1996). Also, the effects on TJPs they describe (e.g. undulated cellular contacts) are probably due to their Caco-2 cultivation method on plain culture surface instead of transwell-filters, leading to artifacts as shown in Appx. 26. By trying to reproduce ZO-1 alterations according to Thaiss et al. (2018), on plain culture plates as well as transwell-filters, the degree of undulated ZO-1 correlated only with the culture surface, but not with glucose level or *G. duodenalis* infection (not shown). Additionally, ODMs incubated under high glucose conditions - infected with *G. duodenalis* or not - also did not show barrier dysfunction or proposed TJ alterations (2.2.3.1).

Another interesting confounder may be the "Giardia lamblia virus" (GLV), which is to date the only known virus to infect (some) *G. duodenalis* isolates (Miller et al., 1988; Sepp et al., 1994) and is related to the *Leishmania*-specific "Leishmania RNA virus-1" (LRV1), which is known to influence severity of leishmaniasis (Ives et al., 2011). It was speculated that also GLV could influence *G. duodenalis* to change the course of giardiasis. However, no correlation regarding GLV infection of *G. duodenalis* isolates to symptomatic or asymptomatic patients were found in the past (Jonckheere & Gordts, 1987). Also, data in this work suggest that (missing concomitant) GLV-infection of trophozoites is not the reason for absence of barrier dysfunction phenotypes (2.1.2.11). Apart from the specific GLV-experiment, no *G. duodenalis* isolate in this work carried GLV. Unfortunately, GLV-infection status of the *G. duodenalis* isolates used by others, was not assessed in any other study on this topic. Considering that in some studies about half of the tested *G. duodenalis* isolates which were collected in different countries are $GLV^+$ (Jonckheere & Gordts, 1987), this virus could still be of relevance even if a potential impact could not be revealed (yet).

The differentiation time of Caco-2 cultures represents an additional confounding factor in this model system. Although Caco-2 reach a plateau phase in TEER at approximately 14 days after seeding (as also shown in this work, 2.1.1), cells are still heterogeneously polarized and differentiated, transitioning to a more homogenous state after more than 30 days of confluent incubation (Vachon & Beaulieu, 1992). Because most of the enterocyte markers are expressed at day 21, and functional differentiation (e.g. enzyme marker) does seemingly not correlate with morphological differentiation (e.g. polarization), the 21-day rule has been established as best compromise (Sambuy et al., 2005; Srinivasan et al., 2015). Unfortunately, many authors do not comply with that rule. Shorter differentiation periods like 5 days (Teoh et al., 2000; Buret et al., 2002), 7 days (Chin et al., 2002), or 14 days (Humen et al., 2011) after seeding are more common. It could be speculated that less differentiated Caco-2 monolayers are more susceptible to disturbing stimuli, or the opposite, if pathogenesis of *G. duodenalis* is linked to a certain enterocyte protein or receptor which is expressed only in fully differentiated monolayers. Either way this could also explain the disparate results in seemingly similar studies (Teoh et al., 2000; Humen et al., 2011; Maia-Brigagao et al., 2012). However, Caco-2 experiments in this work suggest no differences in outcome between standard (21-day) and premature (7-day) differentiation periods (2.1.2.7).

Lastly, Caco-2 cells themselves are a source of potential bias due to their inherent heterogeneity, leading to changes in cell proportions e.g. via bottle-neck effects during the process of passaging (Sambuy et al., 2005). To counteract, several clonal Caco-2 subpopulations have been derived from the parental line with the goal to create a stable population by using more

homogeneous clones, like the Caco-2 bbe subpopulation used also in this work. However, those aging effects may be delayed but are still present even in those Caco-2 populations, as shown here (2.1.1) and elsewhere (Lu et al., 1996; Briske-Anderson et al., 1997; Yu et al., 1997). Moreover, the possibility to select cells with a certain phenotype to create custom Caco-2 lines further increased the complexity of this model and, together with the aging effects, it can be almost assumed that every lab - at a chosen time point - has its own version of the Caco-2 line, as suggested by e.g. basic TEER ranging from ~160 $\Omega \cdot cm^2$ (Teoh et al., 2000) to >1200 $\Omega \cdot cm^2$ (Scott et al., 2002) even in the same(!) lab. Therefore, making comparisons and reproduction of results difficult and questionable.

### 3.1.1 Conclusions from the Caco-2 model

Summarizing, although Caco-2 (bbe) is considered the most suitable cancer-derived cell line to mimic the small intestine and is therefore widely used in different bio-scientific fields, the various confounding factors hidden in details of this model system's application, as well as its own cell-determined limitations, led to the conviction that a robust Caco-2-based model system to simulate the barrier breakdown phenotype of acute *G. duodenalis* infections is not available. Barrier dysfunction studies on *G. duodenalis* differ in so many methodological aspects - and also/therefore regarding their findings - that none of them can be fully compared to another. This work is to date the most elaborated study regarding those (subtle) confounder variables in *G. duodenalis in vitro*-infection setups and investigated several key variables different between such studies (results also published as Kraft et al., 2017). Although many of those variables have the potential to influence the course and outcome of the functional *in vitro* correlate of acute *G. duodenalis* infections, none of them led to an actual barrier dysfunction. Also, no significant differences in CCL20 expression (2.1.3) or elevated levels of other cytokines (Appx. 11) were observed. However, whether or not this may be due to immune-modulatory features of the parasite (Kamda & Singer, 2009; Cotton et al., 2014; 2015) cannot be excluded. Intriguingly, the only condition which enables *G. duodenalis* to obviously harm or destroy the monolayers was the luminal-mock medium TYI-S-33, which was only observed with the ODM model, since, as data suggests, undiluted TYI-S-33 cannot be used together with Caco-2 and for the Caco-2 monolayer acceptable 50% dilutions did not trigger *G. duodenalis* to break the epithelial barrier. It is confusing that studies, differing in several variables, were able to show *Giardia*-induced barrier disruption on Caco-2 (albeit dissimilar or even contradictory in severity, mechanism, and affected TJPs including the pathological phenotype), but this work is not. It raises the hypothesis that a very

basic decisive factor is present in those studies and missing here. It seems that TYI-S-33 could be this factor, however none of the comparable studies ever described its usage in their Caco-2 infection setups.

## 3.2 Results of the new ODM model

The attained experiences with the shortcomings of the Caco-2 model and its unstandardized use by the field, reveals the requirement for a more sophisticated and robust model system to simulate the human small intestinal epithelium. Organoids, as the most recent development in cell culturing, promises the opportunity to establish stable primary cultures with a - theoretically – unlimited potential for growth. Based on small intestinal organoids, or rather their stem cells, monolayers can be derived and used in a transwell-filter setup, likewise traditional monolayers, as the here designated ODM model.

### 3.2.1 ODM model characteristics

By seeding stem cells from spheroid cultures on Matrigel®-coated transwell-filters, duodenal ODMs could be generated reliably and with sufficient consistency (2.2.1.3). Growth to confluence was achieved very fast and distinct morphological and protein-markers for polarization showed up already at day 3 after seeding (2.2.2.1 - 2.2.2.2), which has been also observed for duodenal ODMs by others (Kozuka et al., 2017; implied) as well as ileal and rectal ODMs (VanDussen et al., 2015). Even more, a thick and highly branched glycocalyx developed on and between microvilli (2.2.2.2), unlike reported on any carcinoma-derived cell line but highly resembling what is featured *in vivo* (Frey et al., 1996; Giannasca et al., 1996). Additionally, all under 1.2.1.2 described cellular contact sites can be found and especially proteins of the TJ, determinants of barrier properties like cldn-1 (as barrier forming example), cldn-2 (as pore forming example), and ZO-1 (as example for cytosolic TJ integrity and proper architecture), are present in ODMs (2.2.2.2). Also, measured basic TEER values (2.2.2.2) are comparable to Caco-2 (2.1.1), ODMs of others (Kozuka et al., 2017), and also reasonable regarding data of *ex vivo* biopsies[20] (Srinivasan et al., 2015). Cells became more elongated and cylindrical and also increased their microvilli length over time. However, the most significant changes occur within one week after seeding. Considering that data

[20] Admittedly, comparing TEER values between studies is problematic due to strong methodological confounders as pointed out by others (Yee, 1997; Srinivasan et al., 2015).

and the fact that the epithelium renews itself every 3-5 days (Sato et al., 2009; van der Flier & Clevers, 2009; Park et al., 2016), this work recommends that ODMs do not require extended incubation periods and can be used after one week past seeding (2.2.2.2), which is close to the day 5-7 window suggested by others (Kozuka et al., 2017).
ODMs stayed in monolayer-formation with passing time. Occasionally, pseudostratified layers were found without correlation to incubation time (2.2.2.2). It could be a consequence of higher seeding densities. If organoids were not disseminated sufficiently into single cells or oligo-conglomerates, those larger multilayered structures grew into the monolayer and flatted out with time (2.2.1.3). However, the use of enzymatic digestion to force a single cell state during seeding actually decreased consistency of ODM generation, presumably by affecting cell survival or attachment to the filter by degraded surface receptors. Taken together, the gathered data suggests a trend of ODMs to organize themselves as true monolayers.
By investigating a potential mucus layer, an Alcian blue positive line on the apical membrane of ODMs could be observed (2.2.2.3). However, since GCs are apparently not present on ODMs by default in this work (2.2.2.4), the medium component N-acetylcysteine is a known mucus-solvent (Millar et al., 1985) and the duodenal mucus is much thinner and more aqueous than in the colon and does not even form anchored layers (Johansson et al., 2013; Pelaseyed et al., 2014), the staining is more likely to represent the glycocalyx. The existence of a mucus layer on duodenal ODMs was also not mentioned by others (Kozuka et al., 2017), although GCs were present in their setup.

Noticeable is a mosaic-like pattern of microvilli- and/or glycocalyx-formation between cells (2.2.2.2), which was equally recognizable in young (3 days) as well as old (> month, not shown) ODMs. This could indicate the presence of different populations of cell types. However, heterogenous expression of several enzymes like lactase (Maiuri et al., 1991), sucrase-isomaltase (Rings et al., 1994), and blood group-antigens (Maiuri et al., 1993) in enterocytes only, in patchy or mosaic patterns along the villus, has been described as well. While patchy patterns (more randomly scattered single cells) are speculated to be caused by differentiation-dependent variances due to e.g. different extracellular signals, mosaic patterns (vertical ribbons along the villus axis, or sheets, or any kind of clustering) suggests different clonal origins and are known to occur e.g. in females due to X-inactivation[21] (Stokkers et al., 1994). Different extracellular signaling as a cause for the mosaic patterns on *in vitro* ODMs in this work are quite unlikely, since all factors are available from start and are equally

[21] X-inactivation describes the random permanent inactivation of one of the two copies of the X-chromosome in females, creating (stem) cell populations with different genotypes within one individuum (Lyon, 1961).

disseminated within the medium. The only exception might be signaling with the basal lamina, since Matrigel® can be clumped occasionally, suggesting variability in thickness and therefore probably signal intensity of the Matrigel® coat. However, mosaic patterns do not correlate with growth of cells on Matrigel® clumps. The other explanation (different clonal origins, also the cause of cellular heterogeneity in the Caco-2 line) may be more likely, however at least not in regard to X-inactivation, since ODMs in this work are all derived from the same male patient. Mutations or epigenetic alterations which could have occurred in some stem cells may contribute to this, though passage numbers not exceeding 50 and - in all likelihood - fully functional DNA-damage repair mechanisms (in contrast to carcinoma-derived or immortalized cell lines), renders this also a quite improbable scenario. Especially regarding other studies, which show mosaic-patterns of their ODMs as well (Kozuka et al., 2017). Therefore, those patterns may be a curiosity of the ODM system of unknown origin or are simply a consequence of different cell types.

Regarding the cellular composition of ODMs, it is likely that ECs represent the majority of cells. Morphology, brush border architecture, ALPi-signals, factors of the DM-2 medium (nicotinamide; suppressing differentiation to the secretory lineage), and ECs as the most abundant cells *in vivo* as well as in 3D organoid culture, consolidates this assumption.
Beside ECs, the data suggests the presence of PCs. Lysozyme, a reliable diagnostic antibody (also performing well in murine and human 3D cultures as well as murine duodenal sections, Appx. 14), offered fractions of clearly lysozyme$^+$ cells but also cells with lesser signal intensities (2.2.2.4). It is likely that the most intense signals represent PCs, and the cells with lesser signal intensity could be explained by e.g. ECs, which pinocytosed lysozyme secreted by the PCs, or they represent a semi-differentiated PC state. However, due to those lesser signal intense cells, a reliable quantification of PCs cannot be conducted.
The question of ISC presence is hard to evaluate from the gathered data. ISC-marker LGR5$^+$ offered a uniform but strong signal throughout the monolayer, suggesting all cells have ISC character or at least express ISC marker LGR5. Due to this confusing result and the unreliable performance of the anti-LGR5 antibody in the validation experiment on murine duodenal thin sections (Appx. 14), LGR5 signals were initially considered as false positive (2.2.2.4). However, this may be an incorrect conclusion, since the problem of the LGR5 staining on the duodenal sections was not poor specificity but sensitivity. Lesser cells were stained than expected, which is the opposite of what is observed on ODM stainings. LGR5 may be a problematic target for antibodies *in situ*, which may be the reason other authors use a recombinant GFP-tag on LGR5 (Sato et al., 2009; 2011a; 2011b; Gjorevski et al., 2016; Haber et al., 2017; Qi et al., 2017; Wang et

al., 2017; Broguiere et al., 2018) or a different - but more unspecific marker (Formeister et al., 2009; Umar, 2010; Roche et al., 2015) - like SOX9 (Hiraoka et al., 2015; Qi et al., 2017; Broguiere et al., 2018). Noteworthy is also the occurrence of spherical glycosylated bodies at the apical membrane and along the microvilli (Appx. 28). Those are probably glycocalyceal bodies, which are usually a feature of TCs, but also a marker for stem cell-associated small intestinal tumors and therefore suggesting ISC-presence on ODMs (Marcus et al., 1979; 1981; Morroni et al., 2007; Hoover et al., 2017). The morphology of cells in EM images could also suggest ISCs and PCs (Appx. 28), since the cellular distortions due to environmental constraints of the crypt base *in vivo* (forcing "U"-shape) do not take place on ODMs. Apart from that, ISCs and PCs indeed feature a brush border with microvilli and glycocalyx (Hally, 1958; West et al., 1988; Borg et al., 1993; Gonzalez et al., 2013), therefore also villin should not be considered as a specific marker for ECs as assumed in other studies. Since PCs regulate ISCs (1.2.1.1), it is also not unlikely that ISCs are still present on ODMs and the mosaic pattern regarding microvilli formation can be interpreted as different cell types, as mentioned earlier, as well. Furthermore, the ability of ODMs to induce clear ClCa-1 signals after infection with *G. duodenalis* (2.2.3.7), suggested differentiation to GCs (which is thought to require ISCs), also supports the idea that a fraction of ISCs is still present on ODMs. However, those are all indicators of ISC presence but not real evidence. Further experiments are required to answer this question reliably.

Cells that are most likely not present in standard ODMs in this work are GCs and EECs (2.2.2.4). The status of TCs is questionable because even the recommended marker is not very specific (Gerbe et al., 2012; Middelhoff et al., 2017) and the measured signals suggest an abundance two orders of magnitude below of what would be expected *in vivo* (Saqui-Salces et al., 2011; Gerbe et al., 2012), making with 0,3‰ total abundance also biological significance in the ODM system doubtful.

Data from qRT-PCRs has not been included in this work due to missing proper controls like human duodenal *ex vivo* material and generally low explanatory power. Due to the complexity to get valid readout-data from multi-cell systems to quantify distinct cell populations[22], a de-complexation is required. This can be achieved by single-cell or digital qRT-PCR analysis[23], like other authors

[22] The ΔΔCt-method can only compare conditions (relative) but cannot be used to make a quantitative 'snapshot' of a distinct situation (e.g. getting cell type ratios of an ODM). Absolute quantification (use of a standard) could, but not with (putative) multi-cell systems like ODMs where transcript-dosage effects cannot be distinguished from effects related to different abundances of distinct cell types.

[23] Many qRT-PCRs are conducted in parallel at the single cell level with a binary readout parameter (e.g. lysozyme-threshold passed: yes/no -> GC: yes/no), basically nullifying transcription-dosage related interference, thus facilitating clear statements about cell type abundance.

recently showed (Brazovskaja et al., 2019; Chen et al., 2019; Collin et al., 2019; Harder et al., 2019). Although a (yet) expensive technology and not in the scope of this work, single-cell analysis would be a very helpful tool to dissect and characterize ODM composition and should be contemplated in future works.

Kozuka et al. (2017) described presence of ECs, GCs, and EECs in human ileal and distal colonic ODMs (not actually shown for duodenal or jejunal ODMs, also generated in their work, but it can be assumed). TCs were not investigated. The major differences between this work and Kozuka et al. (2017) are the two medium components nicotinamide and A83-01.
Nicotinamide is used for long-term (> 7 days) growth and maintenance of organoid cultures (Sato et al., 2011a) and known to suppresses sirtuin[24] activity (Denu, 2005). Other authors reported initial growth-facilitating effects of nicotinamide as well but contrarily observed decreased long-term culturing capabilities (Bartfeld et al., 2015). It is usually included in (3D) organoid culture and withdrawn together with SB202190 (p38 MAPK-inhibitor) to facilitate differentiation into GCs and EECs (Sato et al., 2011a; Bartfeld et al., 2015; Kozuka et al., 2017). However, other studies used nicotinamide as well as SB202190 and stemness propagators Wnt3A, prostaglandin $E_2$ (PGE-2), and initial CHIR99021-treatment[25] with the result of achieving GC differentiation by omitting only Wnt3A for 5 days in colonic ODMs (In et al., 2016). In gastric organoids, PGC-positive chief cells, MUC6-positive mucous neck cells and very rare SST-positive enteroendocrine cells were found even with nicotinamide addition (Bartfeld et al., 2015). Therefore, in this work it was tried to achieve some kind of GC and EEC differentiation by SB202190 removal only, since withdrawal of nicotinamide led to collapsing ODMs after one week (similar to what has been observed by Sato *et al.* 2011 on 3D organoids). Apparently, this goal was not achieved, but making putative GC differentiation due to *G. duodenalis* infections (2.2.3.7) even more intriguing.
The other component, A83-01[26], is - according to Kozuka *et al.* 2017 - necessary for proper differentiation. However, this is in contrast to experiences in this work (DM-1 contained this inhibitor but was omitted in DM-2, leading to earlier differentiation; 2.2.1.2, DM-1 data not shown), as well as to reports from others (VanDussen et al., 2015). The actual role of TGF-β signaling in organoids is still unknown (Sato et al., 2011a) and is described as ambivalent regarding proliferation and differentiation (Moses et al., 1990; Bach et al., 2000; Miyoshi et al., 2012; Reynolds et al., 2013; Hahn et al., 2017). Thus, divergent experiences

[24] Sirtuins act as HDACs, moderating epigenetic regulation e.g. apoptosis, stress response and differentiation (Denu, 2005).
[25] CHIR99021 is a GSK3-inhibitor; preventing phosphorylation of β-catenin for degradation and therefore enhancing canonical Wnt-signalling (An et al., 2010).
[26] A83-01 is a TGF-β-receptor (ALK4, 5, 7) inhibitor, preventing SMAD-signaling (Tojo et al., 2005).

with this factor in different setups may not be surprising. However, since the ODM model in this work had the purpose to study infections, interferences with the signaling of TGF-β, which is a cytokine produced and secreted by every leukocyte lineage upon inflammation (Letterio & Roberts, 1998), could confound results. Concluding, TGF-β inhibition should remain avoided in this system.
The addition of insulin-like growth factor 1 (IGF-1) and fibroblast growth factor 2 (FGF-2) was very recently shown to improve multi-differentiation capacity among other benefits (Fujii et al., 2018). It may be worthwhile to evaluate those factors on ODMs to potentially improve future model systems.

#### 3.2.1.1 Conclusions of the ODM model

The ODMs in this work show a high degree of polarization and feature a well-developed brush border, surpassing Caco-2 or other immortalized cell lines. Cellular contact sites and TJPs of interest are present and barrier properties are comparable to ODM data from other authors. Additionally, data suggests the presence of different cell types like ECs and PCs. GCs and EECs were not found, TCs are also not present or exist only in insignificant numbers and the presence of ISCs can only be assumed. Further experiments, on single cell resolution, are required to investigate the cellular composition in more depth. However, it is fair to state that ODMs as electro-physiologically tight epithelial monolayers with a pronounced brush border and glycocalyx, which can support *G. duodenalis* co-culture and even allow the use of luminal mock medium TYI-S-33, are a suitable model system to study *G. duodenalis* infections. Moreover, as a primary cell system which requires only minimal duodenal biopsy material to start cultivation, it could be used synergistically with epidemiological studies. With patients, known to be asymptomatically colonized or acute symptomatically infected with *G. duodenalis*, potential disease-deciding host attributes and characteristics could be easily examined *in vitro*.

### 3.2.2 *Giardia*-induced pathological effects

This work shows that *G. duodenalis* only induced the proposed epithelial barrier dysfunction phenotype of giardiasis if the luminal mock medium TYI-S-33 has been used apically on ODMs (2.2.3.2), and this was true for all assemblages (2.2.3.3) and infection loads (2.2.3.4) tested herein. With usual medium like Caco-2 DMEM, signs of epithelial damage were not observed (2.2.3.1). This is a confusing finding, since almost all studies investigating *Giardia*-induced barrier dysfunction *in vitro* either claimed to use regular DMEM or did not mention a special treatment, e.g. TYI-S-33 or other medium additives, for their infection setups. The only exception is the Caco-2 transwell system of Fisher *et al*. (2013), which features a mixture of 90% DMEM and 10% TYI-S-33 in the apical compartment[27]. However, they detected beginning monolayer disorganization and "hole-formation" as late as 13-21 days after infection (Fisher et al., 2013), whereas other studies described such effects already after 2 h without using TYI-S-33 (Scott et al., 2002; Zhou et al., 2007; Maia-Brigagao et al., 2012).
A possible explanation could be that trophozoites experience increased viability with TYI-S-33, therefore it could be speculated that *G. duodenalis* is simply dying before exerting any harm to the epithelium and studies which detected pathologic effects used high parasite loads, compensating early parasite death. However, the data in this work rejects this hypothesis. Parasite loads in other studies (max. MOI 8) were significantly lower than maximal infection loads (MOI 100) in this work. Trophozoite survival data from TYI-S-33 conditions shows indeed higher viability of *G. duodenalis* (2.2.3.5), but Caco-2 DMEM is sufficient to keep enough parasites alive to still cover the monolayer at day 3 and barely has an influence at day 1 after infection - when most infection experiments show barrier function impairment (Buret et al., 2002; Scott et al., 2002; Zhou et al., 2007; Humen et al., 2011; Maia-Brigagao et al., 2012; Tysnes & Robertson, 2015; and this work 2.2.3.2). Additionally, some studies describe the use of trophozoite sonicates as sufficient to observe barrier dysfunction and therefore completely ruling out parasite viability as a factor (Teoh et al., 2000; Buret et al., 2002; Chin et al., 2002; Scott et al., 2002), which is contradictory to other findings (Humen et al., 2011; and this work 2.1.2.4), however.
Another explanation could be that some studies suffer strong confounders or perhaps a kind of contamination, which is especially suggested for those finding effects as early as 2 h (Scott et al., 2002; Zhou et al., 2007; Maia-Brigagao et al., 2012). It could also explain contradictory data e.g. that already parasite lysates or spent medium exert barrier damage (Teoh et al., 2000; Buret et al., 2002; Chin et al., 2002; Scott et al., 2002)[28], whereas others disagree (Humen et al.,

[27] Higher TYI-S-33 concentrations led to unwanted effects on Caco-2 (Fisher et al., 2013).
[28] It should be noted that those studies are all from the same lab/group.

2011) or are inconclusive (Tysnes & Robertson, 2015); or that isolate WB6 seemed virulent in some studies (Panaro et al., 2007; Humen et al., 2011; Maia-Brigagao et al., 2012; Fisher et al., 2013), but not in others (Chavez et al., 1986; Chin et al., 2002).

Since studies vary so much in experimental detail and results (as shown under 3.1), it is not possible to pinpoint a clear causal relationship between confounder/factor/variable and experimental outcome. This work strongly indicates that TYI-S-33 (or a certain factor in it) triggers *G. duodenalis* virulence in this ODM-setup. It may also induce parasite virulence on Caco-2 or other cell lines, however, this cannot be investigated because of TYI-S-33's harmful effect on cell lines already on its own, as explained earlier (2.1.2.9, 2.2.3.2, also Chavez et al., 1986; Fisher et al., 2013). Investigating the TYI-S-33 specific ingredients is recommended for future works and may elucidate some study discrepancies. Perhaps TYI-S-33 could be modified in a way to prevent harmful side-effects on Caco-2 while maintaining trophozoite virulence.

#### 3.2.2.1 Barrier dysfunction

The detected epithelial damage of *G. duodenalis* infected ODMs in this work was severe and manifold. Cytoskeletal changes were evident by microvilli-depletion and loss of cylindrical cell shape (2.2.3.2, 2.2.3.9, 2.2.3.10, and 2.2.3.11). Cells sometimes seemed to retain lateral connections to their neighboring counterparts (most likely desmosomes) but TJ integrity was lost and TJPs seemed either delocalized (cldn-1 along the lateral membrane, occludin in the cytosol), partially degraded (ZO-1) or completely disappeared (cldn-2), which was accompanied by cellular detachment (2.2.3.9, 2.2.3.11). This is in line with the majority of other studies, also showing *Giardia* sp. induced F-actin changes and specifically microvilli depletion or atrophy (Teoh et al., 2000; Scott et al., 2002; Humen et al., 2011; Maia-Brigagao et al., 2012), which is a well-known pathomechanism also described in non-human hosts (Erlandsen & Chase, 1974; Buret et al., 1990; 1991) and even found in studies without evidence of barrier dysfunction (Chavez et al., 1986; 1995). The reduction of absorptive surface area by villus atrophy or microvilli depletion (Troeger et al., 2007) seems to be the main mode of action of the disease's malabsorption phenotype. Especially the impact on microvilli - presumably as a consequence of membrane tensions, generated by physical depression, which is exerted by the trophozoite's ventral attachment disc ('suction cup') - could be some kind of side-effect, independent from the barrier dysfunction phenotype. However, it can be speculated that the opposite may be the case, and a distorted brush border and terminal web could impair cell-cell anchoring directly via cytosolically disrupted TJ or AJ joints or

indirectly by targeted cell-contact-site-degradation as an adverse host response. It is also imaginable that *Giardia* spp. release effectors that induce such surface changes in order to facilitate attachment. It is worthwhile to investigate this further since microvilli depletion is apparently the most consistent outcome of *Giardia* sp.-host interaction but concurrently one of the most understudied effects (Cotton et al., 2011).

As mentioned, various studies describe effects on TJ complexes, however, many of them seeded Caco-2 cells on plain culture surfaces, which leads to odd phenotypes (shown under Appx. 26), and therefore perhaps fallacious interpretations regarding parasite-induced TJ alterations (e.g. ZO-1 branching, described by Maia-Brigagao et al., 2012). Nevertheless, several specific effects on certain TJPs are equivalently found on cell lines in other studies as well as ODMs in this work. Delocalization effects are described for cldn-1 (Humen et al., 2011; Maia-Brigagao et al., 2012) and can be found on ODMs (2.2.3.11). Effects observed on occludin (2.2.3.11) suggest rearrangement (Humen et al., 2011) or cleavage (Chen et al., 2013), as well. Disruption of ZO-1 (2.2.3.11) could be prevented in other studies by various means, e.g., by EGF- (Buret et al., 2002) or caspase-3 inhibitor treatment (Chin et al., 2002), or MLCK-inhibitor addition (Scott et al., 2002) - especially EGF and caspase-3i interference suggests a link to cell death, whereas MLCK-dependency could indicate secondary effects on TJs due to F-actin reorganization, as mentioned earlier. Loss of cldn-2 (2.2.3.11) has not been described before. The fact that TJPs show different phenotypes, ranging from rearrangement (on site), delocalization (into cytoplasm), or degradation (partial/cleavage to complete disintegration), suggests regulated processes rather than simple parasite-driven destruction (e.g. by proteases), which would affect extracellular domains of TJPs like occludin or cldn-1 and -2 in a more similar way. Also, effects on the cytosolic scaffold protein ZO-1 seem regulated, as mentioned studies suggests, and not secondary to loss of transmembrane TJPs. By receiving a stimulus from *G. duodenalis*, host cells could start to remove the pore-forming claudins - like cldn-2 - from TJCs to increase barrier properties, which could explain the initial TEER increase. However, dilution potentials did not indicated altered $Na^+$-permeabilities before actual barrier dysfunction (cldn-2 allows $Na^+$- and water-flux; Amasheh et al., 2002; Rosenthal et al., 2010), but a strong negative selectivity for $Cl^-$, which rather indicates integration of barrier-forming claudins into the TJC than removal of pore-forming ones (2.2.3.12). Epithelial monolayers could recruit more cldn-1 to the TJ, while simultaneously keeping cldn-2 constant to ensure luminal reflux of $Na^+$, required to maintain the $Na^+$-gradient. The entire loss of cldn-2, as IFAs suggest (2.2.3.11), may occur at later stages. Loss of cldn-2 has also been described in apoptotic cells, whereas cldn-1 expression not changed or even increased (Bojarski et al., 2004). As actual barrier dysfunction takes place, cldn-1 seemed to be delocalized on the whole lateral membrane

(2.2.3.11), which could be a secondary effect of the regulated (Buret et al., 2002; Chin et al., 2002; Scott et al., 2002) removal of cytoplasmatic adaptor protein ZO-1, which, in turn, is released e.g. by caspase-3-mediated occludin cleavage (Bojarski et al., 2004) and/or general F-actin reorganization (Teoh et al., 2000; Scott et al., 2002; Humen et al., 2011; Maia-Brigagao et al., 2012).

#### 3.2.2.2 Cell death

Since ZO-1 removal from the TJC is connected to programmed cell death (Bojarski et al., 2004; Zehendner et al., 2011; Wu et al., 2014), and apoptosis-inducing effects of *G. duodenalis*, although contradictory, were occasionally reported by some studies (Chin et al., 2002; Panaro et al., 2007; Troeger et al., 2007), TUNEL assays were conducted to verify apoptotic effects. Mild signs of apoptosis (up to 6% at day 3 after infection, $p < 0{,}001$) were found (2.2.3.6). Although being higher than the 1.5% apoptotic rate as shown by others on chronic infected human duodenal biopsies (Troeger et al., 2007), it appears too weak to explain the massive destruction observed on ODMs in this work. Since TUNEL is a marker for fragmented DNA, and therefore late stage apoptosis, it could be that apoptotic events were missed (false negative) due to too early analysis. However, after 72 h monolayers were usually collapsed for more than 24 h and therefore apoptosis, if not visible there (especially regarding its kinetics of a few hours, according to Gavrieli et al., 1992; Wolbers et al., 2004), is unlikely to be the cause of barrier dysfunction. The other direction, that apoptosis occurred too early and analysis may have missed it, can, in regard to the TUNEL mechanism, also be excluded. In contrast to caspase-activity assays, in which the activity of certain caspases is measured at a certain time and will diminish later, $TUNEL^+$ fragmented DNA stays fragmented or increases degree of fragmentation further, thus leading to a more biased readout towards an increased signal with progressing time - and also false positives, since some necrotic mechanisms can result in DNA fragmentation as well (Grasl-Kraupp et al., 1995; Torres et al., 1997). Additionally, earlier time points (e.g. 24 h, or 48 h; 2.2.3.6) also did not indicate apoptotic counts exceeding the counts of 72 h observations. An explanation which is more likely to have occurred is that cells with progressed apoptosis, and therefore increased junctional disassembly, may facilitated their removal from the monolayer e.g. by washing procedures during IF stainings. However, with regard to the cellular phenotype of infected ODM cells in EM (2.2.3.10), another explanation can be suggested - ischemic cell death.

Ischemic cell death, or oncosis, is an accidentally initiated but later partially regulated pathway of death (Mills et al., 2002). Whereas apoptosis requires

energy (ATP) and is characterized by cellular shrinkage (Kerr, 1971; Eguchi et al., 1997; Elmore, 2007), oncosis is induced by a lack of ATP, leading to cellular swelling by idle ionic pumps (Majno & Joris, 1995; Mills et al., 2002; Weerasinghe & Buja, 2012). Trump et al. (1997) describe it as follows: "In oncosis, the early changes include marked alterations in cell shape and volume. […] In monolayer cultures, such cells form cytoplasmic blebs; chromatin clumping occurs later, followed by cells pulling apart, rounding up, and often detaching from the substrate."

Findings in this work (2.2.3.9, 2.2.3.10) show rounded cell shapes and detachment, increased vacuolization devoid of organelles, membrane blebs (single blister-formation with cytoplasmatic clearance; not to be confused with membrane budding as seen in apoptosis), and peripheral nuclear condensation (Majno & Joris, 1995; Trump et al., 1997; Mills et al., 2002; Weerasinghe & Buja, 2012). Furthermore, active ionic transporter complexes decrease their activity (2.2.3.12). The loss of cells is also a described consequence (Gonzalez et al., 2015). Significant cell or organelle swelling was not observed. However, this may be due to late observational time points at which swelling could be already decreased because of advancing membrane permeability as necrotic processes started to take place. Opposed to this, typical apoptotic phenotypes like cell shrinkage, membrane budding into apoptotic bodies containing organelles or nuclear fragments, condensed chromatin into irregular-shaped clumps or karyorrhexis were hardly or never observed (Majno & Joris, 1995; Eguchi et al., 1997; Mills et al., 2002; Elmore, 2007; Weerasinghe & Buja, 2012), which is in line with the TUNEL findings. Also, with regard to the rather low (6%) apoptotic rate detected, it is reasonable to assume that cells of *G. duodenalis*-infected ODMs in this work underwent ischemic death in the majority of cases. Or rather, ischemic cell death may be even a reason for the low apoptotic rate, since the death due to energy starvation prevents energy consuming apoptosis. This could also explain why apoptotic counts did not significantly increase further with time, although an accumulation of TUNEL signals was expected. Host cells may die faster due to oncosis than apoptosis takes place. However, confusing is that in some cell line setups (Caco-2 or HCT-8), apoptosis seems to be the driving factor for epithelial destruction, since caspase-3 inhibition abolished ZO-1 disruption and barrier leakage (Chin et al., 2002; Panaro et al., 2007). Although, it cannot be excluded that this is just a carcinoma cell-specific artifact, which is also not consistently found, since other studies on the same cells describe that TJ alterations, without affected cell viability, exist (Maia-Brigagao et al., 2012). Duodenal biopsies used by Troeger et al. (2007), on the other side, with their even lower apoptotic rate of 1.5% (1% in controls), are more in line with findings in this work.

#### 3.2.2.3 ClCa-1$^{+}$/GC emergence

Of highest interest is the finding that GC-specific marker ClCa-1 is expressed on *Giardia*-stressed ODMs (2.2.3.2, 2.2.3.7). ClCa-1 was first speculated to resemble a $Ca^{2+}$-activated $Cl^{-}$-channel (Gruber et al., 1998), but more recent studies showed that it is a secreted self-cleaving protein (Yurtsever et al., 2012), which can activate the calcium-dependent chloride channel TMEM16A (Sala-Rabanal et al., 2015; 2017). It is heavily produced and secreted by GCs along with the mucus (Gibson et al., 2005) and plays also a role in mucin production (Hoshino et al., 2002) as well as mucus homeostasis (Nyström et al., 2018). It has been shown to be an Il-13-controlled key regulator of metaplasia towards GCs (Alevy et al., 2012) and has also been linked to certain carcinoma types (Hu et al., 2018; 2019), although with conflicting results showing both, poor prognosis under low (Yang et al., 2015) and high expression levels (Chen et al., 2018). There are also indicators for immunomodulatory (pro-inflammatory; macrophage-involvement) properties, in the airway epithelium (Ching et al., 2013). Therefore, ClCa-1 seems to serve multiple functions and may not only be considered as GC-marker but perhaps also as important factor in giardiasis.

Il-13, as mentioned earlier (1.2.1.1), is responsible among others for GC hyperplasia. Increased Il-13 serum levels were found in *Giarida* sp.-infections in *in vivo* studies (Matowicka-Karna et al., 2011; Hagel et al., 2014). Interestingly, transcriptomic analyses on Caco-2 do not show significantly elevated levels of either ClCa-1 or Il-13 (Roxström-Lindquist et al., 2005; Ma'ayeh et al., 2015). However, it could also indicate the limitations of carcinoma-derived cell lines, unable to show effects of cellular differentiation. Unfortunately, Troeger et al. (2007), who investigated duodenal biopsies from chronic *G. duodenalis*-infected patients, did not examined GC abundance. However, they found increased anion secretion along with others (Gorowara et al., 1992; 1994; Resta-Lenert et al., 2000), which could hint to increased ClCa-1 expression, driving chloride secretion. Although chloride secretion was found to be reduced in this work (2.2.3.12), the exact mode of action for Theophylline/PGE2 stimulation is still unknown (Grotmol & van Dyke, 1992), hence could simply lead to increased chloride-channel integration (as suggested by Grotmol & van Dyke) rather than transporter activation or channel opening, which is therefore not in conflict with a potential increase in ClCa-1-mediated chloride secretion.

The rationale behind this could be an induced GC hyperplasia to counteract parasite colonization, e.g. via increased mucus production. But also increased chloride secretion (and concurrent $Na^{+}$-transport inhibition to stop counteracting resorptive processes, as data suggests; 2.2.3.11, 2.2.3.12) to induce secretory diarrhea in order to flush trophozoites away is imaginable. Diarrhea as a primitive defense mechanism to remove hazardous agents is a concept, speculated about occasionally (DuPont & Hornick, 1973; Das et al.,

2018), but not considered often. Most likely because it generates more harm than benefit. However, secretory processes outbalance absorption in the crypt, whereas the opposite is the case for the villus region (Thiagarajah et al., 2015; Das et al., 2018). Since the ODM-model in this work seemed to represent rather the crypt base with the presence of PCs, increased secretion as a deliberate mechanism for defense may be valid in this setting. Furthermore, it has been shown that *Giardia* sp. induces crypt hyperplasia (Buret et al., 1992; Koudela & Vitovec, 1998; Araújo et al., 2008; Koot et al., 2009; Halliez et al., 2016). Together with simultaneous villus atrophy (Erlandsen & Chase, 1974; Buret et al., 1992; Oberhuber et al., 1997; Koudela & Vitovec, 1998; Williamson et al., 2000; Araújo et al., 2008; Koot et al., 2009; Bartelt et al., 2013; Ventura et al., 2013; Halliez et al., 2016; Li et al., 2017) and therefore reduced resorption capabilities, it is a possible explanation for the diarrhea apart from the epithelial destruction.

Increased chloride secretion could also be a consequence of ischemic cell death, since degradation of intracellular calcium stores might release $Ca^{2+}$ ions (Majno & Joris, 1995; Trump et al., 1997; Weerasinghe & Buja, 2012), which induces calcium-dependent chloride channels (CaCCs; including but not limited to TMEM16A, which is also activated by ClCa-1 as mentioned earlier). However, this less specifically induced chloride secretion - if had taken place - would have been certainly detected by experiments (e.g. 2.2.3.12). Interference of ischemic death or its subsequent necrotic processes with ClCa-1 signals, on the other side, is inherently unlikely unless the anti-ClCa-1 antibody cross-reacts with other substrates created or released during such processes.

The idea of GC hyperplasia as a direct consequence of *G. duodenalis* infection is corroborated by similar responses of the intestinal epithelium towards other enteric pathogens e.g. helminths (Knight et al., 2008; Lee et al., 2013; Yasuda & Nakanishi, 2018; Zwarycz et al., 2018), bacteria (Mantle et al., 1991; Khare et al., 2009; Yang et al., 2014) and even viruses (Mussarat et al., 2018), as well as the apparent inapplicable alternative explanation; GC hyperplasia to enhance tissue regeneration as response to damage and cell loss (2.2.3.8). Of note, GC hyperplasia can be independent from the Il-13 pathway (Marillier et al., 2008). Though studies investigating GCs in *G. duodenalis* infections are scarce, GC hyperplasia has been described *in/ex vivo* (Williamson et al., 2000; Ponce-Macotela et al., 2008; Ventura et al., 2013), and is also suggested as unspecific defensive mechanism of the host (Ponce-Macotela et al., 2008). Moreover, there is evidence that *Giardia* sp. exerts mucus degrading effects by proteolytic mucin-cleavage (Amat et al., 2017), which could indicate GC hyperplasia as a compensatory response of the host. Taken together, there are supportive indicators that ClCa-$1^+$ cells indeed represent GCs and that they are a direct consequence of *G. duodenalis* infection and not secondary to epithelial damage. However, further efforts should be taken to validate those findings.

#### 3.2.2.4 Conclusions of *Giardia*-induced pathology on ODMs

Concluding, with the new established ODM system it was possible to set up conditions which allowed the replication of the parasite's proposed barrier disrupting effects. *G. duodenalis*, in the presence of luminal mock medium TYI-S-33, induced fulminant monolayer destruction with subsequent total barrier dysfunction between day one and two after infection, which could be only observed with the new ODM model but not with the Caco-2 model. This destruction was connected to TJ impairment, with different TJPs being differently affected, which suggests an interplay of regulated host processes probably (or partially) by intent. Cell death, suggesting oncotic-like death of ODMs for the majority of cells as well as occasional signs of apoptosis seemed to exert significant impact on barrier properties. However, the relation between cell death and TJ integrity is not clear and whether observed TJ effects were a cause of parasite interaction, leading to cell death or vice versa requires further investigation. Additionally, microvilli depletion, as the most reported *Giardia* sp.-induced morphological phenotype on host cells by studies was also observed with the new ODM model. Other findings concerning emerged ClCa-1 signals suggests GC hyperplasia, only described by *in vivo* studies before, portend the power of this new model system.

### 3.2.3 Outlook

Using ODMs as a new approach offers promising possibilities to study *Giardia* sp. infections in greater detail in an advanced *in vitro* setup, much closer to *in vivo* conditions. However, ODM culturing can still be improved to generate even more *in vivo*-like monolayers with all cell types in their respective abundance. To achieve this, the omission of nicotinamide, which blocks secretory lineage differentiation (GCs, EECs), and the setup of a single cell-based analysis system to properly quantify cell type abundances is highly advisable.
Although appearing as a kind of backstep, the Caco-2 model may still be of limited use if it would allow investigations with luminal mock medium TYI-S-33. By switching from cysteine as the primary supplement to setup a redox environment to glutathione, the *in vivo* substance for this purpose (and also the compound created of cysteine components by mammalian cells to reduce cytotoxic cysteine amounts), a less stressful luminal mock medium could be created, which could allow its use in the Caco-2 system to possibly show similar *Giardia*-induced phenotypes.

Regarding observed pathological effects in this work, several new aspects can be targeted for future investigations.
Ischemic cell death has not been described as consequence of *G. duodenalis* infection before but is suggested in this work, although apoptosis, as also described by other research, is taking place as well. Whether this is an artifact of the *in vitro*-culturing (perhaps even related to TYI-S-33 in conjunction with *G. duodenalis*-induced barrier dysfunction as a kind of breakpoint), or a mechanism also found *in vivo*, needs to be determined. However, increased awareness of other kinds of cell death, apart from apoptosis, is recommended since it alone (in its marginal manifestation shown here and elsewhere) cannot explain either, intense monolayer destruction in this work or cases of severe diarrhea.
It is also advisable to investigate the effects of *G. duodenalis*, direct or indirect via host cell regulation, on tight junction complexes. Many studies described them; however mechanistic details remain obscure. Some alterations seem to be a consequence of apoptosis, it could be therefore useful to separate these events for investigation, e.g. by blocking apoptosis or enhancing tight junctions.
Future research should also cover more secretion-specific transporters like CaCCs, NKCC1, CFTR or gradient-building pumps like the important $Na^+/K^+$-ATPase, since alterations in the ionic transport systems can lead to secretory diarrhea and may also be influenced by cell death.
Highest attention deserves the putative emergence of $ClCa\text{-}1^+$ goblet cells. Though described by some *in/ex vivo* studies, GC hyperplasia could never be observed *in vitro* due to the limitations of immortalized cell lines. The ODM

setup, with its intestinal stem cells, however, enables observations of directed differentiation or metaplasia with the ability to interfere at any given time point. This is a huge advantage compared to *in/ex vivo* approaches, which allows only pre-defined interventions and mostly blind or endpoint-only observations. Use of animal models can also be reduced therewith, complying with the first of the 3Rs's principles of laboratory animal science. Increased mucus production may be a plausible consequence of GC hyperplasia, which could have complications for the parasite, and should be examined also with regard to treatment.
Lastly, the OMDs as purely epithelial model (and therefore not a tissue by strict definition) lack also a vital component of gut in health and disease, the immune system. Especially monocytes like dendritic cells or macrophages are pivotal for pathogen sensing and preemptive reaction. Those cells could be seeded into the basal compartment or onto the basal side of the transwell-filter to investigate their reaction and effects on both, parasite and host. This could even be further expanded by a fourth component, the microbiota, on the apical side.

Concluding, the new ODM setup can succeed, where traditional cell lines fail. It facilitates the discovery of more subtle effects, which are necessary to illuminate the complex pathology of *G. duodenalis* and similar parasites, which are obscure, neglected and hard to investigate.

# 4. Material and methods

## 4.1 Material

### 4.1.1 Cell lines and parasite isolates

#### 4.1.1.1 Cell lines

Caco-2 [HTB-37™] ATCC
Human epithelial cells derived from a colon carcinoma of a 72-year-old male.

Caco-2 bbe1 [CRL-2102™] Gift from J.-D. Schulzke, Charité CBF
Human epithelial cells derived from Caco-2 parental cell line, selected on the basis of morphological homogeneity and exclusive apical villin localization.

L-WRN [CRL-3276™] (murine L-cells) ATCC
Murine L-cells of a 100-day-old male C3H/An mouse (L-M(TK-) [CCL-1.3™] cells), transfected with a Wnt-3A expression vector (L-Wnt3A [CRL-2647™]), again transfected with a R-spondin-3 and noggin co-expressing vector (L-WRN [CRL-3276™]).

HEK 293T/17 [CRL-11268™] ATCC
Human epithelial cells derived from a human embryo's kidney, in which the temperature sensitive gene for SV40 T-antigen was inserted. Clone 17 selected for high transfectability.

HA-noggin-Fc (HEK) Gift from H. Clevers, Hubrecht Institute
HEK cells genetically engineered to produce and secrete noggin.

R-Spondin-1-Fc (HEK) Gift from H. Clevers, Hubrecht Institute
HEK cells genetically engineered to produce and secrete R-Spondin-1.

#### 4.1.1.2 Organoid lines

CBF1 "Benjamin" Charité CBF
Human small intestinal epithelial cells derived from duodenal biopsies of a 30-year-old male.

#### 4.1.1.3 *G. duodenalis* isolates

| Name | Assemblage | Source |
|---|---|---|
| GS/H7 [50581™] | (B) | ATCC |
| GS/H7 GLV-infected | (B) | Gift from M. Lalle, Istituto Superiore di Sanità |
| NF | (A) | Gift from A. Buret, University of Calgary |
| P15/E | (E) | Gift from J. Jerlström-Hultqvist, Uppsala University |
| P344/B2 | (B) | Giardia biobank, RKI |
| P387/C1 | (B) | Giardia biobank, RKI |
| P413/H7 | (B) | Giardia biobank, RKI |
| P424/A5 | (B) | Giardia biobank, RKI |
| P458/E2 | (B) | Giardia biobank, RKI |
| P64/F7 | (A) | Giardia biobank, RKI |
| S2 | (A) | Gift from A. Buret, University of Calgary |
| WB6 [50803™] | (A) | ATCC |
| WB6 GLV-infected | (A) | Gift from M. Lalle, Istituto Superiore di Sanità |

### 4.1.2 Chemicals and reagents

#### 4.1.2.1 Antibiotics

| Name | Vendor | Cat. No. | Notes |
|---|---|---|---|
| Amphotericin B | Sigma | A2411 | 250 µg/ml |
| Geneticin® G418 | Thermo Scientific | 10131035 | 50 mg/ml |
| Gentamicin | Capricorn Scientific | GEN-10B | 10 mg/ml |
| Hygromycin B | Sigma | H0654 | 50 mg/ml |
| Penicillin/streptomycin (P/S) | Capricorn Scientific | PS-B | 100x |
| Tetracycline hydrochloride | Merck | 58346 | 10 mg/ml |
| Zeocin™ | Invivogen | ant-zn-1 | 100 mg/ml |

#### 4.1.2.2 Biologicals and Supplements

| Name | Vendor | Cat. No. | Notes |
|---|---|---|---|
| Bacto yeast extract | BD Bioscience | 212750 | |
| Bovine and ovine bile solution | Sigma | B8381 | 52 mg/ml |
| Bovine serum albumin (BSA) | Merck | A7030 | 1% for coating |
| Casein peptone | Merck | 1.07213.1000 | |
| Fetal bovine serum (FBS) | Thermo Scientific | 26170-043 | |
| GlutaMAX™ supplement (100x) | Thermo Scientific | 35050061 | |
| human rec. EGF | Peprotech | AF-100-15 | 50 µg/ml |
| Matrigel® | VWR | 734-0269 | |
| MEM non-essential amino acids solution (NEAA, 100x) | Thermo Scientific | 11140050 | |
| Poly(I:C) | Invivogen | tlrl-pic | 10 mg/ml |
| Supplement B-27 (50x) | Thermo Scientific | 17504044 | |
| Supplement N-2 (100x) | Thermo Scientific | A1370701 | |
| TrypLE™ Express Enzyme (cell dissociation reagent) | Thermo Scientific | 12604013 | |

### 4.1.2.3 Chemical compounds

| Name | Vendor | Cat. No. | Notes |
|---|---|---|---|
| 3-O-methyl-D-glucose ($C_7H_{14}O_6$) | MP Biomedicals | 02151651-CF | |
| 4′,6-Diamidino-2-phenylindole dihydrochloride (DAPI, $C_{16}H_{15}N_5$) | Sigma | D9542 | 2 mg/ml |
| A83-01 ($C_{25}H_{19}N_5S$) | Sigma | SML0788 | 500 µM (DMSO) |
| Acetic acid, glacial ($C_2H_4O_2$) | Carl Roth | 3738.5 | |
| Ammonium ferric citrate ($(NH_4)_5[Fe(C_6H_4O_7)_2]$) | Merck | RES20400-A7 | 22.8 mg/ml |
| Ascorbic Acid ($C_6H_8O_6$) | Fluka | 85210 | |
| Bisbenzimide (Hoechst 33342, $C_{27}H_{28}N_{60}$) | Thermo Scientific | H21492 | 2 mg/ml |
| Calcium chloride ($CaCl_2$) | Carl Roth | A119.1 | |
| Chloroform ($CHCl_3$) | Merck | 102432 | |
| D-Glucose ($C_6H_{12}O_6$) | Fluka | 49159 | |
| Diethanolamin ($C_4H_{11}NO_2$) | Sigma | D8885 | |
| Dimethyl sulfoxide (DMSO, $C_2H_6OS$) | Sigma | D2650 | |
| Disodium phosphate ($Na_2HPO_4$) | Carl Roth | T876.2 | |
| Dipotassium phosphate ($K_2HPO_4$) | Fluka | 60356 | |
| D-Mannitol ($C_6H_{14}O_6$) | Merck | M4125 | |
| Ethanol ($C_2H_6O$) | Carl Roth | 5054.3 | |
| Ethylenediaminetetraacetic acid (EDTA, $C_{10}H_{16}N_2O_8$) | Applichem | A4892,0100 | 0.5 M |
| Fluorescein ($C_{20}H_{12}O_5$) | Sigma | 46955 | 1 M |
| Formononetine ($C_{16}H_{12}O_4$) | Merck | 47752 | 10 mM |
| Haematoxylin ($C_{16}H_{14}O_6$) | Carl Roth | T865.1 | |
| Hydrogen chloride (HCl) | Carl Roth | 4625.1 | |
| L-cysteine hydrochloride monohydrate ($C_3H_7NO_2S \cdot HCl \cdot H_2O$) | Merck | 30129 | 50 mg/ml |
| Lead citrate ($C_{12}H_{10}O_{14}Pb_3$) | Science Services | E22410 | |
| Magnesium chloride ($MgCl_2$) | Carl Roth | KK36.3 | |
| Magnesium sulfate ($MgSO_4$) | NEB | B1003S | |
| Methanol ($CH_4O$) | Carl Roth | 4627.5 | |
| Monopotassium phosphate ($KH_2PO_4$) | Fluka | 60220 | |
| N-Acetylcysteine ($C_5H_9NO_3S$) | Sigma | A9165 | 0.5 M (DMEM) |
| Nicotinamide ($C_6H_6N_2O$) | Sigma | N0636 | 1 M (DMEM) |
| Osmium tetroxide ($OsO_4$) | Carl Roth | 8088.1 | |
| *para*-formaldehyde ($OH(CH_2O)_nH$) | Carl Roth | 0335.3 | 4% |
| *para*-Nitrophenylphosphate (pNPP, $C_6H_6NO_6P$) | NEB | P0757S | 0.5 M |
| Periodic acid ($H_5IO_6$) | Carl Roth | 3257.1 | |
| Polyethylenimine 25k (PEI, $(C_2H_5N)_n$) | Polysciences | 23966-1 | 1 mg/ml |
| Potassium chloride (KCl) | Carl Roth | 6781.1 | |
| Propidium iodide (PI, $C_{27}H_{34}I_2N_4$) | Sigma | 81845 | 2 mg/ml |
| Prostaglandin $E_2$ (PGE2, $C_{20}H_{32}O_5$) | Tocris | 2296 | 10 mM |
| Pure water type 1, PCR grade, sterile ($H_2O$/A. bidest) | Carl Roth | T143 | |
| ROCK-inhibitor Y-27632 Dihydro-chloride ($C_{14}H_{21}N_3O \cdot 2HCl$) | Tocris | 1254 | 10 mM |
| SB202190 ($C_{20}H_{14}FN_3O$) | Cayman Chemicals | 10010399 | 1 mM (DMSO) |
| Sodium chloride (NaCl) | Fluka | 71379 | |
| Sodium hydroxide (NaOH) | Carl Roth | 9356.1 | |
| Staurosporine ($C_{28}H_{26}N_4O_3$) | Merck | 569396 | 1 mM |
| Theophylline ($C_7H_8N_4O_2$) | Tocris | 2795 | 1 M |
| TRIS Pufferan® ($C_4H_{11}NO_3$) | Carl Roth | 4855.2 | |
| Triton™ X-100 ($C_{14}H_{22}O(C_2H_4O)_n$) | Merck | T8787 | |
| Uranyl acetate ($UO_2(CH_3COO)_2 \cdot 2\ H_2O$) | Serva | 77870.02 | |

### 4.1.2.4 Solutions, mixtures and conjugated substances

| Name | Vendor | Cat. No. | Notes |
|---|---|---|---|
| Acid alcohol | | | 3% HCl in 70% ethanol |
| Alcian blue solution | Carl Roth | 3082.1 | 1% Alcian blue in 3% acetic acid |
| Antibiotic mix | | | 1:100 amphotericin B, 1:100 gentamicin, 1:1000 tetracycline |
| Bacillol® AF | Hartmann | 29210 | |
| Carnoy's solution | | | 60% methanol, 30% chloroform 10% glacial acetic acid |
| Entellan® | VWR | 1.07961 | |
| Epon® 812 (Glycidether 100) | Serva | 21045.01 | |
| FITC-dextran 3000 | Sigma | FD4 | 25 mg/ml |
| Fluoromount-G® | Southern Biotech | 0100-01 | |
| HEPES | Thermo Scientific | 15630080 | |
| Klinikfixans | | | 1% formaldehyde, 2,5% glutaraldehyde, 50 mM HEPES |
| Low-melting agarose | Carl Roth | 6351.1 | |
| Luciferase assay reagent II (LARPII) | Promega | E195A | |
| Paraplast paraffin wax | Carl Roth | X880.2 | |
| Passive lysis buffer (PLB) | Promega | E194A | |
| Permeabilization/ blocking solution | | | 0,2% Triton X-100, 1% BSA in $PBS^{+/+}$ (w/o Triton X-100 as blocking solution only) |
| Phalloidin Alexa Fluor™ 546 | Invitrogen | A22283 | 100x |
| pNPP collection buffer (100 ml) | | | 10 mM TRIS, 150 mM NaCl, ad 100 ml $H_2O$, pH 8.0 |
| pNPP reaction solution | | | 75% pNPP sol. (pH 9.5), 25% col. buffer (pH 8.0), make fresh, keep dark |
| pNPP solution (1 ml) | | | 2,5 mg pNPP, 100 mM diethanolamin, 150 mM NaCl, 2 mM $MgCl_2$, ad 1 ml $H_2O$ (pH 9.5), store at -20°C, keep dark |
| Roti®-Histol | Carl Roth | 6640.4 | |
| Schiff's reagent | Sigma | 3952016 | |
| Scott's tap water | Leica | 3802900 | |
| STOP & Glo® reaction mix (buffer/substrate) | Promega | E640A/E641A | |
| Tannic acid | Carl Roth | 4239.1 | |

### 4.1.3 Buffers and culture media

#### 4.1.3.1 Buffers

Dulbecco's Phosphate buffered saline ($PBS^{+/+}$)
137 mM NaCl, 8.0 mM $Na_2HPO_4$, 2.7 mM KCl, 1.5 mM $KH_2PO_4$, 0.5 mM $MgCl_2$, 0.9 mM $CaCl_2$ (pH 7.4), sterilize

Phosphate buffered saline ($PBS^{-/-}$)
137 mM NaCl, 8.0 mM $Na_2HPO_4$, 2.7 mM KCl, 1.5 mM $KH_2PO_4$ (pH 7.4), sterilize

Ringer's solution
5.4 mM KCl, 1 mM $MgSO_4$, 1.2 mM $CaCl_2$, 10 mM HEPES, 10 mM D-glucose (pH 7.4), sterilize; depending on experiment: 280 mM D-mannitol / 140 mM NaCl

#### 4.1.3.2 Culture media (basic or supplemental precursors)

Advanced DMEM/F12 (basic organoid) Thermo Scientific Cat. No. 12634028
DMEM (basic cell lines) Thermo Scientific Cat. No. 31966047
D1 (differentiation supplement 1, 10x)
10x B-27, 10x N-2, 10 mM N-Acetylcysteine, 100 mM Nicotinamide, 5 µM A83-01 in Adv. DMEM/F12, sterilize and store at -20°C
D2 (differentiation supplement 2, 10x)
10x B-27, 10x N-2, 10 mM N-Acetylcysteine, 100 mM Nicotinamide in Adv. DMEM/F12, sterilize and store at -20°C
M1 (basic mix, 10x)
100 mM HEPES, 20 mM GlutaMAX, 10x P/S in Adv. DMEM/F12
M2 (supplement mix, 10x)
10x B-27, 10x N-2, 10 mM N-Acetylcysteine, 100 mM Nicotinamide, 5 µM A83-01, 100 µM SB202190 in Adv. DMEM/F12, sterilize and store at -20°C
TYI-S-33 basic
18 g Casein Peptone, 9 g Bacto yeast extract, 10 g Glucose, 2 g NaCl, 200 mg Ascorbic Acid, 1 g $K_2HPO_4$, 600 mg $KH_2PO_4$, ad 1 l $H_2O$ (pH 7.0), sterilize and store at -20°C

#### 4.1.3.3 Culture media (complete)

Differentiation mix 1 [medium] (DM-1)
10% M1, 10% D1, 10% conditioned noggin, 20% conditioned R-spondin-1, 50% Adv. DMEM/F12, 50 ng/ml human rec. EGF, sterilize, always make fresh
Differentiation mix 2 [medium] (DM-2)
10% M1, 10% D2, 10% conditioned noggin, 20% conditioned R-spondin-1, 50% Adv. DMEM/F12, 50 ng/ml human rec. EGF, sterilize, always make fresh
DMEM (Caco-2)
1x P/S, 10% FBS, 1x NEAA, additional 10 mM HEPES
DMEM (HEK/L-WRN)
1x P/S, 10% FBS
Spheroid mix [medium] (SM)
10% M1, 10% M2, 10% conditioned noggin, 20% conditioned R-spondin-1, 50% conditioned WRN, 50 ng/ml human rec. EGF, sterilize, always make fresh
TYI-S-33 (*Giardia* sp.)
10 ml FBS, 4 ml L-cysteine solution, 1 ml bovine/ovine bile solution, 1x P/S, 100 µl ammonium ferric citrate, ad 100 ml TYI-S-33 basic, store at 4°C not longer than a week

### 4.1.4 General laboratory equipment

#### 4.1.4.1 Glassware

| Name | Vendor | Cat. No. |
|---|---|---|
| 25/100/250/500/1000-ml DURAN® Bottles | Schott | 21801 1453/1753/2458/ 3651/4459/5455 |
| 25/50/100/250/600-ml DURAN® Beakers | Schott | 21106 1406/1706/2402/ 3604/4806 |
| 50/300/500-ml DURAN® Erlenmeyer Flasks | Schott | 21216 1707/3905/4404 |
| 50-ml DURAN® Mixing Cylinder | Schott | 213901706 |
| 5/10-ml Measuring Pipettes AR® glass | Schott | 243452 302/902 |
| Frosted microscope slides and cover slips | Carl Roth | H868.1/LH26.1 |
| Staining Dish Hellendahl Type | Schott | 233150002 |

#### 4.1.4.2 Plasticware and consumables

| Name | Vendor | Cat. No. |
|---|---|---|
| T25/75/150-$cm^2$ tissue culture flasks | TPP | 90 026/076/151 |
| 12/24/96-well tissue culture plates (F-base) | TPP | 920 12/24/96 |
| 40/60/96-mm Ø tissue culture dishes | TPP | 93 040/060/100 |
| 15/50-ml centrifuge tubes | TPP | 910 15/50 |
| Nunclon™Δ flat-sided 10-ml tubes | Thermo Scientific | 156758 |
| 0.5/1.5/2.0-ml Eppendorf® reaction tubes | Neolab | E-23 13/06/07 |
| 0.5/1.5-ml LoBind® tubes | Eppendorf | 00301080 35/51 |
| 0.2-ml PCR tubes | Neolab | 3-011-50-0 |
| 1.2-ml Cryo tubes | TPP | 89020 |
| 10/100/1000-µl ART® barrier pipet tips | Thermo Scientific | 10313272 |
| 20/200-µl PP filter tips | Nerbe Plus | 07-662-8300 |
| 5/10/25-ml serological pipettes | TPP | 940 /05/10/24 |
| Nunc™ white flat-bottomed 96-well plates | Thermo Scientific | 236107 |
| PCF transwell-inserts (0.6 $cm^2$, 0.4 µm pores) | Millicell | PIHP01250 |
| PET transwell-inserts (0.4 $cm^2$, 0.4 µm pores) | Falcon | 3413 |
| Vacuum filtration "rapid"-Filtermax (0.22 µm) | TPP | 99505 |
| Sartorius™ Minisart® sterile filters (0.22 µm) | Thermo Scientific | 10730792 |
| B Braun™ solo cone Leur syringes (10/20-ml) | Fisher Scientific | 12752637 |
| Falcon™ 70 µm cell strainer | Thermo Scientific | C352350 |
| Cell scraper "S"/"M", rotating | TPP | 9900,666667 |
| C-Chip, Neubauer counting chamber | Science Services | NE63508-01 |
| 25-ml reagent reservoirs | Diversified Biotech | RESE-3000 |
| Oxoid™ AnaeroJar™ 2.5 L | Thermo Scientific | AG0025A |
| Gas-pak Oxoid™ AnaeroGen™ 2.5L sachet | Thermo Scientific | 10269582 |
| Bemis™ Parafilm® "M" | Thermo Scientific | 11762644 |
| Rotilabo®-embedding cassettes | Carl Roth | K115.1 |
| Prepartion folders for slides | Carl Roth | K326.2 |

### 4.1.5 Machines, tools and kits

#### 4.1.5.1 Cell lysing apparatuses

| Name | Vendor |
|---|---|
| French Press EmulsiFlex-C3 | Avestin |
| Sonicator Sonopuls HD 70 | Bandelin |

#### 4.1.5.2 Centrifuges

| | |
|---|---|
| Galaxy MiniStar Mini Centrifuge | VWR |
| Centrifuge 5424 R (cooled) | Eppendorf |
| Multifuge X1R (cooled) | Thermo Scientific |

#### 4.1.5.3 Cooling containers or heaters

| | |
|---|---|
| IsoRack+IsoPack (0°C) | Eppendorf |
| Mini Cooler, temperature retention box (-20°C) | VWR |
| Block heater for 1.5-ml tubes or plates (100°C) | Störk Tronic |

#### 4.1.5.4 Freezers and refrigerators

| | |
|---|---|
| Refrigerator 4°C TP 1760 Premium | Liebherr |
| Freezer -25°C GTP 3656 Premium | Liebherr |
| Ultra Low Temperature Freezer -86°C MDF-U73V | Sanyo |

#### 4.1.5.5 Incubators

| | |
|---|---|
| CB 150 $CO_2$-Incubator | Binder |
| HERAcell® 150 $CO_2$-Incubator | Thermo Scientific |

#### 4.1.5.6 Kits

| | |
|---|---|
| Pierce™ BCA Protein Assay Kit (23225) | Thermo Scientific |
| Dual-Luciferase® Reporter Assay System (E1910) | Promega |
| In Situ Cell Death Detection Kit, Fluorescein (11 684 795 910) | Roche |
| Luminex® Human Premixed Multi-Analyte Kit (LXSAH) | R&D Systems |

#### 4.1.5.7 Microscopes

| Name | Vendor |
|---|---|
| AE31 Trinocular | Motic |
| Axioskop 2 | Zeiss |
| AxioVert 25 | Zeiss |
| Leo 1530 Gemini | Zeiss |
| LSM 780 | Zeiss |
| Tecnai™ 12 Spirit | Fei Company |
| Teneo field emission SEM with CCD camera MegaViewG3 | Fei Company/Olympus |
| Observer Z1 | Zeiss |

#### 4.1.5.8 Microscopic sample preparation equipment

| | |
|---|---|
| Automated Critical Point Dryer CPD 300 | Leica |
| Cool' Sputter Coater E 5100 | Polaron |
| Microtome RM2235 | Leica |
| Ultramicrotome UC 7 | Leica |
| Paraffin embedding station EG1160 | Leica |

#### 4.1.5.9 Pipettes

| | |
|---|---|
| Micropipette Transferpette® 2.5/10/20/100/200/1000, adjustable | Brand |
| Multi-channel micropipette Transferpette® M8-50/M8-200, adjustable | Brand |
| Multipette® M4, adjustable and combitips advanced® | Eppendorf |
| Pipetman G P10G/P20G/P100G/P1000G, adjustable | Gilson |
| Pipetting aid accu-jet® pro | Brand |
| Research® plus 10/20/100/200/1000, adjustable | Eppendorf |

#### 4.1.5.10 Pumps

| | |
|---|---|
| VacuSafe pump | Integra |
| VacuSip pump | Integra |

#### 4.1.5.11 Readers and data gathering tools

| | |
|---|---|
| Infinite® M200 plate reader | Tecan |
| Bio-Plex® 200 analyzer | Bio-Rad |
| pH-Meter CG 825 | Schott |
| TriStar LB 941 multimode microplate reader | Berthold |
| Volt-Ohm meter ERS-2 with electrode STX01 | Millicell |

#### 4.1.5.12 Rocking tables, rotators, stirrer, and vortexer

| Name | Vendor |
|---|---|
| Cooke AM69 Microshaker (orbital) | Denley-Tech |
| Problot Rocker 25 (3D) | Kisker |
| WT 16 Shaker (2D) | Biometra |
| Rotator pluriPlix (tube rotator/roller) | PluriSelect |
| Magnetic Stirrer RET basic (heated) | IKA |
| New Brunswick™ Innova® 40/40R (heated) | Eppendorf |
| FVL-2400N Combi-Spin (vortexer/microfuge) | Biosan |
| Minishaker MS1 (vortexer with plate adapter) | IKA |
| Vortex-Genie® 2 | VWR |

#### 4.1.5.13 Other equipment

| | |
|---|---|
| 15/50-ml racks | TPP |
| 1.5/2.0-ml racks | Biozym |
| Disposable Safety Scalpel #11 | Fine Science Tools |
| Dumont #7 - Fine Forceps | Fine Science Tools |
| Customized Ussing-chamber system with electrodes and computer | / |
| Milli-Q Type 1 water purifier Q-POD® Reference | Millicell |
| Safe 2020 Class II Biological Safety Cabinet | Thermo Scientific |
| Waterbath WNB 14 | Memmert |

### 4.1.6 Molecular biological reagents

#### 4.1.6.1 Antibodies (primary/secondary)

| Name | Vendor | Cat. No. |
|---|---|---|
| ALP, intestinal/placental (rabbit, polyclonal) | NSJ Bioreagents | F44184 |
| Chr-A [C-12] (mouse, monoclonal) | Santa Cruz Biotechnology | sc-393941 |
| Chr-A [C-20] (goat, polyclonal) | Santa Cruz Biotechnology | sc-1488 |
| Claudin-1 (rabbit, polyclonal) | Invitrogen | 71-7800 |
| Claudin-2 (rabbit, polyclonal) | Invitrogen | 51-6100 |
| Claudin-4 (mouse, monoclonal 3E2C1) | Invitrogen | 32-9400 |
| Claudin-5 (rabbit, polyclonal) | Invitrogen | 34-1600 |
| Claudin-8 (rabbit, polyclonal) | Invitrogen | 710222 |
| ClCa-1 (rabbit, monoclonal EPR12254-88) | Abcam | ab180851 |
| DCKL-1 (rabbit, polyclonal) | Abcam | ab37994 |
| GLUT2 (rabbit, polyclonal) | Abcam | ab54460 |
| LGR5 [loop2] (rabbit, polyclonal) | Abgent | AP2745d |
| Lysozyme EC 3.2.1.17 (rabbit, polyclonal) | Dako | A009902-2 |
| Muc-2 (mouse, monoclonal Ccp58) | Monosan | MON 6053 |
| Muc-2 [F-2] (mouse, monoclonal) | Santa Cruz Biotechnology | sc-515032 |
| Muc-2 [H-300] (rabbit, polyclonal) | Santa Cruz Biotechnology | sc-15334 |
| Occludin (rabbit, polyclonal) | Invitrogen | 71-1500 |
| Villin [1D2C3] (mouse, monoclonal) | Santa Cruz Biotechnology | sc-58897 |
| Villin [C-19] (goat, polyclonal) | Santa Cruz Biotechnology | sc-7672 |
| ZO-1 (mouse, monoclonal 1/ZO-1) | BD Bioscience | 610967 |
| α-defensin 5 [8c8] (mouse, monoclonal) | Santa Cruz Biotechnology | sc-53997 |

| Name | Vendor | Cat. No. |
|---|---|---|
| Troph-o-Glo Cy3R (anti-Giardia, Cy3 conjugated) | Waterborne Inc. | A900Cy3R-20X |
| IgG-Cy5 (goat, anti-rabbit) | Jackson Immuno Research | 111-175-144 |
| IgG-Cy5 (donkey, anti-goat) | Jackson Immuno Research | 705-175-147 |
| IgG-DTAF (goat, anti-mouse) | Jackson Immuno Research | 115-016-003 |
| IgG-FITC (donkey, anti-mouse) | Jackson Immuno Research | 715-096-151 |

#### 4.1.6.2 Genetic constructs (plasmids)

| Name | Vendor | Cat. No. |
|---|---|---|
| pM50 Super 8x TOPFlash | Addgene | 12456 |
| pM51 Super 8x FOPFlash | Addgene | 12457 |
| pRenilla (pRL-TK) | Promega | E2241 |

### 4.1.7 Software

| Name | Vendor |
|---|---|
| AxioVision 2009 | Zeiss |
| Excel® | Microsoft |
| ImageJ | NIH |
| R | R-Project |
| Word® | Microsoft |
| ZEN blue edition, black edition, 2012 | Zeiss |

## 4.2 Methods

### 4.2.1 Cell, organoid and parasite culturing

#### 4.2.1.1 Caco-2

Caco-2 cells, used for *Giardia*-infection experiments, were grown on plain surface in T25 or T75 flasks under standard incubation conditions (37°C, 5% $CO_2$, humid) and with DMEM (Caco-2) for regular culturing. Upon reaching confluency, cells were washed twice with $PBS^{-/-}$ and split 1:20 or 1:50 by using gentle dissociation reagent TrypLE™ (usually once a week).
For transwell experiments, 100 000 cells (passage no. < 55) were seeded into 0.6 $cm^2$ 0.4 µm-pore transwell filters (PCF). To allow spontaneous differentiation, Caco-2 cells were grown for 21 days on those filters with complete medium exchanges (400 µl apical, 800 µl basal compartment) twice a week. Monolayer formation was monitored throughout this process regularly by TEER. Transwell filter experiments usually started at day 22.

#### 4.2.1.2 L-WRN (murine L cells)

L-WRN cells, used to produce Wnt3A-, R-spondin-3- and noggin-conditioned medium (simultaneously) for organoid culture, were grown in T150 flasks under standard incubation conditions with DMEM (L-WRN) and hygromycin B (0,5mg/ml) and Geneticin® (0,5mg/ml) to select and maintain genetically engineered cells.
By reaching confluence, cells were washed twice with $PBS^{-/-}$ (avoid carryover of drugs) and 25 ml DMEM (no selective antibiotics apart from P/S) were added to the L-WRN monolayer to start conditioned medium production. Every 24 h, medium supernatant was collected and new medium added for up to 4 days. The harvested conditioned medium of one week was combined, sterile-filtered (0.22 µm) using a vacuum pump ("rapid"-Filtermax devices/VacuSafe), aliquoted, and frozen at -20°C. Prior use, its Wnt-activity was assessed quantitatively using TOP/FOP luciferase assays (4.2.2.4).

#### 4.2.1.3 HEK 293T (expressing R-spondin-1-Fc or HA-noggin-Fc)

Two HEK 293T cell lines, transfected with constructs, selective for Zeocin™, to express either Fc-tagged R-spondin-1 or HA- and Fc-tagged noggin, were used for production of R-spondin-1- and noggin- conditioned medium.

Both cell lines were grown in T150 flasks with constant pressure of 300 µg/ml Zeocin™ to maintain transgenic construct-containing cells. Upon confluence, cells were washed twice with $PBS^{-/-}$ (removing Zeocin™) and 25 ml fresh DMEM (no selective antibiotics apart from P/S, also no FBS) were added to the monolayer to start conditioned medium production. After 7 days, medium supernatant was collected, sterile-filtered (0.22 µm) using a vacuum pump ("rapid"-Filtermax devices/VacuSafe), aliquoted and frozen at -20°C. Batch quality of R-spondin-1 or noggin was compared qualitatively against older batches in dilution series on murine organoid cultures.

#### 4.2.1.4 HEK 293T (untransfected)

HEK cells, used to assess quality of Wnt3A-conditioned medium with TOP/FOP luciferase assays, were grown in T25 or T75 flasks under standard incubation conditions and with DMEM (HEK). Cells were washed once with $PBS^{-/-}$ and split 1:20 or 1:50 by using TrypLE™ twice a week to avoid confluent growth and preserve optimal transfection rates.

#### 4.2.1.5 Small intestinal organoids – crypt isolation, spheroid culturing and ODM generation

Organoid isolation and passaging were conducted according to Sato et al. (2009/2011) with modifications.
Several (3-5) human duodenal biopsy specimens (< 5 $mm^2$) were obtained from voluntary, regarding intestine healthy, patient donors during routine inspection by medical personnel of the Charité Berlin. Fresh biopsy material was transferred into ice cold $PBS^{-/-}$ and processed to isolate the crypts immediately. Biopsy specimens were washed twice with ice-cold $PBS^{-/-}$ to remove mucus and reduce potential microbiota load by using the shear forces of a 5-ml serological pipette by gently pipetting the specimens up and down. Afterwards, specimens were transferred into a 50-ml tube with ice-cold 20 ml 2 mM EDTA in $PBS^{-/-}$ and embedded in ice on a rocking table (WT 16 Shaker) for 40 min to facilitate dissociation. EDTA/PBS solution was discarded afterwards, and specimens were transferred into a BSA-coated 12-ml tube with 8 ml fresh and ice-cold $PBS^{-/-}$. The 12-ml tube was manually shaken vigorously for 30 s to extract crypts from the tissue. Afterwards, specimens were allowed to settle down at the tube bottom, the 8 ml were decanted and collected in a new BSA-coated 50-ml-tube. This procedure was repeated 4 times with increasing shaking intensity. The volume of the almost completely filled 50-ml collection tube with isolated crypts was filtered through a 70 µm cell strainer to separate the smaller crypts from

larger villi or remaining connective tissue particles. The flow-through was collected and centrifuged at 500 x *g* for 5 min at 4°C. Supernatant was discarded and merely visible crypt pellet was resuspended in 4°C Adv. DMEM/F12 and transferred into a new BSA-coated 12-ml tube, which was centrifuged again with the same conditions. Supernatant was removed with 200 µl to remain with the crypt pellet. 200 µl of 4°C Matrigel® were added into the tube and mixed with the remaining Adv. DMEM/F12 to gain a 50% dilution of Matrigel® including resuspended crypts. 50 µl droplets of this mixture were seeded in up to 8 wells of a 24-well plate and allowed to polymerize for 20 min at 37°C (standard conditions). 500 µl SM (including antibiotic mix for isolation and 10 µM ROCK-inhibitor Y-27632) was filled into the respective wells with the crypt/Matrigel® droplet and the plate was incubated under standard conditions. Medium was exchanged the subsequent day and switched to regular SM (without additional antibiotics mixture or ROCK-inhibitor) at the next occasion (medium exchanges were done every other day, except weekends). After one week, cultures consisted mainly of spheroids.

Spheroid cultures were passaged twice a week. Fastest expansion is achieved by a high concentration of spheroids per Matrigel® droplet (e.g. Figure 22), most likely due to increased feed-forward signaling of self-propagation. A doubling of spheroid amount is possible every 3-4 days. For passaging, up to six Matrigel® droplets and their spheroids within were resuspended with a 1000 µl pipette tip and collected in a 12-ml tube, filled with ice-cold Adv. DMEM/F12. The 12-ml tubes were centrifuged at 500 x *g* for 5 min at 4°C. Supernatant was decanted and Matrigel® pellet was removed as much as possible whilst avoiding loss of the spheroids, which were dispersed along a gradient within the Matrigel® at the tube bottom (as a rule of thumb: Matrigel®/spheroid pellet remained below tube's 100-µl mark). If several 12-ml tubes were used (e.g. when more than six spheroid wells were passaged) Matrigel®/spheroid pellets were combined into one 12-ml tube and the last step was repeated with more tolerance to remaining Matrigel®. Ice-cold Adv. DMEM/F12 was added to the pellet to gain approximately 1 ml of volume at the tube bottom. By using shear forces of a 200-ml pipette, spheroid structures were torn apart to achieve a suspension of oligo cell conglomerates or even a single cell state for some of them. Afterwards, 12-ml tubes were filled with ice-cold Adv. DMEM/F12 and centrifuged again. Supernatant was removed, leaving enough volume to ensure a 1:2 dilution in Matrigel®, which has been thawed and adjusted to 4°C beforehand (e.g. for a whole 24-well plate of 50-µl Matrigel® droplets, 600 µl resuspended spheroid cells were combined with 600 µl Matrigel®). The Matrigel®/cell mix must be kept at 4°C (IsoPacks used), since higher temperatures (> 8°C) lead to premature Matrigel®-polymerization and lower temperatures risk cellular freezing damage. Under constant mixing by pipetting, 50-µl droplets of the

solution were pipetted into the wells of a new 24-well plate with hurry. Subsequently, the plate was put into an incubator (standard conditions) to allow the Matrigel® to polymerize. After 15-20 min, wells were filled with 500 µl fresh and pre-warmed SM including ROCK-inhibitor Y-27632 to prevent anoikis each time after disruptive passaging. Medium (then without ROCK-inhibitor) has been exchanged every other day (except weekends). Spheroid culture discontinued after 35 passages.

ODM-generation was conducted similar to normal passaging up to and including spheroid disruption, which was also executed with more rigor to gain even smaller oligo cell conglomerates and further increased numbers of single cells to facilitate monolayers with preferably flat topography (e.g. avoid artifacts as shown in early experiments, Figure 24). Alternatively, a TrypLE™ digestion step (5-10 min at 37°C, also recommended to include ROCK-inhibitor) can be introduced but due to varying amounts of remaining Matrigel® particles compared between such procedures, results were usually less consistent. After spheroid dissociation, the 12-ml tube was filled with ice-cold Adv. DMEM/F12 and centrifuged at 500 x *g* for 5 min at 4°C, supernatant removed. The pellet was resuspended with DM-2 including ROCK-inhibitor Y-27632 in a volume to ensure the transfer of 100 µl of this solution into each 0.6 $cm^2$ 0.4 µm-pore transwell-filter (which were put in wells of a 12-well plate). The transwell-filters were apically coated prior seeding with 100 µl of 10% Matigel® solution for at least 3 h at 4°C with subsequent removal of the coating solution and pre-warming step in the incubator (standard conditions) for at least 10 min to establish a fine protein layer for cell attachment. After transfer of 100 µl of cell/DM-2 solution in the apical transwell-filter compartment, additional 400 µl of DM-2 (including ROCK-inhibitor) were pipetted into the same compartment, whereas 800 µl were transferred into the outer, basal compartment (the actual well of the 12-well plate). Plates with transwell-filters and seeded cells were allowed to settle in the incubator (standard conditions) and to develop ODMs for 7 days. DM-2 medium (without ROCK-inhibitor) was exchanged every other day (except weekends). A color shift of the DM-2 medium to yellow in the apical compartment only, indicated a polarized monolayer with solid epithelial barrier function, which was quantitatively assessed by TEER measurements on day 7 (24 h before infection experiments).

#### 4.2.1.6 *G. duodenalis* trophozoites and infection procedure

Trophozoites, used for infection, were cultured in flat-sided 10-ml-tubes with tight cap in TYI-S-33 medium under standard incubation conditions. For passaging, culture tubes were put on ice for approximately 20 min to facilitate

trophozoite-detachment from the tube. Trophozoites were passaged according to the growth rate of the respective isolate (for WB6 ~1:100, 3 times a week) to synchronously achieve an early-confluent state. The day before an infection experiment, trophozoites were passaged as well in this manner and into several tubes to guarantee late logarithmic or early stationary growth phase and sufficient parasite numbers.
To prepare trophozoites for infection experiments, tubes were put on ice as usual and centrifuged at 1000 x *g* for 5 min at 4°C. Supernatant was discarded and trophozoite pellet was resuspended with ice-cold $PBS^{-/-}$ and combined with other flat-sided tubes of the same isolate in a 12-ml tube, filled up to 10 ml. 10 µl of this 10 ml PBS/trophozoite solution was pipetted into a disposable Neubauer chamber for counting (depending on the magnitude of infection load, the 10 µl were diluted to expect 30-100 trophozoites per quadrant for easy but reliable counting). The 12-ml tube was again centrifuged in the meantime, supernatant removed and ice-cold $PBS^{-/-}$ added to gain a concentration which represents the wanted MOI in a 10-100 µl window (usually 20 µl was intended). Either Caco-2 or ODM transwell-filters were TEER-measured and received fresh medium (in case of ODMs, the apical medium was substituted with TYI-S-33) 2-4 h prior infection. Trophozoites were added to the apical compartment and apical volume was adjusted to 500 µl, basal volume to 1000 µl for all transwell filters. Staurosporine was used as positive control for barrier dysfunction in concentrations of 1 µM (Caco-2) or 2 µM (ODMs) in the basal compartment only. If parasite lysates were used, detached and counted trophozoites were resuspended in ice-cold $PBS^{-/-}$ and either lysed with 6x French Press cycles (EmulsiFlex-C3, 1500-1700 bar for 1 min) or 3x sonicated (probe sonicator Sonopuls HD 70, power 72 D, cycle 90 for 30 s) at 4°C, visually assessed for lysis and controlled for protein content with BCA assay after debris-removal with centrifugation (1000 x *g*, 5 min, 4°C). Parasites considered as dead debris or heat-inactivated were incubated at 70°C for 20 min in a block heater.

### 4.2.2 Measurements and assays

#### 4.2.2.1 (Bio)electric methods (TEER, $I_{SC}$, ionic secretion, dilution potentials)

TEER measurements offer a proxy for epithelial barrier dysfunction *in vitro*. By using a Volt-Ohm meter (Millicell® ERS-2) with a chopstick Ag/AgCl electrode (STX01) the electric resistance of a transwell filter can be measured by placing the shorter electrode end into the apical transwell compartment, the longer end into the outer basal plate-well (electrode design adapted to transwell filters, uses AC and could also be arranged the other way around). The blank electric resistance was determined by the mean of twelve 0.6 $cm^2$ 0.4 µm pored PC

transwell-filters with 37°C DMEM (resulting in 134 Ω), which were subtracted from each measurement to gain the corrected TEER values, corresponding to the cell layer ($R^{layer} = R^{total} - R^{blank}$). Electric resistance values were then standardized to the surface of 1 $cm^2$ ($\Omega \cdot cm^2$). Tight cell monolayers offer higher electric resistance values. Smaller values of this resistance suggest leakage and therefore an impaired barrier function or non-confluent growth. TEER measurements were used for barrier dysfunction experiments as well as monitoring of monolayer formation. It is important to note that TEER is sensitive to temperature and measurements must be conducted quick and preferably on a heating block suitable for a 12 well plate. To avoid contamination or carryover, the chopstick electrode should be cleaned and disinfected. In this work a sequence of three beakers or 50-ml tubes filled with pure water (cleaning), 80% ethanol (disinfection), and pure water again (removal of disinfectant) was used before initial measurements and between different conditions. The final cleaning step at the end of the procedure was in 5 min of Bacillol® AF. The electrode was stored semidry in a parafilm-sealed 12-ml tube.

TEER measurements were also conducted in an Ussing-chamber setup (at Charité Berlin, Campus Benjamin Franklin), which allows further readouts like the $I_{SC}$, dilution potentials and impedance (Ussing & Zerahn, 1951). A regular 0.6 $cm^2$ transwell filter (provided that its small basal feet are removed e.g. by clipping off with forceps) were clamped between two hemichambers, representing the basal and apical side, respectively. Both sides included reservoirs and water-jacketed gas lifts which were filled with 10 ml Ringer's solution and were equilibrated with 100% $O_2$ and 37°C temperature by a secondary circulation system. Build-in electrodes allowed constant electric measurements. Resistance of bathing solution and filter was measured prior to each experiment and subtracted. The hemichambers were open at the top and allowed interference with this system, e.g. by applying substances which were also quickly dispersed as a welcomed side effect of the active gas circulation. A customized computer system recorded TEER readout and controlled electric input of additional electrodes, functioning as current injectors for $I_{SC}$ measurements, which require to set epithelial ionic transport-generated voltage to 0 mV. The amount of current to do this represents the $I_{SC}$.

For measuring electrogenic $Cl^-$ secretion, monolayers were stimulated by PGE2 (1 µM, basal side) and theophylline (10 mM, both sides). The subsequent increase in $I_{SC}$ ($\Delta I_{SC}$) was measured. After reaching steady state, the effect of theophylline and PGE2 was antagonized by bumetanide (10 µM, basal side) and the $I_{SC}$ decrease was measured.
For measuring glucose-dependent $Na^+$ absorption, a glucose free Ringer's solution was used. After equilibration for one hour, aliquots of standard

medium supplemented with 3-O-methyl-D-glucose (non-metabolizable) were added at 10-min intervals, resulting in final concentrations of 4, 8, 16, 32, and 48 mM and $\Delta I_{SC}$ was determined.
Sodium and chloride permeabilities were determined from dilution potentials and the Goldman-Hodgkin-Katz equation (Amasheh et al., 2002; Günzel et al., 2009; Yu et al., 2009). Briefly, NaCl dilution potentials were measured by switching one hemichamber to a solution containing a reduced concentration of NaCl and all other components identical to standard Ringer's solution. Osmolality was balanced by mannitol.

#### 4.2.2.2 Fluorescein/FITC-dextran permeability

Barrier leakage can also be investigated by the transfer of a marker or labeled inert substance from one side of the monolayer (e.g. the apical side) to the other (e.g. into the basal compartment). However, in contrast to TEER, this method can be confounded by cellular uptake (e.g. pinocytosis) and transcellular transport. Two approaches were used in this work: FITC-dextran (large molecule permeability; 3000 Da) in the regular transwell setup and fluorescein (small molecule permeability; 332 Da) in an Ussing-chamber setup.
To investigate FITC-dextran permeability in the transwell-setup, 50 µl samples of basal CTRL- medium were taken and added into three wells of a solid white flat-bottomed 96-well plate with 150 µl $PBS^{-/-}$ to measure blank value for later subtraction. 20 µl of FITC-dextran solution (25 mg/ml) were added to the apical filter compartments (final concentration 1 mg/ml or ~0.3 mM). Treated transwell-filters were subsequently incubated under standard conditions for 2 h. Afterwards, 50 µl of the apical volume of CTRL- filters were used to determine maximum fluorescence intensity and 50 µl of the basal compartment for each monolayer to test were added to 150 µl $PBS^{-/-}$ in the white 96-well plate, respectively and in triplicates. Plate was shaken shortly on a rocking table and fluorometric analysis was conducted with a Tecan Infinite® M200 plate reader (excitation 485 nm; emission 525 nm; bandwidth 20 nm). Linearity was assessed with standards of known concentration and plotted exemplarily also for similar experiments in Appx. 29. Blank values were subtracted (limit of detection was passed if blank-corrected samples exceeded 3 standard deviations of the blanks), and basal fluorescence intensities were put in relation of maximal apical intensity.

Flux studies in Ussing-chambers were performed under short-circuit conditions. For flux measurements, after apical addition of fluorescein (0.1 mM) basal samples were taken at 0, 10, 20, 30, and 40 min. Tracer fluxes and apparent permeabilities were calculated from the amount of fluorescein in the basal

compartment measured fluorometrically by Tecan Infinite® M200 plate reader as well.

#### 4.2.2.3 Alkaline phosphatase activity assay (pNPP/pNP)

ALPi dephosphorylates pNPP to pNP, which can be photometrically measured at 405 nm absorbance, therefore functioning as readout parameter for cellular ALPi activity. Monolayers were washed two times with 37°C warmed $PBS^{+/+}$ and were subsequently treated with 500 µl pNPP-reaction solution apically and 1000 µl $PBS^{+/+}$ basally. After 10 min of standard 37°C incubation, 100 µl of apical supernatant were pipetted into wells of a 96-well plate, which were filled with 100 µl of 1 M NaOH solution per well to block further reactions. 100 µl of the original pNPP-reaction solution was used in the same way as blank. For analysis, absorption values were put in relation to older monolayers. As a side note, this treatment seems to be destructive and led to TEER declines after several hours and was therefore not used for regular differentiation monitoring.

#### 4.2.2.4 TOP/FOP luciferase assay (Wnt quality assessment)

The quality of produced Wnt-conditioned medium was assessed by measuring activity of Wnt on HEK cells, transfected with reporter plasmids in a dual reporter system (Glaeser et al., 2016). Dual reporter systems express and measure two individual reporter enzymes simultaneously. The first reporter (e.g firefly luciferase) gives information about the magnitude of an investigated effect (here Wnt-activity), correlated to an experimental condition (here batches to test). The second reporter (e.g. Renilla luciferase) provides an internal control to which the first reporter can be normalized in order to minimize experimental variability introduced by e.g. differences in transfection or lysis efficiency. Therefore, the transfection of HEK cells with two plasmids simultaneously is required (Wnt-reporter and transfection reporter). For Wnt-activity, the plasmid pM50 Super 8x TOPFlash (eight TCF/LEF sites upstream of a firefly luciferase reporter, which activate expression by binding β-catenin, which in turn is a downstream Wnt-signaling molecule) is used and a plasmid with mutated TCF/LEF binding sites (pM51 Super 8x FOPFlash) serves as negative control/background reporter expression. Each of them was combined with a pRenilla control plasmid, expressing Renilla luciferase in a low constitutive manner.
30,000 HEK 293T cells were seeded into each well of a 24-well plate on the day before. At day of the transfection, a mixture of serum-free DMEM and

27.5 µg/ml PEI with either 5 µg/ml pM50 TOP and 0.5 µg/ml pRenilla, as well as 5 µg/ml pM51 FOP and 0.5 µg/ml pRenilla was made by vortexing and incubating 15 min at RT. 200 µl of the medium/plasmid solutions were added into each HEK-well (old medium was removed first) in a pattern that one half of the plate received TOP/Renilla and the other half received FOP/Renilla. Plate was incubated O/N and medium was exchanged with DMEM (CTRL-) or 50%-dilutions of the Wnt-conditioned medium (3 wells TOP- and 3 wells FOP-transfected HEK cells for each batch to test) on the next day. At the day after, medium was removed and cells were lysed with 100 µl passive lysis buffer (PLB) according to kit Dual-Luciferase® Reporter Assay System (Promega, E1910) instructions by rocking 20 min at RT. Incomplete lysis could be prevented, if necessary, by freezing the plate at -80°C with subsequent thawing to freeze-fracture cells. 5 µl of each well's lysed solution were pipetted into new wells of a white 96-well flat-bottomed plate. The plate was put into a TriStar LB 941 multimode microplate reader and the machine was programmed to inject 50 µl of luciferase assay reagent II (LARPII) into each well with subsequent measurement of bioluminescence (1 s delay, continuous measurement for 7 s). Afterwards, reaction was stopped, firefly luciferase signals quenched, and Renilla luciferase reaction started by injecting 50 µl STOP & Glo® reaction mix and Renilla signal was measured subsequently (1 s delay, continuous measurement for 7 s). TOP/FOP signals were normalized by Renilla signals, the ratio of TOP to FOP signals determines Wnt-activity. Batches were excluded if a certain threshold was not reached (lower 30-fold); others were diluted to meet the standards of the current Wnt batch in use.

#### 4.2.2.5 Fixation for microscopic analysis

Apical and basal medium of monolayers at the end of experiments were removed and subsequently fixed by mainly 4% (*para*-)formaldehyde (20 min at RT) or -20°C cold methanol (20 min at -20°C), depending on capabilities of primary antibodies or to achieve increased trophozoite preservation. Carnoy's solution (O/N) was used for some histological stainings for better mucus preservation (Swidsinski et al., 2005; Hansson & Johansson, 2010; Earle et al., 2015). A customized mix "Klinikfixans" (O/N) was used for electron microscopic analysis. Monolayers were processed for histochemical or cytochemical stainings or immediate microscopic examination or stored in $PBS^{+/+}$ at 4°C for not longer than four days.

#### 4.2.2.6 Histochemistry

Histochemistry uses chemical stainings to visualize more or less specific certain areas, tissue properties or molecules with specific chemical features (e.g. staining of lipids, glycosylated proteins, fibers, DNA, etc.). Histochemistry was conducted to investigate mucus. Therefore, the combination of periodic acid–Schiff (PAS) and/or Alcian blue was used, which bind and stain polysaccharides in general (PAS) or acidic polysaccharides only (Alcian blue) of glycoproteins. The rationale of the co-staining is that all the acidic mucins will be stained (dark blue) by the preceding Alcian blue treatment, which also chemically blocks them, preventing further reactions with PAS during this technique. Neutral mucins which are solely stainable by PAS will subsequently be demonstrated in a contrasting manner (magenta). The combination of the two stainings is perhaps the most sensitive histological method to detect mucus. However, due to their properties, those chemicals also stain the glycocalyx.
After removal of fixative, monolayers in transwell-filters were rinsed with pure water and Alcian blue solution was applied for 15 min with a subsequent washing step for 2 min softly under tap water and then rinsed with pure water, followed by 5 min of 0.5% periodic acid. Another washing step with pure water was followed by staining with Schiff's reagent for 10 min. After a washing step for 5 min under tap water, monolayer's nuclei were stained with haematoxylin solution for 1 min. Thereafter, transwell-filters were washed under running tap water again and treated with acid alcohol (3% HCl in 70% ethanol) to remove excessive staining. After another washing step, Scott's tap water was used for bluing, followed by a washing step with regular tap water. After dehydration, monolayers were removed from the transwell-inserts by punching and mounted with Entellan® on glass slides. In order to investigate cross-sections, monolayers after fixative-removal were immediately extracted from the transwell-inserts and 2% low-melting agarose was dropped on top (apically) to solidify the monolayers. Afterwards, solid monolayers were placed into embedding cassettes for regular paraffin embedding. In short, monolayers were dehydrated with increasing ethanol concentrations (70%, 80%, 95%, 100%; each for 1 h and 2-3 times exchange of ethanol solutions). Afterwards, Roti®-Histol (as xylene substituent) was applied for 1 h (3 times exchanged) to remove ethanol. Paraffin wax at 56-58°C was applied for 1.5 h and monolayers were embedded into paraffin blocks. Blocks were trimmed to an optimal cutting surface and 10 µm slices (smaller ones are problematic due to the filter-membrane) were cut using a microtome (RM 2235). Thin-sections/ribbons, swimming in the water bath were put on glass slides, which were subsequently dried for several hours. Rehydration was initiated with Roti®-Histol O/N and exchanged with a fresh charge on the next day for 1 h. Section-mounted slides were then treated with decreasing ethanol concentrations (100%, 95%, 80%,

70%, 50%; each for 5 min). Afterwards, Alcian blue and/or PAS stainings were conducted similar as described for the whole transwell-filters.

#### 4.2.2.7 Immunofluorescence assay (IFA)

IFA's use antibodies to specifically bind the protein of interest. In a second step, those primary antibodies are bound by anti-(primary)antibodies which are labeled with fluorophores to visualize the primary antibody and therefore the target-protein.
Fixative was removed and monolayers were washed once with $PBS^{+/+}$ and treated with permeabilization/blocking solution apically and basally for at least 2 h. Afterwards, solution was removed and 100 µl primary antibody solution (1:300 – 1:1000, depending on batch and antibody) was added into the apical compartment and 500 µl blocking solution in the basal compartment. Monolayers were placed either at 37°C for 1 h or 4°C O/N. Thereafter, monolayers were washed thoroughly four times with $PBS^{+/+}$ to remove unbound primary antibodies. The same staining procedure was repeated for the secondary antibodies (1:600). If F-actin staining was desired, labeled phalloidin (1:100) was included in this step as well. Afterwards, monolayers were washed once with $PBS^{+/+}$ and treated apically with 100 µl DAPI or Hoechst 33342 solution (1:1000) for 20 min at RT in the dark. Subsequently, monolayers were washed thoroughly three times with $PBS^{+/+}$. For desalination, monolayers were shortly (< 3 s) immersed in a beaker with pure, deionized water and thereafter shortly (< 3 s) immersed in a second beaker with 80% ethanol to facilitate drying. Almost dry (but not dried-out) transwell-filters were rolled between thumb and forefinger to turn 360°, which allowed the removal of the actual filter membrane and its fixed cell layer with a straight pointed scalpel (e.g. blade No. 11) with a move resembling the opening of a can. Up to six membranes were carefully placed onto a glass slide and semi-hardening Fluoromount-G® was dripped on top of and between them. The slides were sealed with a cover slip, placed in a way to avoid inclusion of air bubbles, and stored at 4°C for later microscopic analysis.

#### 4.2.2.8 TUNEL assay

Terminal deoxynucleotidyl transferase dUTP nick end labeling (TUNEL) is a direct staining method for apoptosis or cell death, which fragments the DNA. It makes use of the enzyme terminal deoxynucleotide transferase (TdT), which can attach fluorescein-labeled deoxynucleotides (like dUTP) to the 3'-hydroxyl

terminus of DNA breaks and therefore make DNA fragmentation visible (Crowley et al., 2016).
Staining was conducted according to protocol (*In Situ* Cell Death Detection Kit, Fluorescein; Roche; Cat. No. 11 684 795 910, Version 17), slightly adapted to the IFA protocol under 4.2.2.7.
In short, 50 µl of the kit's enzyme solution (ES) was mixed with 450 µl of the label solution (LS). Monolayers were treated according to 4.2.2.7 up to (or in case of simultaneous IFA also including) the primary antibody staining step. 100 µl of the TUNEL mixture (ES and LS) was added to the apical filter compartment and 500 µl of blocking solution into the basal compartment. Incubation at 37°C for 1 h was followed by the remaining IFA protocol (nuclear staining, mounting, etc.). As a side note, secondary antibodies can also be combined with the TUNEL mixture to increase protocol efficiency.

#### 4.2.2.9 Luminex® assay

The enzyme-linked immunosorbent assay (ELISA)-based Luminex® assay offers multiplexing capabilities to quantify proteins of interest by using a mixture of color-coded polystyrene beads, which are pre-coated with target-specific antibodies. A second antibody, specific for the same target but biotinylated, leads to the formation of an antibody[bead]-antigen-antibody[biotin] sandwich. Added Phycoerythrin (PE)-conjugated streptavidin binds to the biotinylated antibodies. With a dual-laser flow-based detection instrument (e.g. Bio-Rad® Bio-Plex® 200 analyzer) lasers can classify color-coded beads to determine the target protein as well as the magnitude of the PE-signal to indicate the amount of target protein (H. Graham et al., 2019).
Procedure was conducted according to protocol (Luminex® Human Premixed Multi-Analyte Kit; R&D Systems; Cat. No. LXSAH) instructions as follows.
Apical medium supernatant of (un)infected monolayers had been saved and cryo-stored at -80°C previously. After thawing, a 1:2 dilution (75 µL of sample + 75 µL of calibrator diluent RD6-52), as suggested for cell cultures by the kit instructions, was mixed thoroughly. Standards for the proteins of interest were reconstituted in the respective volumes given in the certificate of analysis for 15 min with gently agitation and diluted according to instructions with calibrator diluent RD6-52 in a series of five 3-fold dilutions (100 µl reconstituted standard to 200 µl calibrator diluent RD6-52). The undiluted standard solution serves as highest standard, pure calibrator diluent RD6-52 as blank. The microparticle cocktail was centrifuged at 1000 x *g* for 30 s to settle all beads at the bottom, followed by gently vortexing to resuspend them again without losing particles in the cap region of the vial. The microparticle cocktail was then diluted in diluent RD2-1 in a provided mixing bottle, protecting from

light (500 µl microparticle cocktail to 5 ml diluent RD2-1). The biotinylated antibody mix was centrifuged, vortexed and diluted in RD2-1 like the microparticle cocktail. 100x PE-conjugated streptavidin was diluted to a 1x concentration by addition of 55 µL of streptavidin-PE to 5.5 mL of wash buffer (WB).
Filter-bottomed microplate was pre-wetted by filling each well with 100 µl of WB. The liquid was removed through the filter at the plate bottom by using a customized vacuum manifold to accommodate microplate design. After this and each subsequent wash cycle, the plate bottom was blotted with a paper towel to prevent wicking. The diluted microparticle cocktail was again resuspended and 50 µl of the mixture was added into each well of the pre-wetted filter plate. 50 µl of prepared standard or sample was added per well and the plate was covered with a foil and incubated for 2 h at RT on a horizontal orbital microplate shaker (0.12'' orbit at 500 rpm). Using the vacuum manifold device, liquid was removed and washed with 100 µl WB per well. The washing procedure was repeated two additional times. Afterwards, 50 µl of biotinylated antibody mix was added to each well and a new foil was used to cover the plate for the subsequent incubation for 1 h at RT on the orbital shaker (same conditions). The liquid removal and washing procedures were repeated as previously described. Thereafter, 50 µl of streptavidin-PE were added to each well and covered with foil again to incubate for 30 min at RT on orbital shaker (same conditions). The washing procedure was repeated the same way. Afterwards, beads were resuspended in the wells with 100 µl WB and 2 min incubation at RT on orbital shaker (same conditions). Analysis was conducted immediately thereafter with a Bio-Rad® Bio-Plex® 200 analyzer and quantified according to the respective standard curves using the lowest concentrations as the limits of detection.

#### 4.2.2.10 Trophozoite vitality

To investigate survival of *G. duodenalis* trophozoites within an infection experiment on monolayers, 1 µl of propidium iodide (PI, 2mg/ml; final 6 µM) for life/death staining, and 1 µl of formononetin (10 mM; final 20 µM) to paralyze and detach trophozoites without killing, were added to the apical compartment and incubated for 5 min. After thoroughly mixing the apical medium, a 20-µl sample was taken on a glass slide and examined under a fluorescence microscope to determine the ratio of dead ($PI^+$; excitation: 488 nm, emission: 590 nm) trophozoites to total trophozoite numbers by investigating 10 randomized locations per slide.
To also assess reproductive capacity of trophozoites (trophozoites may live but could be too stressed to reproduce), monolayers were treated with 1 µl of formononetin (10 mM; final 20 µM; or alternatively treated 5 times with ice cold

TYI-S-33) for trophozoite detachment and, after thoroughly mixing, the apical medium was combined with 10 ml fresh ice-cold TYI-S-33 and centrifuged at 1000 x *g* for 5 min at 4°C to remove formononetin. Trophozoite pellet was resuspended in 500 µl TYI-S-33, counted, and a dilution series was made with factor 3,17 (to pass one $\log_{10}$-dimension every other dilution step) by pipetting 46 µl of the solution into 100 µl fresh TYI-S-33, mixing, and then 46 µl of it again in the next 100 µl of TYI-S-33. This was repeated until statistically no trophozoites were left (12 steps, basically a 96-well flat bottom plate with 8 replicates). Plates were incubated in a sealed container (OXOID™ AnaeroJar™ 2.5 L, Thermo Scientific) with gas-pak sachets (Oxoid™ AnaeroGen™ 2.5L) to create an oxygen-deprived environment. Plates were incubated for up to 72 h under standard conditions. Wells with or without established *G. duodenalis* culture were counted in a binary manner (growth yes/no). According to Poisson distribution a dilution which represents less or equal 3 growth-positive out of 8 replicates reaches statistical significance ($p < 0.05$). Therefore, the lowest dilution in which more than 3 wells still offered growth was considered as minimal parasite amount to start a colony (and therefore proof replication). The respective amount of trophozoites was calculated according to this dilution, gaining the minimal number of trophozoites to generate a new culture, which was used for comparison of different time points after infection.

### 4.2.3 Microscopic analysis

#### 4.2.3.1 Light microscopy

Light-microscopic images were taken using bright field (BF), dark field (DF) or phase-contrast techniques like differential interference contrast (DIC) with and without fluorescence filters on Zeiss microscope systems such as Axioskop 2 or Observer Z1 (for more advanced techniques). ZEN software (ZEN blue edition, 2012 for Observer Z1) or AxioVision 2009 software (for Axioskop 2) was used to acquire images. For overviews, mostly 2.5x 10x, or 20x objectives were used, also in tile mode (2x2 to 5x5) to map wider regions without sacrificing resolution. For time series, plate layout and precise positions were saved for recovery. 40x or 63x objectives (with water- or oil-immersion, respectively) were used for higher resolutions and more detailed images. PC transwell-filters (PCF) are not suitable for light microscopy, therefore PET transwell-filters were used for top-view images of monolayers. To counter selective bias, either randomized positions were taken for image acquisition or tile images to map the full membrane/Matrigel®-droplet/region of interest almost entirely.

#### 4.2.3.2 Confocal laser-scanning microscopy (cLSM)

Fluorescence-microscopic images (e.g. from IFAs) were taken by Zeiss LSM 780 microscope system and ZEN (black edition) software at RKI's ZBS4 facility. Confocal laser-scanning microscopes offer higher quality micrographs at higher resolutions due to monochromatic light and a confocal pinhole to minimize scatter (Bayguinov et al., 2018). In contrast to light (transmission) microscopy, PC transwell-filters are suitable for fluorescence (emission) microscopy. 10x or 20x objectives for larger regions, 63x (oil-immersion) objectives for higher details were used. Lasers were chosen to excite respective fluorophores and intensities were adapted to the maximal emitted signal strength for each wavelength in each experiment. Gain (master) values of the detector were adjusted to remain in the linear amplification zone (not exceeding value 750). Digital gain or offset were not used. If (as usual) multiple stainings and therefore fluorophores were used simultaneously, acquisition with "best signal" was chosen as scanning method in the "smart setup" (serial scanning of each laser/wavelength) to avoid spectral overlap. Pinhole (determining confocal section thickness) was adapted to resolution and was either ~2 Airy units for lower, and ~1 Airy units for higher resolution images and, as far as possible, equal or very similar for all wavelengths within one acquisition and experiment. Acquisition was conducted with one line-step but mean-based averaging of 2 scans in bi-directional mode. Scanning speed values were between 6 and 8 (lower numbers for better quality at the expense of increased acquisition time). Occasionally, zoom-feature was used at 0.6 to increase field of view. For most experiments, z-stacks (setting: "optimal" section thickness) were made to map the complete vertical extent of monolayers. Investigated regions were randomized by blind navigation along the monolayer, but in case of z-stacks slightly biased towards flatter areas to reduce z-stack thickness and therefore acquisition time. However, monolayer flatness was assessed by observing the spatial level of nuclear signals only, which should not correlate to any investigated parameter.

#### 4.2.3.3 Scanning electron microscopy (SEM)

Light (photon)-based microscopy faces the problem that a resolution, lower than the wavelength of an applied (laser) beam, cannot be resolved, therefore limiting maximum magnification. Electron beams, however, offer wavelengths up to six dimensions shorter than visible light, therefore increasing resolving power enormously to properly visualize structures as small as 1 Å. SEM is used on samples with either or both, a sputter coated gold/palladium-alloy or osmium tetroxide post-fixation (adding metal atoms at or in the membrane

surface). If electrons hit this surface, they lose energy which is converted into heat, low-energy secondary electron, high-energy backscattered electron, light, and X-ray emission. All of that can be detected and give information about surface composition and topography (Gordon, 2014).
Fragments of 3 mm diameter were punched of monolayers, previously fixed by Klinikfixans for at least 2 h. Fragments were washed with pure water, post-fixed with osmium tetroxide (1% in pure water) for 1 h to add contrast, washed again and dehydrated with increasing amounts of ethanol (30%-100%, 10% steps) to facilitate supercritical drying with $CO_2$ (CPD 300) to preserve fine structures. Sample fragments were put on stubs and sputter coated with Au/Pd alloy (Polaron E5100). Examination was conducted under high vacuum conditions in a field emission SEM (Leo 1530 Gemini) at electron high tension (EHT) of 3.0 kV using the in-lens secondary electron detector, 30.00 µm aperture size, and a working distance (WD) of 3.9 - 4.2 mm.

#### 4.2.3.4 Transmission electron microscopy (TEM)

In contrast to SEM, TEM accelerates electrons to actually travel through the sample in a fashion similar to light microscopy. Therefore, very thin sample sections are required (Winey et al., 2014).
Initial sample preparation was similar to SEM sample treatment. After the washing step with pure water to remove unbound osmium tetroxide, sample fragments were treated with tannic acid (0.1% in 50 mM HEPES) to increase visibility of fibrillary structures (e.g. microvilli, microfilaments), block-contrasted with uranyl acetate (2% in pure water) for negative staining, stepwise dehydrated with ethanol series (30%-100%), and embedded in epoxy resin Epon® 812 which was allowed to polymerize for 48 h at 60°C. Blocks were trimmed and ultra-thin sections (~60 nm) were prepared with an ultramicrotome (UC 7). Sections were further contrasted by uranyl acetate and lead citrate (both 2% in pure water) counterstaining.
For examination, a TEM (Tecnai™ 12 Spirit) at 120 kV and a charge-coupled-device (CCD) camera (MegaViewG3), or a Teneo field emission SEM with a scanning transmission electron microscopy (STEM)-detector operated at 25 kV and 10 mm WD for organizational reasons, was used.

#### 4.2.3.5 Post-processing of microscopic images

Post-processing was reduced as much as possible but was sometimes necessary to increase image quality and to facilitate interpretation of some fluorescence

micrographs. Background was digitally reduced, or signal intensity was digitally increased according to equalized relative thresholds within one experiment's histogram data (pixel intensity in relation to amount) in a reasonable manner to increase contrast only. Tiles were stitched automatically by ZEN software to assemble tile images. Occasionally z-stacks were transformed via maximum intensity projection to compress the whole signal readout of a monolayer to a single image.
Image files were generated from raw or post-processed files of the proprietary czi- or zvi- format by generating TIFF files with universal lossless Lempel–Ziv–Welch (LZW) data compression algorithm. Also, 3D-projections and videos (avi-format) were created with ZEN (blue edition) software.

### 4.2.4 Statistics and computational analysis

#### 4.2.4.1 Signal quantification

To quantify cells positive for a certain marker (e.g. TUNEL$^+$ or ClCa-1$^+$ cells), several randomized picture-samples were taken per monolayer/condition and analyzed by a custom algorithm for ImageJ software to count nuclei (for total cell amount), ClCa-1$^+$ cells or TUNEL$^+$ cells (Appx. 30).

#### 4.2.4.2 Statistical significance testing

Testing for statistical significance was conducted using one-way Analysis of Variance (ANOVA) with subsequent post-hoc Tukey HSD test (including correction for multiple comparisons) on $\log_2$ ratios (e.g. $\log_2$[TEER infected at 48h / TEER before infection]) to compare different conditions for each time point (e.g. TEER $\log_2$ ratios of infected monolayers at 24 h vs. TEER $\log_2$ ratios of uninfected monolayers at 24 h) using programming language R (R Core Team, 2015). Normality was assessed visually with Q-Q plots and mathematically using Shapiro–Wilk test. R packages "ANOVAreplication" (Zondervan-Zwijnenburg, 2019), "car" (Fox & Weisberg, 2019), "dplyr" (Wickham et al., 2019), and "pwr" (Champely, 2018) were used. Appx. 31-Appx. 35 show examples Generation of ratios, comparisons, normalizations, log-transformations, corrections, and other simple data transformations and calculations were conducted mostly with Microsoft Excel®.

#### 4.2.4.3 Visualization and data plotting

For graphical visualization of the data, Microsoft Excel® or R and R package "ggplot2" (Wickham, 2016), "RColorBrewer" (Neuwirth, 2014), and "scales" (Wickham, 2018) were used. Color-combinations within plots in this work were chosen to be distinguishable for three types of colorblindness. Appx. 32 shows an example.

# References


Abdel-Hafeez, E. H., Belal, U. S., Abdellatif, M. Z. M., Naoi, K., and Norose, K. (2013). Breast-feeding protects infantile diarrhea caused by intestinal protozoan infections. *The Korean journal of parasitology* 51, 519–524. doi: 10.3347/kjp.2013.51.5.519

Adam, R. D. (2001). Biology of Giardia lamblia. *Clin. Microbiol. Rev.* 14, 447–475. doi: 10.1128/CMR.14.3.447-475.2001

Aggarwal, A., and Nash, T. E. (1988). Antigenic variation of Giardia lamblia in vivo. *Infection and immunity* 56, 1420–1423.

Albert-Bayo, M., Paracuellos, I., González-Castro, A. M., Rodríguez-Urrutia, A., Rodríguez-Lagunas, M. J., Alonso-Cotoner, C., et al. (2019). Intestinal Mucosal Mast Cells: Key Modulators of Barrier Function and Homeostasis. *Cells* 8. doi: 10.3390/cells8020135

Alevy, Y. G., Patel, A. C., Romero, A. G., Patel, D. A., Tucker, J., Roswit, W. T., et al. (2012). IL-13-induced airway mucus production is attenuated by MAPK13 inhibition. *The Journal of clinical investigation* 122, 4555–4568. doi: 10.1172/JCI64896

Allain, T., Amat, C. B., Motta, J.-P., Manko, A., and Buret, A. G. (2017). Interactions of Giardia sp. with the intestinal barrier: Epithelium, mucus, and microbiota. *Tissue barriers* 5, e1274354. doi: 10.1080/21688370.2016.1274354

Allaire, J. M., Crowley, S. M., Law, H. T., Chang, S.-Y., Ko, H.-J., and Vallance, B. A. (2018). The Intestinal Epithelium: Central Coordinator of Mucosal Immunity. *Trends in immunology* 39, 677–696. doi: 10.1016/j.it.2018.04.002

Al-Mekhlafi, H. M., Al-Maktari, M. T., Jani, R., Ahmed, A., Anuar, T. S., Moktar, N., et al. (2013). Burden of Giardia duodenalis infection and its adverse effects on growth of schoolchildren in rural Malaysia. *PLoS neglected tropical diseases* 7, e2516. doi: 10.1371/journal.pntd.0002516

Amasheh, S., Meiri, N., Gitter, A. H., Schöneberg, T., Mankertz, J., Schulzke, J. D., et al. (2002). Claudin-2 expression induces cation-selective channels in tight junctions of epithelial cells. *Journal of cell science* 115, 4969–4976. doi: 10.1242/jcs.00165

Amat, C. B., Motta, J.-P., Fekete, E., Moreau, F., Chadee, K., and Buret, A. G. (2017). Cysteine Protease-Dependent Mucous Disruptions and Differential Mucin Gene Expression in Giardia duodenalis Infection. *The American journal of pathology* 187, 2486–2498. doi: 10.1016/j.ajpath.2017.07.009

An, W. F., Germain, A. R., Bishop, J. A., Nag, P. P., Metkar, S., Ketterman, J., et al. (2010). *Probe Reports from the NIH Molecular Libraries Program: Discovery of Potent and Highly Selective Inhibitors of GSK3b*. Bethesda (MD).

Andersen, Y. S., Gillin, F. D., and Eckmann, L. (2006). Adaptive immunity-dependent intestinal hypermotility contributes to host defense against Giardia spp. *Infection and immunity* 74, 2473–2476. doi: 10.1128/IAI.74.4.2473-2476.2006

Anderson, R. C., Young, W., Clerens, S., Cookson, A. L., McCann, M. J., Armstrong, K. M., et al. (2013). Human oral isolate Lactobacillus fermentum AGR1487 reduces intestinal barrier integrity by increasing the turnover of microtubules in Caco-2 cells. *PloS one* 8, e78774. doi: 10.1371/journal.pone.0078774

Ankarklev, J., Jerlström-Hultqvist, J., Ringqvist, E., Troell, K., and Svärd, S. G. (2010). Behind the smile: cell biology and disease mechanisms of Giardia species. *Nature reviews. Microbiology* 8, 413–422. doi: 10.1038/nrmicro2317

Araújo, N. S., Mundim, M. J. S., Gomes, M. A., Amorim, R. M. R., Viana, J. C., Queiroz, R. P., et al. (2008). Giardia duodenalis: pathological alterations in gerbils, Meriones unguiculatus, infected with different dosages of trophozoites. *Experimental parasitology* 118, 449–457. doi: 10.1016/j.exppara.2007.10.007

Artis, D., Wang, M. L., Keilbaugh, S. A., He, W., Brenes, M., Swain, G. P., et al. (2004). RELMbeta/FIZZ2 is a goblet cell-specific immune-effector molecule in the gastrointestinal

tract. *Proceedings of the National Academy of Sciences of the United States of America* 101, 13596–13600. doi: 10.1073/pnas.0404034101

Artursson, P. (1990). Epithelial transport of drugs in cell culture. I: A model for studying the passive diffusion of drugs over intestinal absorptive (Caco-2) cells. *Journal of pharmaceutical sciences* 79, 476–482.

Ayabe, T., Satchell, D. P., Wilson, C. L., Parks, W. C., Selsted, M. E., and Ouellette, A. J. (2000). Secretion of microbicidal alpha-defensins by intestinal Paneth cells in response to bacteria. *Nature immunology* 1, 113–118. doi: 10.1038/77783

Bach, S. P., Renehan, A. G., and Potten, C. S. (2000). Stem cells: the intestinal stem cell as a paradigm. *Carcinogenesis* 21, 469–476. doi: 10.1093/carcin/21.3.469

Barker, N., van Es, J. H., Kuipers, J., Kujala, P., van den Born, M., Cozijnsen, M., et al. (2007). Identification of stem cells in small intestine and colon by marker gene Lgr5. *Nature* 449, 1003–1007. doi: 10.1038/nature06196

Baron-Delage, S., Mahraoui, L., Cadoret, A., Veissiere, D., Taillemite, J. L., Chastre, E., et al. (1996). Deregulation of hexose transporter expression in Caco-2 cells by ras and polyoma middle T oncogenes. *The American journal of physiology* 270, G314-23. doi: 10.1152/ajpgi.1996.270.2.G314

Bartelt, L. A., and Platts-Mills, J. A. (2016). Giardia: a pathogen or commensal for children in high-prevalence settings? *Current opinion in infectious diseases* 29, 502–507. doi: 10.1097/QCO.0000000000000293

Bartelt, L. A., Roche, J., Kolling, G., Bolick, D., Noronha, F., Naylor, C., et al. (2013). Persistent G. lamblia impairs growth in a murine malnutrition model. *J. Clin. Invest.* 123, 2672–2684. doi: 10.1172/JCI67294

Bartelt, L. A., and Sartor, R. B. (2015). Advances in understanding Giardia: determinants and mechanisms of chronic sequelae. *F1000prime reports* 7, 62. doi: 10.12703/P7-62

Bartfeld, S., Bayram, T., van de Wetering, M., Huch, M., Begthel, H., Kujala, P., et al. (2015). In vitro expansion of human gastric epithelial stem cells and their responses to bacterial infection. *Gastroenterology* 148, 126-136.e6. doi: 10.1053/j.gastro.2014.09.042

Bayguinov, P. O., Oakley, D. M., Shih, C.-C., Geanon, D. J., Joens, M. S., and Fitzpatrick, J. A. J. (2018). Modern Laser Scanning Confocal Microscopy. *Current protocols in cytometry* 85, e39. doi: 10.1002/cpcy.39

Bénéré, E., van Assche, T., van Ginneken, C., Peulen, O., Cos, P., and Maes, L. (2012). Intestinal growth and pathology of Giardia duodenalis assemblage subtype A(I), A(II), B and E in the gerbil model. *Parasitology* 139, 424–433. doi: 10.1017/S0031182011002137

Bernander, R., Palm, J. E., and Svärd, S. G. (2001). Genome ploidy in different stages of the Giardia lamblia life cycle. *Cellular microbiology* 3, 55–62.

Betanzos, A., Schnoor, M., Javier-Reyna, R., García-Rivera, G., Bañuelos, C., Pais-Morales, J., et al. (2014). Analysis of the epithelial damage produced by Entamoeba histolytica infection. *Journal of visualized experiments : JoVE*. doi: 10.3791/51668

Bhargava, A., Cotton, J. A., Dixon, B. R., Gedamu, L., Yates, R. M., and Buret, A. G. (2015). Giardia duodenalis Surface Cysteine Proteases Induce Cleavage of the Intestinal Epithelial Cytoskeletal Protein Villin via Myosin Light Chain Kinase. *PloS one* 10, e0136102. doi: 10.1371/journal.pone.0136102

Bilenko, N., Levy, A., Dagan, R., Deckelbaum, R. J., El-On, Y., and Fraser, D. (2004). Does co-infection with Giardia lamblia modulate the clinical characteristics of enteric infections in young children? *European journal of epidemiology* 19, 877–883.

Bingham, A. K., Jarroll, E. L., Meyer, E. A., and Radulescu, S. (1979). Giardia sp. physical factors of excystation in vitro, and excystation vs eosin exclusion as determinants of viability. *Experimental parasitology* 47, 284–291.

Birchenough, G. M. H., Johansson, M. E. V., Gustafsson, J. K., Bergström, J. H., and Hansson, G. C. (2015). New developments in goblet cell mucus secretion and function. *Mucosal immunology* 8, 712–719. doi: 10.1038/mi.2015.32

Blume, L.-F., Denker, M., Gieseler, F., and Kunze, T. (2010). Temperature corrected transepithelial electrical resistance (TEER) measurement to quantify rapid changes in paracellular permeability. *Die Pharmazie* 65, 19–24.

Boj, S. F., Hwang, C.-I., Baker, L. A., Chio, I. I. C., Engle, D. D., Corbo, V., et al. (2015). Organoid models of human and mouse ductal pancreatic cancer. *Cell* 160, 324–338. doi: 10.1016/j.cell.2014.12.021

Bojarski, C., Weiske, J., Schoneberg, T., Schroder, W., Mankertz, J., Schulzke, J.-D., et al. (2004). The specific fates of tight junction proteins in apoptotic epithelial cells. *Journal of cell science* 117, 2097–2107. doi: 10.1242/jcs.01071

Borg, M., Phillips, A. D., Smith, M. W., and Brown, D. (1993). Enteric disease in early childhood inhibits microvillus expression by potential stem cells. *Clinical science (London, England : 1979)* 84, 377–379.

Brazovskaja, A., Treutlein, B., and Camp, J. G. (2019). High-throughput single-cell transcriptomics on organoids. *Current opinion in biotechnology* 55, 167–171. doi: 10.1016/j.copbio.2018.11.002

Briske-Anderson, M. J., Finley, J. W., and Newman, S. M. (1997). The influence of culture time and passage number on the morphological and physiological development of Caco-2 cells. *Proceedings of the Society for Experimental Biology and Medicine. Society for Experimental Biology and Medicine (New York, N.Y.)* 214, 248–257.

Broguiere, N., Isenmann, L., Hirt, C., Ringel, T., Placzek, S., Cavalli, E., et al. (2018). Growth of Epithelial Organoids in a Defined Hydrogel. *Advanced materials (Deerfield Beach, Fla.)* 30, e1801621. doi: 10.1002/adma.201801621

Buchel, L. A., Gorenflot, A., Chochillon, C., Savel, J., and Gobert, J. G. (1987). In vitro excystation of Giardia from humans: a scanning electron microscopy study. *The Journal of parasitology* 73, 487–493.

Buret, A., Gall, D. G., and Olson, M. E. (1990). Effects of murine giardiasis on growth, intestinal morphology, and disaccharidase activity. *The Journal of parasitology* 76, 403–409.

Buret, A., Gall, D. G., and Olson, M. E. (1991). Growth, activities of enzymes in the small intestine, and ultrastructure of microvillous border in gerbils infected with Giardia duodenalis. *Parasitology research* 77, 109–114.

Buret, A., Hardin, J. A., Olson, M. E., and Gall, D. G. (1992). Pathophysiology of small intestinal malabsorption in gerbils infected with Giardia lamblia. *Gastroenterology* 103, 506–513.

Buret, A. G. (2007). Mechanisms of epithelial dysfunction in giardiasis. *Gut* 56, 316–317. doi: 10.1136/gut.2006.107771

Buret, A. G., Chin, A. C., and Scott, K. G. (2003). Infection of human and bovine epithelial cells with Cryptosporidium andersoni induces apoptosis and disrupts tight junctional ZO-1: effects of epidermal growth factor. *International journal for parasitology* 33, 1363–1371.

Buret, A. G., Mitchell, K., Muench, D. G., and Scott, K. G. (2002). Giardia lamblia disrupts tight junctional ZO-1 and increases permeability in non-transformed human small intestinal epithelial monolayers: effects of epidermal growth factor. *Parasitology* 125, 11–19.

Burridge, K. (2017). Focal adhesions: a personal perspective on a half century of progress. *The FEBS journal* 284, 3355–3361. doi: 10.1111/febs.14195

Caloni, F., Spotti, M., Pompa, G., Zucco, F., Stammati, A., and Angelis, I. de (2002). Evaluation of Fumonisin B(1) and its metabolites absorption and toxicity on intestinal cells line Caco-2. *Toxicon : official journal of the International Society on Toxinology* 40, 1181–1188.

Camilleri, M., Sellin, J. H., and Barrett, K. E. (2017). Pathophysiology, Evaluation, and Management of Chronic Watery Diarrhea. *Gastroenterology* 152, 515-532.e2. doi: 10.1053/j.gastro.2016.10.014

Campbell, H. K., Maiers, J. L., and DeMali, K. A. (2017). Interplay between tight junctions & adherens junctions. *Experimental cell research* 358, 39–44. doi: 10.1016/j.yexcr.2017.03.061

Carlson, D. W., and Finger, D. R. (2004). Beaver fever arthritis. *Journal of clinical rheumatology : practical reports on rheumatic & musculoskeletal diseases* 10, 86–88. doi: 10.1097/01.rhu.0000120979.11380.16

Champely, S. (2018). *pwr: Basic Functions for Power Analysis: R package version 1.2-2*.

Chantret, I., Rodolosse, A., Barbat, A., Dussaulx, E., Brot-Laroche, E., Zweibaum, A., et al. (1994). Differential expression of sucrase-isomaltase in clones isolated from early and late passages of the cell line Caco-2: evidence for glucose-dependent negative regulation. *Journal of cell science* 107 (Pt 1), 213–225.

Chavez, B., Cedillo-Rivera, R., and Martinez-Palomo, A. (1992). Giardia lamblia: ultrastructural study of the in vitro effect of benzimidazoles. *The Journal of protozoology* 39, 510–515.

Chavez, B., Gonzalez-Mariscal, L., Cedillo-Rivera, R., and Martinez-Palomo, A. (1995). Giardia lamblia: in vitro cytopathic effect of human isolates. *Experimental parasitology* 80, 133–138.

Chavez, B., Knaippe, F., Gonzalez-Mariscal, L., and Martinez-Palomo, A. (1986). Giardia lamblia: electrophysiology and ultrastructure of cytopathology in cultured epithelial cells. *Experimental parasitology* 61, 379–389.

Chen, J., Lau, B. T., Andor, N., Grimes, S. M., Handy, C., Wood-Bouwens, C., et al. (2019). Single-cell transcriptome analysis identifies distinct cell types and niche signaling in a primary gastric organoid model. *Sci. Rep.* 9, 4536. doi: 10.1038/s41598-019-40809-x

Chen, T.-J., He, H.-L., Shiue, Y.-L., Yang, C.-C., Lin, L.-C., Tian, Y.-F., et al. (2018). High chloride channel accessory 1 expression predicts poor prognoses in patients with rectal cancer receiving chemoradiotherapy. *International journal of medical sciences* 15, 1171–1178. doi: 10.7150/ijms.26685

Chen, T.-L., Chen, S., Wu, H.-W., Lee, T.-C., Lu, Y.-Z., Wu, L.-L., et al. (2013). Persistent gut barrier damage and commensal bacterial influx following eradication of Giardia infection in mice. *Gut pathogens* 5, 26. doi: 10.1186/1757-4749-5-26

Cheng, H., and Leblond, C. P. (1974). Origin, differentiation and renewal of the four main epithelial cell types in the mouse small intestine. V. Unitarian Theory of the origin of the four epithelial cell types. *The American journal of anatomy* 141, 537–561. doi: 10.1002/aja.1001410407

Chin, A. C., Teoh, D. A., Scott, K. G.-E., Meddings, J. B., Macnaughton, W. K., and Buret, A. G. (2002). Strain-dependent induction of enterocyte apoptosis by Giardia lamblia disrupts epithelial barrier function in a caspase-3-dependent manner. *Infection and immunity* 70, 3673–3680.

Ching, J. C. H., Lobanova, L., and Loewen, M. E. (2013). Secreted hCLCA1 is a signaling molecule that activates airway macrophages. *PloS one* 8, e83130. doi: 10.1371/journal.pone.0083130

Clayburgh, D. R., Le Shen, and Turner, J. R. (2004). A porous defense: the leaky epithelial barrier in intestinal disease. *Laboratory investigation; a journal of technical methods and pathology* 84, 282–291. doi: 10.1038/labinvest.3700050

Collin, J., Queen, R., Zerti, D., Dorgau, B., Hussain, R., Coxhead, J., et al. (2019). Deconstructing Retinal Organoids: Single Cell RNA-Seq Reveals the Cellular Components of Human Pluripotent Stem Cell-Derived Retina. *Stem cells (Dayton, Ohio)* 37, 593–598. doi: 10.1002/stem.2963

Cotton, J. A., Amat, C. B., and Buret, A. G. (2015). Disruptions of Host Immunity and Inflammation by Giardia Duodenalis: Potential Consequences for Co-Infections in the Gastro-Intestinal Tract. *Pathogens (Basel, Switzerland)* 4, 764–792. doi: 10.3390/pathogens4040764

Cotton, J. A., Beatty, J. K., and Buret, A. G. (2011). Host parasite interactions and pathophysiology in Giardia infections. *International journal for parasitology* 41, 925–933. doi: 10.1016/j.ijpara.2011.05.002

Cotton, J. A., Motta, J.-P., Schenck, L. P., Hirota, S. A., Beck, P. L., and Buret, A. G. (2014). Giardia duodenalis infection reduces granulocyte infiltration in an in vivo model of bacterial toxin-induced colitis and attenuates inflammation in human intestinal tissue. *PloS one* 9, e109087. doi: 10.1371/journal.pone.0109087

Crowley, L. C., Marfell, B. J., and Waterhouse, N. J. (2016). Detection of DNA Fragmentation in Apoptotic Cells by TUNEL. *Cold Spring Harbor protocols* 2016. doi: 10.1101/pdb.prot087221

Curtis, G. H., Patrick, M. K., Catto-Smith, A. G., and Gall, D. G. (1990). Intestinal anaphylaxis in the rat. Effect of chronic antigen exposure. *Gastroenterology* 98, 1558–1566.

Dagci, H., Ustun, S., Taner, M. S., Ersoz, G., Karacasu, F., and Budak, S. (2002). Protozoon infections and intestinal permeability. *Acta tropica* 81, 1–5.

D'Anchino, M., Orlando, D., and Feudis, L. de (2002). Giardia lamblia infections become clinically evident by eliciting symptoms of irritable bowel syndrome. *The Journal of infection* 45, 169–172.

Das, S., Jayaratne, R., and Barrett, K. E. (2018). The Role of Ion Transporters in the Pathophysiology of Infectious Diarrhea. *Cellular and molecular gastroenterology and hepatology* 6, 33–45. doi: 10.1016/j.jcmgh.2018.02.009

Delacour, D., Salomon, J., Robine, S., and Louvard, D. (2016). Plasticity of the brush border - the yin and yang of intestinal homeostasis. *Nature reviews. Gastroenterology & hepatology*. doi: 10.1038/nrgastro.2016.5

Denu, J. M. (2005). The Sir 2 family of protein deacetylases. *Current opinion in chemical biology* 9, 431–440. doi: 10.1016/j.cbpa.2005.08.010

Di Campbell, McPhail, G., Lunn, P. G., Elia, M., and Jeffries, D. J. (2004). Intestinal inflammation measured by fecal neopterin in Gambian children with enteropathy: association with growth failure, Giardia lamblia, and intestinal permeability. *Journal of pediatric gastroenterology and nutrition* 39, 153–157.

Diamond, L. S., Harlow, D. R., and Cunnick, C. C. (1978). A new medium for the axenic cultivation of Entamoeba histolytica and other Entamoeba. *Transactions of the Royal Society of Tropical Medicine and Hygiene* 72, 431–432. doi: 10.1016/0035-9203(78)90144-x

Dizdar, V., Hausken, T., Larum, O. D., Gilja, O. H., Langeland, N., and Hanevik, K. (2018). Prolonged duodenal mucosal lymphocyte alterations in patients with and without post infectious functional gastrointestinal disorders after Giardia infection. *The Journal of infectious diseases*. doi: 10.1093/infdis/jiy690

Dormond, M., Gutierrez, R. L., and Porter, C. K. (2016). Giardia lamblia infection increases risk of chronic gastrointestinal disorders. *Tropical diseases, travel medicine and vaccines* 2, 17. doi: 10.1186/s40794-016-0030-0

DuPont, H. L. (2013). Giardia: both a harmless commensal and a devastating pathogen. *The Journal of clinical investigation* 123, 2352–2354. doi: 10.1172/JCI69932

DuPont, H. L., and Hornick, R. B. (1973). Adverse effect of lomotil therapy in shigellosis. *JAMA* 226, 1525–1528.

Earle, K. A., Billings, G., Sigal, M., Lichtman, J. S., Hansson, G. C., Elias, J. E., et al. (2015). Quantitative Imaging of Gut Microbiota Spatial Organization. *Cell host & microbe* 18, 478–488. doi: 10.1016/j.chom.2015.09.002

Edlind, T. D., Hang, T. L., and Chakraborty, P. R. (1990). Activity of the anthelmintic benzimidazoles against Giardia lamblia in vitro. *Journal of Infectious Diseases* 162, 1408–1411. doi: 10.1093/infdis/162.6.1408

Eguchi, Y., Shimizu, S., and Tsujimoto, Y. (1997). Intracellular ATP levels determine cell death fate by apoptosis or necrosis. *Cancer research* 57, 1835–1840.

Elmore, S. (2007). Apoptosis: a review of programmed cell death. *Toxicologic pathology* 35, 495–516. doi: 10.1080/01926230701320337

El-Shewy, K. A., and Eid, R. A. (2005). In vivo killing of Giardia trophozoites harbouring bacterial endosymbionts by intestinal Paneth cells: an ultrastructural study. *Parasitology* 130, 269–274.

Engle, M. J., Goetz, G. S., and Alpers, D. H. (1998). Caco-2 cells express a combination of colonocyte and enterocyte phenotypes. *Journal of cellular physiology* 174, 362–369. doi: 10.1002/(SICI)1097-4652(199803)174:3<362:AID-JCP10>3.0.CO;2-B

Erlandsen, S. L., and Chase, D. G. (1974). Morphological alterations in the microvillous border of villous epithelial cells produced by intestinal microorganisms. *The American journal of clinical nutrition* 27, 1277–1286. doi: 10.1093/ajcn/27.11.1277

Erlandsen, S. L., Macechko, P. T., van Keulen, H., and Jarroll, E. L. (1996). Formation of the Giardia cyst wall: studies on extracellular assembly using immunogold labeling and high resolution field emission SEM. *The Journal of eukaryotic microbiology* 43, 416–429.

Escobedo, A. A., Hanevik, K., Almirall, P., Cimerman, S., and Alfonso, M. (2014). Management of chronic Giardia infection. *Expert review of anti-infective therapy* 12, 1143–1157. doi: 10.1586/14787210.2014.942283

Evans-Osses, I., Mojoli, A., Monguio-Tortajada, M., Marcilla, A., Aran, V., Amorim, M., et al. (2017). Microvesicles released from Giardia intestinalis disturb host-pathogen response in vitro. *European journal of cell biology* 96, 131–142. doi: 10.1016/j.ejcb.2017.01.005

Fajdiga, S., Koninkx, J. F. J. G., Tooten, P. C. J., and Marinsek-Logar, R. (2006). Interference of Salmonella enteritidis and Lactobacillus spp. with IL-8 levels and transepithelial electrical resistance of enterocyte-like Caco-2 cells. *Folia microbiologica* 51, 268–272.

Farhadi, A., Banan, A., Fields, J., and Keshavarzian, A. (2003). Intestinal barrier: an interface between health and disease. *Journal of gastroenterology and hepatology* 18, 479–497.

Farthing, M. J. (1997). The molecular pathogenesis of giardiasis. *Journal of pediatric gastroenterology and nutrition* 24, 79–88.

Faso, C., and Hehl, A. B. (2011). Membrane trafficking and organelle biogenesis in Giardia lamblia: use it or lose it. *International journal for parasitology* 41, 471–480. doi: 10.1016/j.ijpara.2010.12.014

Faso, C., Konrad, C., Schraner, E. M., and Hehl, A. B. (2013). Export of cyst wall material and Golgi organelle neogenesis in Giardia lamblia depend on endoplasmic reticulum exit sites. *Cellular microbiology* 15, 537–553. doi: 10.1111/cmi.12054

Fassio, F., Facioni, M. S., and Guagnini, F. (2018). Lactose Maldigestion, Malabsorption, and Intolerance: A Comprehensive Review with a Focus on Current Management and Future Perspectives. *Nutrients* 10. doi: 10.3390/nu10111599

Feng, Y., and Xiao, L. (2011). Zoonotic potential and molecular epidemiology of Giardia species and giardiasis. *Clinical microbiology reviews* 24, 110–140. doi: 10.1128/CMR.00033-10

Fiorentino, M., Ding, H., Blanchard, T. G., Czinn, S. J., Sztein, M. B., and Fasano, A. (2013). Helicobacter pylori-induced disruption of monolayer permeability and proinflammatory cytokine secretion in polarized human gastric epithelial cells. *Infection and immunity* 81, 876–883. doi: 10.1128/IAI.01406-12

Fisher, B. S., Estrano, C. E., and Cole, J. A. (2013). Modeling long-term host cell-Giardia lamblia interactions in an in vitro co-culture system. *PloS one* 8, e81104. doi: 10.1371/journal.pone.0081104

Fogh, J., Fogh, J. M., and Orfeo, T. (1977). One hundred and twenty-seven cultured human tumor cell lines producing tumors in nude mice. *Journal of the National Cancer Institute* 59, 221–226. doi: 10.1093/jnci/59.1.221

Formeister, E. J., Sionas, A. L., Lorance, D. K., Barkley, C. L., Lee, G. H., and Magness, S. T. (2009). Distinct SOX9 levels differentially mark stem/progenitor populations and enteroendocrine cells of the small intestine epithelium. *American journal of physiology. Gastrointestinal and liver physiology* 296, G1108-18. doi: 10.1152/ajpgi.00004.2009

Fox, J., and Weisberg, S. (2019). *An {R} Companion to Applied Regression*. Thousand Oaks (CA): Sage.

Fraser, D., Bilenko, N., Deckelbaum, R. J., Dagan, R., El-On, J., and Naggan, L. (2000). Giardia lamblia carriage in Israeli Bedouin infants: risk factors and consequences. *Clinical infectious diseases : an official publication of the Infectious Diseases Society of America* 30, 419–424. doi: 10.1086/313722

Frey, A., Giannasca, K. T., Weltzin, R., Giannasca, P. J., Reggio, H., Lencer, W. I., et al. (1996). Role of the glycocalyx in regulating access of microparticles to apical plasma membranes of

intestinal epithelial cells: implications for microbial attachment and oral vaccine targeting. *The Journal of experimental medicine* 184, 1045–1059. doi: 10.1084/jem.184.3.1045

Frisch, S. M., and Francis, H. (1994). Disruption of epithelial cell-matrix interactions induces apoptosis. *The Journal of cell biology* 124, 619–626. doi: 10.1083/jcb.124.4.619

Fujii, M., Matano, M., Toshimitsu, K., Takano, A., Mikami, Y., Nishikori, S., et al. (2018). Human Intestinal Organoids Maintain Self-Renewal Capacity and Cellular Diversity in Niche-Inspired Culture Condition. *Cell stem cell* 23, 787-793.e6. doi: 10.1016/j.stem.2018.11.016

Fujita, J. (1999). Cold shock response in mammalian cells. *Journal of molecular microbiology and biotechnology* 1, 243–255.

Furuse, M., Fujita, K., Hiiragi, T., Fujimoto, K., and Tsukita, S. (1998). Claudin-1 and -2: novel integral membrane proteins localizing at tight junctions with no sequence similarity to occludin. *The Journal of cell biology* 141, 1539–1550. doi: 10.1083/jcb.141.7.1539

Furuse, M., Hirase, T., Itoh, M., Nagafuchi, A., Yonemura, S., and Tsukita, S. (1993). Occludin: a novel integral membrane protein localizing at tight junctions. *The Journal of cell biology* 123, 1777–1788. doi: 10.1083/jcb.123.6.1777

Gao, D., Vela, I., Sboner, A., Iaquinta, P. J., Karthaus, W. R., Gopalan, A., et al. (2014). Organoid cultures derived from patients with advanced prostate cancer. *Cell* 159, 176–187. doi: 10.1016/j.cell.2014.08.016

Garzon, M., Pereira-da-Silva, L., Seixas, J., Papoila, A. L., Alves, M., Ferreira, F., et al. (2017). Association of enteric parasitic infections with intestinal inflammation and permeability in asymptomatic infants of Sao Tome Island. *Pathogens and global health* 111, 116–127. doi: 10.1080/20477724.2017.1299831

Gassler, N. (2017). Paneth cells in intestinal physiology and pathophysiology. *World journal of gastrointestinal pathophysiology* 8, 150–160. doi: 10.4291/wjgp.v8.i4.150

Gavrieli, Y., Sherman, Y., and Ben-Sasson, S. A. (1992). Identification of programmed cell death in situ via specific labeling of nuclear DNA fragmentation. *The Journal of cell biology* 119, 493–501. doi: 10.1083/jcb.119.3.493

Gerbe, F., Legraverend, C., and Jay, P. (2012). The intestinal epithelium tuft cells: specification and function. *Cellular and molecular life sciences : CMLS* 69, 2907–2917. doi: 10.1007/s00018-012-0984-7

Gerbe, F., Sidot, E., Smyth, D. J., Ohmoto, M., Matsumoto, I., Dardalhon, V., et al. (2016). Intestinal epithelial tuft cells initiate type 2 mucosal immunity to helminth parasites. *Nature* 529, 226–230. doi: 10.1038/nature16527

Gericke, B., Amiri, M., and Naim, H. Y. (2016). The multiple roles of sucrase-isomaltase in the intestinal physiology. *Molecular and cellular pediatrics* 3, 2. doi: 10.1186/s40348-016-0033-y

Giannasca, K. T., Giannasca, P. J., and Neutra, M. R. (1996). Adherence of Salmonella typhimurium to Caco-2 cells: identification of a glycoconjugate receptor. *Infection and immunity* 64, 135–145.

Gibson, A., Lewis, A. P., Affleck, K., Aitken, A. J., Meldrum, E., and Thompson, N. (2005). hCLCA1 and mCLCA3 are secreted non-integral membrane proteins and therefore are not ion channels. *The Journal of biological chemistry* 280, 27205–27212. doi: 10.1074/jbc.M504654200

Gillin, F. D., Reiner, D. S., Gault, M. J., Douglas, H., Das, S., Wunderlich, A., et al. (1987). Encystation and expression of cyst antigens by Giardia lamblia in vitro. *Science (New York, N.Y.)* 235, 1040–1043.

Gjorevski, N., Sachs, N., Manfrin, A., Giger, S., Bragina, M. E., Ordóñez-Morán, P., et al. (2016). Designer matrices for intestinal stem cell and organoid culture. *Nature* 539, 560–564. doi: 10.1038/nature20168

Glaeser, K., Boutros, M., and Gross, J. C. (2016). Biochemical Methods to Analyze Wnt Protein Secretion. *Methods in molecular biology (Clifton, N.J.)* 1481, 17–28. doi: 10.1007/978-1-4939-6393-5_3

Gonzalez, L. M., Moeser, A. J., and Blikslager, A. T. (2015). Animal models of ischemia-reperfusion-induced intestinal injury: progress and promise for translational research. *American journal of physiology. Gastrointestinal and liver physiology* 308, G63-75. doi: 10.1152/ajpgi.00112.2013

Gonzalez, L. M., Williamson, I., Piedrahita, J. A., Blikslager, A. T., and Magness, S. T. (2013). Cell lineage identification and stem cell culture in a porcine model for the study of intestinal epithelial regeneration. *PloS one* 8, e66465. doi: 10.1371/journal.pone.0066465

Gordon, R. E. (2014). Electron microscopy: a brief history and review of current clinical application. *Methods in molecular biology (Clifton, N.J.)* 1180, 119–135. doi: 10.1007/978-1-4939-1050-2_7

Gorowara, S., Ganguly, N. K., Mahajan, R. C., and Walia, B. N. (1992). Study on the mechanism of Giardia lamblia induced diarrhoea in mice. *Biochimica et biophysica acta* 1138, 122–126. doi: 10.1016/0925-4439(92)90051-n

Gorowara, S., Ganguly, N. K., Mahajan, R. C., and Walia, B. N. (1994). Involvement of intracellular calcium stores in Giardia lamblia induced diarrhoea in mice. *FEMS microbiology letters* 120, 231–236. doi: 10.1111/j.1574-6968.1994.tb07038.x

Goto, R., Mascie-Taylor, C. G., and Lunn, P. G. (2009). Impact of intestinal permeability, inflammation status and parasitic infections on infant growth faltering in rural Bangladesh. *The British journal of nutrition* 101, 1509–1516. doi: 10.1017/S0007114508083554

Goto, R., Panter-Brick, C., Northrop-Clewes, C. A., Manahdhar, R., and Tuladhar, N. R. (2002). Poor intestinal permeability in mildly stunted Nepali children: associations with weaning practices and Giardia lamblia infection. *The British journal of nutrition* 88, 141–149.

Graham, H., Chandler, D. J., and Dunbar, S. A. (2019). The genesis and evolution of bead-based multiplexing. *Methods (San Diego, Calif.)* 158, 2–11. doi: 10.1016/j.ymeth.2019.01.007

Graham, W. V., He, W., Marchiando, A. M., Zha, J., Singh, G., Li, H.-S., et al. (2019). Intracellular MLCK1 diversion reverses barrier loss to restore mucosal homeostasis. *Nature medicine* 25, 690–700. doi: 10.1038/s41591-019-0393-7

Grasl-Kraupp, B., Ruttkay-Nedecky, B., Koudelka, H., Bukowska, K., Bursch, W., and Schulte-Hermann, R. (1995). In situ detection of fragmented DNA (TUNEL assay) fails to discriminate among apoptosis, necrosis, and autolytic cell death: a cautionary note. *Hepatology (Baltimore, Md.)* 21, 1465–1468.

Grencis, R. K., and Worthington, J. J. (2016). Tuft Cells: A New Flavor in Innate Epithelial Immunity. *Trends in parasitology* 32, 583–585. doi: 10.1016/j.pt.2016.04.016

Gribble, F. M., and Reimann, F. (2016). Enteroendocrine Cells: Chemosensors in the Intestinal Epithelium. *Annual review of physiology* 78, 277–299. doi: 10.1146/annurev-physiol-021115-105439

Grotmol, T., and van Dyke, R. W. (1992). Prostaglandin- and theophylline-induced C1 secretion in rat distal colon is inhibited by microtubule inhibitors. *Digestive diseases and sciences* 37, 1709–1717.

Gruber, A. D., Elble, R. C., Ji, H. L., Schreur, K. D., Fuller, C. M., and Pauli, B. U. (1998). Genomic cloning, molecular characterization, and functional analysis of human CLCA1, the first human member of the family of Ca2+-activated Cl- channel proteins. *Genomics* 54, 200–214. doi: 10.1006/geno.1998.5562

Günzel, D., Amasheh, S., Pfaffenbach, S., Richter, J. F., Kausalya, P. J., Hunziker, W., et al. (2009). Claudin-16 affects transcellular Cl- secretion in MDCK cells. *The Journal of physiology* 587, 3777–3793. doi: 10.1113/jphysiol.2009.173401

Haber, A. L., Biton, M., Rogel, N., Herbst, R. H., Shekhar, K., Smillie, C., et al. (2017). A single-cell survey of the small intestinal epithelium. *Nature* 551, 333–339. doi: 10.1038/nature24489

Hagel, I., Puccio, F., López, E., Lugo, D., Cabrera, M., and Di Prisco, M. C. (2014). Intestinal parasitic infections and atopic dermatitis among Venezuelan Warao Amerindian pre- school children. *Pediatric allergy and immunology : official publication of the European Society of Pediatric Allergy and Immunology* 25, 276–282. doi: 10.1111/pai.12190

Hahn, S., Nam, M.-O., Noh, J. H., Lee, D. H., Han, H. W., Kim, D. H., et al. (2017). Organoid-based epithelial to mesenchymal transition (OEMT) model: from an intestinal fibrosis perspective. *Sci. Rep.* 7, 2435. doi: 10.1038/s41598-017-02190-5

Halbleib, J. M., and Nelson, W. J. (2006). Cadherins in development: cell adhesion, sorting, and tissue morphogenesis. *Genes & development* 20, 3199–3214. doi: 10.1101/gad.1486806

Halliez, M. C. M., Motta, J.-P., Feener, T. D., Guerin, G., LeGoff, L., Francois, A., et al. (2016). Giardia duodenalis induces para-cellular bacterial translocation and causes post-infectious visceral hypersensitivity. *American journal of physiology. Gastrointestinal and liver physiology*, 144. doi: 10.1152/ajpgi.00144.2015

Hally, A. D. (1958). The fine structure of the Paneth cell. *Journal of anatomy* 92, 268–277.

Hanevik, K. (2016). Giardia lamblia - Pathogen or Commensal? *Clinical infectious diseases : an official publication of the Infectious Diseases Society of America*. doi: 10.1093/cid/ciw392

Hanevik, K., Wensaas, K.-A., Rortveit, G., Eide, G. E., Morch, K., and Langeland, N. (2014). Irritable bowel syndrome and chronic fatigue 6 years after giardia infection: a controlled prospective cohort study. *Clinical infectious diseases : an official publication of the Infectious Diseases Society of America* 59, 1394–1400. doi: 10.1093/cid/ciu629

Hansen, G. H., Niels-Christiansen, L.-L., Immerdal, L., and Danielsen, E. M. (2006). Antibodies in the small intestine: mucosal synthesis and deposition of anti-glycosyl IgA, IgM, and IgG in the enterocyte brush border. *American journal of physiology. Gastrointestinal and liver physiology* 291, G82-90. doi: 10.1152/ajpgi.00021.2006

Hansson, G. C., and Johansson, M. E. (2010). The inner of the two Muc2 mucin-dependent mucus layers in colon is devoid of bacteria. *Gut microbes* 1, 51–54. doi: 10.4161/gmic.1.1.10470

Harder, J. L., Menon, R., Otto, E. A., Zhou, J., Eddy, S., Wys, N. L., et al. (2019). Organoid single cell profiling identifies a transcriptional signature of glomerular disease. *JCI insight* 4. doi: 10.1172/jci.insight.122697

Hardin, J. A., Buret, A. G., Olson, M. E., Kimm, M. H., and Gall, D. G. (1997). Mast cell hyperplasia and increased macromolecular uptake in an animal model of giardiasis. *The Journal of parasitology* 83, 908–912.

Harris, J., and Shields, R. (1970). Absorption and secretion of water and electrolytes by the intact human colon in diffuse untreated proctocolitis. *Gut* 11, 27–33. doi: 10.1136/gut.11.1.27

Hasnain, S. Z., Gallagher, A. L., Grencis, R. K., and Thornton, D. J. (2013). A new role for mucins in immunity: insights from gastrointestinal nematode infection. *The international journal of biochemistry & cell biology* 45, 364–374. doi: 10.1016/j.biocel.2012.10.011

Hayflick, L. (1979). The cell biology of aging. *The Journal of investigative dermatology* 73, 8–14.

Helander, H. F., and Fändriks, L. (2014). Surface area of the digestive tract - revisited. *Scandinavian journal of gastroenterology* 49, 681–689. doi: 10.3109/00365521.2014.898326

Herbert, D.'B. R., Yang, J.-Q., Hogan, S. P., Groschwitz, K., Khodoun, M., Munitz, A., et al. (2009). Intestinal epithelial cell secretion of RELM-beta protects against gastrointestinal worm infection. *The Journal of experimental medicine* 206, 2947–2957. doi: 10.1084/jem.20091268

Hetsko, M. L., McCaffery, J. M., Svärd, S. G., Meng, T. C., Que, X., and Gillin, F. D. (1998). Cellular and transcriptional changes during excystation of Giardia lamblia in vitro. *Experimental parasitology* 88, 172–183. doi: 10.1006/expr.1998.4246

Heyworth, M. F. (2016). Giardia duodenalis genetic assemblages and hosts. *Parasite (Paris, France)* 23, 13. doi: 10.1051/parasite/2016013

Hidalgo, I. J., Raub, T. J., and Borchardt, R. T. (1989). Characterization of the human colon carcinoma cell line (Caco-2) as a model system for intestinal epithelial permeability. *Gastroenterology* 96, 736–749. doi: 10.1016/0016-5085(89)90897-4

Hiraoka, K., Hayashi, T., Kaneko, R., Nasu-Nishimura, Y., Koyama-Nasu, R., Kawasaki, Y., et al. (2015). SOX9-mediated upregulation of LGR5 is important for glioblastoma tumorigenicity. *Biochemical and biophysical research communications* 460, 216–221. doi: 10.1016/j.bbrc.2015.03.012

Hollm-Delgado, M.-G., Gilman, R. H., Bern, C., Cabrera, L., Sterling, C. R., Black, R. E., et al. (2008). Lack of an adverse effect of Giardia intestinalis infection on the health of Peruvian children. *American journal of epidemiology* 168, 647–655. doi: 10.1093/aje/kwn177

Hoover, B., Baena, V., Kaelberer, M. M., Getaneh, F., Chinchilla, S., and Bohórquez, D. V. (2017). The intestinal tuft cell nanostructure in 3D. *Sci. Rep.* 7, 1652. doi: 10.1038/s41598-017-01520-x

Hoshino, M., Morita, S., Iwashita, H., Sagiya, Y., Nagi, T., Nakanishi, A., et al. (2002). Increased expression of the human Ca2+-activated Cl- channel 1 (CaCC1) gene in the asthmatic airway. *American journal of respiratory and critical care medicine* 165, 1132–1136. doi: 10.1164/ajrccm.165.8.2107068

Howitt, M. R., Lavoie, S., Michaud, M., Blum, A. M., Tran, S. V., Weinstock, J. V., et al. (2016). Tuft cells, taste-chemosensory cells, orchestrate parasite type 2 immunity in the gut. *Science (New York, N.Y.)* 351, 1329–1333. doi: 10.1126/science.aaf1648

Hu, D., Ansari, D., Bauden, M., Zhou, Q., and Andersson, R. (2019). The Emerging Role of Calcium-activated Chloride Channel Regulator 1 in Cancer. *Anticancer research* 39, 1661–1666. doi: 10.21873/anticanres.13271

Hu, D., Ansari, D., Zhou, Q., Sasor, A., Hilmersson, K. S., Bauden, M., et al. (2018). Calcium-activated chloride channel regulator 1 as a prognostic biomarker in pancreatic ductal adenocarcinoma. *BMC cancer* 18, 1096. doi: 10.1186/s12885-018-5013-2

Huch, M., Dorrell, C., Boj, S. F., van Es, J. H., Li, V. S. W., van de Wetering, M., et al. (2013). In vitro expansion of single Lgr5+ liver stem cells induced by Wnt-driven regeneration. *Nature* 494, 247–250. doi: 10.1038/nature11826

Huch, M., Gehart, H., van Boxtel, R., Hamer, K., Blokzijl, F., Verstegen, M. M. A., et al. (2015). Long-term culture of genome-stable bipotent stem cells from adult human liver. *Cell* 160, 299–312. doi: 10.1016/j.cell.2014.11.050

Huch, M., Knoblich, J. A., Lutolf, M. P., and Martinez-Arias, A. (2017). The hope and the hype of organoid research. *Development (Cambridge, England)* 144, 938–941. doi: 10.1242/dev.150201

Humen, M. A., Pérez, P. F., and Liévin-Le Moal, V. (2011). Lipid raft-dependent adhesion of Giardia intestinalis trophozoites to a cultured human enterocyte-like Caco-2/TC7 cell monolayer leads to cytoskeleton-dependent functional injuries. *Cellular microbiology* 13, 1683–1702. doi: 10.1111/j.1462-5822.2011.01647.x

Ignatius, R., Gahutu, J. B., Klotz, C., Steininger, C., Shyirambere, C., Lyng, M., et al. (2012). High prevalence of Giardia duodenalis Assemblage B infection and association with underweight in Rwandan children. *PLoS neglected tropical diseases* 6, e1677. doi: 10.1371/journal.pntd.0001677

Ikenouchi, J., Furuse, M., Furuse, K., Sasaki, H., Tsukita, S., and Tsukita, S. (2005). Tricellulin constitutes a novel barrier at tricellular contacts of epithelial cells. *The Journal of cell biology* 171, 939–945. doi: 10.1083/jcb.200510043

In, J. G., Foulke-Abel, J., Estes, M. K., Zachos, N. C., Kovbasnjuk, O., and Donowitz, M. (2016). Human mini-guts: new insights into intestinal physiology and host-pathogen interactions. *Nature reviews. Gastroenterology & hepatology* 13, 633–642. doi: 10.1038/nrgastro.2016.142

Ives, A., Ronet, C., Prevel, F., Ruzzante, G., Fuertes-Marraco, S., Schutz, F., et al. (2011). Leishmania RNA virus controls the severity of mucocutaneous leishmaniasis. *Science (New York, N.Y.)* 331, 775–778. doi: 10.1126/science.1199326

Janáky, R., Varga, V., Hermann, A., Saransaari, P., and Oja, S. S. (2000). Mechanisms of L-cysteine neurotoxicity. *Neurochemical research* 25, 1397–1405.

Janoff, E. N., Smith, P. D., and Blaser, M. J. (1988). Acute antibody responses to Giardia lamblia are depressed in patients with AIDS. *Journal of Infectious Diseases* 157, 798–804. doi: 10.1093/infdis/157.4.798

Janssen, M. E. W., Takagi, Y., Parent, K. N., Cardone, G., Nibert, M. L., and Baker, T. S. (2015). Three-dimensional structure of a protozoal double-stranded RNA virus that infects the

enteric pathogen Giardia lamblia. *Journal of virology* 89, 1182–1194. doi: 10.1128/JVI.02745-14

Jerlström-Hultqvist, J., Ankarklev, J., and Svärd, S. G. (2010). Is human giardiasis caused by two different Giardia species? *Gut microbes* 1, 379–382. doi: 10.4161/gmic.1.6.13608

Jiménez, J. C., Fontaine, J., Grzych, J.-M., Dei-Cas, E., and Capron, M. (2004). Systemic and mucosal responses to oral administration of excretory and secretory antigens from Giardia intestinalis. *Clinical and diagnostic laboratory immunology* 11, 152–160. doi: 10.1128/cdli.11.1.152-160.2004

Jochems, P. G. M., Garssen, J., van Keulen, A. M., Masereeuw, R., and Jeurink, P. V. (2018). Evaluating Human Intestinal Cell Lines for Studying Dietary Protein Absorption. *Nutrients* 10. doi: 10.3390/nu10030322

Johansson, M. E. V., Sjövall, H., and Hansson, G. C. (2013). The gastrointestinal mucus system in health and disease. *Nature reviews. Gastroenterology & hepatology* 10, 352–361. doi: 10.1038/nrgastro.2013.35

Jonckheere, J. F. de, and Gordts, B. (1987). Occurrence and transfection of a Giardia virus. *Molecular and biochemical parasitology* 23, 85–89. doi: 10.1016/0166-6851(87)90190-3

Kamda, J. D., and Singer, S. M. (2009). Phosphoinositide 3-kinase-dependent inhibition of dendritic cell interleukin-12 production by Giardia lamblia. *Infection and immunity* 77, 1–9. doi: 10.1128/IAI.00718-08

Karthaus, W. R., Iaquinta, P. J., Drost, J., Gracanin, A., van Boxtel, R., Wongvipat, J., et al. (2014). Identification of multipotent luminal progenitor cells in human prostate organoid cultures. *Cell* 159, 163–175. doi: 10.1016/j.cell.2014.08.017

Katelaris, P. H., Naeem, A., and Farthing, M. J. (1995). Attachment of Giardia lamblia trophozoites to a cultured human intestinal cell line. *Gut* 37, 512–518.

Keister, D. B. (1983). Axenic culture of Giardia lamblia in TYI-S-33 medium supplemented with bile. *Transactions of the Royal Society of Tropical Medicine and Hygiene* 77, 487–488.

Kerr, J. F. (1971). Shrinkage necrosis: a distinct mode of cellular death. *The Journal of pathology* 105, 13–20. doi: 10.1002/path.1711050103

Keselman, A., Li, E., Maloney, J., and Singer, S. M. (2016). The Microbiota Contributes to CD8+ T Cell Activation and Nutrient Malabsorption following Intestinal Infection with Giardia duodenalis. *Infection and immunity* 84, 2853–2860. doi: 10.1128/IAI.00348-16

Keystone, J. S., Krajden, S., and Warren, M. R. (1978). Person-to-person transmission of Giardia lamblia in day-care nurseries. *Canadian Medical Association journal* 119, 241-2, 247-8.

Khare, S., Nunes, J. S., Figueiredo, J. F., Lawhon, S. D., Rossetti, C. A., Gull, T., et al. (2009). Early phase morphological lesions and transcriptional responses of bovine ileum infected with Mycobacterium avium subsp. paratuberculosis. *Veterinary pathology* 46, 717–728. doi: 10.1354/vp.08-VP-0187-G-FL

Kiela, P. R., and Ghishan, F. K. (2016). Physiology of Intestinal Absorption and Secretion. *Best practice & research. Clinical gastroenterology* 30, 145–159. doi: 10.1016/j.bpg.2016.02.007

Kim, S.-H., Turnbull, J., and Guimond, S. (2011). Extracellular matrix and cell signalling: the dynamic cooperation of integrin, proteoglycan and growth factor receptor. *The Journal of endocrinology* 209, 139–151. doi: 10.1530/JOE-10-0377

Kindon, H., Pothoulakis, C., Thim, L., Lynch-Devaney, K., and Podolsky, D. K. (1995). Trefoil peptide protection of intestinal epithelial barrier function: cooperative interaction with mucin glycoprotein. *Gastroenterology* 109, 516–523.

Klotz, C., and Aebischer, T. (2015). The Immunological Enigma of Human Giardiasis. *Curr Trop Med Rep* 2, 119–127. doi: 10.1007/s40475-015-0050-2

Klotz, C., Aebischer, T., and Seeber, F. (2012). Stem cell-derived cell cultures and organoids for protozoan parasite propagation and studying host-parasite interaction. *International journal of medical microbiology : IJMM* 302, 203–209. doi: 10.1016/j.ijmm.2012.07.010

Knight, P. A., Brown, J. K., and Pemberton, A. D. (2008). Innate immune response mechanisms in the intestinal epithelium: potential roles for mast cells and goblet cells in the expulsion of adult Trichinella spiralis. *Parasitology* 135, 655–670. doi: 10.1017/S0031182008004319

Knoop, K. A., McDonald, K. G., McCrate, S., McDole, J. R., and Newberry, R. D. (2015). Microbial sensing by goblet cells controls immune surveillance of luminal antigens in the colon. *Mucosal immunology* 8, 198–210. doi: 10.1038/mi.2014.58

Koh, W. H., Geurden, T., Paget, T., O'Handley, R., Steuart, R. F., Thompson, R. C. A., et al. (2013). Giardia duodenalis assemblage-specific induction of apoptosis and tight junction disruption in human intestinal epithelial cells: effects of mixed infections. *The Journal of parasitology* 99, 353–358. doi: 10.1645/GE-3021.1

Koot, B. G. P., ten Kate, Fiebo J W, Juffrie, M., Rosalina, I., Taminiau, Jan J A M, and Benninga, M. A. (2009). Does Giardia lamblia cause villous atrophy in children? A retrospective cohort study of the histological abnormalities in giardiasis. *Journal of pediatric gastroenterology and nutrition* 49, 304–308. doi: 10.1097/MPG.0b013e31818de3c4

Kosek, M. N. (2017). Causal Pathways from Enteropathogens to Environmental Enteropathy: Findings from the MAL-ED Birth Cohort Study. *EBioMedicine* 18, 109–117. doi: 10.1016/j.ebiom.2017.02.024

Kotloff, K. L., Nataro, J. P., Blackwelder, W. C., Nasrin, D., Farag, T. H., Panchalingam, S., et al. (2013). Burden and aetiology of diarrhoeal disease in infants and young children in developing countries (the Global Enteric Multicenter Study, GEMS): a prospective, case-control study. *Lancet (London, England)* 382, 209–222. doi: 10.1016/S0140-6736(13)60844-2

Koudela, B., Nohýnková, E., Vítovec, J., Pakandl, M., and Kulda, J. (1991). Giardia infection in pigs: detection and in vitro isolation of trophozoites of the Giardia intestinalis group. *Parasitology* 102 Pt 2, 163–166.

Koudela, B., and Vitovec, J. (1998). Experimental giardiasis in goat kids. *Veterinary parasitology* 74, 9–18.

Kowalczyk, A. P., and Green, K. J. (2013). Structure, function, and regulation of desmosomes. *Progress in molecular biology and translational science* 116, 95–118. doi: 10.1016/B978-0-12-394311-8.00005-4

Kozuka, K., He, Y., Koo-McCoy, S., Kumaraswamy, P., Nie, B., Shaw, K., et al. (2017). Development and Characterization of a Human and Mouse Intestinal Epithelial Cell Monolayer Platform. *Stem cell reports* 9, 1976–1990. doi: 10.1016/j.stemcr.2017.10.013

Kraft, M. R., Klotz, C., Bücker, R., Schulzke, J.-D., and Aebischer, T. (2017). Giardia's Epithelial Cell Interaction In Vitro: Mimicking Asymptomatic Infection? *Frontiers in cellular and infection microbiology* 7, 421. doi: 10.3389/fcimb.2017.00421

Krause, G., Winkler, L., Piehl, C., Blasig, I., Piontek, J., and Müller, S. L. (2009). Structure and function of extracellular claudin domains. *Annals of the New York Academy of Sciences* 1165, 34–43. doi: 10.1111/j.1749-6632.2009.04057.x

Krug, S. M., Amasheh, S., Richter, J. F., Milatz, S., Günzel, D., Westphal, J. K., et al. (2009). Tricellulin forms a barrier to macromolecules in tricellular tight junctions without affecting ion permeability. *Molecular biology of the cell* 20, 3713–3724. doi: 10.1091/mbc.e09-01-0080

Lalle, M., and Hanevik, K. (2018). Treatment-refractory giardiasis: challenges and solutions. *Infection and drug resistance* 11, 1921–1933. doi: 10.2147/IDR.S141468

Lancaster, M. A., Renner, M., Martin, C.-A., Wenzel, D., Bicknell, L. S., Hurles, M. E., et al. (2013). Cerebral organoids model human brain development and microcephaly. *Nature* 501, 373–379. doi: 10.1038/nature12517

Lee, J.-J., Kim, D., Pyo, K.-H., Kim, M.-K., Kim, H.-J., Chai, J.-Y., et al. (2013). STAT6 expression and IL-13 production in association with goblet cell hyperplasia and worm expulsion of Gymnophalloides seoi from C57BL/6 mice. *The Korean journal of parasitology* 51, 589–594. doi: 10.3347/kjp.2013.51.5.589

Leroy, A., Lauwaet, T., Bruyne, G. de, Cornelissen, M., and Mareel, M. (2000). Entamoeba histolytica disturbs the tight junction complex in human enteric T84 cell layers. *FASEB journal : official publication of the Federation of American Societies for Experimental Biology* 14, 1139–1146.

Letterio, J. J., and Roberts, A. B. (1998). Regulation of immune responses by TGF-beta. *Annual review of immunology* 16, 137–161. doi: 10.1146/annurev.immunol.16.1.137

Li, E., Stenson, W. F., Kunz-Jenkins, C., Swanson, P. E., Duncan, R., and Stanley, S. L. (1994). Entamoeba histolytica interactions with polarized human intestinal Caco-2 epithelial cells. *Infection and immunity* 62, 5112–5119.

Li, E., Zhao, A., Shea-Donohue, T., and Singer, S. M. (2007). Mast cell-mediated changes in smooth muscle contractility during mouse giardiasis. *Infection and immunity* 75, 4514–4518. doi: 10.1128/IAI.00596-07

Li, E., Zhou, P., and Singer, S. M. (2006). Neuronal nitric oxide synthase is necessary for elimination of Giardia lamblia infections in mice. *Journal of immunology (Baltimore, Md. : 1950)* 176, 516–521. doi: 10.4049/jimmunol.176.1.516

Li, L., and Clevers, H. (2010). Coexistence of quiescent and active adult stem cells in mammals. *Science (New York, N.Y.)* 327, 542–545. doi: 10.1126/science.1180794

Li, X., Zhang, X., Gong, P., Xia, F., Li, L., Yang, Z., et al. (2017). TLR2-/- Mice Display Decreased Severity of Giardiasis via Enhanced Proinflammatory Cytokines Production Dependent on AKT Signal Pathway. *Frontiers in immunology* 8, 1186. doi: 10.3389/fimmu.2017.01186

Lievin-Le Moal, V., and Servin, A. L. (2013). Pathogenesis of human enterovirulent bacteria: lessons from cultured, fully differentiated human colon cancer cell lines. *Microbiology and molecular biology reviews : MMBR* 77, 380–439. doi: 10.1128/MMBR.00064-12

Liévin-Le Moal, V. (2013). Dysfunctions at human intestinal barrier by water-borne protozoan parasites: lessons from cultured human fully differentiated colon cancer cell lines. *Cellular microbiology* 15, 860–869. doi: 10.1111/cmi.12126

Liévin-Le Moal, V., and Servin, A. L. (2006). The front line of enteric host defense against unwelcome intrusion of harmful microorganisms: mucins, antimicrobial peptides, and microbiota. *Clin. Microbiol. Rev.* 19, 315–337. doi: 10.1128/CMR.19.2.315-337.2006

Litleskare, S., Wensaas, K.-A., Eide, G. E., Hanevik, K., Kahrs, G. E., Langeland, N., et al. (2015). Perceived food intolerance and irritable bowel syndrome in a population 3 years after a giardiasis-outbreak: a historical cohort study. *BMC gastroenterology* 15, 164. doi: 10.1186/s12876-015-0393-0

Liu, Q., Mittal, R., Emami, C. N., Iversen, C., Ford, H. R., and Prasadarao, N. V. (2012). Human isolates of Cronobacter sakazakii bind efficiently to intestinal epithelial cells in vitro to induce monolayer permeability and apoptosis. *The Journal of surgical research* 176, 437–447. doi: 10.1016/j.jss.2011.10.030

Liu, S. M., Brown, D. M., O'Donoghue, P., Upcroft, P., and Upcroft, J. A. (2000). Ferredoxin involvement in metronidazole resistance of Giardia duodenalis. *Molecular and biochemical parasitology* 108, 137–140.

Lloyd, D., Harris, J. C., Maroulis, S., Biagini, G. A., Wadley, R. B., Turner, M. P., et al. (2000). The microaerophilic flagellate Giardia intestinalis: oxygen and its reaction products collapse membrane potential and cause cytotoxicity. *Microbiology (Reading, England)* 146 Pt 12, 3109–3118. doi: 10.1099/00221287-146-12-3109

Lo, D. D. (2018). Vigilance or Subversion? Constitutive and Inducible M Cells in Mucosal Tissues. *Trends in immunology* 39, 185–195. doi: 10.1016/j.it.2017.09.002

Lu, S., Gough, A. W., Bobrowski, W. F., and Stewart, B. H. (1996). Transport properties are not altered across Caco-2 cells with heightened TEER despite underlying physiological and ultrastructural changes. *Journal of pharmaceutical sciences* 85, 270–273. doi: 10.1021/js950269u

Lu, Z., Ding, L., Lu, Q., and Chen, Y.-H. (2013). Claudins in intestines: Distribution and functional significance in health and diseases. *Tissue barriers* 1, e24978. doi: 10.4161/tisb.24978

Luciano, L., and Reale, E. (1990). Brush cells of the mouse gallbladder. A correlative light- and electron-microscopical study. *Cell and tissue research* 262, 339–349.

Lugo-Martínez, V.-H., Petit, C. S., Fouquet, S., Le Beyec, J., Chambaz, J., Pinçon-Raymond, M., et al. (2009). Epidermal growth factor receptor is involved in enterocyte anoikis through the dismantling of E-cadherin-mediated junctions. *American journal of physiology. Gastrointestinal and liver physiology* 296, G235-44. doi: 10.1152/ajpgi.90313.2008

Lujan, H. D., Mowatt, M. R., and Nash, T. E. (1996). Lipid requirements and lipid uptake by Giardia lamblia trophozoites in culture. *The Journal of eukaryotic microbiology* 43, 237–242.

Lyon, M. F. (1961). Gene action in the X-chromosome of the mouse (Mus musculus L.). *Nature* 190, 372–373.

Ma'ayeh, S. Y., Knörr, L., and Svärd, S. G. (2015). Transcriptional profiling of Giardia intestinalis in response to oxidative stress. *International journal for parasitology* 45, 925–938. doi: 10.1016/j.ijpara.2015.07.005

Mahe, M. M., Aihara, E., Schumacher, M. A., Zavros, Y., Montrose, M. H., Helmrath, M. A., et al. (2013). Establishment of Gastrointestinal Epithelial Organoids. *Current protocols in mouse biology* 3, 217–240. doi: 10.1002/9780470942390.mo130179

Mahraoui, L., Rodolosse, A., Barbat, A., Dussaulx, E., Zweibaum, A., Rousset, M., et al. (1994). Presence and differential expression of SGLT1, GLUT1, GLUT2, GLUT3 and GLUT5 hexose-transporter mRNAs in Caco-2 cell clones in relation to cell growth and glucose consumption. *The Biochemical journal* 298 Pt 3, 629–633. doi: 10.1042/bj2980629

Maia-Brigagao, C., Morgado-Diaz, J. A., and Souza, W. de (2012). Giardia disrupts the arrangement of tight, adherens and desmosomal junction proteins of intestinal cells. *Parasitology international* 61, 280–287. doi: 10.1016/j.parint.2011.11.002

Maiuri, L., Raia, V., Fiocca, R., Solcia, E., Cornaggia, M., Norèn, O., et al. (1993). Mosaic differentiation of human villus enterocytes: patchy expression of blood group A antigen in A nonsecretors. *Gastroenterology* 104, 21–30.

Maiuri, L., Raia, V., Potter, J., Swallow, D., Ho, M. W., Fiocca, R., et al. (1991). Mosaic pattern of lactase expression by villous enterocytes in human adult-type hypolactasia. *Gastroenterology* 100, 359–369.

Majno, G., and Joris, I. (1995). Apoptosis, oncosis, and necrosis. An overview of cell death. *The American journal of pathology* 146, 3–15.

Malago, J. J., Koninkx, J. F. J. G., Ovelgonne, H. H., van Asten, F. J. A. M., Swennenhuis, J. F., and van Dijk, J. E. (2003). Expression levels of heat shock proteins in enterocyte-like Caco-2 cells after exposure to Salmonella enteritidis. *Cell stress & chaperones* 8, 194–203.

Manko, A., Motta, J.-P., Cotton, J. A., Feener, T., Oyeyemi, A., Vallance, B. A., et al. (2017). Giardia co-infection promotes the secretion of antimicrobial peptides beta-defensin 2 and trefoil factor 3 and attenuates attaching and effacing bacteria-induced intestinal disease. *PloS one* 12, e0178647. doi: 10.1371/journal.pone.0178647

Mantle, M., Atkins, E., Kelly, J., Thakore, E., Buret, A., and Gall, D. G. (1991). Effects of Yersinia enterocolitica infection on rabbit intestinal and colonic goblet cells and mucin: morphometrics, histochemistry, and biochemistry. *Gut* 32, 1131–1138. doi: 10.1136/gut.32.10.1131

Marcus, P. B. (1981). Glycocalyceal bodies and their role in tumor typing. *Journal of submicroscopic cytology* 13, 483–500.

Marcus, P. B., Martin, J. H., Green, R. H., and Krouse, M. A. (1979). Glycocalyceal bodies and microvillous core rootlets: their value in tumor typing. *Archives of pathology & laboratory medicine* 103, 89–92.

Mariano, C., Sasaki, H., Brites, D., and Brito, M. A. (2011). A look at tricellulin and its role in tight junction formation and maintenance. *European journal of cell biology* 90, 787–796. doi: 10.1016/j.ejcb.2011.06.005

Marillier, R. G., Michels, C., Smith, E. M., Fick, L. C. E., Leeto, M., Dewals, B., et al. (2008). IL-4/IL-13 independent goblet cell hyperplasia in experimental helminth infections. *BMC immunology* 9, 11. doi: 10.1186/1471-2172-9-11

Marshman, E., Booth, C., and Potten, C. S. (2002). The intestinal epithelial stem cell. *BioEssays : news and reviews in molecular, cellular and developmental biology* 24, 91–98. doi: 10.1002/bies.10028

Martinez-Rico, C., Pincet, F., Perez, E., Thiery, J. P., Shimizu, K., Takai, Y., et al. (2005). Separation force measurements reveal different types of modulation of E-cadherin-based adhesion by nectin-1 and -3. *The Journal of biological chemistry* 280, 4753–4760. doi: 10.1074/jbc.M412544200

Martìn-Padura, I., Lostaglio, S., Schneemann, M., Williams, L., Romano, M., Fruscella, P., et al. (1998). Junctional adhesion molecule, a novel member of the immunoglobulin superfamily that distributes at intercellular junctions and modulates monocyte transmigration. *The Journal of cell biology* 142, 117–127. doi: 10.1083/jcb.142.1.117

Mashimo, H., Wu, D. C., Podolsky, D. K., and Fishman, M. C. (1996). Impaired defense of intestinal mucosa in mice lacking intestinal trefoil factor. *Science (New York, N.Y.)* 274, 262–265.

Mastronicola, D., Falabella, M., Forte, E., Testa, F., Sarti, P., and Giuffrè, A. (2015). Antioxidant defence systems in the protozoan pathogen Giardia intestinalis. *Molecular and biochemical parasitology*. doi: 10.1016/j.molbiopara.2015.12.002

Matowicka-Karna, J., Kralisz, M., and Kemona, H. (2011). Assessment of the levels of nitric oxide (NO) and cytokines (IL-5, IL-6, IL-13, TNF, IFN-gamma) in giardiosis. *Folia histochemica et cytobiologica* 49, 280–284.

McCracken, K. W., Catá, E. M., Crawford, C. M., Sinagoga, K. L., Schumacher, M., Rockich, B. E., et al. (2014). Modelling human development and disease in pluripotent stem-cell-derived gastric organoids. *Nature* 516, 400–404. doi: 10.1038/nature13863

McCracken, K. W., Howell, J. C., Wells, J. M., and Spence, J. R. (2011). Generating human intestinal tissue from pluripotent stem cells in vitro. *Nature protocols* 6, 1920–1928. doi: 10.1038/nprot.2011.410

McDole, J. R., Wheeler, L. W., McDonald, K. G., Wang, B., Konjufca, V., Knoop, K. A., et al. (2012). Goblet cells deliver luminal antigen to CD103+ dendritic cells in the small intestine. *Nature* 483, 345–349. doi: 10.1038/nature10863

McKenzie, G. J., Bancroft, A., Grencis, R. K., and McKenzie, A. N. (1998). A distinct role for interleukin-13 in Th2-cell-mediated immune responses. *Current biology : CB* 8, 339–342.

Meloni, B. P., Thompson, R. C., Reynoldson, J. A., and Seville, P. (1990). Albendazole: a more effective antigiardial agent in vitro than metronidazole or tinidazole. *Transactions of the Royal Society of Tropical Medicine and Hygiene* 84, 375–379. doi: 10.1016/0035-9203(90)90324-8

Menzies, I. S., Zuckerman, M. J., Nukajam, W. S., Somasundaram, S. G., Murphy, B., Jenkins, A. P., et al. (1999). Geography of intestinal permeability and absorption. *Gut* 44, 483–489.

Mesonero, J., Mahraoui, L., Matosin, M., Rodolosse, A., Rousset, M., and Brot-Laroche, E. (1994). Expression of the hexose transporters GLUT1-GLUT5 and SGLT1 in clones of Caco-2 cells. *Biochemical Society transactions* 22, 681–684.

Middelhoff, M., Westphalen, C. B., Hayakawa, Y., Yan, K. S., Gershon, M. D., Wang, T. C., et al. (2017). Dclk1-expressing tuft cells: critical modulators of the intestinal niche? *American journal of physiology. Gastrointestinal and liver physiology* 313, G285-G299. doi: 10.1152/ajpgi.00073.2017

Millar, A. B., Pavia, D., Agnew, J. E., Lopez-Vidriero, M. T., Lauque, D., and Clarke, S. W. (1985). Effect of oral N-acetylcysteine on mucus clearance. *British journal of diseases of the chest* 79, 262–266.

Miller, R. L., Wang, A. L., and Wang, C. C. (1988). Identification of Giardia lamblia isolates susceptible and resistant to infection by the double-stranded RNA virus. *Experimental parasitology* 66, 118–123.

Mills, E. M., Xu, D., Fergusson, M. M., Combs, C. A., Xu, Y., and Finkel, T. (2002). Regulation of cellular oncosis by uncoupling protein 2. *The Journal of biological chemistry* 277, 27385–27392. doi: 10.1074/jbc.M111860200

Miyoshi, H., Ajima, R., Luo, C. T., Yamaguchi, T. P., and Stappenbeck, T. S. (2012). Wnt5a potentiates TGF-β signaling to promote colonic crypt regeneration after tissue injury. *Science (New York, N.Y.)* 338, 108–113. doi: 10.1126/science.1223821

Miyoshi, H., and Stappenbeck, T. S. (2013). In vitro expansion and genetic modification of gastrointestinal stem cells in spheroid culture. *Nature protocols* 8, 2471–2482. doi: 10.1038/nprot.2013.153

Miyoshi, H., VanDussen, K. L., Malvin, N. P., Ryu, S. H., Wang, Y., Sonnek, N. M., et al. (2017). Prostaglandin E2 promotes intestinal repair through an adaptive cellular response of the epithelium. *The EMBO journal* 36, 5–24. doi: 10.15252/embj.201694660

Moltke, J. von, Ji, M., Liang, H.-E., and Locksley, R. M. (2016). Tuft-cell-derived IL-25 regulates an intestinal ILC2-epithelial response circuit. *Nature* 529, 221–225. doi: 10.1038/nature16161

Monis, P. T., Caccio, S. M., and Thompson, R. C. A. (2009). Variation in Giardia: towards a taxonomic revision of the genus. *Trends in parasitology* 25, 93–100. doi: 10.1016/j.pt.2008.11.006

Moon, C., VanDussen, K. L., Miyoshi, H., and Stappenbeck, T. S. (2014). Development of a primary mouse intestinal epithelial cell monolayer culture system to evaluate factors that modulate IgA transcytosis. *Mucosal immunology* 7, 818–828. doi: 10.1038/mi.2013.98

Morrison, H. G., McArthur, A. G., Gillin, F. D., Aley, S. B., Adam, R. D., Olsen, G. J., et al. (2007). Genomic minimalism in the early diverging intestinal parasite Giardia lamblia. *Science (New York, N.Y.)* 317, 1921–1926. doi: 10.1126/science.1143837

Morroni, M., Cangiotti, A. M., and Cinti, S. (2007). Brush cells in the human duodenojejunal junction: an ultrastructural study. *Journal of anatomy* 211, 125–131. doi: 10.1111/j.1469-7580.2007.00738.x

Moses, H. L., Yang, E. Y., and Pietenpol, J. A. (1990). TGF-beta stimulation and inhibition of cell proliferation: new mechanistic insights. *Cell* 63, 245–247.

Muhsen, K., Cohen, D., and Levine, M. M. (2014). Can Giardia lamblia infection lower the risk of acute diarrhea among preschool children? *Journal of tropical pediatrics* 60, 99–103. doi: 10.1093/tropej/fmt085

Müller, N., Stäger, S., and Gottstein, B. (1996). Serological analysis of antigenic heterogeneity of Giardia lamblia variant surface proteins. *Infection and immunity* 64, 1385–1390.

Muñoz, J., Stange, D. E., Schepers, A. G., van de Wetering, M., Koo, B.-K., Itzkovitz, S., et al. (2012). The Lgr5 intestinal stem cell signature: robust expression of proposed quiescent '+4' cell markers. *The EMBO journal* 31, 3079–3091. doi: 10.1038/emboj.2012.166

Mussarat, A., Manohar, M., Verma, A. K., Upparahalli Venkateshaiah, S., Zaidi, A., Sanders, N. L., et al. (2018). Intestinal overexpression of interleukin (IL)-15 promotes tissue eosinophilia and goblet cell hyperplasia. *Immunology and cell biology* 96, 273–283. doi: 10.1111/imcb.1036

Mustata, R. C., Vasile, G., Fernandez-Vallone, V., Strollo, S., Lefort, A., Libert, F., et al. (2013). Identification of Lgr5-independent spheroid-generating progenitors of the mouse fetal intestinal epithelium. *Cell reports* 5, 421–432. doi: 10.1016/j.celrep.2013.09.005

Nakao, J. H., Collier, S. A., and Gargano, J. W. (2017). Giardiasis and Subsequent Irritable Bowel Syndrome: A Longitudinal Cohort Study Using Health Insurance Data. *The Journal of infectious diseases* 215, 798–805. doi: 10.1093/infdis/jiw621

Nash, T. E. (1997). Antigenic variation in Giardia lamblia and the host's immune response. *Philosophical transactions of the Royal Society of London. Series B, Biological sciences* 352, 1369–1375. doi: 10.1098/rstb.1997.0122

Nash, T. E., Herrington, D. A., Losonsky, G. A., and Levine, M. M. (1987). Experimental human infections with Giardia lamblia. *The Journal of infectious diseases* 156, 974–984.

Nash, T. E., McCutchan, T., Keister, D., Dame, J. B., Conrad, J. D., and Gillin, F. D. (1985). Restriction-endonuclease analysis of DNA from 15 Giardia isolates obtained from humans and animals. *Journal of Infectious Diseases* 152, 64–73. doi: 10.1093/infdis/152.1.64

Nauli, A. M., and Whittimore, J. D. (2015). Using Caco-2 Cells to Study Lipid Transport by the Intestine. *Journal of visualized experiments : JoVE*, e53086. doi: 10.3791/53086

Neutra, M. R. (1998). Current concepts in mucosal immunity. V Role of M cells in transepithelial transport of antigens and pathogens to the mucosal immune system. *The American journal of physiology* 274, G785-91. doi: 10.1152/ajpgi.1998.274.5.G785

Neuwirth, E. (2014). *RColorBrewer: ColorBrewer Palettes: R package version 1.1-2*.

Nielsen, M. S., Axelsen, L. N., Sorgen, P. L., Verma, V., Delmar, M., and Holstein-Rathlou, N.-H. (2012). Gap junctions. *Comprehensive Physiology* 2, 1981–2035. doi: 10.1002/cphy.c110051

Nusrat, A., Turner, J. R., and Madara, J. L. (2000). Molecular physiology and pathophysiology of tight junctions. IV. Regulation of tight junctions by extracellular stimuli: nutrients, cytokines, and immune cells. *American journal of physiology. Gastrointestinal and liver physiology* 279, G851-7. doi: 10.1152/ajpgi.2000.279.5.G851

Nyström, E. E. L., Birchenough, G. M. H., van der Post, S., Arike, L., Gruber, A. D., Hansson, G. C., et al. (2018). Calcium-activated Chloride Channel Regulator 1 (CLCA1) Controls Mucus Expansion in Colon by Proteolytic Activity. *EBioMedicine* 33, 134–143. doi: 10.1016/j.ebiom.2018.05.031

Oberhuber, G., Kastner, N., and Stolte, M. (1997). Giardiasis: a histologic analysis of 567 cases. *Scandinavian journal of gastroenterology* 32, 48–51.

Ogle, C. K., Noel, J. G., Guo, X., Wells, D. A., Valente, J. F., Ogle, J. D., et al. (2002). The ability of endotoxin-stimulated enterocytes to produce bactericidal factors. *Critical care medicine* 30, 428–434.

Ohno, H. (2016). Intestinal M cells. *Journal of biochemistry* 159, 151–160. doi: 10.1093/jb/mvv121

Paget, T. A., Jarroll, E. L., Manning, P., Lindmark, D. G., and Lloyd, D. (1989). Respiration in the cysts and trophozoites of Giardia muris. *Journal of general microbiology* 135, 145–154. doi: 10.1099/00221287-135-1-145

Panaro, M. A., Cianciulli, A., Mitolo, V., Mitolo, C. I., Acquafredda, A., Brandonisio, O., et al. (2007). Caspase-dependent apoptosis of the HCT-8 epithelial cell line induced by the parasite Giardia intestinalis. *FEMS immunology and medical microbiology* 51, 302–309. doi: 10.1111/j.1574-695X.2007.00304.x

Parenti, D. M. (1989). Characterization of a thiol proteinase in Giardia lamblia. *Journal of Infectious Diseases* 160, 1076–1080. doi: 10.1093/infdis/160.6.1076

Park, J.-H., Kotani, T., Konno, T., Setiawan, J., Kitamura, Y., Imada, S., et al. (2016). Promotion of Intestinal Epithelial Cell Turnover by Commensal Bacteria: Role of Short-Chain Fatty Acids. *PloS one* 11, e0156334. doi: 10.1371/journal.pone.0156334

Pavlova, V., Paunova-Krasteva, T., Stoitsova, S., and Nikolova, E. (2015). Distribution patterns of carbohydrates in murine glycocalyx. *Biotechnology, biotechnological equipment* 29, 357–362. doi: 10.1080/13102818.2014.999214

Peglion, F., Llense, F., and Etienne-Manneville, S. (2014). Adherens junction treadmilling during collective migration. *Nature cell biology* 16, 639–651. doi: 10.1038/ncb2985

Pelaseyed, T., Bergström, J. H., Gustafsson, J. K., Ermund, A., Birchenough, G. M. H., Schütte, A., et al. (2014). The mucus and mucins of the goblet cells and enterocytes provide the first defense line of the gastrointestinal tract and interact with the immune system. *Immunological reviews* 260, 8–20. doi: 10.1111/imr.12182

Peterson, M. D., and Mooseker, M. S. (1992). Characterization of the enterocyte-like brush border cytoskeleton of the C2BBe clones of the human intestinal cell line, Caco-2. *Journal of cell science* 102 (Pt 3), 581–600.

Pickett, J. A., and Edwardson, J. M. (2006). Compound exocytosis: mechanisms and functional significance. *Traffic (Copenhagen, Denmark)* 7, 109–116. doi: 10.1111/j.1600-0854.2005.00372.x

Pinto, M., Robine, S., and Appay, M. D. (1983). Enterocyte-like differentiation and polarization of the human colon carcinoma cell line CACO-2 in culture. *Biology of the Cell* 47.

Poley, J. R. (1988). Loss of the glycocalyx of enterocytes in small intestine: a feature detected by scanning electron microscopy in children with gastrointestinal intolerance to dietary protein. *Journal of pediatric gastroenterology and nutrition* 7, 386–394.

Ponce-Macotela, M., González-Maciel, A., Reynoso-Robles, R., and Martínez-Gordillo, M. N. (2008). Goblet cells: are they an unspecific barrier against Giardia intestinalis or a gate? *Parasitology research* 102, 509–513. doi: 10.1007/s00436-007-0790-6

Potten, C. S., Booth, C., and Pritchard, D. M. (1997). The intestinal epithelial stem cell: the mucosal governor. *International journal of experimental pathology* 78, 219–243. doi: 10.1046/j.1365-2613.1997.280362.x

Potten, C. S., Kovacs, L., and Hamilton, E. (1974). Continuous labelling studies on mouse skin and intestine. *Cell and tissue kinetics* 7, 271–283.

Poxleitner, M. K., Carpenter, M. L., Mancuso, J. J., Wang, C.-J. R., Dawson, S. C., and Cande, W. Z. (2008). Evidence for karyogamy and exchange of genetic material in the binucleate intestinal parasite Giardia intestinalis. *Science (New York, N.Y.)* 319, 1530–1533. doi: 10.1126/science.1153752

Prucca, C. G., Slavin, I., Quiroga, R., Elías, E. V., Rivero, F. D., Saura, A., et al. (2008). Antigenic variation in Giardia lamblia is regulated by RNA interference. *Nature* 456, 750–754. doi: 10.1038/nature07585

Qi, Z., Li, Y., Zhao, B., Xu, C., Liu, Y., Li, H., et al. (2017). BMP restricts stemness of intestinal Lgr5+ stem cells by directly suppressing their signature genes. *Nature communications* 8, 13824. doi: 10.1038/ncomms13824

R Core Team (2015). R: A Language and Environment for Statistical Computing.

Raetz, M., Hwang, S.-H., Wilhelm, C. L., Kirkland, D., Benson, A., Sturge, C. R., et al. (2013). Parasite-induced TH1 cells and intestinal dysbiosis cooperate in IFN-γ-dependent elimination of Paneth cells. *Nature immunology* 14, 136–142. doi: 10.1038/ni.2508

Rees, L. E. N., Cogan, T. A., Dodson, A. L., Birchall, M. A., Bailey, M., and Humphrey, T. J. (2008). Campylobacter and IFNgamma interact to cause a rapid loss of epithelial barrier integrity. *Inflammatory bowel diseases* 14, 303–309. doi: 10.1002/ibd.20325

Rendtorff, R. C., and HOLT, C. J. (1954). The experimental transmission of human intestinal protozoan parasites. IV. Attempts to transmit Endamoeba coli and Giardia lamblia cysts by water. *American journal of hygiene* 60, 327–338.

Resta-Lenert, S., Langford, T. D., Gillin, F. D., and Barrett, K. E. (2000). Altered chloride secretory responses in HT29/Cl.19A cells infected with giardia lamblia. *Gastroenterology* 118, A684. doi: 10.1016/S0016-5085(00)84871-4

Reynolds, N., O'Shaughnessy, A., and Hendrich, B. (2013). Transcriptional repressors: multifaceted regulators of gene expression. *Development (Cambridge, England)* 140, 505–512. doi: 10.1242/dev.083105

Rings, E. H., Krasinski, S. D., van Beers, E. H., Moorman, A. F., Dekker, J., Montgomery, R. K., et al. (1994). Restriction of lactase gene expression along the proximal-to-distal axis of rat small intestine occurs during postnatal development. *Gastroenterology* 106, 1223–1232.

Robert Koch-Institut. *SurvStat@RKI 2.0*.

Robertson, L. J., Hanevik, K., Escobedo, A. A., Mørch, K., and Langeland, N. (2010). Giardiasis--why do the symptoms sometimes never stop? *Trends in parasitology* 26, 75–82. doi: 10.1016/j.pt.2009.11.010

Roche, K. C., Gracz, A. D., Liu, X. F., Newton, V., Akiyama, H., and Magness, S. T. (2015). SOX9 maintains reserve stem cells and preserves radioresistance in mouse small intestine. *Gastroenterology* 149, 1553-1563.e10. doi: 10.1053/j.gastro.2015.07.004

Rogawski, E. T., Bartelt, L. A., Platts-Mills, J. A., Seidman, J. C., Samie, A., Havt, A., et al. (2017). Determinants and Impact of Giardia Infection in the First 2 Years of Life in the MAL-ED Birth Cohort. *Journal of the Pediatric Infectious Diseases Society*. doi: 10.1093/jpids/piw082

Rosenthal, R., Milatz, S., Krug, S. M., Oelrich, B., Schulzke, J.-D., Amasheh, S., et al. (2010). Claudin-2, a component of the tight junction, forms a paracellular water channel. *Journal of cell science* 123, 1913–1921. doi: 10.1242/jcs.060665

Roxström-Lindquist, K., Palm, D., Reiner, D., Ringqvist, E., and Svärd, S. G. (2006). Giardia immunity--an update. *Trends in parasitology* 22, 26–31. doi: 10.1016/j.pt.2005.11.005

Roxström-Lindquist, K., Ringqvist, E., Palm, D., and Svärd, S. (2005). Giardia lamblia-induced changes in gene expression in differentiated Caco-2 human intestinal epithelial cells. *Infection and immunity* 73, 8204–8208. doi: 10.1128/IAI.73.12.8204–8208.2005

Rubin, W., Ross, L. L., Sleisenger, M. H., and Weser, E. (1966). An electron microscopic study of adult celiac disease. *Laboratory investigation; a journal of technical methods and pathology* 15, 1720–1747.

Sala-Rabanal, M., Yurtsever, Z., Berry, K. N., Nichols, C. G., and Brett, T. J. (2017). Modulation of TMEM16A channel activity by the von Willebrand factor type A (VWA) domain of the calcium-activated chloride channel regulator 1 (CLCA1). *The Journal of biological chemistry* 292, 9164–9174. doi: 10.1074/jbc.M117.788232

Sala-Rabanal, M., Yurtsever, Z., Nichols, C. G., and Brett, T. J. (2015). Secreted CLCA1 modulates TMEM16A to activate Ca(2+)-dependent chloride currents in human cells. *eLife* 4. doi: 10.7554/eLife.05875

Sambuy, Y., Angelis, I. de, Ranaldi, G., Scarino, M. L., Stammati, A., and Zucco, F. (2005). The Caco-2 cell line as a model of the intestinal barrier: influence of cell and culture-related factors on Caco-2 cell functional characteristics. *Cell biology and toxicology* 21, 1–26. doi: 10.1007/s10565-005-0085-6

Saqui-Salces, M., Keeley, T. M., Grosse, A. S., Qiao, X. T., El-Zaatari, M., Gumucio, D. L., et al. (2011). Gastric tuft cells express DCLK1 and are expanded in hyperplasia. *Histochemistry and cell biology* 136, 191–204. doi: 10.1007/s00418-011-0831-1

Sato, A. (2007). Tuft cells. *Anatomical science international* 82, 187–199. doi: 10.1111/j.1447-073x.2007.00188.x

Sato, A., Hisanaga, Y., Inoue, Y., Nagato, T., and Toh, H. (2002). Three-dimensional structure of apical vesicles of tuft cells in the main excretory duct of the rat submandibular gland. *European journal of morphology* 40, 235–239.

Sato, T., and Clevers, H. (2013). Growing self-organizing mini-guts from a single intestinal stem cell: mechanism and applications. *Science (New York, N.Y.)* 340, 1190–1194. doi: 10.1126/science.1234852

Sato, T., Stange, D. E., Ferrante, M., Vries, R. G. J., van Es, J. H., van den Brink, S., et al. (2011a). Long-term expansion of epithelial organoids from human colon, adenoma, adenocarcinoma, and Barrett's epithelium. *Gastroenterology* 141, 1762–1772. doi: 10.1053/j.gastro.2011.07.050

Sato, T., van Es, J. H., Snippert, H. J., Stange, D. E., Vries, R. G., van den Born, M., et al. (2011b). Paneth cells constitute the niche for Lgr5 stem cells in intestinal crypts. *Nature* 469, 415–418. doi: 10.1038/nature09637

Sato, T., Vries, R. G., Snippert, H. J., van de Wetering, M., Barker, N., Stange, D. E., et al. (2009). Single Lgr5 stem cells build crypt-villus structures in vitro without a mesenchymal niche. *Nature* 459, 262–265. doi: 10.1038/nature07935

Saurabh, K., Nag, V. L., Khera, D., and Elhence, P. (2017). Giardiasis mimicking celiac disease in a patient of common variable immunodeficiency. *Tropical parasitology* 7, 125–127. doi: 10.4103/tp.TP_45_16

Schafer, F. Q., and Buettner, G. R. (2001). Redox environment of the cell as viewed through the redox state of the glutathione disulfide/glutathione couple. *Free radical biology & medicine* 30, 1191–1212.

Schneeberger, E. E., and Lynch, R. D. (2004). The tight junction: a multifunctional complex. *American journal of physiology. Cell physiology* 286, C1213-28. doi: 10.1152/ajpcell.00558.2003

Schupp, D. G., Januschka, M. M., Sherlock, L. A., Stibbs, H. H., Meyer, E. A., Bemrick, W. J., et al. (1988). Production of viable Giardia cysts in vitro: determination by fluorogenic dye staining, excystation, and animal infectivity in the mouse and Mongolian gerbil. *Gastroenterology* 95, 1–10.

Scott, K. G., Meddings, J. B., Kirk, Lees-Miller, S. P., and Buret, A. G. (2002). Intestinal infection with Giardia spp. reduces epithelial barrier function in a myosin light chain kinase-dependent fashion. *Gastroenterology* 123, 1179–1190.

Sepp, T., Wang, A. L., and Wang, C. C. (1994). Giardiavirus-resistant Giardia lamblia lacks a virus receptor on the cell membrane surface. *Journal of virology* 68, 1426–1431.

Serrander, R., Magnusson, K. E., and Sundqvist, T. (1984). Acute infections with Giardia lamblia and rotavirus decrease intestinal permeability to low-molecular weight polyethylene glycols (PEG 400). *Scandinavian journal of infectious diseases* 16, 339–344.

Singer, S. M., and Nash, T. E. (2000). The role of normal flora in Giardia lamblia infections in mice. *The Journal of infectious diseases* 181, 1510–1512. doi: 10.1086/315409

Singh, K. D., Bhasin, D. K., Rana, S. V., Vaiphei, K., Katyal, R., Vinayak, V. K., et al. (2000). Effect of Giardia lamblia on duodenal disaccharidase levels in humans. *Tropical gastroenterology : official journal of the Digestive Diseases Foundation* 21, 174–176.

Smith, P. D., Gillin, F. D., Kaushal, N. A., and Nash, T. E. (1982a). Antigenic analysis of Giardia lamblia from Afghanistan, Puerto Rico, Ecuador, and Oregon. *Infection and immunity* 36, 714–719.

Smith, P. D., Gillin, F. D., Spira, W. M., and Nash, T. E. (1982b). Chronic giardiasis: studies on drug sensitivity, toxin production, and host immune response. *Gastroenterology* 83, 797–803.

Solaymani-Mohammadi, S., and Singer, S. M. (2011). Host immunity and pathogen strain contribute to intestinal disaccharidase impairment following gut infection. *Journal of immunology (Baltimore, Md. : 1950)* 187, 3769–3775. doi: 10.4049/jimmunol.1100606

Songhet, P., Barthel, M., Stecher, B., Müller, A. J., Kremer, M., Hansson, G. C., et al. (2011). Stromal IFN-γR-signaling modulates goblet cell function during Salmonella Typhimurium infection. *PloS one* 6, e22459. doi: 10.1371/journal.pone.0022459

Spence, J. R., Mayhew, C. N., Rankin, S. A., Kuhar, M. F., Vallance, J. E., Tolle, K., et al. (2011). Directed differentiation of human pluripotent stem cells into intestinal tissue in vitro. *Nature* 470, 105–109. doi: 10.1038/nature09691

Srinivasan, B., Kolli, A. R., Esch, M. B., Abaci, H. E., Shuler, M. L., and Hickman, J. J. (2015). TEER measurement techniques for in vitro barrier model systems. *Journal of laboratory automation* 20, 107–126. doi: 10.1177/2211068214561025

Stadelmann, B., Merino, M. C., Lo Persson, and Svärd, S. G. (2012). Arginine consumption by the intestinal parasite Giardia intestinalis reduces proliferation of intestinal epithelial cells. *PloS one* 7, e45325. doi: 10.1371/journal.pone.0045325

Stahley, S. N., and Kowalczyk, A. P. (2015). Desmosomes in acquired disease. *Cell and tissue research* 360, 439–456. doi: 10.1007/s00441-015-2155-2

Steffansen, B., Pedersen, M. D. L., Laghmoch, A. M., and Nielsen, C. U. (2017). SGLT1-Mediated Transport in Caco-2 Cells Is Highly Dependent on Cell Bank Origin. *Journal of pharmaceutical sciences* 106, 2664–2670. doi: 10.1016/j.xphs.2017.04.033

Sternini, C., Anselmi, L., and Rozengurt, E. (2008). Enteroendocrine cells: a site of 'taste' in gastrointestinal chemosensing. *Current opinion in endocrinology, diabetes, and obesity* 15, 73–78. doi: 10.1097/MED.0b013e3282f43a73

Stevens, D. P. (1982). Giardiasis: host-pathogen biology. *Reviews of infectious diseases* 4, 851–858.

Stokkers, P., van den Berg, M., Büller, H., and Rings, E. (1994). Patchy and mosaic protein expression in the small intestine. *Journal of pediatric gastroenterology and nutrition* 19, 133–135.

Sun, H., Chow, E. C., Liu, S., Du, Y., and Pang, K. S. (2008). The Caco-2 cell monolayer: usefulness and limitations. *Expert opinion on drug metabolism & toxicology* 4, 395–411. doi: 10.1517/17425255.4.4.395

Suzuki, T. (2013). Regulation of intestinal epithelial permeability by tight junctions. *Cellular and molecular life sciences : CMLS* 70, 631–659. doi: 10.1007/s00018-012-1070-x

Swidsinski, A., Weber, J., Loening-Baucke, V., Hale, L. P., and Lochs, H. (2005). Spatial organization and composition of the mucosal flora in patients with inflammatory bowel disease. *Journal of clinical microbiology* 43, 3380–3389. doi: 10.1128/JCM.43.7.3380-3389.2005

Takahashi, Y., Sato, S., Kurashima, Y., Yamamoto, T., Kurokawa, S., Yuki, Y., et al. (2018). A Refined Culture System for Human Induced Pluripotent Stem Cell-Derived Intestinal Epithelial Organoids. *Stem cell reports* 10, 314–328. doi: 10.1016/j.stemcr.2017.11.004

Takasato, M., Er, P. X., Becroft, M., Vanslambrouck, J. M., Stanley, E. G., Elefanty, A. G., et al. (2014). Directing human embryonic stem cell differentiation towards a renal lineage generates a self-organizing kidney. *Nature cell biology* 16, 118–126. doi: 10.1038/ncb2894

Takebe, T., Sekine, K., Enomura, M., Koike, H., Kimura, M., Ogaeri, T., et al. (2013). Vascularized and functional human liver from an iPSC-derived organ bud transplant. *Nature* 499, 481–484. doi: 10.1038/nature12271

Takeichi, M. (2014). Dynamic contacts: rearranging adherens junctions to drive epithelial remodelling. *Nature reviews. Molecular cell biology* 15, 397–410. doi: 10.1038/nrm3802

Taupin, D., and Podolsky, D. K. (2003). Trefoil factors: initiators of mucosal healing. *Nature reviews. Molecular cell biology* 4, 721–732. doi: 10.1038/nrm1203

Teal, E., Bertaux-Skeirik, N., Chakrabarti, J., Holokai, L., and Zavros, Y. (2018). Establishment of Human- and Mouse-Derived Gastric Primary Epithelial Cell Monolayers from Organoids. *Methods in molecular biology (Clifton, N.J.)* 1817, 145–155. doi: 10.1007/978-1-4939-8600-2_15

Teoh, D. A., Kamieniecki, D., Pang, G., and Buret, A. G. (2000). Giardia lamblia rearranges F-actin and alpha-actinin in human colonic and duodenal monolayers and reduces transepithelial electrical resistance. *The Journal of parasitology* 86, 800–806. doi: 10.1645/0022-3395(2000)086[0800:GLRFAA]2.0.CO;2

Teshima, C. W., and Meddings, J. B. (2008). The measurement and clinical significance of intestinal permeability. *Current gastroenterology reports* 10, 443–449.

Thaiss, C. A., Levy, M., Grosheva, I., Zheng, D., Soffer, E., Blacher, E., et al. (2018). Hyperglycemia drives intestinal barrier dysfunction and risk for enteric infection. *Science (New York, N.Y.)* 359, 1376–1383. doi: 10.1126/science.aar3318

Thiagarajah, J. R., Donowitz, M., and Verkman, A. S. (2015). Secretory diarrhoea: mechanisms and emerging therapies. *Nature reviews. Gastroenterology & hepatology* 12, 446–457. doi: 10.1038/nrgastro.2015.111

Thomason, H. A., Scothern, A., McHarg, S., and Garrod, D. R. (2010). Desmosomes: adhesive strength and signalling in health and disease. *The Biochemical journal* 429, 419–433. doi: 10.1042/BJ20100567

Thompson, R. A., and Monis, P. (2012). "Giardia—From Genome to Proteome," in *Advances in Parasitology Volume 78* (Elsevier), 57–95.

Thompson, R. C. A., and Monis, P. T. (2004). Variation in Giardia: implications for taxonomy and epidemiology. *Advances in parasitology* 58, 69–137. doi: 10.1016/S0065-308X(04)58002-8

Tojo, M., Hamashima, Y., Hanyu, A., Kajimoto, T., Saitoh, M., Miyazono, K., et al. (2005). The ALK-5 inhibitor A-83-01 inhibits Smad signaling and epithelial-to-mesenchymal transition by transforming growth factor-beta. *Cancer science* 96, 791–800. doi: 10.1111/j.1349-7006.2005.00103.x

Tordesillas, L., and Berin, M. C. (2018). Mechanisms of Oral Tolerance. *Clinical reviews in allergy & immunology* 55, 107–117. doi: 10.1007/s12016-018-8680-5

Torres, C. de, Munell, F., Ferrer, I., Reventós, J., and Macaya, A. (1997). Identification of necrotic cell death by the TUNEL assay in the hypoxic-ischemic neonatal rat brain. *Neuroscience letters* 230, 1–4.

Tovar, J., León-Avila, G., Sánchez, L. B., Sutak, R., Tachezy, J., van der Giezen, M., et al. (2003). Mitochondrial remnant organelles of Giardia function in iron-sulphur protein maturation. *Nature* 426, 172–176. doi: 10.1038/nature01945

Troeger, H., Epple, H.-J., Schneider, T., Wahnschaffe, U., Ullrich, R., Burchard, G.-D., et al. (2007). Effect of chronic Giardia lamblia infection on epithelial transport and barrier function in human duodenum. *Gut* 56, 328–335. doi: 10.1136/gut.2006.100198

Trump, B. F., Berezesky, I. K., Chang, S. H., and Phelps, P. C. (1997). The pathways of cell death: oncosis, apoptosis, and necrosis. *Toxicologic pathology* 25, 82–88. doi: 10.1177/019262339702500116

Turner, J. R. (2009). Intestinal mucosal barrier function in health and disease. *Nature reviews. Immunology* 9, 799–809. doi: 10.1038/nri2653

Turner, J. R., Lencer, W. I., Carlson, S., and Madara, J. L. (1996). Carboxy-terminal vesicular stomatitis virus G protein-tagged intestinal Na+-dependent glucose cotransporter (SGLT1): maintenance of surface expression and global transport function with selective perturbation of transport kinetics and polarized expression. *The Journal of biological chemistry* 271, 7738–7744.

Turner, J.-E., Stockinger, B., and Helmby, H. (2013). IL-22 mediates goblet cell hyperplasia and worm expulsion in intestinal helminth infection. *PLoS pathogens* 9, e1003698. doi: 10.1371/journal.ppat.1003698

Tysnes, K. R., and Robertson, L. J. (2015). Investigation of effects of Giardia duodenalis on transcellular and paracellular transport in enterocytes using in vitro Ussing chamber experiments. *Parasitology* 142, 691–697. doi: 10.1017/S0031182014001772

Ugolev, A. M., Timofeeva, N. M., Smirnova, L. F., Delaey, P., Gruzdkov, A. A., Iezuitova, N. N., et al. (1977). Membrane and intracellular hydrolysis of peptides: differentiation, role and interrelations with transport. *Ciba Foundation symposium*, 221–243.

Umar, S. (2010). Intestinal stem cells. *Current gastroenterology reports* 12, 340–348. doi: 10.1007/s11894-010-0130-3

Ussing, H. H., and Zerahn, K. (1951). Active transport of sodium as the source of electric current in the short-circuited isolated frog skin. *Acta physiologica Scandinavica* 23, 110–127. doi: 10.1111/j.1748-1716.1951.tb00800.x

Vachon, P. H., and Beaulieu, J. F. (1992). Transient mosaic patterns of morphological and functional differentiation in the Caco-2 cell line. *Gastroenterology* 103, 414–423.

van der Flier, L. G., and Clevers, H. (2009). Stem cells, self-renewal, and differentiation in the intestinal epithelium. *Annual review of physiology* 71, 241–260. doi: 10.1146/annurev.physiol.010908.163145

VanDussen, K. L., Marinshaw, J. M., Shaikh, N., Miyoshi, H., Moon, C., Tarr, P. I., et al. (2015). Development of an enhanced human gastrointestinal epithelial culture system to facilitate patient-based assays. *Gut* 64, 911–920. doi: 10.1136/gutjnl-2013-306651

Ventura, L. L. A., Oliveira, D. R., Viana, J. C., Santos, J. F. G., Caliari, M. V., and Gomes, M. A. (2013). Impact of protein malnutrition on histological parameters of experimentally infected animals with Giardia lamblia. *Experimental parasitology* 133, 391–395. doi: 10.1016/j.exppara.2013.01.007

Wang, A. L., and Wang, C. C. (1986). Discovery of a specific double-stranded RNA virus in Giardia lamblia. *Molecular and biochemical parasitology* 21, 269–276.

Wang, Y., DiSalvo, M., Gunasekara, D. B., Dutton, J., Proctor, A., Lebhar, M. S., et al. (2017). Self-renewing Monolayer of Primary Colonic or Rectal Epithelial Cells. *Cellular and molecular gastroenterology and hepatology* 4, 165-182.e7. doi: 10.1016/j.jcmgh.2017.02.011

Ward, W., Alvarado, L., Rawlings, N. D., Engel, J. C., Franklin, C., and McKerrow, J. H. (1997). A primitive enzyme for a primitive cell: the protease required for excystation of Giardia. *Cell* 89, 437–444.

Wattel, W., and Geuze, J. J. (1978). The cells of the rat gastric groove and cardia. An ultrastructural and carbohydrate histochemical study, with special reference to the fibrillovesicular cells. *Cell and tissue research* 186, 375–391.

Weerasinghe, P., and Buja, L. M. (2012). Oncosis: an important non-apoptotic mode of cell death. *Experimental and molecular pathology* 93, 302–308. doi: 10.1016/j.yexmp.2012.09.018

Wensaas, K.-A., Langeland, N., Hanevik, K., Morch, K., Eide, G. E., and Rortveit, G. (2012). Irritable bowel syndrome and chronic fatigue 3 years after acute giardiasis: historic cohort study. *Gut* 61, 214–219. doi: 10.1136/gutjnl-2011-300220

West, A. B., Isaac, C. A., Carboni, J. M., Morrow, J. S., Mooseker, M. S., and Barwick, K. W. (1988). Localization of villin, a cytoskeletal protein specific to microvilli, in human ileum and colon and in colonic neoplasms. *Gastroenterology* 94, 343–352.

Wickham, H. (2016). *ggplot2: Elegant graphics for data analysis*. Cham: Springer.

Wickham, H. (2018). *scales: Scale Functions for Visualization: R package version 1.0.0*.

Wickham, H., François, R., Henry, L., and Müller, K. (2019). *dplyr: A Grammar of Data Manipulation: R package version 0.8.3*.

Williamson, A. L., O'Donoghue, P. J., Upcroft, J. A., and Upcroft, P. (2000). Immune and pathophysiological responses to different strains of Giardia duodenalis in neonatal mice. *International journal for parasitology* 30, 129–136.

Winey, M., Meehl, J. B., O'Toole, E. T., and Giddings, T. H. (2014). Conventional transmission electron microscopy. *Molecular biology of the cell* 25, 319–323. doi: 10.1091/mbc.E12-12-0863

Wolbers, F., Buijtenhuijs, P., Haanen, C., and Vermes, I. (2004). Apoptotic cell death kinetics in vitro depend on the cell types and the inducers used. *Apoptosis : an international journal on programmed cell death* 9, 385–392.

Worbs, T., Bode, U., Yan, S., Hoffmann, M. W., Hintzen, G., Bernhardt, G., et al. (2006). Oral tolerance originates in the intestinal immune system and relies on antigen carriage by dendritic cells. *The Journal of experimental medicine* 203, 519–527. doi: 10.1084/jem.20052016

Worthington, J. J., Reimann, F., and Gribble, F. M. (2018). Enteroendocrine cells-sensory sentinels of the intestinal environment and orchestrators of mucosal immunity. *Mucosal immunology* 11, 3–20. doi: 10.1038/mi.2017.73

Wu, Z., Mirza, H., Teo, J. D. W., and Tan, K. S. W. (2014). Strain-dependent induction of human enterocyte apoptosis by blastocystis disrupts epithelial barrier and ZO-1 organization in a caspase 3- and 9-dependent manner. *BioMed research international* 2014, 209163. doi: 10.1155/2014/209163

Yang, B., Cao, L., Liu, J., Xu, Y., Milne, G., Chan, W., et al. (2015). Low expression of chloride channel accessory 1 predicts a poor prognosis in colorectal cancer. *Cancer* 121, 1570–1580. doi: 10.1002/cncr.29235

Yang, J.-Y., Lee, S.-N., Chang, S.-Y., Ko, H.-J., Ryu, S., and Kweon, M.-N. (2014). A mouse model of shigellosis by intraperitoneal infection. *The Journal of infectious diseases* 209, 203–215. doi: 10.1093/infdis/jit399

Yasuda, K., and Nakanishi, K. (2018). Host responses to intestinal nematodes. *International immunology* 30, 93–102. doi: 10.1093/intimm/dxy002

Yee, S. (1997). In vitro permeability across Caco-2 cells (colonic) can predict in vivo (small intestinal) absorption in man--fact or myth. *Pharmaceutical research* 14, 763–766.

Yonemura, S. (2017). Actin filament association at adherens junctions. *The journal of medical investigation : JMI* 64, 14–19. doi: 10.2152/jmi.64.14

Yu, A. S. L., Cheng, M. H., Angelow, S., Günzel, D., Kanzawa, S. A., Schneeberger, E. E., et al. (2009). Molecular basis for cation selectivity in claudin-2-based paracellular pores: identification of an electrostatic interaction site. *The Journal of general physiology* 133, 111–127. doi: 10.1085/jgp.200810154

Yu, H., Cook, T. J., and Sinko, P. J. (1997). Evidence for diminished functional expression of intestinal transporters in Caco-2 cell monolayers at high passages. *Pharmaceutical research* 14, 757–762.

Yu, L. C., Huang, C. Y., Kuo, W. T., Sayer, H., Turner JR, and Buret, A. G. (2008). SGLT-1-mediated glucose uptake protects human intestinal epithelial cells against Giardia duodenalis-induced apoptosis. *International journal for parasitology* 38, 923–934. doi: 10.1016/j.ijpara.2007.12.004

Yu, L. C. H., Flynn, A. N., Turner, J. R., and Buret, A. G. (2005). SGLT-1-mediated glucose uptake protects intestinal epithelial cells against LPS-induced apoptosis and barrier defects: a novel cellular rescue mechanism? *FASEB journal : official publication of the Federation of American Societies for Experimental Biology* 19, 1822–1835. doi: 10.1096/fj.05-4226com

Yurtsever, Z., Sala-Rabanal, M., Randolph, D. T., Scheaffer, S. M., Roswit, W. T., Alevy, Y. G., et al. (2012). Self-cleavage of human CLCA1 protein by a novel internal metalloprotease domain controls calcium-activated chloride channel activation. *The Journal of biological chemistry* 287, 42138–42149. doi: 10.1074/jbc.M112.410282

Zehendner, C. M., Librizzi, L., Curtis, M. de, Kuhlmann, C. R. W., and Luhmann, H. J. (2011). Caspase-3 contributes to ZO-1 and Cl-5 tight-junction disruption in rapid anoxic neurovascular unit damage. *PloS one* 6, e16760. doi: 10.1371/journal.pone.0016760

Zeller, P., Bricks, T., Vidal, G., Jacques, S., Anton, P. M., and Leclerc, E. (2015). Multiparametric temporal analysis of the Caco-2/TC7 demonstrated functional and differentiated monolayers as early as 14 days of culture. *European journal of pharmaceutical sciences : official journal of the European Federation for Pharmaceutical Sciences* 72, 1–11. doi: 10.1016/j.ejps.2015.02.013

Zhou, P., Li, E., Shea-Donohue, T., and Singer, S. M. (2007). Tumour necrosis factor alpha contributes to protection against Giardia lamblia infection in mice. *Parasite immunology* 29, 367–374. doi: 10.1111/j.1365-3024.2007.00953.x

Zoellner, H., Hofler, M., Beckmann, R., Hufnagl, P., Vanyek, E., Bielek, E., et al. (1996). Serum albumin is a specific inhibitor of apoptosis in human endothelial cells. *Journal of cell science* 109 (Pt 10), 2571–2580.

Zondervan-Zwijnenburg, M.A.J. (2019). *ANOVAreplication: Test ANOVA Replications by Means of the Prior Predictive p-Value: R package version 1.1.4*.

Zwarycz, B., Gracz, A. D., and Magness, S. T. (2018). Organoid Cultures for Assessing Intestinal Epithelial Differentiation and Function in Response to Type-2 Inflammation. *Methods in molecular biology (Clifton, N.J.)* 1799, 397–417. doi: 10.1007/978-1-4939-7896-0_29

# Appendix

Appx. 1 Adjusted p-values (Tukey-test) for Figure 9 (different MOIs; Caco-2 bbe/parental)

| **Comparison of conditions** | **Time p.i.** | **Adj. p-value** | **Significance** |
|---|---|---|---|
| CTRL+ (bbe)-CTRL- (bbe) | 2 | 0,0009 | *** |
| WB6 MOI 1 (bbe)-CTRL- (bbe) | 2 | 1,0000 | ns |
| WB6 MOI 10 (bbe)-CTRL- (bbe) | 2 | 0,7184 | ns |
| WB6 MOI 100 (bbe)-CTRL- (bbe) | 2 | 0,0052 | ** |
| WB6 MOI 10 (bbe)-WB6 MOI 1 (bbe) | 2 | 0,7987 | ns |
| WB6 MOI 100 (bbe)-WB6 MOI 1 (bbe) | 2 | 0,0145 | * |
| WB6 MOI 100 (bbe)-WB6 MOI 10 (bbe) | 2 | 0,0464 | * |
| CTRL+ (bbe)-CTRL- (bbe) | 24 | 0,0000 | **** |
| WB6 MOI 1 (bbe)-CTRL- (bbe) | 24 | 0,9809 | ns |
| WB6 MOI 10 (bbe)-CTRL- (bbe) | 24 | 0,1815 | ns |
| WB6 MOI 100 (bbe)-CTRL- (bbe) | 24 | 0,0171 | * |
| WB6 MOI 10 (bbe)-WB6 MOI 1 (bbe) | 24 | 0,6666 | ns |
| WB6 MOI 100 (bbe)-WB6 MOI 1 (bbe) | 24 | 0,1154 | ns |
| WB6 MOI 100 (bbe)-WB6 MOI 10 (bbe) | 24 | 0,4994 | ns |
| CTRL+ (bbe)-CTRL- (bbe) | 48 | 0,0000 | **** |
| WB6 MOI 1 (bbe)-CTRL- (bbe) | 48 | 0,7918 | ns |
| WB6 MOI 10 (bbe)-CTRL- (bbe) | 48 | 0,2094 | ns |
| WB6 MOI 100 (bbe)-CTRL- (bbe) | 48 | 0,1064 | ns |
| WB6 MOI 10 (bbe)-WB6 MOI 1 (bbe) | 48 | 0,9538 | ns |
| WB6 MOI 100 (bbe)-WB6 MOI 1 (bbe) | 48 | 0,6977 | ns |
| WB6 MOI 100 (bbe)-WB6 MOI 10 (bbe) | 48 | 0,9292 | ns |
| | | | |
| CTRL+ (parental)-CTRL- (parental) | 2 | 0,0011 | ** |
| WB6 MOI 10 (parental)-CTRL- (parental) | 2 | 0,9402 | ns |
| WB6 MOI 100 (parental)-CTRL- (parental) | 2 | 0,0076 | ** |
| WB6 MOI 100 (parental)-WB6 MOI 10 (parental) | 2 | 0,0158 | * |
| CTRL+ (parental)-CTRL- (parental) | 24 | 0,0000 | **** |
| WB6 MOI 10 (parental)-CTRL- (parental) | 24 | 0,3138 | ns |
| WB6 MOI 100 (parental)-CTRL- (parental) | 24 | 0,0834 | ns |
| WB6 MOI 100 (parental)-WB6 MOI 10 (parental) | 24 | 0,7667 | ns |
| CTRL+ (parental)-CTRL- (parental) | 48 | 0,0000 | **** |
| WB6 MOI 10 (parental)-CTRL- (parental) | 48 | 0,3406 | ns |
| WB6 MOI 100 (parental)-CTRL- (parental) | 48 | 0,1177 | ns |
| WB6 MOI 100 (parental)-WB6 MOI 10 (parental) | 48 | 0,8538 | ns |

Appx. 2 Adjusted p-values (Tukey-test) for Figure 11 (*Giardia*-attachment dependency)

| **Comparison of conditions** | **Time p.i.** | **Adj. p-value** | **Significance** |
|---|---|---|---|
| CTRL- (F+t24)-CTRL- (F+t0) | 2 | 0,3304 | ns |
| CTRL- (F+t24)-CTRL- (F+t0) | 24 | 0,6326 | ns |
| CTRL- (F+t24)-CTRL- (F+t0) | 48 | 0,3054 | ns |
| CTRL- (F+t24)-CTRL- (F+t0) | 72 | 0,5403 | ns |
| | | | |
| WB6 (F+t0)-CTRL- (F+t0) | 2 | 0,1433 | ns |
| WB6 (F+t0)-CTRL- (F+t0) | 24 | 0,0254 | * |
| WB6 (F+t0)-CTRL- (F+t0) | 48 | 0,5160 | ns |
| WB6 (F+t0)-CTRL- (F+t0) | 72 | 0,2064 | ns |
| | | | |
| WB6 (F+t24)-CTRL- (F+t24) | 2 | 0,6810 | ns |
| WB6 (F+t24)-CTRL- (F+t24) | 24 | 0,0220 | * |
| WB6 (F+t24)-CTRL- (F+t24) | 48 | 0,0135 | * |
| WB6 (F+t24)-CTRL- (F+t24) | 72 | 0,0100 | ** |
| | | | |
| WB6 (F+t24)-WB6 (F+t0) | 2 | 0,9540 | ns |
| WB6 (F+t24)-WB6 (F+t0) | 24 | 0,5722 | ns |
| WB6 (F+t24)-WB6 (F+t0) | 48 | 0,9495 | ns |
| WB6 (F+t24)-WB6 (F+t0) | 72 | 0,9540 | ns |

Appx. 3 Adjusted p-values (Tukey-test) for Figure 12 (parasite products)

| **Comparison of conditions** | **Time p.i.** | **Adj. p-value** | **Significance** |
|---|---|---|---|
| CTRL+-CTRL- | 2 | 0,0000 | **** |
| WB6-CTRL- | 2 | 0,4027 | ns |
| WB6 heat-inactivated-CTRL- | 2 | 0,9034 | ns |
| WB6 lysate (FP)-CTRL- | 2 | 0,1409 | ns |
| WB6 lysate (S)-CTRL- | 2 | 0,2096 | ns |
| CTRL SN-CTRL- | 2 | 0,7166 | ns |
| WB6 SN-CTRL- | 2 | 0,9949 | ns |
| CTRL+-CTRL- | 24 | 0,0000 | **** |
| WB6-CTRL- | 24 | 0,0115 | * |
| WB6 heat-inactivated-CTRL- | 24 | 0,9997 | ns |
| WB6 lysate (FP)-CTRL- | 24 | 0,9733 | ns |
| WB6 lysate (S)-CTRL- | 24 | 0,9341 | ns |
| CTRL SN-CTRL- | 24 | 0,9950 | ns |
| WB6 SN-CTRL- | 24 | 0,9597 | ns |
| CTRL+-CTRL- | 48 | 0,0000 | **** |
| WB6-CTRL- | 48 | 0,2335 | ns |
| WB6 heat-inactivated-CTRL- | 48 | 1,0000 | ns |
| WB6 lysate (FP)-CTRL- | 48 | 0,9994 | ns |
| WB6 lysate (S)-CTRL- | 48 | 0,9964 | ns |
| CTRL SN-CTRL- | 48 | 0,9946 | ns |
| WB6 SN-CTRL- | 48 | 1,0000 | ns |
| CTRL+-CTRL- | 72 | 0,0000 | **** |
| WB6 lysate (S)-CTRL- | 72 | 0,7462 | ns |
| CTRL SN-CTRL- | 72 | 0,7334 | ns |
| WB6 SN-CTRL- | 72 | 0,5957 | ns |
| | | | |
| WB6 SN-CTRL SN | 2 | 0,9909 | ns |
| WB6 SN-CTRL SN | 24 | 0,7800 | ns |
| WB6 SN-CTRL SN | 48 | 0,9831 | ns |
| WB6 SN-CTRL SN | 72 | 0,9989 | ns |

Appx. 4 Adjusted p-values (Tukey-test) for Figure 13 (parasite survival in Caco-2 system)

| **Comparison of time p.i.** | **Condition** | **Adj. p-value** | **Significance** |
|---|---|---|---|
| 48-24 | MOI 20 | 0,1370 | ns |
| 72-24 | MOI 20 | 0,0000 | **** |
| 72-48 | MOI 20 | 0,0000 | **** |

Appx. 5 Adjusted p-values (Tukey-test) for Figure 14 (*G. duodenalis* isolates)

| **Comparison of conditions** | **Time p.i.** | **Adj. p-value** | **Significance** |
|---|---|---|---|
| CTRL+-CTRL- | 2 | 0,0000 | **** |
| WB6-CTRL- | 2 | 0,0496 | * |
| NF-CTRL- | 2 | 0,0084 | ** |
| S2-CTRL- | 2 | 0,0134 | * |
| P64/F7-CTRL- | 2 | 0,2675 | ns |
| GS-CTRL- | 2 | 0,0446 | * |
| P424/A5-CTRL- | 2 | 0,0002 | *** |
| P458/E2-CTRL- | 2 | 0,0067 | ** |
| P344/B2-CTRL- | 2 | 0,0001 | **** |
| P387/C1-CTRL- | 2 | 0,0002 | *** |
| P413/H7-CTRL- | 2 | 0,0006 | *** |
| P15/E-CTRL- | 2 | 0,0262 | * |
| NF-WB6 | 2 | 1,0000 | ns |
| S2-WB6 | 2 | 1,0000 | ns |
| P64/F7-WB6 | 2 | 1,0000 | ns |
| GS-WB6 | 2 | 1,0000 | ns |
| P424/A5-WB6 | 2 | 0,9863 | ns |
| P458/E2-WB6 | 2 | 1,0000 | ns |
| P344/B2-WB6 | 2 | 0,9760 | ns |
| P387/C1-WB6 | 2 | 0,9879 | ns |
| P413/H7-WB6 | 2 | 0,9979 | ns |
| P15/E-WB6 | 2 | 1,0000 | ns |
| S2-NF | 2 | 1,0000 | ns |
| P64/F7-NF | 2 | 0,9981 | ns |
| GS-NF | 2 | 1,0000 | ns |
| P424/A5-NF | 2 | 0,9998 | ns |
| P458/E2-NF | 2 | 1,0000 | ns |
| P344/B2-NF | 2 | 0,9994 | ns |
| P387/C1-NF | 2 | 0,9999 | ns |
| P413/H7-NF | 2 | 1,0000 | ns |
| P15/E-NF | 2 | 1,0000 | ns |
| P64/F7-S2 | 2 | 0,9994 | ns |
| GS-S2 | 2 | 1,0000 | ns |
| P424/A5-S2 | 2 | 0,9993 | ns |
| P458/E2-S2 | 2 | 1,0000 | ns |
| P344/B2-S2 | 2 | 0,9982 | ns |
| P387/C1-S2 | 2 | 0,9994 | ns |
| P413/H7-S2 | 2 | 1,0000 | ns |
| P15/E-S2 | 2 | 1,0000 | ns |
| GS-P64/F7 | 2 | 1,0000 | ns |
| P424/A5-P64/F7 | 2 | 0,8185 | ns |
| P458/E2-P64/F7 | 2 | 0,9969 | ns |
| P344/B2-P64/F7 | 2 | 0,7657 | ns |
| P387/C1-P64/F7 | 2 | 0,8287 | ns |
| P413/H7-P64/F7 | 2 | 0,9231 | ns |
| P15/E-P64/F7 | 2 | 0,9999 | ns |
| P424/A5-GS | 2 | 0,9888 | ns |
| P458/E2-GS | 2 | 1,0000 | ns |
| P344/B2-GS | 2 | 0,9798 | ns |

| Comparison of conditions | Time p.i. | Adj. p-value | Significance |
|---|---|---|---|
| P387/C1-GS | 2 | 0,9901 | ns |
| P413/H7-GS | 2 | 0,9984 | ns |
| P15/E-GS | 2 | 1,0000 | ns |
| P458/E2-P424/A5 | 2 | 0,9999 | ns |
| P344/B2-P424/A5 | 2 | 1,0000 | ns |
| P387/C1-P424/A5 | 2 | 1,0000 | ns |
| P413/H7-P424/A5 | 2 | 1,0000 | ns |
| P15/E-P424/A5 | 2 | 0,9963 | ns |
| P344/B2-P458/E2 | 2 | 0,9997 | ns |
| P387/C1-P458/E2 | 2 | 0,9999 | ns |
| P413/H7-P458/E2 | 2 | 1,0000 | ns |
| P15/E-P458/E2 | 2 | 1,0000 | ns |
| P387/C1-P344/B2 | 2 | 1,0000 | ns |
| P413/H7-P344/B2 | 2 | 1,0000 | ns |
| P15/E-P344/B2 | 2 | 0,9923 | ns |
| P413/H7-P387/C1 | 2 | 1,0000 | ns |
| P15/E-P387/C1 | 2 | 0,9968 | ns |
| P15/E-P413/H7 | 2 | 0,9997 | ns |
| CTRL+-CTRL- | 24 | 0,0000 | **** |
| WB6-CTRL- | 24 | 0,0000 | **** |
| NF-CTRL- | 24 | 0,0000 | **** |
| S2-CTRL- | 24 | 0,0000 | **** |
| P64/F7-CTRL- | 24 | 0,0000 | **** |
| GS-CTRL- | 24 | 0,0000 | **** |
| P424/A5-CTRL- | 24 | 0,0000 | **** |
| P458/E2-CTRL- | 24 | 0,0000 | **** |
| P344/B2-CTRL- | 24 | 0,0000 | **** |
| P387/C1-CTRL- | 24 | 0,0000 | **** |
| P413/H7-CTRL- | 24 | 0,0000 | **** |
| P15/E-CTRL- | 24 | 0,0000 | **** |
| NF-WB6 | 24 | 1,0000 | ns |
| S2-WB6 | 24 | 1,0000 | ns |
| P64/F7-WB6 | 24 | 1,0000 | ns |
| GS-WB6 | 24 | 1,0000 | ns |
| P424/A5-WB6 | 24 | 0,9178 | ns |
| P458/E2-WB6 | 24 | 0,9994 | ns |
| P344/B2-WB6 | 24 | 0,9950 | ns |
| P387/C1-WB6 | 24 | 0,9945 | ns |
| P413/H7-WB6 | 24 | 0,9980 | ns |
| P15/E-WB6 | 24 | 1,0000 | ns |
| S2-NF | 24 | 1,0000 | ns |
| P64/F7-NF | 24 | 1,0000 | ns |
| GS-NF | 24 | 0,9998 | ns |
| P424/A5-NF | 24 | 0,8663 | ns |
| P458/E2-NF | 24 | 0,9977 | ns |
| P344/B2-NF | 24 | 0,9871 | ns |
| P387/C1-NF | 24 | 0,9861 | ns |
| P413/H7-NF | 24 | 0,9941 | ns |
| P15/E-NF | 24 | 1,0000 | ns |
| P64/F7-S2 | 24 | 1,0000 | ns |
| GS-S2 | 24 | 1,0000 | ns |
| P424/A5-S2 | 24 | 0,9455 | ns |
| P458/E2-S2 | 24 | 0,9998 | ns |
| P344/B2-S2 | 24 | 0,9977 | ns |
| P387/C1-S2 | 24 | 0,9975 | ns |
| P413/H7-S2 | 24 | 0,9992 | ns |
| P15/E-S2 | 24 | 1,0000 | ns |
| GS-P64/F7 | 24 | 1,0000 | ns |
| P424/A5-P64/F7 | 24 | 0,9623 | ns |

| Comparison of conditions | Time p.i. | Adj. p-value | Significance |
|---|---|---|---|
| P458/E2-P64/F7 | 24 | 0,9999 | ns |
| P344/B2-P64/F7 | 24 | 0,9989 | ns |
| P387/C1-P64/F7 | 24 | 0,9987 | ns |
| P413/H7-P64/F7 | 24 | 0,9997 | ns |
| P15/E-P64/F7 | 24 | 1,0000 | ns |
| P424/A5-GS | 24 | 0,9992 | ns |
| P458/E2-GS | 24 | 1,0000 | ns |
| P344/B2-GS | 24 | 1,0000 | ns |
| P387/C1-GS | 24 | 1,0000 | ns |
| P413/H7-GS | 24 | 1,0000 | ns |
| P15/E-GS | 24 | 1,0000 | ns |
| P458/E2-P424/A5 | 24 | 1,0000 | ns |
| P344/B2-P424/A5 | 24 | 1,0000 | ns |
| P387/C1-P424/A5 | 24 | 1,0000 | ns |
| P413/H7-P424/A5 | 24 | 1,0000 | ns |
| P15/E-P424/A5 | 24 | 0,9633 | ns |
| P344/B2-P458/E2 | 24 | 1,0000 | ns |
| P387/C1-P458/E2 | 24 | 1,0000 | ns |
| P413/H7-P458/E2 | 24 | 1,0000 | ns |
| P15/E-P458/E2 | 24 | 0,9999 | ns |
| P387/C1-P344/B2 | 24 | 1,0000 | ns |
| P413/H7-P344/B2 | 24 | 1,0000 | ns |
| P15/E-P344/B2 | 24 | 0,9989 | ns |
| P413/H7-P387/C1 | 24 | 1,0000 | ns |
| P15/E-P387/C1 | 24 | 0,9988 | ns |
| P15/E-P413/H7 | 24 | 0,9997 | ns |
| CTRL+-CTRL- | 48 | 0,0000 | **** |
| WB6-CTRL- | 48 | 0,0000 | **** |
| NF-CTRL- | 48 | 0,0000 | **** |
| S2-CTRL- | 48 | 0,0000 | **** |
| P64/F7-CTRL- | 48 | 0,0000 | **** |
| GS-CTRL- | 48 | 0,0000 | **** |
| P424/A5-CTRL- | 48 | 0,0000 | **** |
| P458/E2-CTRL- | 48 | 0,0000 | **** |
| P344/B2-CTRL- | 48 | 0,0000 | **** |
| P387/C1-CTRL- | 48 | 0,0000 | **** |
| P413/H7-CTRL- | 48 | 0,0000 | **** |
| P15/E-CTRL- | 48 | 0,0000 | **** |
| NF-WB6 | 48 | 0,6258 | ns |
| S2-WB6 | 48 | 0,7598 | ns |
| P64/F7-WB6 | 48 | 1,0000 | ns |
| GS-WB6 | 48 | 1,0000 | ns |
| P424/A5-WB6 | 48 | 1,0000 | ns |
| P458/E2-WB6 | 48 | 1,0000 | ns |
| P344/B2-WB6 | 48 | 1,0000 | ns |
| P387/C1-WB6 | 48 | 0,9998 | ns |
| P413/H7-WB6 | 48 | 1,0000 | ns |
| P15/E-WB6 | 48 | 1,0000 | ns |
| S2-NF | 48 | 1,0000 | ns |
| P64/F7-NF | 48 | 0,4238 | ns |
| GS-NF | 48 | 0,5785 | ns |
| P424/A5-NF | 48 | 0,2110 | ns |
| P458/E2-NF | 48 | 0,8121 | ns |
| P344/B2-NF | 48 | 0,5388 | ns |
| P387/C1-NF | 48 | 0,1522 | ns |
| P413/H7-NF | 48 | 0,6247 | ns |
| P15/E-NF | 48 | 0,9295 | ns |
| P64/F7-S2 | 48 | 0,5645 | ns |
| GS-S2 | 48 | 0,7175 | ns |

| Comparison of conditions | Time p.i. | Adj. p-value | Significance |
|---|---|---|---|
| P424/A5-S2 | 48 | 0,3154 | ns |
| P458/E2-S2 | 48 | 0,9046 | ns |
| P344/B2-S2 | 48 | 0,6803 | ns |
| P387/C1-S2 | 48 | 0,2371 | ns |
| P413/H7-S2 | 48 | 0,7588 | ns |
| P15/E-S2 | 48 | 0,9738 | ns |
| GS-P64/F7 | 48 | 1,0000 | ns |
| P424/A5-P64/F7 | 48 | 1,0000 | ns |
| P458/E2-P64/F7 | 48 | 1,0000 | ns |
| P344/B2-P64/F7 | 48 | 1,0000 | ns |
| P387/C1-P64/F7 | 48 | 1,0000 | ns |
| P413/H7-P64/F7 | 48 | 1,0000 | ns |
| P15/E-P64/F7 | 48 | 0,9997 | ns |
| P424/A5-GS | 48 | 1,0000 | ns |
| P458/E2-GS | 48 | 1,0000 | ns |
| P344/B2-GS | 48 | 1,0000 | ns |
| P387/C1-GS | 48 | 0,9999 | ns |
| P413/H7-GS | 48 | 1,0000 | ns |
| P15/E-GS | 48 | 1,0000 | ns |
| P458/E2-P424/A5 | 48 | 0,9992 | ns |
| P344/B2-P424/A5 | 48 | 1,0000 | ns |
| P387/C1-P424/A5 | 48 | 1,0000 | ns |
| P413/H7-P424/A5 | 48 | 1,0000 | ns |
| P15/E-P424/A5 | 48 | 0,9911 | ns |
| P344/B2-P458/E2 | 48 | 1,0000 | ns |
| P387/C1-P458/E2 | 48 | 0,9968 | ns |
| P413/H7-P458/E2 | 48 | 1,0000 | ns |
| P15/E-P458/E2 | 48 | 1,0000 | ns |
| P387/C1-P344/B2 | 48 | 1,0000 | ns |
| P413/H7-P344/B2 | 48 | 1,0000 | ns |
| P15/E-P344/B2 | 48 | 1,0000 | ns |
| P413/H7-P387/C1 | 48 | 0,9999 | ns |
| P15/E-P387/C1 | 48 | 0,9774 | ns |
| P15/E-P413/H7 | 48 | 1,0000 | ns |

Appx. 6 Adjusted p-values (Tukey-test) for Figure 17 (TYI-S-33 medium)

| **Comparison of conditions** | **Time p.i.** | **Adj. p-value** | **Significance** |
|---|---|---|---|
| CTRL+ (DMEM)-CTRL- (DMEM) | 2 | 0,0000 | **** |
| WB6 (DMEM)-CTRL- (DMEM) | 2 | 1,0000 | ns |
| CTRL (TYI-S-33)-CTRL- (DMEM) | 2 | 0,0000 | **** |
| WB6 (TYI-S-33)-CTRL- (DMEM) | 2 | 0,0000 | **** |
| CTRL (50% TYI-S-33)-CTRL- (DMEM) | 2 | 0,0000 | **** |
| WB6 (50% TYI-S-33)-CTRL- (DMEM) | 2 | 0,0000 | **** |
| CTRL (50% TYI-S-33)-CTRL (TYI-S-33) | 2 | 0,0049 | ** |
| WB6 (TYI-S-33)-CTRL (TYI-S-33) | 2 | 1,0000 | ns |
| WB6 (50% TYI-S-33)-CTRL (50% TYI-S-33) | 2 | 0,2640 | ns |
| CTRL+ (DMEM)-CTRL- (DMEM) | 24 | 0,0000 | **** |
| WB6 (DMEM)-CTRL- (DMEM) | 24 | 0,6739 | ns |
| CTRL (TYI-S-33)-CTRL- (DMEM) | 24 | 0,0001 | **** |
| WB6 (TYI-S-33)-CTRL- (DMEM) | 24 | 0,9995 | ns |
| CTRL (50% TYI-S-33)-CTRL- (DMEM) | 24 | 0,3715 | ns |
| WB6 (50% TYI-S-33)-CTRL- (DMEM) | 24 | 0,0047 | ** |
| CTRL (50% TYI-S-33)-CTRL (TYI-S-33) | 24 | 0,0306 | * |
| WB6 (TYI-S-33)-CTRL (TYI-S-33) | 24 | 0,0010 | *** |
| WB6 (50% TYI-S-33)-CTRL (50% TYI-S-33) | 24 | 0,2644 | ns |
| CTRL+ (DMEM)-CTRL- (DMEM) | 33 | 0,0000 | **** |
| WB6 (DMEM)-CTRL- (DMEM) | 33 | 0,3013 | ns |
| CTRL (TYI-S-33)-CTRL- (DMEM) | 33 | 0,0000 | **** |
| WB6 (TYI-S-33)-CTRL- (DMEM) | 33 | 0,0000 | **** |
| CTRL (50% TYI-S-33)-CTRL- (DMEM) | 33 | 0,5060 | ns |
| WB6 (50% TYI-S-33)-CTRL- (DMEM) | 33 | 0,0006 | *** |
| CTRL (50% TYI-S-33)-CTRL (TYI-S-33) | 33 | 0,0000 | **** |
| WB6 (TYI-S-33)-CTRL (TYI-S-33) | 33 | 0,9840 | ns |
| WB6 (50% TYI-S-33)-CTRL (50% TYI-S-33) | 33 | 0,0418 | * |
| CTRL+ (DMEM)-CTRL- (DMEM) | 48 | 0,0000 | **** |
| WB6 (DMEM)-CTRL- (DMEM) | 48 | 0,3168 | ns |
| CTRL (TYI-S-33)-CTRL- (DMEM) | 48 | 0,0000 | **** |
| WB6 (TYI-S-33)-CTRL- (DMEM) | 48 | 0,0000 | **** |
| CTRL (50% TYI-S-33)-CTRL- (DMEM) | 48 | 0,5548 | ns |
| WB6 (50% TYI-S-33)-CTRL- (DMEM) | 48 | 0,0003 | *** |
| CTRL (50% TYI-S-33)-CTRL (TYI-S-33) | 48 | 0,0000 | **** |
| WB6 (TYI-S-33)-CTRL (TYI-S-33) | 48 | 0,9980 | ns |
| WB6 (50% TYI-S-33)-CTRL (50% TYI-S-33) | 48 | 0,0181 | * |
| CTRL+ (DMEM)-CTRL- (DMEM) | 72 | 0,0000 | **** |
| WB6 (DMEM)-CTRL- (DMEM) | 72 | 0,0118 | * |
| CTRL (50% TYI-S-33)-CTRL- (DMEM) | 72 | 0,0049 | ** |
| WB6 (50% TYI-S-33)-CTRL- (DMEM) | 72 | 0,0000 | **** |
| WB6 (50% TYI-S-33)-CTRL (50% TYI-S-33) | 72 | 0,0000 | **** |

Appx. 7 Adjusted p-values (Tukey-test) for Figure 18 (oxygen-deprivation)

| **Comparison of conditions** | **Time p.i.** | **Adj. p-value** | **Significance** |
|---|---|---|---|
| CTRL+ (aerobic)-CTRL- (aerobic) | 4 | 0,0012 | ** |
| WB6 (aerobic)-CTRL- (aerobic) | 4 | 0,4458 | ns |
| CTRL- (oxygen-deprived)-CTRL- (aerobic) | 4 | 0,9854 | ns |
| WB6 (oxygen-deprived)-WB6 (aerobic) | 4 | 0,8526 | ns |
| WB6 (oxygen-deprived)-CTRL- (oxygen-deprived) | 4 | 0,9982 | ns |
| CTRL+ (aerobic)-CTRL- (aerobic) | 24 | 0,0000 | **** |
| WB6 (aerobic)-CTRL- (aerobic) | 24 | 0,0022 | ** |
| CTRL- (oxygen-deprived)-CTRL- (aerobic) | 24 | 0,0153 | * |
| WB6 (oxygen-deprived)-WB6 (aerobic) | 24 | 0,4663 | ns |
| WB6 (oxygen-deprived)-CTRL- (oxygen-deprived) | 24 | 0,0570 | ns |
| CTRL+ (aerobic)-CTRL- (aerobic) | 48 | 0,0000 | **** |
| WB6 (aerobic)-CTRL- (aerobic) | 48 | 0,0003 | *** |
| CTRL- (oxygen-deprived)-CTRL- (aerobic) | 48 | 0,0017 | ** |
| WB6 (oxygen-deprived)-WB6 (aerobic) | 48 | 0,0701 | ns |
| WB6 (oxygen-deprived)-CTRL- (oxygen-deprived) | 48 | 0,0053 | ** |
| CTRL+ (aerobic)-CTRL- (aerobic) | 72 | 0,0000 | **** |
| WB6 (aerobic)-CTRL- (aerobic) | 72 | 0,0001 | **** |
| CTRL- (oxygen-deprived)-CTRL- (aerobic) | 72 | 0,0003 | *** |
| WB6 (oxygen-deprived)-WB6 (aerobic) | 72 | 0,0141 | * |
| WB6 (oxygen-deprived)-CTRL- (oxygen-deprived) | 72 | 0,0024 | ** |
| CTRL+ (aerobic)-CTRL- (aerobic) | 139 | 0,0003 | *** |
| WB6 (aerobic)-CTRL- (aerobic) | 139 | 0,2994 | ns |
| CTRL- (oxygen-deprived)-CTRL- (aerobic) | 139 | 0,0000 | **** |
| WB6 (oxygen-deprived)-WB6 (aerobic) | 139 | 0,0000 | **** |
| WB6 (oxygen-deprived)-CTRL- (oxygen-deprived) | 139 | 0,0278 | * |

Appx. 8 Adjusted p-values (Tukey-test) for Figure 16 (glucose influence)

| **Comparison of conditions** | **Time p.i.** | **Adj. p-value** | **Significance** |
|---|---|---|---|
| CTRL+-CTRL- | 2 | 0,0031 | ** |
| CTRL- (low glucose)-CTRL- | 2 | 0,9998 | ns |
| WB6 (low glucose)-CTRL- | 2 | 0,9917 | ns |
| WB6-CTRL- | 2 | 0,9984 | ns |
| CTRL (high glucose)-CTRL- | 2 | 1,0000 | ns |
| WB6 (high glucose)-CTRL- | 2 | 1,0000 | ns |
| WB6 M10-CTRL- | 2 | 1,0000 | ns |
| WB6 (low glucose)-CTRL- (low glucose) | 2 | 1,0000 | ns |
| CTRL (high glucose)-CTRL- (low glucose) | 2 | 1,0000 | ns |
| WB6-WB6 (low glucose) | 2 | 1,0000 | ns |
| WB6 (high glucose)-CTRL (high glucose) | 2 | 1,0000 | ns |
| WB6 M10-WB6 (high glucose) | 2 | 1,0000 | ns |
| CTRL+-CTRL- | 24 | 0,0000 | **** |
| CTRL- (low glucose)-CTRL- | 24 | 1,0000 | ns |
| WB6 (low glucose)-CTRL- | 24 | 0,8967 | ns |
| WB6-CTRL- | 24 | 0,9530 | ns |
| CTRL (high glucose)-CTRL- | 24 | 1,0000 | ns |
| WB6 (high glucose)-CTRL- | 24 | 0,9998 | ns |
| WB6 M10-CTRL- | 24 | 1,0000 | ns |
| WB6 (low glucose)-CTRL- (low glucose) | 24 | 0,9705 | ns |
| CTRL (high glucose)-CTRL- (low glucose) | 24 | 1,0000 | ns |
| WB6-WB6 (low glucose) | 24 | 1,0000 | ns |
| WB6 (high glucose)-CTRL (high glucose) | 24 | 1,0000 | ns |
| WB6 M10-WB6 (high glucose) | 24 | 1,0000 | ns |
| CTRL+-CTRL- | 48 | 0,0000 | **** |
| CTRL- (low glucose)-CTRL- | 48 | 1,0000 | ns |
| WB6 (low glucose)-CTRL- | 48 | 0,9306 | ns |
| WB6-CTRL- | 48 | 0,9572 | ns |
| CTRL (high glucose)-CTRL- | 48 | 1,0000 | ns |
| WB6 (high glucose)-CTRL- | 48 | 0,9991 | ns |
| WB6 M10-CTRL- | 48 | 0,9996 | ns |
| WB6 (low glucose)-CTRL- (low glucose) | 48 | 0,9817 | ns |
| CTRL (high glucose)-CTRL- (low glucose) | 48 | 1,0000 | ns |
| WB6-WB6 (low glucose) | 48 | 1,0000 | ns |
| WB6 (high glucose)-CTRL (high glucose) | 48 | 0,9996 | ns |
| WB6 M10-WB6 (high glucose) | 48 | 1,0000 | ns |

Appx. 9 Adjusted p-values (Tukey-test) for Figure 19 (GLV-influence)

| **Comparison of conditions** | **Time p.i.** | **Adj. p-value** | **Significance** |
|---|---|---|---|
| CTRL+-CTRL- | 2 | 0,0002 | *** |
| GS-CTRL- | 2 | 0,7956 | ns |
| GS (GLV)-CTRL- | 2 | 0,5856 | ns |
| WB6-CTRL- | 2 | 0,0133 | * |
| WB6 (GLV)-CTRL- | 2 | 0,9533 | ns |
| Poly(I:C)-CTRL- | 2 | 1,0000 | ns |
| GS (GLV)-GS | 2 | 0,9998 | ns |
| WB6-GS | 2 | 0,1756 | ns |
| WB6 (GLV)-GS (GLV) | 2 | 0,9848 | ns |
| Poly(I:C)-GS (GLV) | 2 | 0,8567 | ns |
| WB6 (GLV)-WB6 | 2 | 0,0934 | ns |
| Poly(I:C)-WB6 (GLV) | 2 | 0,9963 | ns |
| CTRL+-CTRL- | 24 | 0,0000 | **** |
| GS-CTRL- | 24 | 0,0000 | **** |
| GS (GLV)-CTRL- | 24 | 0,0000 | **** |
| WB6-CTRL- | 24 | 0,0000 | **** |
| WB6 (GLV)-CTRL- | 24 | 0,0000 | **** |
| Poly(I:C)-CTRL- | 24 | 0,9886 | ns |
| GS (GLV)-GS | 24 | 0,9522 | ns |
| WB6-GS | 24 | 0,1057 | ns |
| WB6 (GLV)-GS (GLV) | 24 | 0,9928 | ns |
| Poly(I:C)-GS (GLV) | 24 | 0,0000 | **** |
| WB6 (GLV)-WB6 | 24 | 0,1712 | ns |
| Poly(I:C)-WB6 (GLV) | 24 | 0,0000 | **** |
| CTRL+-CTRL- | 48 | 0,0000 | **** |
| GS-CTRL- | 48 | 0,0000 | **** |
| GS (GLV)-CTRL- | 48 | 0,0000 | **** |
| WB6-CTRL- | 48 | 0,0000 | **** |
| WB6 (GLV)-CTRL- | 48 | 0,0000 | **** |
| Poly(I:C)-CTRL- | 48 | 0,2046 | ns |
| GS (GLV)-GS | 48 | 0,9830 | ns |
| WB6-GS | 48 | 0,6720 | ns |
| WB6 (GLV)-GS (GLV) | 48 | 1,0000 | ns |
| Poly(I:C)-GS (GLV) | 48 | 0,0000 | **** |
| WB6 (GLV)-WB6 | 48 | 0,9847 | ns |
| Poly(I:C)-WB6 (GLV) | 48 | 0,0000 | **** |

Appx. 10 Adjusted p-values (Tukey-test) for Figure 20 (FITC-dextran permeability)

| **Comparison of conditions** | **Time p.i.** | **Adj. p-value** | **Significance** |
|---|---|---|---|
| CTRL+-CTRL- | 24 | 0,0000 | **** |
| WB6-CTRL- | 24 | 0,9679 | ns |
| WB6 (GLV)-CTRL- | 24 | 1,0000 | ns |
| GS-CTRL- | 24 | 1,0000 | ns |
| GS (GLV)-CTRL- | 24 | 0,9822 | ns |
| CTRL- (low glucose)-CTRL- | 24 | 1,0000 | ns |
| WB6 (low glucose)-CTRL- | 24 | 1,0000 | ns |
| CTRL- (no FBS, 7-day)-CTRL- | 24 | 1,0000 | ns |
| WB6 (no FBS, 7-day)-CTRL- | 24 | 0,1871 | ns |
| WB6 (GLV)-WB6 | 24 | 0,9996 | ns |
| GS-WB6 | 24 | 1,0000 | ns |
| WB6 (low glucose)-WB6 | 24 | 0,9970 | ns |
| GS (GLV)-WB6 (GLV) | 24 | 0,9996 | ns |
| GS (GLV)-GS | 24 | 0,9999 | ns |
| WB6 (low glucose)-CTRL- (low glucose) | 24 | 1,0000 | ns |
| WB6 (no FBS, 7-day)-CTRL- (no FBS, 7-day) | 24 | 0,6254 | ns |
| CTRL+-CTRL- | 48 | 0,0000 | **** |
| WB6-CTRL- | 48 | 1,0000 | ns |
| WB6 (GLV)-CTRL- | 48 | 0,9988 | ns |
| GS-CTRL- | 48 | 0,9961 | ns |
| GS (GLV)-CTRL- | 48 | 0,8735 | ns |
| CTRL- (low glucose)-CTRL- | 48 | 0,8081 | ns |
| WB6 (low glucose)-CTRL- | 48 | 0,9702 | ns |
| CTRL- (no FBS, 7-day)-CTRL- | 48 | 0,7670 | ns |
| WB6 (no FBS, 7-day)-CTRL- | 48 | 1,0000 | ns |
| WB6 (GLV)-WB6 | 48 | 1,0000 | ns |
| GS-WB6 | 48 | 0,9999 | ns |
| WB6 (low glucose)-WB6 | 48 | 0,8918 | ns |
| GS (GLV)-WB6 (GLV) | 48 | 0,9995 | ns |
| GS (GLV)-GS | 48 | 0,9999 | ns |
| WB6 (low glucose)-CTRL- (low glucose) | 48 | 0,9998 | ns |
| WB6 (no FBS, 7-day)-CTRL- (no FBS, 7-day) | 48 | 0,7697 | ns |

Appx. 11 Overview of all tested cytokines in the Luminex® assay

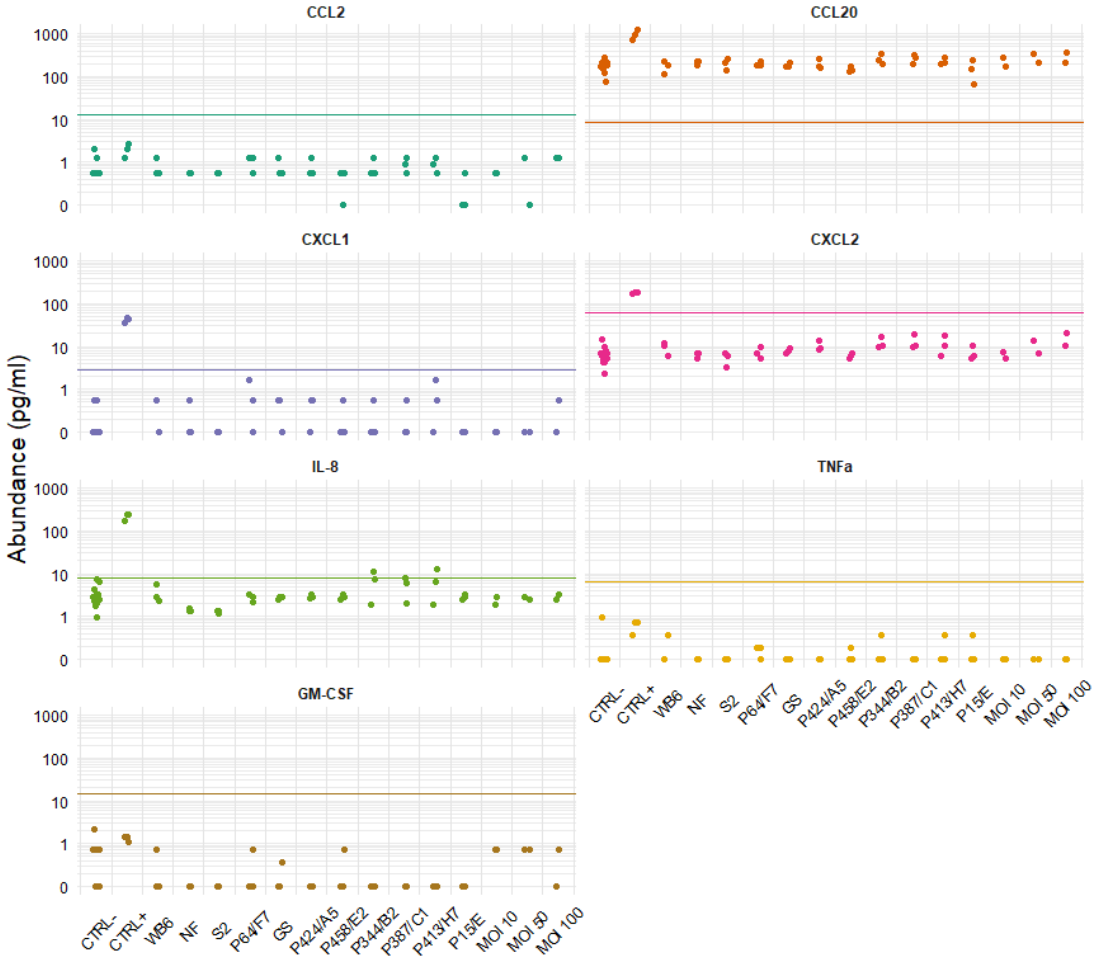


Apart from CCL20 (in detail shown in Figure 21), abundances of all other tested cytokines (CCL2, CXCL1, CXCL2, IL-8, TNFα, and GM-CSF) were below respective detection limits (colored horizontal lines) for most of the tested conditions. Only CTRL+ (1 µM staurosporine) was within detection limits for CXCL1, CXCL2, and IL-8.

Appx. 12 Adjusted p-values (Tukey-test) for Figure 21 (CCL20 abundance)

| **Comparison of conditions** | **Adj. p-value** | **Significance** |
|---|---|---|
| CTRL+-CTRL- | 0,0000 | **** |
| WB6-CTRL- | 1,0000 | ns |
| NF-CTRL- | 1,0000 | ns |
| S2-CTRL- | 1,0000 | ns |
| P64/F7-CTRL- | 1,0000 | ns |
| GS-CTRL- | 1,0000 | ns |
| P424/A5-CTRL- | 1,0000 | ns |
| P458/E2-CTRL- | 1,0000 | ns |
| P344/B2-CTRL- | 0,9614 | ns |
| P387/C1-CTRL- | 0,9443 | ns |
| P413/H7-CTRL- | 0,9990 | ns |
| P15/E-CTRL- | 1,0000 | ns |
| MOI 10-CTRL- | 1,0000 | ns |
| MOI 50-CTRL- | 0,9632 | ns |
| MOI 100-CTRL- | 0,8808 | ns |
| WB6-CTRL+ | 0,0000 | **** |
| NF-CTRL+ | 0,0000 | **** |
| S2-CTRL+ | 0,0000 | **** |
| P64/F7-CTRL+ | 0,0000 | **** |
| GS-CTRL+ | 0,0000 | **** |
| P424/A5-CTRL+ | 0,0000 | **** |
| P458/E2-CTRL+ | 0,0000 | **** |
| P344/B2-CTRL+ | 0,0000 | **** |
| P387/C1-CTRL+ | 0,0000 | **** |
| P413/H7-CTRL+ | 0,0000 | **** |
| P15/E-CTRL+ | 0,0000 | **** |
| MOI 10-CTRL+ | 0,0000 | **** |
| MOI 50-CTRL+ | 0,0000 | **** |
| MOI 100-CTRL+ | 0,0000 | **** |
| NF-WB6 | 1,0000 | ns |
| S2-WB6 | 1,0000 | ns |
| P64/F7-WB6 | 1,0000 | ns |
| GS-WB6 | 1,0000 | ns |
| P424/A5-WB6 | 1,0000 | ns |
| P458/E2-WB6 | 1,0000 | ns |
| P344/B2-WB6 | 0,9938 | ns |
| P387/C1-WB6 | 0,9904 | ns |
| P413/H7-WB6 | 0,9999 | ns |
| P15/E-WB6 | 1,0000 | ns |
| S2-NF | 1,0000 | ns |
| P64/F7-NF | 1,0000 | ns |
| GS-NF | 1,0000 | ns |
| P424/A5-NF | 1,0000 | ns |
| P458/E2-NF | 0,9993 | ns |
| P344/B2-NF | 1,0000 | ns |
| P387/C1-NF | 1,0000 | ns |
| P413/H7-NF | 1,0000 | ns |
| P15/E-NF | 0,9996 | ns |
| P64/F7-S2 | 1,0000 | ns |
| GS-S2 | 1,0000 | ns |
| P424/A5-S2 | 1,0000 | ns |
| P458/E2-S2 | 0,9999 | ns |
| P344/B2-S2 | 1,0000 | ns |
| P387/C1-S2 | 0,9999 | ns |
| P413/H7-S2 | 1,0000 | ns |
| P15/E-S2 | 1,0000 | ns |
| GS-P64/F7 | 1,0000 | ns |
| P424/A5-P64/F7 | 1,0000 | ns |

| Comparison of conditions | Adj. p-value | Significance |
|---|---|---|
| P458/E2-P64/F7 | 1,0000 | ns |
| P344/B2-P64/F7 | 0,9998 | ns |
| P387/C1-P64/F7 | 0,9995 | ns |
| P413/H7-P64/F7 | 1,0000 | ns |
| P15/E-P64/F7 | 1,0000 | ns |
| P424/A5-GS | 1,0000 | ns |
| P458/E2-GS | 1,0000 | ns |
| P344/B2-GS | 0,9983 | ns |
| P387/C1-GS | 0,9971 | ns |
| P413/H7-GS | 1,0000 | ns |
| P15/E-GS | 1,0000 | ns |
| P458/E2-P424/A5 | 1,0000 | ns |
| P344/B2-P424/A5 | 0,9999 | ns |
| P387/C1-P424/A5 | 0,9998 | ns |
| P413/H7-P424/A5 | 1,0000 | ns |
| P15/E-P424/A5 | 1,0000 | ns |
| P344/B2-P458/E2 | 0,9331 | ns |
| P387/C1-P458/E2 | 0,9145 | ns |
| P413/H7-P458/E2 | 0,9926 | ns |
| P15/E-P458/E2 | 1,0000 | ns |
| P387/C1-P344/B2 | 1,0000 | ns |
| P413/H7-P344/B2 | 1,0000 | ns |
| P15/E-P344/B2 | 0,9470 | ns |
| P413/H7-P387/C1 | 1,0000 | ns |
| P15/E-P387/C1 | 0,9311 | ns |
| P15/E-P413/H7 | 0,9950 | ns |
| | | |
| MOI 50-MOI 10 | 1,0000 | ns |
| MOI 100-MOI 10 | 1,0000 | ns |
| MOI 100-MOI 50 | 1,0000 | ns |

Appx. 13 Adjusted p-values (Tukey-test) for Figure 31 (time-dependent ODM thickening)

| Comparison of conditions | Adj. p-value | Significance |
|---|---|---|
| day 9-day 3 | 0,0110 | * |
| day 15-day 3 | 0,0041 | ** |
| day 15-day 9 | 0,6113 | ns |

Appx. 14 Antibody validation on murine duodenal sections for Figure 33
(primary antibodies in red, F-actin in cyan, nuclei in dark blue, 20 µm scale)

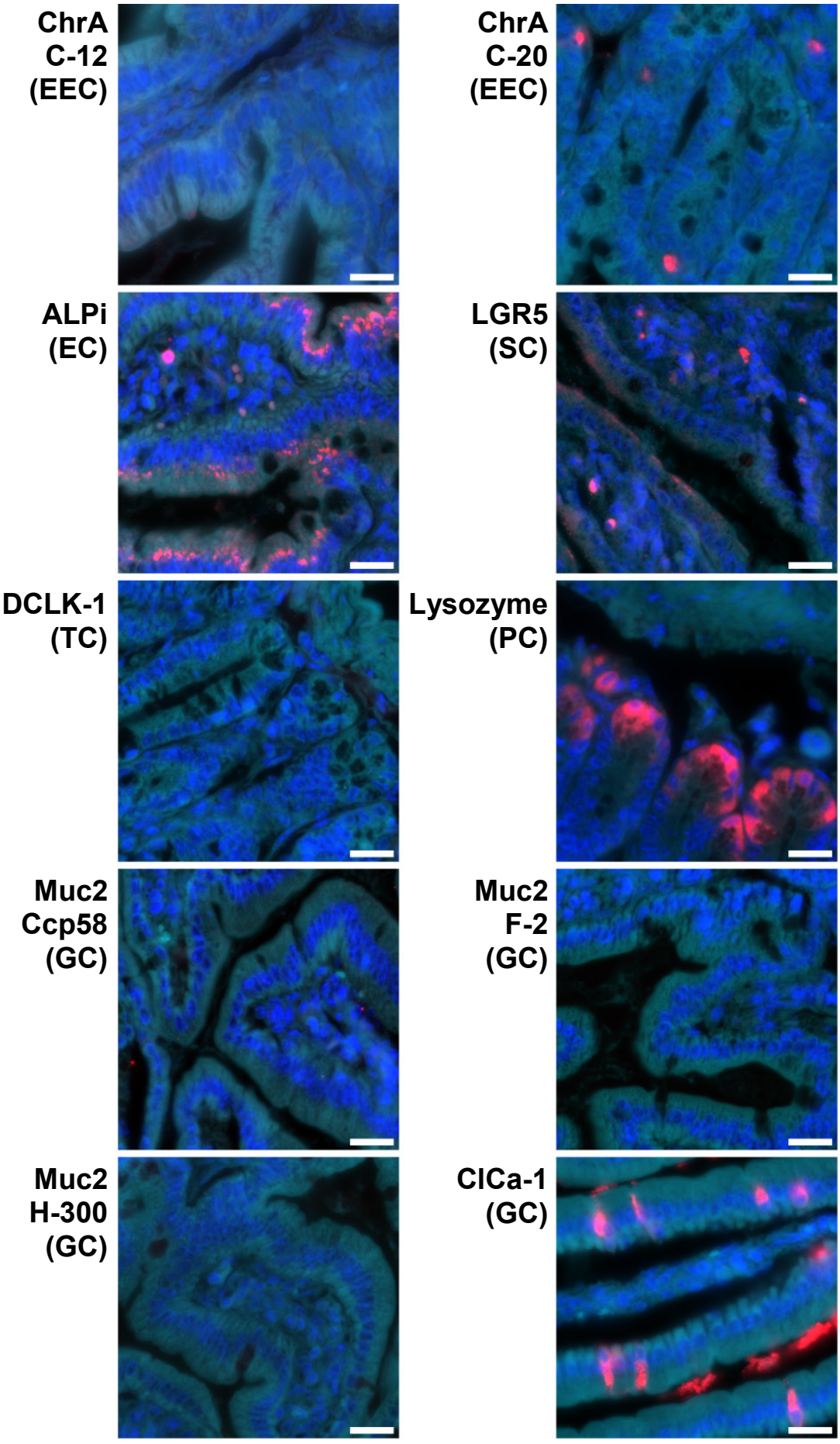

Appx. 15 Adjusted p-values (Tukey-test) for Figure 34 (ODM-infection)

| **Comparison of conditions** | **Time p.i.** | **Adj. p-value** | **Significance** |
|---|---|---|---|
| CTRL+-CTRL- | 2 | 0,9391 | ns |
| WB6-CTRL- | 2 | 0,2307 | ns |
| WB6 heat-inactivated-CTRL- | 2 | 0,0090 | ** |
| WB6 heat-inactivated-WB6 | 2 | 0,1618 | ns |
| CTRL+-CTRL- | 24 | 0,0000 | **** |
| WB6-CTRL- | 24 | 0,0451 | * |
| WB6 heat-inactivated-CTRL- | 24 | 0,2191 | ns |
| WB6 heat-inactivated-WB6 | 24 | 0,6809 | ns |
| CTRL+-CTRL- | 48 | 0,0000 | **** |
| WB6-CTRL- | 48 | 0,7333 | ns |
| WB6 heat-inactivated-CTRL- | 48 | 0,8553 | ns |
| WB6 heat-inactivated-WB6 | 48 | 0,9945 | ns |

Appx. 16 Adjusted p-values (Tukey-test) for Figure 35 (glucose influence)

| **Comparison of conditions** | **Time p.i.** | **Adj. p-value** | **Significance** |
|---|---|---|---|
| CTRL+-CTRL- | 2 | 0,9917 | ns |
| WB6 M10-CTRL- | 2 | 1,0000 | ns |
| CTRL (high glucose)-CTRL- | 2 | 1,0000 | ns |
| WB6 (high glucose)-CTRL- | 2 | 0,9872 | ns |
| WB6 (high glucose)-WB6 M10 | 2 | 0,9878 | ns |
| WB6 (high glucose)-CTRL (high glucose) | 2 | 0,9756 | ns |
| CTRL+-CTRL- | 24 | 0,0000 | **** |
| WB6 M10-CTRL- | 24 | 0,9024 | ns |
| CTRL (high glucose)-CTRL- | 24 | 0,9792 | ns |
| WB6 (high glucose)-CTRL- | 24 | 0,9602 | ns |
| WB6 (high glucose)-WB6 M10 | 24 | 0,9994 | ns |
| WB6 (high glucose)-CTRL (high glucose) | 24 | 0,7623 | ns |
| CTRL+-CTRL- | 48 | 0,0000 | **** |
| WB6 M10-CTRL- | 48 | 0,0471 | * |
| CTRL (high glucose)-CTRL- | 48 | 0,4055 | ns |
| WB6 (high glucose)-CTRL- | 48 | 0,1002 | ns |
| WB6 (high glucose)-WB6 M10 | 48 | 0,9262 | ns |
| WB6 (high glucose)-CTRL (high glucose) | 48 | 0,0174 | * |
| CTRL+-CTRL- | 72 | 0,0000 | **** |
| WB6 M10-CTRL- | 72 | 0,4905 | ns |
| CTRL (high glucose)-CTRL- | 72 | 0,9822 | ns |
| WB6 (high glucose)-CTRL- | 72 | 0,7188 | ns |
| WB6 (high glucose)-WB6 M10 | 72 | 0,9876 | ns |
| WB6 (high glucose)-CTRL (high glucose) | 72 | 0,4689 | ns |

Appx. 17 Adjusted p-values (Tukey-test) for Figure 36 (TYI-S-33 influence)

| **Comparison of conditions** | **Time p.i.** | **Adj. p-value** | **Significance** |
|---|---|---|---|
| CTRL+-CTRL- (DMEM) | 2 | 0,0018 | ** |
| WB6 (DMEM)-CTRL- (DMEM) | 2 | 0,9172 | ns |
| CTRL- (TYI-S-33)-CTRL- (DMEM) | 2 | 1,0000 | ns |
| WB6 (TYI-S-33)-CTRL- (DMEM) | 2 | 1,0000 | ns |
| WB6 (TYI-S-33)-WB6 (DMEM) | 2 | 0,8806 | ns |
| WB6 (TYI-S-33)-CTRL- (TYI-S-33) | 2 | 1,0000 | ns |
| CTRL+-CTRL- (DMEM) | 24 | 0,0000 | **** |
| WB6 (DMEM)-CTRL- (DMEM) | 24 | 0,8021 | ns |
| CTRL- (TYI-S-33)-CTRL- (DMEM) | 24 | 0,9997 | ns |
| WB6 (TYI-S-33)-CTRL- (DMEM) | 24 | 0,3109 | ns |
| WB6 (TYI-S-33)-WB6 (DMEM) | 24 | 0,0487 | * |
| WB6 (TYI-S-33)-CTRL- (TYI-S-33) | 24 | 0,2278 | ns |
| CTRL+-CTRL- (DMEM) | 48 | 0,0000 | **** |
| WB6 (DMEM)-CTRL- (DMEM) | 48 | 0,0082 | ** |
| CTRL- (TYI-S-33)-CTRL- (DMEM) | 48 | 0,9806 | ns |
| WB6 (TYI-S-33)-CTRL- (DMEM) | 48 | 0,0000 | **** |
| WB6 (TYI-S-33)-WB6 (DMEM) | 48 | 0,0000 | **** |
| WB6 (TYI-S-33)-CTRL- (TYI-S-33) | 48 | 0,0000 | **** |
| CTRL+-CTRL- (DMEM) | 72 | 0,0000 | **** |
| WB6 (DMEM)-CTRL- (DMEM) | 72 | 0,0039 | ** |
| CTRL- (TYI-S-33)-CTRL- (DMEM) | 72 | 0,6024 | ns |
| WB6 (TYI-S-33)-CTRL- (DMEM) | 72 | 0,0000 | **** |
| WB6 (TYI-S-33)-WB6 (DMEM) | 72 | 0,0000 | **** |
| WB6 (TYI-S-33)-CTRL- (TYI-S-33) | 72 | 0,0000 | **** |

Appx. 18 Adjusted p-values (Tukey-test) for Figure 39 (*G. duodenalis* isolates)

| **Comparison of conditions** | **Time p.i.** | **Adj. p-value** | **Significance** |
|---|---|---|---|
| CTRL+-CTRL- | 2 | 0,0428 | * |
| NF-CTRL- | 2 | 0,9038 | ns |
| GS-CTRL- | 2 | 0,3899 | ns |
| P64/F7-CTRL- | 2 | 0,2277 | ns |
| P15/E-CTRL- | 2 | 0,2780 | ns |
| GS-NF | 2 | 0,8613 | ns |
| P64/F7-NF | 2 | 0,6208 | ns |
| P15/E-NF | 2 | 0,7134 | ns |
| P64/F7-GS | 2 | 0,9943 | ns |
| P15/E-GS | 2 | 0,9993 | ns |
| P15/E-P64/F7 | 2 | 1,0000 | ns |
| CTRL+-CTRL- | 24 | 0,0000 | **** |
| NF-CTRL- | 24 | 0,0079 | ** |
| GS-CTRL- | 24 | 0,0022 | ** |
| P64/F7-CTRL- | 24 | 0,0094 | ** |
| P15/E-CTRL- | 24 | 0,0184 | * |
| GS-NF | 24 | 0,6040 | ns |
| P64/F7-NF | 24 | 0,9999 | ns |
| P15/E-NF | 24 | 0,9228 | ns |
| P64/F7-GS | 24 | 0,5053 | ns |
| P15/E-GS | 24 | 0,2346 | ns |
| P15/E-P64/F7 | 24 | 0,9695 | ns |
| CTRL+-CTRL- | 48 | 0,0004 | *** |
| NF-CTRL- | 48 | 0,0122 | * |
| GS-CTRL- | 48 | 0,0117 | * |
| P64/F7-CTRL- | 48 | 0,1544 | ns |
| P15/E-CTRL- | 48 | 0,6289 | ns |
| GS-NF | 48 | 1,0000 | ns |
| P64/F7-NF | 48 | 0,2676 | ns |
| P15/E-NF | 48 | 0,0594 | ns |
| P64/F7-GS | 48 | 0,2549 | ns |
| P15/E-GS | 48 | 0,0566 | ns |
| P15/E-P64/F7 | 48 | 0,7486 | ns |
| CTRL+-CTRL- | 72 | 0,0000 | **** |
| NF-CTRL- | 72 | 0,0000 | **** |
| GS-CTRL- | 72 | 0,0001 | **** |
| P64/F7-CTRL- | 72 | 0,0001 | **** |
| P15/E-CTRL- | 72 | 0,0001 | **** |
| GS-NF | 72 | 0,8963 | ns |
| P64/F7-NF | 72 | 0,3801 | ns |
| P15/E-NF | 72 | 0,1593 | ns |
| P64/F7-GS | 72 | 0,8601 | ns |
| P15/E-GS | 72 | 0,4752 | ns |
| P15/E-P64/F7 | 72 | 0,9585 | ns |

Appx. 19 Adjusted p-values (Tukey-test) for Figure 40 (parasite load dependency)

| **Comparison of conditions** | **Time p.i.** | **Adj. p-value** | **Significance** |
|---|---|---|---|
| CTRL+-CTRL- | 2 | 0,0000 | **** |
| WB6 MOI 1-CTRL- | 2 | 1,0000 | ns |
| WB6 MOI 5-CTRL- | 2 | 0,7704 | ns |
| WB6 MOI 10-CTRL- | 2 | 0,5247 | ns |
| WB6 MOI 5-WB6 MOI 1 | 2 | 0,6576 | ns |
| WB6 MOI 10-WB6 MOI 1 | 2 | 0,3835 | ns |
| WB6 MOI 10-WB6 MOI 5 | 2 | 0,9906 | ns |
| CTRL+-CTRL- | 24 | 0,0000 | **** |
| WB6 MOI 1-CTRL- | 24 | 0,9998 | ns |
| WB6 MOI 5-CTRL- | 24 | 0,1459 | ns |
| WB6 MOI 10-CTRL- | 24 | 0,5902 | ns |
| WB6 MOI 5-WB6 MOI 1 | 24 | 0,0530 | ns |
| WB6 MOI 10-WB6 MOI 1 | 24 | 0,3689 | ns |
| WB6 MOI 10-WB6 MOI 5 | 24 | 0,8407 | ns |
| CTRL+-CTRL- | 48 | 0,0000 | **** |
| WB6 MOI 1-CTRL- | 48 | 0,0028 | ** |
| WB6 MOI 5-CTRL- | 48 | 0,0000 | **** |
| WB6 MOI 10-CTRL- | 48 | 0,0000 | **** |
| WB6 MOI 5-WB6 MOI 1 | 48 | 0,0000 | **** |
| WB6 MOI 10-WB6 MOI 1 | 48 | 0,0000 | **** |
| WB6 MOI 10-WB6 MOI 5 | 48 | 0,4135 | ns |
| CTRL+-CTRL- | 72 | 0,0000 | **** |
| WB6 MOI 1-CTRL- | 72 | 0,0000 | **** |
| WB6 MOI 5-CTRL- | 72 | 0,0000 | **** |
| WB6 MOI 10-CTRL- | 72 | 0,0000 | **** |
| WB6 MOI 5-WB6 MOI 1 | 72 | 0,0030 | ** |
| WB6 MOI 10-WB6 MOI 1 | 72 | 0,0010 | *** |
| WB6 MOI 10-WB6 MOI 5 | 72 | 0,9639 | ns |

Appx. 20 Adjusted p-values (Tukey-test) for Figure 41 (parasite survival in new system)

| **Comparison of time p.i.** | **Condition** | **Adj. p-value** | **Significance** |
|---|---|---|---|
| 48-24 | MOI 1 | 0,9594 | ns |
| 72-24 | MOI 1 | 0,9781 | ns |
| 72-48 | MOI 1 | 0,9970 | ns |
| 48-24 | MOI 5 | 0,0714 | ns |
| 72-24 | MOI 5 | 0,1176 | ns |
| 72-48 | MOI 5 | 0,9194 | ns |
| 48-24 | MOI 10 | 0,9522 | ns |
| 72-24 | MOI 10 | 0,6748 | ns |
| 72-48 | MOI 10 | 0,5094 | ns |

Appx. 21 Adjusted p-values (Tukey-test) for Figure 42 (quantification of TUNEL$^+$ cells)

| **Comparison of conditions** | **Time p.i.** | **Adj. p-value** | **Significance** |
|---|---|---|---|
| CTRL+-CTRL- | 24 | 0,0000 | **** |
| WB6 MOI 1-CTRL- | 24 | 0,9067 | ns |
| WB6 MOI 5-CTRL- | 24 | 0,9999 | ns |
| WB6 MOI 10-CTRL- | 24 | 0,8114 | ns |
| CTRL+-CTRL- | 48 | 0,0000 | **** |
| WB6 MOI 1-CTRL- | 48 | 0,5498 | ns |
| WB6 MOI 5-CTRL- | 48 | 0,5309 | ns |
| WB6 MOI 10-CTRL- | 48 | 0,0171 | * |
| CTRL+-CTRL- | 72 | 0,0000 | **** |
| WB6 MOI 1-CTRL- | 72 | 0,1415 | ns |
| WB6 MOI 5-CTRL- | 72 | 0,0002 | *** |
| WB6 MOI 10-CTRL- | 72 | 0,0002 | *** |

Appx. 22 Adjusted p-values (Tukey-test) for Figure 43 (quantification of ClCa$^+$ cells)

| **Comparison of conditions** | **Time p.i.** | **Adj. p-value** | **Significance** |
|---|---|---|---|
| CTRL+-CTRL- | 24 | 0,0000 | **** |
| WB6 MOI 1-CTRL- | 24 | 1,0000 | ns |
| WB6 MOI 5-CTRL- | 24 | 0,0649 | ns |
| WB6 MOI 10-CTRL- | 24 | 0,7566 | ns |
| CTRL+-CTRL- | 48 | 0,0000 | **** |
| WB6 MOI 1-CTRL- | 48 | 0,5206 | ns |
| WB6 MOI 5-CTRL- | 48 | 0,9215 | ns |
| WB6 MOI 10-CTRL- | 48 | 0,0000 | **** |
| CTRL+-CTRL- | 72 | 0,0000 | **** |
| WB6 MOI 1-CTRL- | 72 | 0,0926 | ns |
| WB6 MOI 5-CTRL- | 72 | 0,0000 | **** |
| WB6 MOI 10-CTRL- | 72 | 0,0000 | **** |

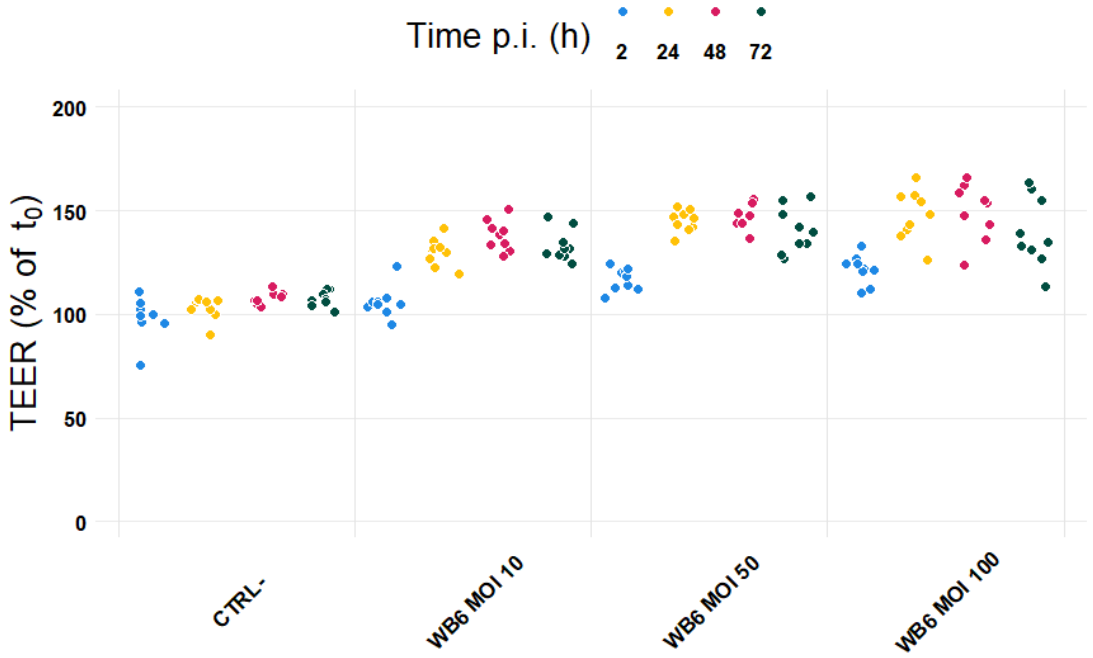


Appx. 23 Additional investigations on MOI.
TEER changes of Caco-2 bbe monolayers, normalized to measurements before infection, are shown when infected with WB6 loads of MOI 10, MOI 50 and MOI 100. MOI 10 showed a significantly lower increase than the two higer conditions. With passing time, differences disappeared. Data points represent individual monolayers, n=9. Time after infection is color coded. Absolute TEER was 245.1 Ω·cm² (SD 36.9 Ω·cm²) at t0. Appx. 24 contains relevant probability values (Tukey post-hoc test).

Appx. 24 Adjusted p-values (Tukey-test) for Appx. 23 (additional MOI investigations)

| **Comparison of conditions** | **Time p.i.** | **Adj. p-value** | **Significance** |
|---|---|---|---|
| WB6 MOI 10-CTRL- | 2 | 0,1384 | ns |
| WB6 MOI 50-CTRL- | 2 | 0,0001 | **** |
| WB6 MOI 100-CTRL- | 2 | 0,0000 | **** |
| WB6 MOI 50-WB6 MOI 10 | 2 | 0,0329 | * |
| WB6 MOI 100-WB6 MOI 10 | 2 | 0,0020 | ** |
| WB6 MOI 100-WB6 MOI 50 | 2 | 0,7003 | ns |
| WB6 MOI 10-CTRL- | 24 | 0,0000 | **** |
| WB6 MOI 50-CTRL- | 24 | 0,0000 | **** |
| WB6 MOI 100-CTRL- | 24 | 0,0000 | **** |
| WB6 MOI 50-WB6 MOI 10 | 24 | 0,0021 | ** |
| WB6 MOI 100-WB6 MOI 10 | 24 | 0,0004 | *** |
| WB6 MOI 100-WB6 MOI 50 | 24 | 0,9350 | ns |
| WB6 MOI 10-CTRL- | 48 | 0,0000 | **** |
| WB6 MOI 50-CTRL- | 48 | 0,0000 | **** |
| WB6 MOI 100-CTRL- | 48 | 0,0000 | **** |
| WB6 MOI 50-WB6 MOI 10 | 48 | 0,0932 | ns |
| WB6 MOI 100-WB6 MOI 10 | 48 | 0,0420 | * |
| WB6 MOI 100-WB6 MOI 50 | 48 | 0,9832 | ns |
| WB6 MOI 10-CTRL- | 72 | 0,0000 | **** |
| WB6 MOI 50-CTRL- | 72 | 0,0000 | **** |
| WB6 MOI 100-CTRL- | 72 | 0,0000 | **** |
| WB6 MOI 50-WB6 MOI 10 | 72 | 0,4946 | ns |
| WB6 MOI 100-WB6 MOI 10 | 72 | 0,6714 | ns |
| WB6 MOI 100-WB6 MOI 50 | 72 | 0,9914 | ns |

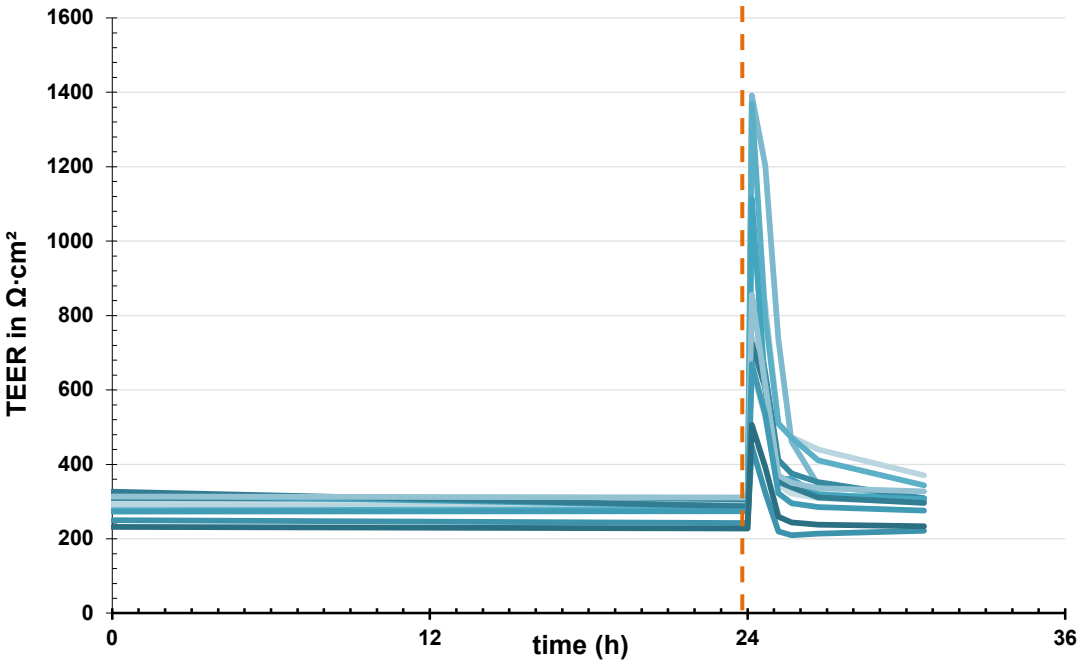


Appx. 25 Highly increased TEER and variance after ice-cold washing steps of Caco-2 bbe. Development of absolute TEER of 12 individual Caco-2 bbe monolayers before and after five ice-cold $PBS^{-/-}$ washing steps at 24 h (orange dashed line) is shown. Usual but cold DMEM was applied afterwards, followed by standard incubation at 37°C. Washing steps introduced high variances of measured TEER, which were not fully normalized even after 6 h.

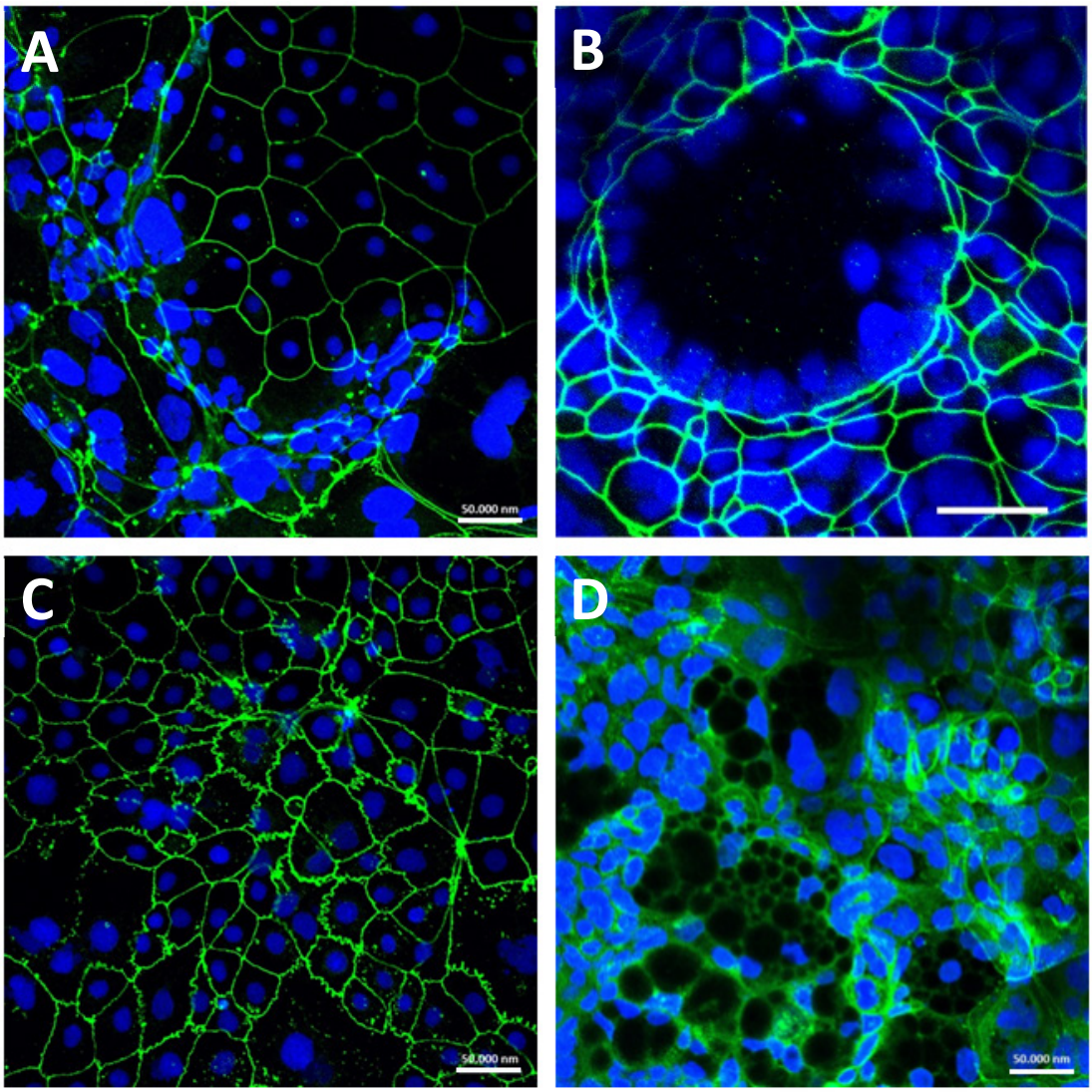


Appx. 26 Caco-2 artifacts.
Caco-2 bbe cells were grown on plain culture plate surfaces of chamber slides. After 21-days of differentiation, cells underwent immunofluorescence (IF) staining of ZO-1 (green; A, B, C) and cldn-4 (D) as well as nuclear staining with DAPI. Micrographs show odd Caco-2 phenotypes like unequal cellular distribution (A), formation of large liquid filled structures (B), undulated cellular contacts (C) and formation of intra- and extracellular vesicles (D). Such phenotypes are linked to cultivation on plain, non-transwell surfaces. Of note, the use of transwell-filters with 3 µm pores led to growth of numerous Caco-2 cells through those pores, subsequently generating a second monolayer of the opposite filter side (data not shown). This also seemed to increase the abundance of shown cellular artifacts. Hence, the use of filter with smaller (0.4 µm) pores is strongly recommended to prevent both of this. Scale bars indicate 50 µm.

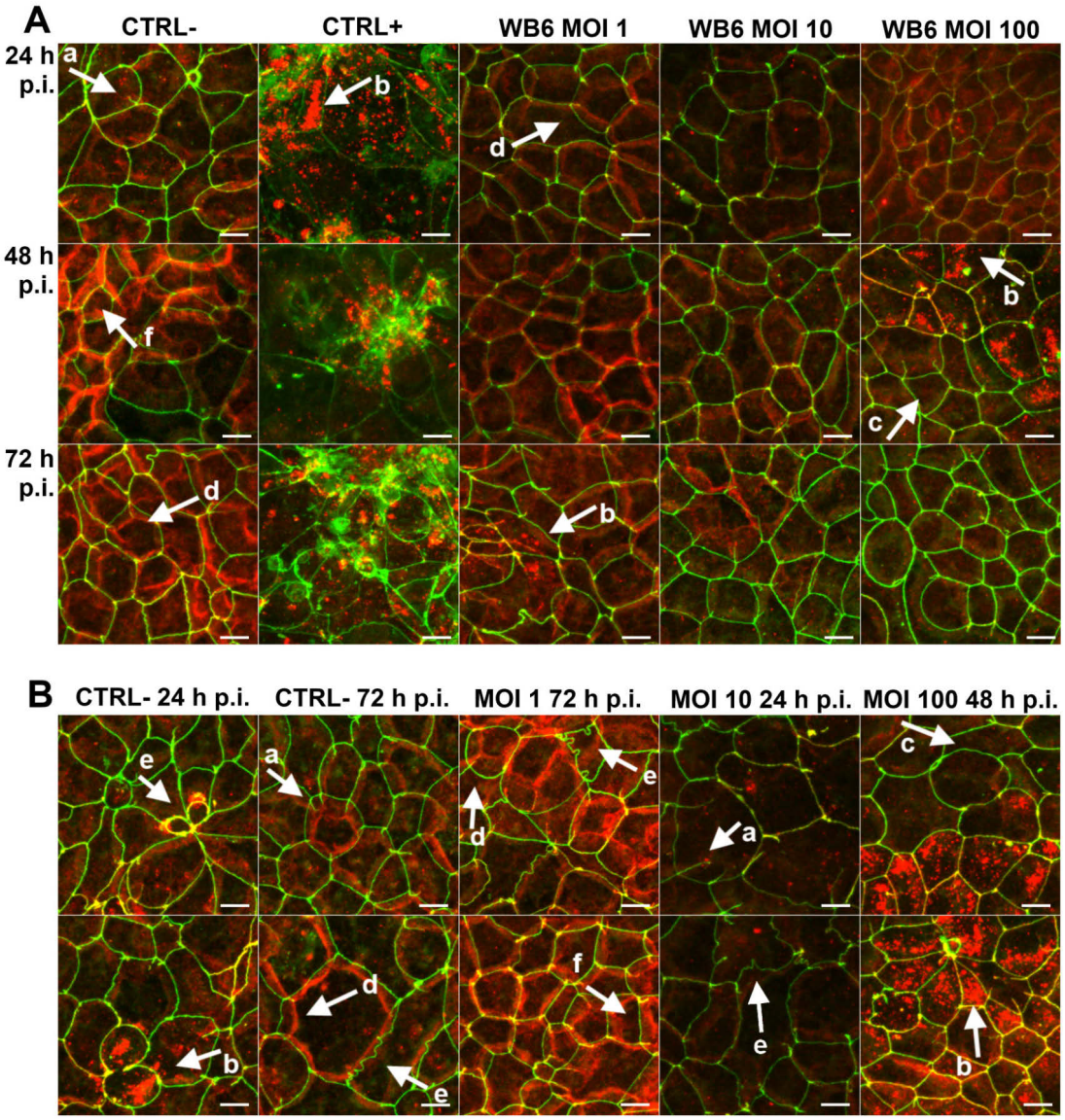


Appx. 27 Diverse effects on tight junction proteins without correlation to infection. Micrographs are derived from z-stacks, spanning whole cells, by using maximum intensity projection to gain complete cell-wide signals and depict tight junction proteins ZO-1 (green) and claudin-1 (red) in Caco-2 bbe monolayer, comparing uninfected control (CTRL−), 1 µM staurosporine control (CTRL+) and *G. duodenalis* isolate WB6 of MOI 1, 10 and 100 after 24, 48, and 72 h (**A**). An additional selection of micrographs is shown in (**B**), illustrating different TJP phenotypes which can be found in Caco-2 monolayers, without correlations to the tested conditions. Arrows in (**A**, **B**) indicate observed random phenotypes like ZO-1 "branching" (a), claudin-1 flocculation and delocalization (b) or its absence directly next to it (c), mismatch of ZO-1 and claudin-1 localization (d), odd cellular contacts (e), and areas of increased claudin-1 presence (f). Scale bars indicate 10 µm.

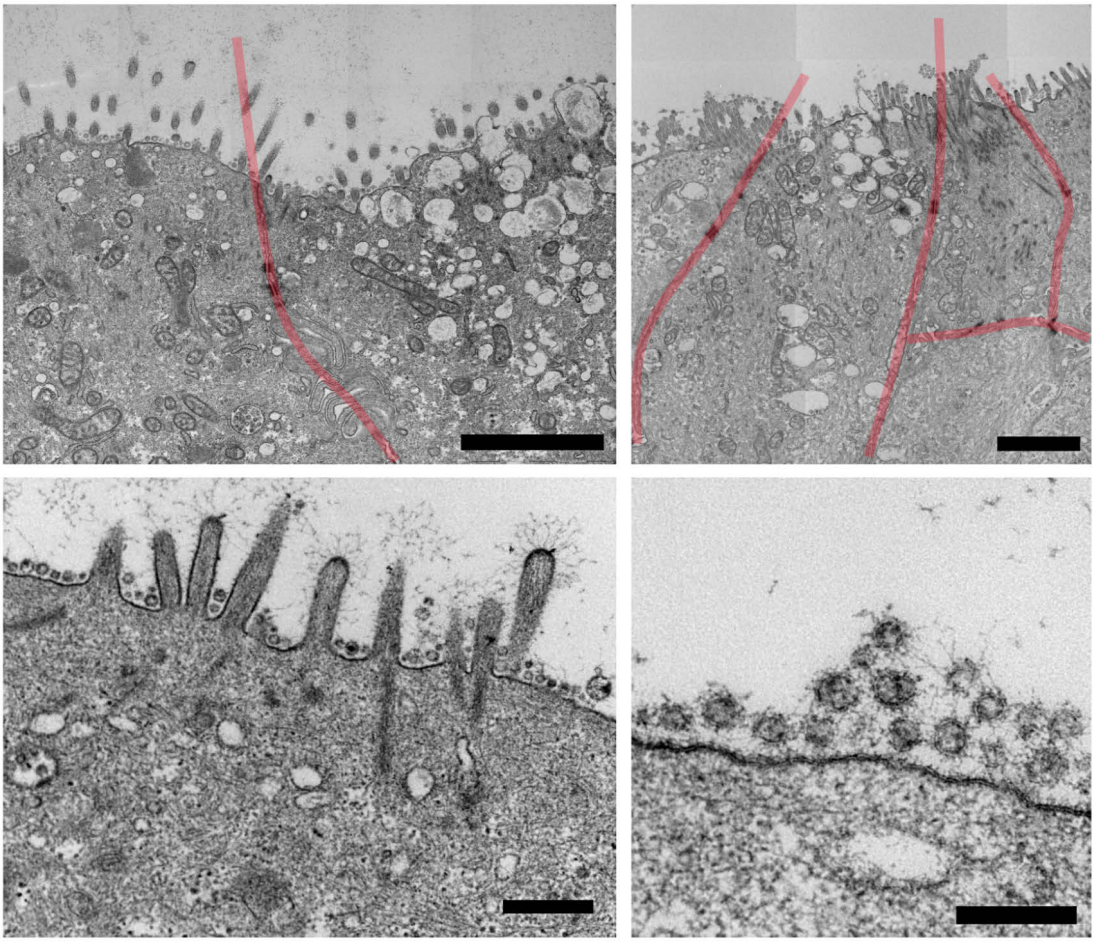

Appx. 28 Vesicle-rich cells and glycocalyceal bodies.
Top panel shows cells with a high content of apical vesicles (historically termed “secretory granules”). There are cells with almost none of such vesicles, some with a very high amount (like shown) but also many intermediate types. This pattern would match the lysozyme-stainings, observed in IFAs, and therefore could suggest the presence of PCs. Bottom panel shows small, granular, extracellular bodies with varying size, which feature a glycocalyx (fine web-like lines, compare to microvilli tips left) on the top of the apical membrane between microvilli. Those particles could represent glycocalyceal bodies, which can also be found on TCs and small intestinal tumors. Cell borders are indicated in red. Scale bars indicate 2 µm for top panel, 500 nm (bottom left) and 200 nm (bottom right).

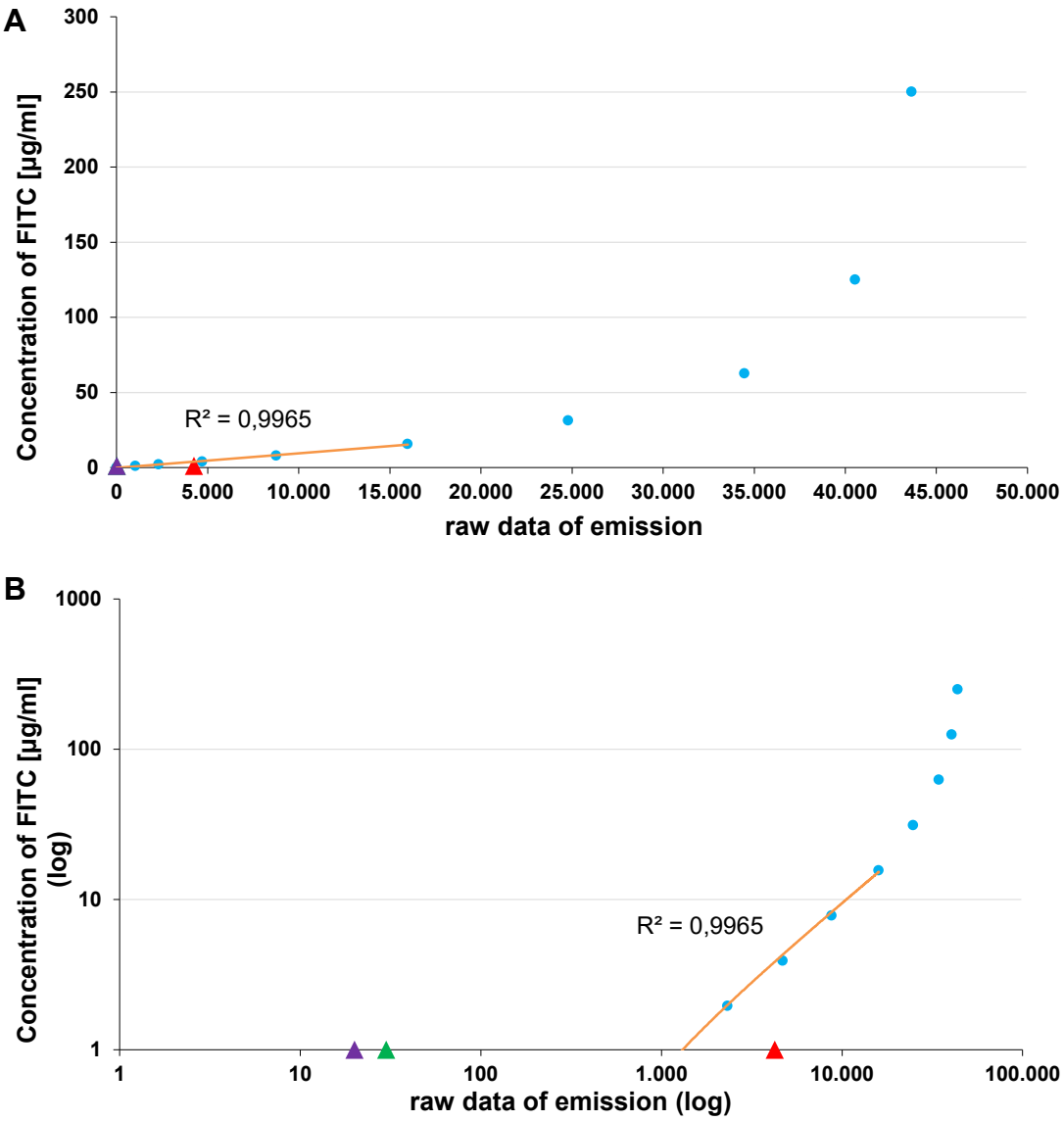


Appx. 29 Standard curve of Figure 20 (Caco-2 permeability)

Shown are normal (**A**) and log-transformed (**B**) plots of standard curves. Blue dots represent dilutions of known concentrations, orange line indicates linear dynamic range of the assay. Triangles indicate limit of detection (violet), lowest measured value (green), highest measured value (red). A zero-value cannot be plotted in log coordinates, but linearity applied down to 0, as seen in **A**. This figure also serves as exemple for other experiments using standard curves (e.g. Luminex® assay, BCA assay, etc.), which are not shown in this work.

```
run("8-bit");
setAutoThreshold("Default dark");
//run("Threshold...");
setThreshold(10, 255);
setOption("BlackBackground", false);
run("Convert to Mask");
run("Watershed");
run("Analyze Particles...", "size=0.03-Infinity show=Outlines display exclude");
```

Appx. 30 ImageJ script to count signals of IFA micrographs.

The code of the algorithm for counting nuclei or ClCa-1⁺ cells, is shown. For counting TUNEL⁺ cells, threshold-parameter was set to (20, 255) to be less sensitive to background interference and size-parameter was set to (0.02-Infinity) to include signals of slightly smaller size, since nuclei offered TUNEL signals sometimes only in a partial area or were smaller due to karyorrhexis. Due to those fixed parameters, it is important to run analysis on micrographs with the same resolution as well as similar intensity values (as done in this work).

```
TEERdata <- read.csv2("/RLocalDir/Data/9f CBF Debris R input log.csv")

View(TEERdata)
str(TEERdata)


### preparations

## load packages
library(ggplot2)
library(RColorBrewer)
library(dplyr)
library(pwr)
library(car)
library(ANOVAreplication)

## formatting to properly read data
TEERdata$condition <- as.factor(TEERdata$condition) # condition is a factor
TEERdata$time <- as.factor(TEERdata$time) # time should also be a factor
str(TEERdata)

## resort categorys
condis <- c("CTRL-", "CTRL+", "WB6", "WB6 heat-inactivated")
TEERdata$condition <- factor(TEERdata$condition, levels = condis)
```

Appx. 31 R script to format data input.

The code of the algorithm to format the input data containing columns for time, condition, TEER (absolute), TEER (normalized % to t0), and TEER (log2-ratios) is shown. This procedure prepares the data for further downstream analysis. Comments are in blue. Data of Figure 34 (first ODM infection) serves as example. Other analyses, which are not shown, e.g. for Luminex® data were conducted in a similar way.

```
### plots

# formatting for plot only (e.g. linebreaks)
condisformat <- c("CTRL-", "CTRL+", "WB6", "WB6\nheat-inactivated")

## remove t0 values for plot because normalized data will be shown
TEERdataNOt0 <- subset(TEERdata, time!=0, drop = TRUE)

## improve visualization

# apply random jitter to avoid stacking of points, dodge to separate groups
posn.jd <- position jitterdodge(jitter.width = 0.5,
                                dodge.width = 1.0)

# apply colorblind-friendly colors
TimeColors <- c("#1E88E5", "#FFC107", "#D81B60", "#004D40", "#CC79A7")

## create main scaffold, use normalized (% of t0) data
Main.Plot <- ggplot(TEERdataNOt0,
                    aes(x = condition,
                        y = TEERnorm,
                        fill = time))

## create final aesthetics
Main.Plot + geom_point(position = posn.jd,
                       size = 3,
                       shape=21,
                       color = "white") +
  geom vline(xintercept = seq(0.5, 13.5, 1),
             col = "grey90", linetype = 1) +
  scale_x_discrete("", labels = condisformat) +
  coord_cartesian(ylim = c(0, 200)) + # always adjust to max value of data
  scale_y_continuous(expression(paste("TEER (% of  ",t[0], ")")),
                     breaks = seq(0, 250, 50), # always adjust to max value of data
                     expand = c(0, 8)) +
  theme minimal() +
  theme(panel.grid.major.x = element_blank(),
        panel.grid.minor.y = element_blank(),
        axis.title.y = element_text(colour = "black",
                                    size = 20),
        axis.text = element text(colour = "black",
                                 face = "bold",
                                 size = 13),
        axis.text.x = element_text(angle = 45,
                                   hjust = 0.5,
                                   vjust = 0.5),
        legend.position = "top",
        legend.spacing.x = unit(10.0, 'points'),
        legend.text = element_text(colour = "black",
                                   face = "bold",
                                   size = 13,
                                   margin = margin(t = 0)),
        legend.title = element text(colour = "black",
                                    face = "plain",
                                    size = 20)) +
  guides(fill = guide legend(label.position = "bottom",
                             title.position = "left",
                             title.vjust = 0.4)) +
  scale fill manual("Time p.i. (h)", values = TimeColors)

## save directly from Plots-panel at 560 px height
```

Appx. 32 R script to plot diagrams.

The code of the algorithm to plot the input data, formatted in Appx. 31, is shown. Comments are in blue. Data of Figure 34 (first ODM infection) serves as example. Other analyses, which are not shown, e.g. for Luminex® data were conducted in a similar way.

```
### statistical pre-analysis (using log2-transformed data)

## check for normality, using all TEER values before infection

# visually
qqPlot(subset(TEERdata, time == 0)$TEERlog)

# if significant, hypothesis of normality should be refused
shapiro.test(subset(TEERdata, time == 0)$TEERlog)

## power t-test (paired), absolute data

# required to calc effect size (mean difference in relation to SD);
# also to indicate absolute TEER values at start in fig. description
meant0 <- mean(na.omit(subset(TEERdata, time == 0)$TEERab))
meant0
sdt0 <- sd(na.omit(subset(TEERdata, time == 0)$TEERab))
sdt0

# power assumed to observe 50% de-/increase in absolute TEER
pwr.t.test(n=3,
           d=(meant0-(meant0/2))/sdt0,
           power = NULL,
           sig.level = 0.05,
           type = "paired",
           alternative = "two.sided")

# with 80% power, a difference of ...Ohm*cm² can be indicated
effectsize <- pwr.t.test(n=3,
                         d=NULL,
                         power = 0.8,
                         sig.level = 0.05,
                         type = "paired",
                         alternative = "two.sided")$d * sdt0
effectsize

# or expressed in ...%
effectsize/meant0*100


## power ANOVA, log2-transformed data

# required to calc effect size
# (pooled SD of all groups in relation to SD within groups)
AOV.sdt0 <- sd(na.omit(subset(TEERdata, time == 0)$TEERlog))
AOV.sdt0

pool_trafo <- data.frame(y=TEERdata$TEERlog, g=TEERdata$condition)
pool_trafoNONA <- na.omit(pool_trafo)
AOV.SDpool <- pooled.sd(pool trafoNONA)
AOV.SDpool

# power assumed to observe differences according to ANOVA definition
pwr.anova.test(k = length(condis),
               n = 3,
               f = AOV.SDpool/AOV.sdt0,
               sig.level = 0.05)
```

Appx. 33 R script to pre-analyze data.

The code of the algorithm to pre-analyze (normally distributed, power-analysis) the input data, formatted in Appx. 31, is shown. Comments are in blue. Data of Figure 34 (first ODM infection) serves as example. Appx. 34 show computed Q-Q plot and Shapiro-Wilk test for normality. Calculated power to observe a 50% de-/increase of TEER was 95%, with 80% power, a decrease of 57.15 Ω·cm² (36,2%) can be investigated (paired t-test). One-way ANOVA had 100% power. Other analyses, which are not shown, e.g. for Luminex® data were conducted in a similar way.

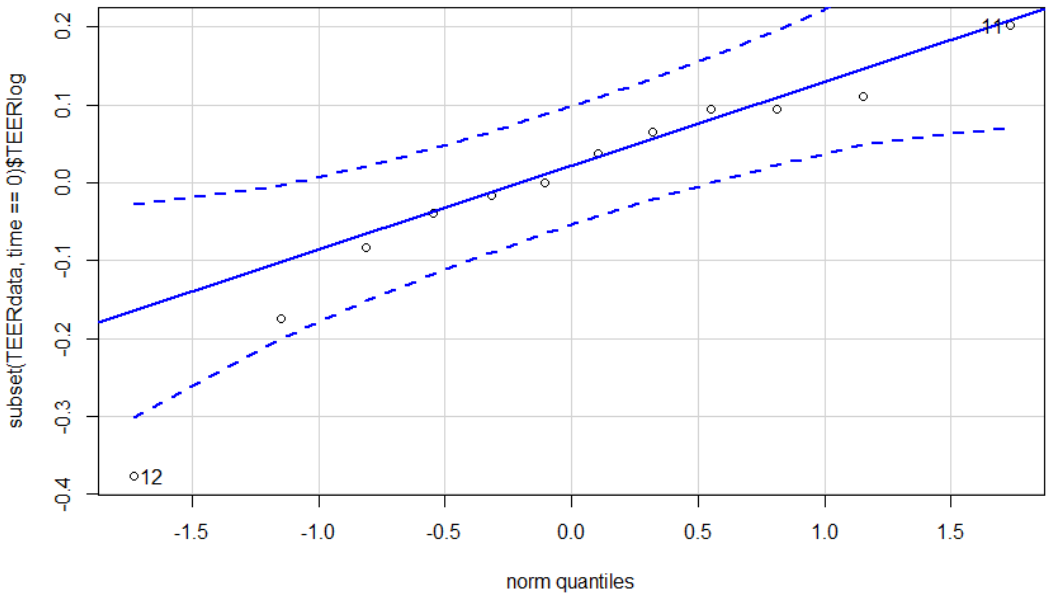


Appx. 34 Example Q-Q plot.

Shown is the Q-Q plot, generated from data of Figure 34 according to Appx. 33. Values along the blue line, within the dashed channel suggested normal distribution. Using Shapiro-Wilk normality test, the null-hypothesis (data is not normally distributed) could not be refused ($p = 0.2015$).

```
### ANOVA & Tukey post-hoc testing correction

## filter parameters to run ANOVA separate for each time point (dependent variable)
t0 <- TEERdata$time == 0
t2 <- TEERdata$time == 2
t24 <- TEERdata$time == 24
t48 <- TEERdata$time == 48


## this compares conditions to CTRL- condition for each time point,
## e.g. WB6 infected after 24 h with CTRL- after 24 h

## for t0
TEER.AOV.con.t0 = aov(TEERlog ~ condition, data = TEERdata[t0, ])
summary(TEER.AOV.con.t0) # ANOVA
AOV.data.con.t0 <- TukeyHSD(TEER.AOV.con.t0, conf.level = 0.95) # Tukey post-hoc
AOV.output.con.t0 <- data.frame(AOV.data.con.t0$condition) # adjust data format
AOV.output.con.t0 <- cbind(rownames(AOV.output.con.t0), AOV.output.con.t0)
rownames(AOV.output.con.t0) <- NULL
colnames(AOV.output.con.t0) <- c("comparison", "diff","lwr","upr", "p.adj")
AOV.output.con.t0$time <- 0 # add time again to table
AOV.output.con.t0

# filter for comparison of conditions to CTRL-
AOV.interest.con.t0 <- filter(AOV.output.con.t0,
                              grepl("-CTRL-", AOV.output.con.t0[,1]))
AOV.interest.con.t0

# filter for sig. p-values
AOV.interest.sig.con.t0 <- AOV.interest.con.t0 %>% filter(p.adj < 0.05)
AOV.interest.sig.con.t0


# [...] repeat last sections for all time points, change respective parameters t0
```

Appx. 35 R script to analyze data for statistically significant differences.

The code of the algorithm to analyze the input data, formatted in Appx. 31, using one-way ANOVA and Tukey post-hoc test, is shown. Comments are in blue. Data of Figure 34 (first ODM infection) serves as example. Other analyses, which are not shown, e.g. for Luminex® data were conducted in a similar way. Appx. 15 showed computed results

Erklärung:

Hiermit erkläre ich, Martin R. Kraft (geb. 17.11.1988, Berlin), die Dissertation selbstständig und nur unter Verwendung der angegebenen Hilfen und Hilfsmittel angefertigt zu haben.
Ich habe mich anderwärts nicht um einen Doktorgrad beworben und besitze keinen entsprechenden Doktorgrad.
Ich erkläre, dass ich die Dissertation oder Teile davon nicht bereits bei einer anderen wissenschaftlichen Einrichtung eingereicht habe und dass sie dort weder angenommen noch abgelehnt wurde.
Ich erkläre die Kenntnisnahme der dem Verfahren zugrunde liegenden Promotionsordnung der Lebenswissenschaftlichen Fakultät der Humboldt-Universität zu Berlin vom 5. März 2015.
Weiterhin erkläre ich, dass keine Zusammenarbeit mit gewerblichen Promotionsbearbeiterinnen/Promotionsberatern stattgefunden hat und dass die Grundsätze der Humboldt-Universität zu Berlin zur Sicherung guter wissenschaftlicher Praxis eingehalten wurden.

Declaration:

I, Martin R. Kraft (born 17th November 1988, Berlin), hereby declare that I completed the doctoral thesis independently based on the stated resources and aids.
I have not applied for a doctoral degree elsewhere and do not have a corresponding doctoral degree.
I have not submitted the doctoral thesis, or parts of it, to another academic institution and the thesis has not been accepted or rejected.
I declare that I have acknowledged the Doctoral Degree Regulations which underlie the procedure of the Faculty of Life Sciences of Humboldt-Universität zu Berlin, as amended on 5th March 2015.
Furthermore, I declare that no collaboration with commercial doctoral degree supervisors took place, and that the principles of Humboldt-Universität zu Berlin for ensuring good academic practice were abided by.

.....

Datum / Unterschrift
Date / signature